Signalling, desensitization and resensitization of neuromedin U receptors

Thesis submitted for the degree of

Doctor of Philosophy

University of Leicester

By

Khaled Alhosaini

Department of Cell Physiology and Pharmacology

University of Leicester

September 2011

ABSTRACT

The neuropeptides neuromedin U (NmU) and neuromedin S (NmS) show a high degree of conservation across species, primarily at the amidated *C*-terminus. NmU in particular is widely distributed in both the central nervous system and periphery and is involved in a plethora of physiological and pathological events. NmU and NmS mediate their actions via two family A, G protein-coupled receptors, NMU1 and NMU2, which share ~50% homology. The present study confirmed receptor coupling to $G\alpha_{q/11}$, leading to increases in intracellular [Ca^{2+}] and activation of extracellular signal-regulated protein kinase (ERK), as well as coupling to $G\alpha_{i/o}$, leading to pertussis toxin-sensitive inhibition of adenylyl cyclase activity. This study also confirmed that different NmU analogues bind pseudo-irreversibly to recombinantly expressed NMUs and has shown receptor-dependent internalization of a fluorescently-tagged version of NmU. *C*-terminal eGFP-tagged NMUs showed co-internalization of ligand and receptor within ~2.5 min of ligand exposure. Cell-surface, receptor-bound ligand could be removed by a rapid (20 s), pH 2.0 washing without detrimental effect on signal transduction or cell viability, allowing examination of desensitization and resensitization in the absence of cell-surface, ligand-bound receptors. Desensitization of NMU2-mediated Ca^{2+} responses (that was independent of continued ligand binding) occurred within minutes of exposure to human (h) NmU-25. Acute exposure (5 min) to a maximum concentration of hNmU-25 followed by recovery in the absence (pH 2.0 wash) or the presence (pH 7.4 wash) of cell-surface, receptor-bound hNmU-25 showed that the continued presence of ligand markedly delayed receptor resensitization. Receptor internalization via a dynamin-dependent pathway was crucial for resensitization of NMU1 and NMU2. Further, resensitization was dependent on endosomal acidification, recycling and endothelin-converting enzyme-1 (ECE-1) activity, but not *de novo* protein synthesis. This suggests that processing of hNmU-25 by ECE-1 in acidified endosomes is critical for resensitization. Inhibition of ECE-1 also prolonged NMU-mediated ERK activation, suggesting G protein-independent signalling by a ligand-receptor dependent complex within endosomes. Although no significant differences were demonstrated in potency and signalling between the NMU subtypes or their ligands, resensitization (and potentially therefore G protein-dependent/independent signalling) was influenced by both the ligand (nature and length of the *N*-terminus) and the receptor (NMU1 versus NMU2).

ACKNOWLEDGEMENTS

I would like to sincerely thank my supervisor Dr Gary Willars for giving me this opportunity to do my PhD, working with the most interesting signalling molecules (GPCRs). Thank you for your extraordinary patience, encouragement and support throughout my laboratory work, talks and writing this thesis. I am also very grateful for the support of Professor John Challiss, whose supervision I have been honoured by and learned from enormously. Thank you indeed for the unlimited encouragement, scientific hints and the great deal of time and efforts to correct my thesis. You have both been unique examples of scientist who dedicate their lives for the advancement of science.

Many thanks also to my thesis committee members John Mitcheson and Nina Storey. Thank you Nina for your constant smile and for the provision of fresh cardiac myocytes. I would also like to thank Rajendra Mistry, Sophie Bradley, Neil Johnston, Jianling Xie Zhang and Carl Nelson for their invaluable help with several techniques.

Special thanks for Yan Huang for the great deal of time and efforts expended to teach me how to generate epitope-tagged constructs. I could not have succeeded without your endless molecular knowledge.

I would also like to extend my thanks to all members of CPP and to the many friends that I have made across the university who have helped make my PhD journey a golden time in my life.

This PhD would not have been possible without funding from King Saud University Scholarship and the government of Saudi Arabia.

Finally, my greatest appreciation goes to my parents, wife, Lama, and children, Fahad, Jumanah and Lubna. Thank you all so very much for your love, support and tolerance.

Lama a special thank you is owed to you for your kind words of encouragement and support during my regular moments of stress and for having the belief in me that I could do it. Thank you for taking over my part of responsibility for the house and our children to allow me to focus on my study. Without you, this thesis would never have been possible.

This thesis is dedicated

To my mother, my father and my wife for

their support and love

Khaled

ABBREVIATIONS

7TM	Seven transmembrane α-helices
A_3	Adenosine receptor
AC	Adenylyl cyclase
ACTH	Adrenocorticotropic hormone
AP-2	Adaptor protein-2
APS	Ammonium persulphate
ARC	Arcuate nucleus
ATP	Adenosine triphosphate
BSA	Bovine serum albumin
CA1	Cornu ammonis area in hippocampus 1
Ca^{2+}	Calcium
$[Ca^{2+}]_i$	Intracellular calcium concentration
cAMP	Adenosine cyclic-3',5'-monophosphate
CCE	Capacitative Ca^{2+} entry
Cch	Carbachol
cDNA	Complementary DNA
CFA	Complete Freund's adjuvant
CHO	Chinese hamster ovary cell-line
cNmU-25	Chicken NmU-25
cNmU-9	Chicken NmU-9
CNS	Central nervous system
CPP	Clathrin-coated pits
CRAC	Ca^{2+} release-activating Ca^{2+} channel
CRH	Corticotropic-releasing hormone
***C*-terminal**	Carboxy-terminal
Cy3B-pNmU-8	pNmU-8 fluorescently-tagged at N-terminal with Cy3B
DAG	Diacylglycerol
DMEM	Dulbecco's modified Eagle's medium
DMSO	Dimethyl sulphoxide
dNmU-25	Dog NmU-25
dNmU-8	Dog NmU-8
dNTPs	Deoxyribonucleotide triphosphate
D-PBS	Dulbecco's phosphate-buffered saline
DTT	Dithiothreitol
EDTA	Ethylenediaminetetraacetic acid
eGFP	Enhanced green fluorescent protein
ELISA	Enzyme-linked immunosorbent assay
ER	Endoplasmic reticulum
ERK	Extracellular signal-regulated kinase
ET_A	Endothelin A receptor
FACS	Fluorescence-activated cell-sorting
FBS	Fetal bovine serum
FITC	Fluorescein 5-isothiocyanate
Fluo-4-AM	Fluo-4-acetoxymethylester
FM-3	Previous name of neuromedin U receptor subtype-1
FM-4	Previous name of neuromedin U receptor subtype-2
fNmU-17	Frog NmU-17
fNmU-23	Frog NmU-23
fNmU-25	Frog NmU-25
G protein	Heterotrimeric guanine nucleotide-binding protein
G-418	Geneticin

$GABA_B$	Gamma-aminobutyric acid receptor type B
GAP	GTPase-activating protein
GDP	Guanosine diphosphate
GEF	Guanine-nucleotide exchange factor
gfNmU-21	Goldfish NmU-21
gfNmU-25	Goldfish NmU-25
gfNmU-38	Goldfish NmU-38
GIT	Gastrointestinal tract
GLP-1	Glucagon-like peptide 1
GPCR	G protein-coupled receptor
gpNmU-9	Guinea pig NmU-9
GPR66	Previous name of neuromedin U receptor subtype-1
GRK	G protein-coupled receptor kinase
GTP	Guanosine triphosphate
HEK	Human embryonic kidney
HEK-NMU1	HEK 293 cells stably expressing NMU1
HEK-NMU1-eGFP	HEK 293 cells stably expressing C-terminal eGFP-tagged NMU1
HEK-NMU2	HEK 293 cells stably expressing NMU2
HEK-NMU2-eGFP	HEK 293 cells stably expressing C-terminal eGFP-tagged NMU2
hNmS-33	Human NmS-33
hNmU-25	Human NmU-25
HPA	Hypothalamic-pituitary axis
i3	Third intracellular loop
IBMX	Isobutylmethylxanthine
ICC	immunocytochemistry
ICV	Intracerebroventricular
IL	Interleukin
$InsP_x$	Inositol (poly)phosphates
IP_3	inositol 1,4,5-trisphoshate
IV	Intravenous
JqNmU-25	Japanese quail NmU-25
K_d	Dissociation constant
KHB	Krebs-HEPES buffer or Krebs-Henseleit buffer
KNRK cells	K-ras-transformed normal rat kidney cell-line
KYSE140 cells	Human oesophageal cancer cell-line
MAPK	Mitogen-activated protein kinase
MDC	Monodansylcadaverine
MEM	Minimum essential medium
mNmS-36	Mouse NmS-33
mRNA	Messenger RNA
NK cells	Natural killer cells
NK1	Neurokinin 1 receptor
NmS	Neuromedin S
NmU	Neuromedin U
$NmU^{-/-}$	genetically lacking the NmU gene
NMU1	Neuromedin U receptor subtype-1
$NMU1^{-/-}$	genetically lacking the NMU1 gene
NMU1-eGFP	Neuromedin U receptor subtype-1 tagged with eGFP
NMU2	Neuromedin U receptor subtype-2
$NMU2^{-/-}$	genetically lacking the NMU2 gene
NMU2-eGFP	Neuromedin U receptor subtype-2 tagged with eGFP
NmU-LI	NmU-like immunoreactivity
NMUR1	NMU1 gene
NMUR2	NMU2 gene

NSCLC cells	Non-small lung cancer cells
***N*-terminal**	Amino-terminal
NTS	Nucleus tractus solitarius
OD	Optical density
PAO	Phenylarsine oxide
PBS	Phosphate-buffered saline
pCASMCs	Porcine coronary artery smooth muscle cells
PCR	Polymerase chain reaction
pERK	Phosphorylated extracellular signal-regulated kinase
PIP_2	Phosphatidylinositol-4,5-bisphosphate
PKA	Protein kinase A
PKC	Protein kinase C
PLCβ	Phospholipase Cβ
pNmU-25	Porcine NmU-25
pNmU-8	Porcine NmU-8
Pomc	Pro-opiomelanocortin
PSS	Physiological salt solution
PTX	Pertussis toxin
PVDF	Polyvinylidene difluoride
PVN	Paraventricular nucleus
qRT-PCR	Quantitative reverse-transcriptase PCR
r.p.m.	Revolution per minute
rbNmU-25	Rabbit NmU-25
RGS	Regulator of G protein signalling
rNmS-36	Rat NmS-36
rNmU-23	Rat NmU-23
RPMI 1640	Royal Park Memorial Institute culture medium
RT	Room temperature
SCN	Suprachiasmatic nucleus
SDS	Sodium dodecyl sulfate
SERCA	Sarcoplasmic/endoplasmic reticulum Ca^{2+}-ATPase pump
siRNA	Short interfering RNA
SM-19712	selective ECE-1 inhibitor (4-chloro-N-[[(4-cyano-3-methyl-1-phenyl-1H-pyrazol-5-yl)amino]carbonyl] benzenesulfonamide, monosodium salt)
SMGS	Smooth muscle growth supplement
TBST	Tris buffered saline with tween
TCA	Trichloroacetic acid
TEMED	N, N, N', N'-tetramethylethylenediamine
TGR-1	Previous name of neuromedin U receptor subtype-2
tNmS-17	Toad NmS-17
tNmS-33	Toad NmS-33
TRPC	(Transient receptor potential cation) channels
U-II	urotensin II
UTP	Uridine-5'-triphosphate
VFM	Venus flytra module
α-MSH	α-melanocyte-stimulating hormone

PUBLICATIONS

Peer reviewed abstracts and poster presentations

Al-Hosaini, K., Challiss, R.A.J. and Willars, G.B (2010) Irreversible binding of neuromedin U to its type 2 receptor (NMU2): relationship to loss and recovery of agonist-mediated Ca^{2+} signalling. British Pharmacological Society, 3rd Focused Meeting on Cell Signalling, Leicester, UK. April 2009. Poster presentation.

Al-Hosaini, K., Challiss, R.A.J. and Willars, G.B (2010) Role of receptor recycling in the recovery of Ca^{2+} signalling by recombinantly expressed neuromedin U 2 receptors (NMU2). 16th World Congress of Basic and Clinical Pharmacology, Copenhagen, Denmark. July 2010. Poster presentation.

Table of contents

Chapter 1

Introduction

1.1 Background

The importance of neuropeptides as signalling molecules was first demonstrated in the 1970s by the fact that with the exception of dopamine, most hypothalamic signalling molecules were identified as small peptides (Hokfelt *et al.*, 2003; Salio *et al.*, 2006). Among hundreds of G protein-coupled receptors (GPCRs) in the human genome, neuropeptides are ligands for approximately 20% of these (Rashid *et al.*, 2004). Neuropeptides play key roles in the central nervous system, such as modulation of pain, addiction, depression, seizure activity and appetite, while in the gastrointestinal tract (GIT), they regulate motility, enzyme secretion, absorption, and smooth muscle tone (Hokfelt *et al.*, 2003; Rashid *et al.*, 2004).

Several differences have been identified between neuropeptides and other smaller signalling molecules, such as neurotransmitters, including mechanisms of synthesis and storage, as well as their signalling functions (Hokfelt *et al.*, 2003). For instance, neuropeptide release in neurons has been reported to require higher frequencies of discharge compared to the lower frequencies necessary for small molecule neurotransmitter release. Neuropeptides are often found together with one or even two small molecule neurotransmitters, which can result in combinations of fast (2–5 ms) and slow (100–500 ms) synaptic communication (Hokfelt *et al.*, 2003). Neuropeptides are generally larger than small molecule neurotransmitters, being composed of 3–100 amino acid residues. These have the capacity to contain more chemical information and possess several recognition sites for receptor interaction (Hokfelt *et al.*, 2003; Salio *et al.*, 2006). Thus, neuropeptides bind to receptors with high affinity (pM-to-nM affinities) compared to lower affinity (μM) binding of small molecule neurotransmitters. Additionally, termination of small molecule neurotransmitter action is mainly achieved by reuptake mechanisms, while neuropeptides are broken down by peptidases, either at the cell-surface or following cellular uptake (Hokfelt *et al.*, 2003).

Endogenous neuropeptide ligands for GPCRs are generally produced as a result of enzymatic cleavage of a precursor protein (prepropeptide) to give fragments that are

biologically active peptides specific for one or more GPCRs. Further, different gene products can also encode peptides that activate similar receptors (Rashid *et al.*, 2004). Post-translational modification of amino acid residues in neuropeptide ligands can regulate their potency or specificity and certain other modifications may be absolutely required for signalling, such as *C*-terminal α-amidation, octanoylation and sulphation (Rashid *et al.*, 2004).

1.2 Neuromedin U and neuromedin S

1.2.1 Discovery and species differences

Neuromedin U (NmU) and S (NmS) are members of a family of neuropeptides known as the neuromedins. With the exception of NmS, all neuromedin family members were originally isolated from porcine spinal cord in the early 1980s due to their ability to contract smooth muscle of rat uterus or guinea pig ileum (Kangawa *et al.*, 1983a; Minamino *et al.*, 1984b; Minamino *et al.*, 1983b; Minamino *et al.*, 1984a; Minamino *et al.*, 1984c; Minamino *et al.*, 1985a; Mori *et al.*, 2005). Two porcine neuropeptides were purified and characterized as NmU; both a 25 (pNmU-25) and 8 (pNmU-8) amino acid neuropeptides. These show potent contractile effects on strips of rat uterine smooth muscle (the suffix U represents their ability to contract rat uterus smooth muscle strips). NmS was first isolated in 2005 from rat brain extract and the suffix "S" given due to its high expression in the suprachiasmatic nucleus (SCN) (Mori *et al.*, 2005).

NmU has been isolated from many species including, rat (rNmU-23) (Conlon *et al.*, 1988; Domin *et al.*, 1986; Domin *et al.*, 1987; Minamino *et al.*, 1988), frog (fNmU-25, fNmU-23 and fNmU-17) (Domin *et al.*, 1989; Lee *et al.*, 2005; Salmon *et al.*, 2000), guinea pig (gpNmU-9) (Murphy *et al.*, 1990), dog (dNmU-25 and dNmU-8) (O'Harte *et al.*, 1991a), chicken (cNmU-25 and cNmU-9) (Domin *et al.*, 1992; O'Harte *et al.*, 1991b), Japanese quail (JqNmU-25) (Shousha *et al.*, 2005), rabbit (rbNmU-25) (Kage *et al.*, 1991), human (hNmU-25) (Austin *et al.*, 1995) and goldfish (gfNmU-21, gfNmU-25 and gfNmU-38) (Maruyama *et al.*, 2008). The cDNA encoding NmS has been isolated from brain extract of human (hNmS-33), rat (rNmS-36) and mouse (mNmS-36) (Mori *et al.*,

2005) and from the dermal venoms of *Eurasian bombinid* toads (tNmS-17 and tNmS-33) (Chen *et al.*, 2006).

A study of the cDNA encoding the protein precursor of rNmU-23 (Lo *et al.*, 1992) and hNmU-25 (Austin *et al.*, 1995) showed that in both cDNAs, NmU is synthesized and located within the *C*-terminus of a 174 amino acid precursor protein. The precursor protein from both species show 74% homology and four out of five proteolytic processing sites in the rat precursor are present in the human version, indicating evolutionary conservation of the precursor between these two species (Brighton *et al.*, 2004b).

1.2.2 Structure-activity relationships

The gene for NmU in man is located on chromosome 4q12 while the NmS gene is located on chromosome 2q11.2. Analysis of the amino acid sequence and structure of NmU and NmS from different species **(Figure 1.1)** has revealed three main aspects: conservation of the amino acid sequence especially at the *C*-terminus; an amidated *C*-terminus and; variation of *N*-terminal length. The different analogues of NmU and NmS isolated from mammalian and non-mammalian species **(Figure 1.1)** show a significant level of conservation and homology. For example, the *C*-terminal heptapeptid (FLFRPRN-NH_2) is conserved in all mammalian species, while the *C*-terminal five amino acids (FRPRN-NH_2) are totally conserved amongst all species with the exception of isoforms isolated from goldfish (Maruyama *et al.*, 2008). NmS isoforms of all species from which it has been identified share the same *C*-terminal undecapeptide (Chen *et al.*, 2006). In certain mammalian forms, such as pNmU-25 (Minamino *et al.*, 1985a) and dNmU-25 (O'Harte *et al.*, 1991a), it has been suggested that the presence of a dibasic pairing (Arg^{16} and Arg^{17}) before the last eight *C*-terminal amino acids serve as a proteolytic cleavage site allowing the generation of the biologically active octapeptide, NmU-8. This potential dibasic cleavage site does not exist in the other elongated versions of NmU such as those found in rabbit, frog or human and shorter versions of NmU have not been reported in these species. Interestingly, although the longer version of chicken NmU lacks Arg^{17} (where it is substituted by Gly), a shorter nonapeptide (NmU-9) has been detected and it has been suggested that Arg^{16}-Gly^{17} is also a cleavage site (O'Harte *et al.*, 1991b). However, it

should be noted that Arg^{16}-Gly^{17} is also found in NmU of other species (e.g. hNmU-25) without detecting a shorter version.

The highly conserved heptapeptide at the *C*-terminus of NmU and NmS seems to be crucial for their biological activity. For example, single amino acid substitution of the residues of NmU-8 by either Gly or the inactive *D*-moiety significantly reduced contractile activity on chicken crop smooth muscle. Indeed, replacing Arg^7 with Gly abolished the contractile effect (Hashimoto *et al.*, 1991). Similarly, replacement of any of the last *C*-terminal seven amino acids of NmU-8 by Ala (particularly Arg^7 and Asn^8) dramatically reduced the potency for Ca^{2+} mobilization in cells expressing NMU2 (Funes *et al.*, 2002).

Incorporation of an amide group at the *C*-terminus is found in approximately 50% of peptides with therapeutic use and it has been suggested to play an essential role in both ligand-receptor interaction and in the protection of the peptide against the proteolytic activity of carboxypeptidases (Rink *et al.*, 2010). Amidation of the *C*-terminal asparagine residue is crucial for NmU, since synthetic pNmU-8 lacking this loses its hypertensive effect and contractile activity in both rat uterus (Minamino *et al.*, 1985a) and chicken crop smooth muscle (Kawai *et al.*, 2006). At the cellular level, non-amidated NmU-8 (10 μM) failed to evoke Ca^{2+} responses in cells recombinantly expressing human NMU1, where the amidated version resulted in a concentration-dependent increase in intercellular Ca^{2+} ($[Ca^{2+}]_i$) with an EC_{50} of 10 nM (Hedrick *et al.*, 2000). Furthermore, in cells expressing mouse NMUs, non-amidated NmU-8 (100 μM) did not induce Ca^{2+} signalling while NmU-8-NH_2 caused an elevation of $[Ca^{2+}]_i$ with an EC_{50} value of 20 nM and 3 nM in NMU1 and NMU2, respectively (Funes *et al.*, 2002).

Unlike the highly conserved *C*-terminus, most of the variation in amino acid sequence of NmU or NmS from different species occurs at the *N*-terminus (Figure 1.1). However, some conservation can be seen within *N*-terminal residues. For example, in NmU-25 from different species, Gln^8 is conserved and Asp^4-Glu^5 are also present with the exception of goldfish NmU-25, while Pro^{10} is absent only in chicken NmU-25. It has been suggested that these differences play a role in the potency and duration of action as pNmU-25 induces a longer hypertensive effect than pNmU-8 in rat and the contractile effect was three times as potent as pNmU-8 on rat uterus (Minamino *et al.*, 1985a). Furthermore,

examination of the contractile effect of synthesized fragments of rNmU-23 using chicken crop smooth muscle revealed that bioactivity was directly proportional to the length of the peptide (Sakura *et al.*, 1991).

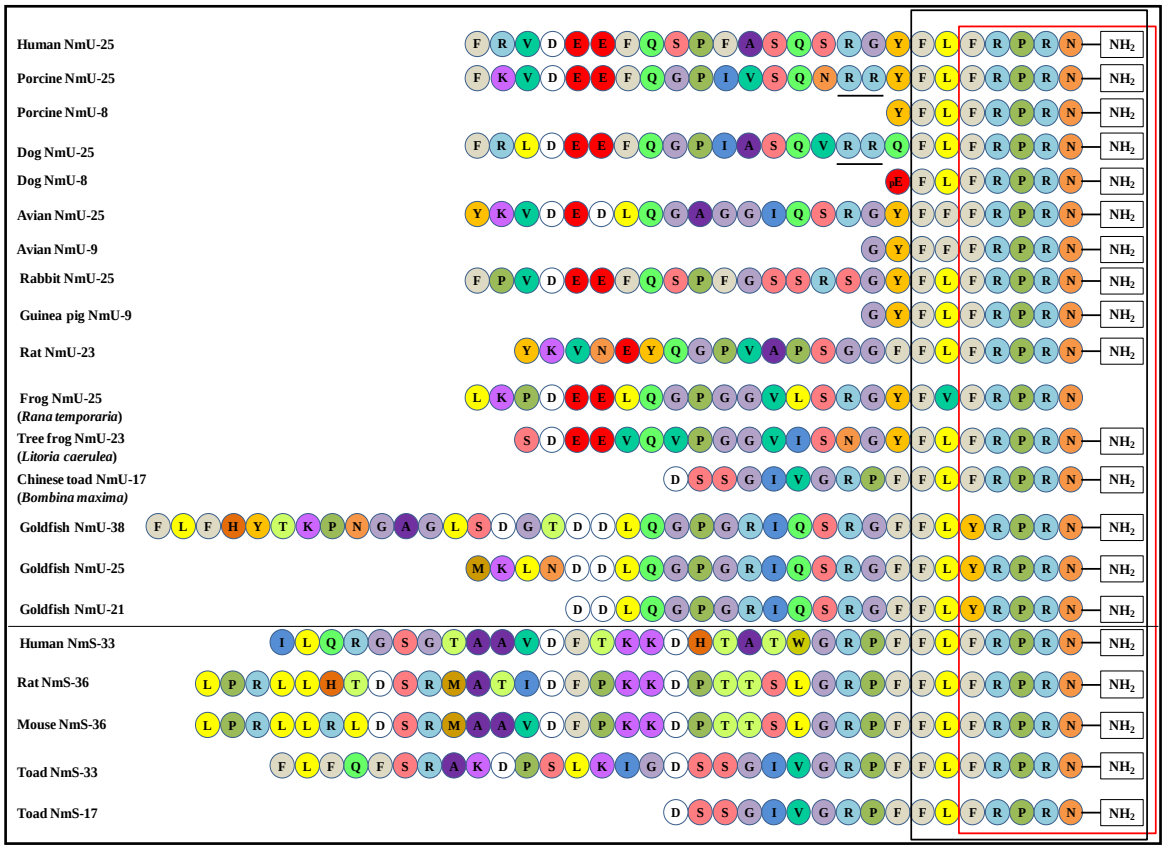

Figure 1.1. Amino acid sequences of NmU and NmS isolated from different species. Each amino acid is given a specific colour for the purpose of clarifying structural homology. An amide group is indicated in all species at the *C*-terminal asparagine (N-NH2) except in fNmU-25, where amidation has not been confirmed (Domin *et al.*, 1989). The potential dibasic cleavage site, Arg16-Arg17 that is present in certain species is also shown (R-R). The sequences show the conserved *C*-terminus pentapeptide (red box) in all species with the exception of gfNmU (Maruyama *et al.*, 2008). NmU and NmS sequences also have an identical *C*-terminal heptapeptide in all mammalian species (black box).

1.2.3 Distribution of NmU and NmS

NmU is commonly termed a gut-brain peptide due to its high expression in these tissues. The tissue distribution of NmU and its precursor has been thoroughly studied in mammals, especially in rat and human (Austin *et al.*, 1995; Domin *et al.*, 1987; Domin *et al.*, 1989; Fujii *et al.*, 2000; Szekeres *et al.*, 2000). NmU shows higher expression in gastrointestinal tract (GIT) than brain (Austin *et al.*, 1995; Szekeres *et al.*, 2000) while NmS are mainly expressed in the central nervous system (CNS) (Mori *et al.*, 2005). These studies used immunocytochemistry (ICC) and/or enzyme-linked immunosorbent assays (ELISA) to detect peptide like immunoreactivity (e.g. NmU-LI) and/or quantitative reverse transcriptase polymerase chain reaction (qRT-PCR) to detect NmU mRNA.

1.3 Neuromedin U receptors (NMU)

Two G protein-coupled receptors (GPCRs) have been identified for NmU and NmS. According to IUPHAR nomenclature and the Guide to Receptors and Channels (Alexander *et al.*, 2008; Sharman *et al.*, 2011

), these are termed NMU1 and NMU2. Before the discovery and de-orphanization of NMUs, specific binding sites for radiolabelled rNmU-23 ([^{125}I]-rNmU-23) had been shown in membranes prepared from rat uterus (Nandha *et al.*, 1993). The binding was time-, pH- and temperature-dependent and reduced by the addition of the non-hydrolysable form of GTP (GTPγS) in a concentration-dependent manner thereby suggesting that binding affinity was G protein-dependent (Nandha *et al.*, 1993). Five years later, the FM-3 receptor (now known as NMU1) was cloned from both mouse T-cell cDNA and a human cDNA library based on its homology to two GPCRs: the growth hormone secretagogue receptor (now known as the ghrelin receptor, 33% homology) and; the neurotensin-1 (NT1) receptor (29% homology) (Tan *et al.*, 1998). The protein sequences of FM-3 from mouse and human are 73% homologous.

The use of reverse pharmacology and high-throughput screening of functional responses such as $[Ca^{2+}]_i$ elevation, archidonic acid release, inositol (poly)phosphate ($InsP_x$) accumulation assay subsequently facilitated the identification and characterization of NMUs. Firstly, FM-3 (also known as GPR66) was cloned from human, mouse and rat

cDNA libraries and reported as a cognate receptor for NmU analogues (Fujii *et al.*, 2000; Howard *et al.*, 2000; Kojima *et al.*, 2000; Raddatz *et al.*, 2000; Szekeres *et al.*, 2000). A second GPCR (TGR-1 or FM-4) was also cloned from human and rat cDNA libraries and de-orphanized. This had 51% sequence homology to NMU1 (Howard *et al.*, 2000) and was subsequently identified as a receptor for NmU and termed NMU2 (Hosoya *et al.*, 2000; Howard *et al.*, 2000; Raddatz *et al.*, 2000; Shan *et al.*, 2000). In cell-lines expressing recombinant NMUs, other members of the neuromedin family or neuropeptides having some homology with NmU were unable to bind or evoke a response even at micromolar concentrations (Brighton *et al.*, 2004b). In contrast, NmU analogues showed high affinity and induced NmU-mediated signalling at sub-nanomolar concentrations (Kojima *et al.*, 2000; Raddatz *et al.*, 2000; Szekeres *et al.*, 2000). The human receptors, NMU1 and NMU2 share 73% and 75% homology with rat receptors, NMU1 and NMU2, respectively (Howard *et al.*, 2000). Furthermore, NMU1 and NMU2 show 73-79% and 81% homology to the mouse receptors, NMU1 and NMU2 respectively (Funes *et al.*, 2002; Tan *et al.*, 1998).

1.3.1 Structural characteristics of NMU

Both NMU1 and NMU2 exhibit many of the characteristics of family A GPCRs with typical seven-transmembrane helices (Figure 3) and the presence of a conserved E/DRY (Asp-Arg-Tyr) amino acid sequence between the third transmembrane domain and the beginning of the second intracellular loop. This is considered to be responsible for maintaining the inactive state of family A GPCRs to regulate both ligand binding and G protein coupling (Rovati *et al.*, 2007; Strader *et al.*, 1994). Similar to other members of family A GPCRs, there are two cysteine residues present in the extracellular domain of both receptors which may allow the formation of a disulfide bridge to maintain protein folding, ligand binding and a stable conformation of the receptor (Strader *et al.*, 1994). Even though variations in *N*-terminal amino acid sequence of NMUs have been reported (Raddatz *et al.*, 2000; Shan *et al.*, 2000; Tan *et al.*, 1998), all versions bind NmU and show functional activity (Brighton *et al.*, 2004b). Due to the fact that both receptors subtypes have two initiation codons (ATG) at the beginning of the sequence, two

sequences for NMU1 have been predicted: either a shorter version, 403 amino acids (Tan *et al.*, 1998) or; a longer version of 426 amino acids (Raddatz *et al.*, 2000). However, the shorter version has a stronger Kozak sequence suggesting that this is likely to be the form expressed physiologically (Brighton *et al.*, 2004b). Similarly, two NMU2 amino acid sequences have been suggested with either 412 amino acids (Hosoya *et al.*, 2000; Howard *et al.*, 2000) or 415 amino acids (Raddatz *et al.*, 2000; Shan *et al.*, 2000). Again, the shorter isoform has a stronger Kozak sequence (see review by Brighton et al. 2004b).

The amino acid sequence similarity between NMU1 and NMU2 is mainly confined to the transmembrane domain, while variations occur at the third intracellular (i3) loop where NMU2 is shorter than NMU1. Additionally, the NMU2 *C*-terminus consists of 88 amino acids which is longer than the 70 amino acid *C*-terminus of NMU1. Both NMUs also have putative phosphorylation sites within their intracellular domains potentially for protein kinase A, protein kinase C and casein kinases I and II. Phosphorylation sites targeted by G protein-coupled receptor kinases (GRKs) usually found within the intracellular regions of many GPCRs remain to be defined (Brighton *et al.*, 2004b). The *C*-terminus of NMU2 contains a specific sequence, (-YQSF) that is considered a tyrosine motif (Y-X-X-Ø, where Y denotes Tyr, X is any amino acid, and Ø is a bulky hydrophobic residue) that binds directly to the clathrin-coated pit (CCP) µ2 subunit of the adaptor protein AP-2, facilitating CCP-mediated GPCR ligand-dependent and constitutive internalization (Marchese *et al.*, 2008).

a) NMU1

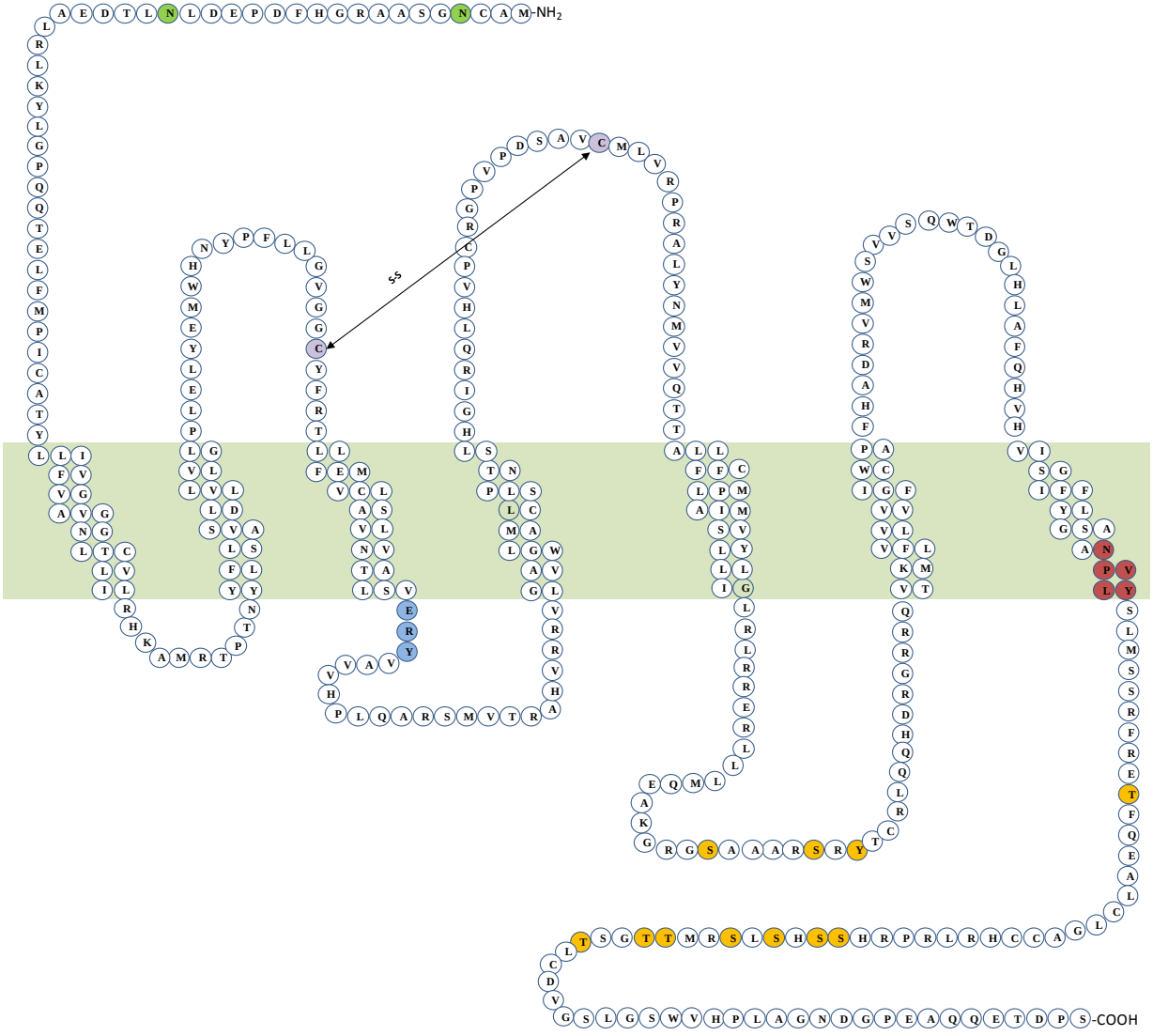

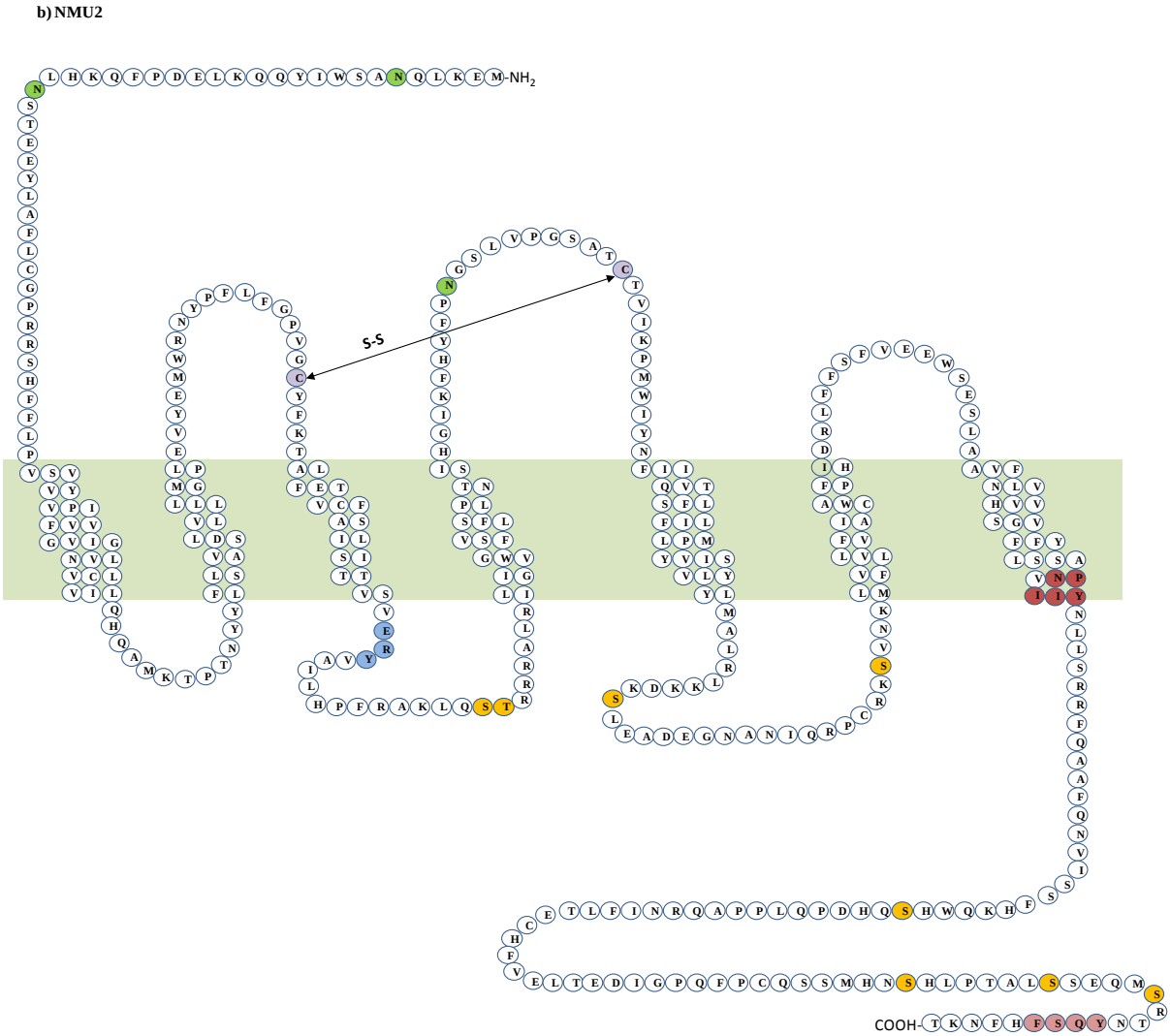

Figure 1.2 Schematic representations of the secondary structures of NMU1 and NMU2. The seven transmembrane α-helices of NMU1 (a, GenBank: EAW70966.1) and NMU2 (b, GenBank: AAF82755.1) were predicted by HMMTOP software, V 2.0 (Tusnady *et al.*, 2001). Structural characteristics of both receptors are indicated including the conserved cysteine residues (purple) for disulfide bond formation between the first and second extracellular loop, E/DRY motif (blue) and serine/threonine phosphorylation sites (orange), NPXXY motif (red) and N-glycosylation residues (green). The conserved Tyr motif in NMU2 (-YQSF) also indicated in pink and suggested to play a role in CPP-mediated internalization (Marchese *et al.*, 2008).

1.3.2 Distribution of NMUs

Since the discovery of NMUs, many studies have been performed to distinguish their tissue distribution and physiological roles, especially in rat and human. NMUs exhibit distinct distributions, where NMU1 shows predominant, but not exclusive expression in the periphery and the expression of NMU2 is primarily in the CNS (Fujii *et al.*, 2000; Gartlon *et al.*, 2004; Guan *et al.*, 2001; Hosoya *et al.*, 2000; Howard *et al.*, 2000; Raddatz *et al.*, 2000; Shan *et al.*, 2000; Szekeres *et al.*, 2000). This highlights the potential importance of each receptor subtype in a set of pathophysiological roles **(Section 1.3)**.

1.3.2.1 Tissue distribution of NMU1

1.3.2.1.1 Peripheral distribution

In rat peripheral tissues, highest levels of NMU1 mRNA are found in the duodenum, jejunum, ileum, lung and spleen while moderate levels are detected in femur, caecum, colon and rectum (Fujii *et al.*, 2000; Gartlon *et al.*, 2004; Hsu *et al.*, 2007). Low levels of NMU1 message are present in thyroid, thymus, adipose, trachea, pancreas, kidney, stomach, mammary gland and uterus while these studies could not detect NMU1 mRNA in the adrenals and testis (Fujii *et al.*, 2000; Hsu *et al.*, 2007). In contrast to the previous reports, it has been recently shown that both NMU1 transcripts and protein are found in the medullary and cortical area of adrenal gland (Rucinski *et al.*, 2007; Trejter *et al.*, 2008; Ziolkowska *et al.*, 2008). Lastly, in isolated rat pancreatic islets, a study using RT-PCR and Western blotting demonstrated the presence of NMU1 mRNA and protein respectively (Kaczmarek *et al.*, 2006).

In human, quantitative RT-PCR, Northern blot and dot blot analyses suggest a wide distribution of NMU1 mRNA in the periphery, with significant levels in adipose tissue, duodenum, jejunum, small intestine, adrenal cortex, bone marrow and testis. Moderate amounts of NMU1 mRNA are found in spleen, stomach, lung, trachea, mammary gland, kidney, pancreas, prostate, uterus, heart and placenta (Gartlon *et al.*, 2004; Hedrick *et al.*, 2000; Howard *et al.*, 2000; Raddatz *et al.*, 2000; Szekeres *et al.*, 2000). Transcripts of NMU1 are also observed in considerable levels in human ileum smooth muscle, caecum, gallbladder, long saphenous vein and all colon segments (Jones *et al.*, 2006). The

expression is variable in colon; for example, the highest levels are in the upper segments (i.e. ascending and transverse) while the lower segments (descending and sigmoid) have lower levels of NMU1 transcripts. Investigation of hNmU-25 and NMUs expression in the cardiovascular system shows that NMU1 mRNA is mainly in the left ventricle, coronary artery and saphenous vein (Mitchell *et al.*, 2009). This study also has supported the existence of NMU1 protein in the left ventricle. Furthermore, [^{125}I]-hNmU-25 binds with high affinity to a wide range of cardiovascular tissues, especially the left ventricle and coronary artery and NMU1-LI is present in intra-myocardial, coronary artery and saphenous vein vascular smooth muscle (Mitchell *et al.*, 2009). In goldfish, NMU1 mRNA is only detected in the ovary (Maruyama *et al.*, 2011).

Several studies have reported the existence of NMU1 in specific cell types such as the mouse Th2 cell clone (Johnson *et al.*, 2004), mouse primary mast cells (Moriyama *et al.*, 2005), human blood eosinophils (Moriyama *et al.*, 2006b), human primary acute myeloid leukemia (AML) cells and human leukemic K562 cell-line (Shetzline *et al.*, 2004), human smooth muscle and endothelial cells of cardiovascular tissues (Mitchell *et al.*, 2009). NMU1 message has been also reported in human immune cells such as natural killer (NK cells), leukocytes (Hedrick *et al.*, 2000), human goblet cells of the ileum (Howard *et al.*, 2000), human lymphocytes (Szekeres *et al.*, 2000) and human hematopoietic CD34(+) cells (Gambone *et al.*, 2011). NMU1 mRNA has also been detected in several human pancreatic cancer cell-lines such as Panc1, colo357, BxPC3, AsPC1, Capan1, MiaPaca2, SU.86.86 and T3M4 but at levels lower than NMU2 (Ketterer *et al.*, 2009).

1.3.2.1.2 Central distribution

Expression of NMU1 mRNA has been demonstrated only at low levels in the amygdala (Gartlon *et al.*, 2004), cerebellum, cortex, hippocampus, hypothalamus, medulla oblongata, striatum, thalamus, spinal cord and in small-medium diameter neurons of dorsal root ganglia but was not found in pituitary (Fujii *et al.*, 2000; Yu *et al.*, 2003). Although in mouse, no NMU1 mRNA could be detected in the CNS (Funes *et al.*, 2002), a recent study has demonstrated the expression of NMU1 mRNA, protein and NMU1-LI

in small neurons of the dorsal root ganglia (Wang *et al.*, 2011) and in hippocampal neurons (Zhang *et al.*, 2010).

In human, although NMU1 message has been below detection level centrally in some studies (Gartlon *et al.*, 2004; Hedrick *et al.*, 2000; Howard *et al.*, 2000), NMU1 mRNA has been reported in cerebellum, amygdala, cortex, hippocampus, hypothalamus, medulla oblongata, thalamus and spinal cord, dorsal root ganglion and pituitary gland (Raddatz *et al.*, 2000; Szekeres *et al.*, 2000). However, it is noteworthy here that the levels of NMU1 mRNA detected in the CNS are 5-25 fold lower than expression levels in the periphery (Brighton *et al.*, 2004b). In *Caenorhabditis elegans* (*C. elegans*), a homologue of mammalian NMU1 has been reported in the sensory neurons, interneurons and somatic gonad (Maier *et al.*, 2010). In goldfish, NMU1 mRNA levels are high in the brain and pituitary (Maruyama *et al.*, 2011).

1.3.2.2 Tissue distribution of NMU2

1.3.2.2.1 Peripheral distribution

A growing number of studies have revealed the existence of NMU2 at both mRNA and protein level in a range of peripheral tissues. In rat, the highest level of NMU2 mRNA expression is in the uterus (Fujii *et al.*, 2000; Hosoya *et al.*, 2000) and high-moderate levels are in the ovary (Fujii *et al.*, 2000; Gartlon *et al.*, 2004; Hosoya *et al.*, 2000). Low levels of NMU2 mRNA have been detected in several rat peripheral tissues including thymus, adipose, salivary gland, lung, small intestine, large intestine, stomach, bladder, testis and costal cartilage (Fujii *et al.*, 2000; Hosoya *et al.*, 2000). In comparison to the growing evidence of NMU1 in adrenal gland, several investigations have confirmed the absence of NMU2 mRNA or protein (Fujii *et al.*, 2000; Hsu *et al.*, 2007; Rucinski *et al.*, 2007; Trejter *et al.*, 2008; Ziolkowska *et al.*, 2008). Further, in contrast to the high expression level of NMU2 mRNA in rat uterus, NMU2 mRNA in human and dog, respectively are mostly absent in the uterus, which suggests species-dependent distribution of NMU2 (Raddatz *et al.*, 2000; Shan *et al.*, 2000; Westfall *et al.*, 2002). Alternatively, this difference may be due to the effect of oestrogen on the expression of NMU2 since oestrogen enhances NMU expression in rat (Nandha *et al.*, 1999). In pig,

NMU2 mRNA is present in a wide variety of tissues such as ovary, jejunum, heart, lung, liver, spleen, adrenal gland, kidney, uterus, colon and thymus and low NMU2 message is found in duodenum and thyroid gland (Yang *et al.*, 2010). In goldfish peripheral tissues, NMU2 message is detected in the ovary (higher than NMU1 mRNA), testis, kidney and gut (Maruyama *et al.*, 2011).

In human, as with NMU1, testis show the highest levels of NMU2 message expression (comparable to levels seen in CNS), while moderate levels are observed in lung (Raddatz *et al.*, 2000; Shan *et al.*, 2000). Low levels of NMU2 transcripts have also been reported in heart, trachea, small intestine, kidney, stomach, mammary gland, prostate and thyroid (Raddatz *et al.*, 2000; Shan *et al.*, 2000). The existence of NMU2 transcripts in gallbladder, ileum, caecum, long saphenous vein and all segments of colon have been demonstrated but at levels lower than those for NMU1 mRNA (Jones *et al.*, 2006).

At the cellular level, freshly isolated rat calvarial osteoblast-like (ROB) cells showed low expression of NMU2 mRNA but this increased significantly on culture (Rucinski *et al.*, 2008). In contrast, the expression of message for NmU showed the opposite (Rucinski *et al.*, 2008). It has been recently reported that NMU2 mRNA presents at much higher level than NMU1 mRNA in human pancreatic cancer cell-lines such as SU.86.86, AsPC1 and Capan1 (Ketterer *et al.*, 2009).

1.3.2.2.2 Central distribution

The predominantly central expression of NMU2 and its distribution is consistent with the distribution of its ligands, NmU and NmS**,** suggesting the important physiological roles of NmU and NmS. Using *in situ* hybridization, rat hypothalamus has demonstrated the highest NMU2 mRNA level, mainly in the wall of the third ventricle with moderate levels in the paraventricular nucleus (PVN) and cornu ammonis area 1 (CA1) region of the hippocampus (Guan *et al.*, 2001; Howard *et al.*, 2000). The medulla oblongata, spinal cord, hippocampus (Fujii *et al.*, 2000; Hosoya *et al.*, 2000) and striatum (Gartlon *et al.*, 2004) show moderate-low levels of NMU2 mRNA. The high expression of NMU2 in specific regions of rat brain is also supported by a binding study where [^{125}I]rNmU-23

showed high binding in the limbic system including the hypothalamus, amygadala and hippocampus (Mangold *et al.*, 2008). Low levels of NMU2 transcripts are also present in the cerebellum, cortex and thalamus (Fujii *et al.*, 2000; Gartlon *et al.*, 2004; Hosoya *et al.*, 2000). In mouse, high amounts of NMU2 message are in the hypothalamus, spinal cord, medulla and pons (Funes *et al.*, 2002). In pig, it has been recently shown that NMU2 mRNA is expressed in spinal cord, medulla oblongata, pons, pituitary and hypothalamus (Yan, 2010). In goldfish NMU2 mRNA is detected in brain and pituitary (Maruyama *et al.*, 2011).

In human, quantitative RT-PCR, Northen blot, dot blot and *in situ* hybridization studies have suggested the existence of significant amounts of NMU2 mRNA in spinal cord, hippocampus, medulla oblongata, pituitary, pontine reticular formation and thalamus while the hypothalamus and cortex show moderate expression (Howard *et al.*, 2000; Raddatz *et al.*, 2000; Shan *et al.*, 2000). These studies have been also reported low NMU2 mRNA levels in amygdala, cerebellum and dorsal root ganglia.

1.4 Pathophysiological roles of NmU

Following the discovery of NmU due to its ability to contract smooth muscle of rat uterus, NmU and NmS have been found to be involved in a broad spectrum of physiological and pathological activities in both the CNS and periphery.

1.4.1 Contractile effects on smooth muscle

The ability of porcine NmU analogues to contract rat uterus smooth muscle was the first physiological role identified for NmU (Minamino *et al.*, 1985a). NmU is also able to contract many other types of smooth muscle (Dass *et al.*, 2007; Jones *et al.*, 2006; Mitchell *et al.*, 2009; Prendergast *et al.*, 2006; Westfall *et al.*, 2002). The contractile effect of NmU in a wide range of tissues such as human ileum, rat and mouse stomach is concentration-dependent and direct, since contraction is unaffected by atropine and tetrodotoxin (Benito-Orfila *et al.*, 1991; Dass *et al.*, 2007; Maggi *et al.*, 1990). Desensitization of the contractile response to NmU seems to be tissue-specific since the

contractile response to pNmU-8 in canine urinary bladder partially desensitized on addition of NmU even after a prolonged, 45 min wash (Westfall *et al.*, 2002). Additionally, the lack of repetitive contractile effect was observed on cumulative additions of gpNmU-9 (0.01-1 μM) in guinea pig uterus (Prendergast *et al.*, 2006). In contrast, the magnitude of responses to repetitive challenges with rNmU-23 (1μM) is unaffected in strips of rat colonic smooth muscle even when reducing washing times between stimulations to 1 min (Brighton *et al.*, 2008).

Several studies have investigated the involvement of either NMU1 or NMU2 in NmU-mediated contraction using receptor knockout animals. In mouse uterus and vas deferens, NmU-mediated contraction was similar in either wild-type or $NMU1^{-/-}$ knockout mice suggesting an NMU2-mediated contraction, while in mouse fundus and gall bladder the contraction was abolished in $NMU1^{-/-}$ implying NMU1 involvement (Prendergast *et al.*, 2006). Furthermore, potentiation of electrical field-stimulated contraction in wild-type or $NMU2^{-/-}$ mice distal colon by NmU was equal highlighting an NMU1-mediated contraction (Dass *et al.*, 2007). In man, mRNA analysis indicated expression of only NMU1 in coronary artery (Mitchell *et al.*, 2009), longitudinal smooth muscle of saphenous vein (Jones *et al.*, 2006; Mitchell *et al.*, 2009) and circular smooth muscle of ascending colon (Jones *et al.*, 2006) suggesting that NMU1 is responsible for contractile effect of NmU in these tissues. Together, the involvement of specific NMU subtypes in NmU-mediated contraction is likely to be tissue-dependent.

1.4.2 Effect on food intake, temperature and locomotor activity

The first evidence of the anorexigenic property of NmU was demonstrated by direct intracerebroventricular (ICV) injection of NmU in rat, which results in decreased food intake, body weight and causes a transient increase in body temperature and locomotor activity (Howard *et al.*, 2000). Further, the level of NmU mRNA was significantly lower in 24 h and 48 h fasted rats compared to those having free access to food (Howard *et al.*, 2000). Together with the distinct distribution of NmU and its receptors **(Section 1.2.2.2.2)** in brain regions involved in regulation of food intake such as the arcuate nucleus (ARC) and PVN of the hypothalamus, these data suggest a role for NmU in the regulation of

food intake (Graham *et al.*, 2003; Hanada *et al.*, 2003; Howard *et al.*, 2000; Ivanov *et al.*, 2002; Kojima *et al.*, 2000; Nakazato *et al.*, 2000; Niimi *et al.*, 2001; Wren *et al.*, 2002). The central anorexigenic role of NmU is supported by the observation that ICV administration of NmU antiserum (anti-NmU IgG) enhance dark-phase feeding and increased body weight in the rat (Jethwa *et al.*, 2005; Kojima *et al.*, 2000). It has also been reported that based on measurement of NmU mRNA, in obese rats and mice, hypothalamic NmU expression is lower than their lean counterparts (Howard *et al.*, 2000; Ivanov *et al.*, 2002).

Transgenic manipulations of NMUs expression in animal models have further helped to elucidate the effects of NmU on satiety and body fat composition. Mice genetically lacking the NmU gene ($NmU^{-/-}$) have confirmed the role of NmU in body weight control as these mice exhibit hyperphagia, adiposity, attenuation of locomotor activity, decreased oxygen consumption, reduced metabolism and hyperleptinemia, even with a highly restricted diet (Hanada *et al.*, 2004). ICV infusion of NmU in this model significantly decreases fat mass (Sato *et al.*, 2007). Additionally, over-expression of NmU in mice resulted in lean, hypophagic mice compared to wild-type mice (Kowalski *et al.*, 2005). The immunoreactivity of C-Fos, a marker of cell activation, was detected in many brain regions and nuclei upon ICV administration of NmU, including the supraoptic nucleus, dorsomedial and lateral hypothalamic areas, nucleus tractus solitaries, amygdala, ventrolateral medulla, ARC and PVN (Ivanov *et al.*, 2002; Ozaki *et al.*, 2002). The PVN and ARC are considered important for NmU-mediated central energy homeostasis since microinjection of NmU in these areas in the rat resulted in satiety, increased locomotor activity and temperature (Novak *et al.*, 2006; Wren *et al.*, 2002).

The exact mechanism(s) by which NmU produce such effects on feeding and satiety is thought to involve a neuronal network with other appetite-regulating peptides (Hanada *et al.*, 2004). In $NmU^{-/-}$ knockout mice, quantitative *in-situ* hybridization suggested down-regulation of the appetite inhibitor peptides, corticotropic-releasing hormone (CRH, (Morley *et al.*, 1982)) in PVN and pro-opiomelanocortin (Pomc) in the ARC, while ICV administration of NmU up-regulated CRH mRNA in PVN but not Pomc mRNA in ARC. This suggests CRH involvement in NmU action rather than Pomc (Hanada *et al.*, 2004). The satiety hormone leptin (Campfield *et al.*, 1995) has also been suggested to regulate

NmU action, since ICV injection with anti-NmU IgG prior to intraperitoneal administration of leptin partially blocked the satiety effect of leptin. Thus, leptin may exert at least some of its effects on food intake through the NmU pathway (Jethwa *et al.*, 2005; Jethwa *et al.*, 2006). However, another study found that anti-NmU IgG did not block leptin-mediated effects on satiety (Nakahara *et al.*, 2010). Interestingly, leptin enhanced the production of NmU *ex-vivo* in rat hypothalamic extracts (Wren *et al.*, 2002) but did not induce expression of NmU mRNA in the ARC (Hanada *et al.*, 2004). Systemic administration of leptin to wild-type or $NmU^{-/-}$ mice decreased body weight and food intake suggesting an independent role of leptin (Hanada *et al.*, 2004). Further, ICV administration of NmU in transgenic mice expressing mutant leptin (*ob/ob*), mutant leptin receptors (*db/db*) or rats lacking leptin receptors (Zucker fatty rats *fa/fa*) resulted in a satiety effect similar to that seen in control animals, suggesting leptin-independent satiety effects of NmU (Hanada *et al.*, 2004).

NmS also share similar physiological role. In man, the chromosomal location of the NmS gene is in agreement with polygenic traits proposed in obesity (Mori *et al.*, 2005). In rat hypothalamus, NmS is expressed more highly than NmU (Rucinski *et al.*, 2007). The anorexigenic effect of NmS is more potent and longer than that of NmU (Ida *et al.*, 2005). NmS also induces the expression of both CRH mRNA and Pomc mRNA in PVN and ARC respectively, while pre-treatment with either CRH or an α-melanocyte-stimulating hormone (α-MSH) antagonist inhibited the anorexigenic effect of NmS (Ida *et al.*, 2005; Miyazato *et al.*, 2008). Further, rNmS-36 did not have any antagonistic effects in Japanese quail as observed with rNmU-23 where it showed anorexigenic effects and an increase in both temperature and locomotor activity (rNmU-23 antagonize satiety effect of JqNmU-25 in Japanese quail) (Shousha *et al.*, 2005; Shousha *et al.*, 2006). The difference between NmS and NmU in terms of potentiating CRH and Pomc are controversial since another group demonstrated no significant difference in the increase of expression of both CRH and Pomc mRNA by either NmS or NmU (Nakahara *et al.*, 2010). Further, this latter study showed that anti-NmS IgG, but not anti-NmU IgG blocks leptin-mediated anorexigenic effects.

Several lines of evidence suggest that both neuromedin peptides produce central effect on energy homeostasis via NMU2 but not NMU1. Thus, there is a preferential

central distribution of NMU2 mRNA in the CNS especially in the hypothalamic regions (see **Section 1.2.2.2.2**) including the PVN in both rat and mouse (Graham *et al.*, 2003; Guan *et al.*, 2001; Howard *et al.*, 2000; Mangold *et al.*, 2008). Transgenic mice lacking NMU2 ($NMU2^{-/-}$) did not show a significant difference from the wild-type animals in food intake, body weight or locomotor activity (Bechtold *et al.*, 2009; Peier *et al.*, 2009; Zeng *et al.*, 2006). Further, knocking-out NMU2 in mouse abolished the locomotor and satiety effects of ICV administration of either NmU or NmS (Bechtold *et al.*, 2009; Zeng *et al.*, 2006). Oral administration of a selective, natural NMU2 agonist, EUK2010, inhibited both food intake and body weight in rat and mice and up-regulated leptin in white fat of mouse (Fang *et al.*, 2006). Interestingly, a recent study using transgenic $NMU2^{-/-}$ mice showed that female but not male $NMU2^{-/-}$ mice subjected to diet-induced obesity (diet of > 60% fat for 9 weeks) increased body weight (especially body fat) by approximately 29%, suggesting that the satiety effect of NmU is via NMU2 in female but not male mice (Egecioglu *et al.*, 2009). On the other hand, $NMU2^{-/-}$ mice show small but significant loss of body weight upon ICV administration of NmU or NmS suggesting NMU1 involvement or another receptor yet to be characterized (Peier *et al.*, 2009). Furthermore, recent evidence of NMU1 involvement in inhibition of food intake and body weight following peripheral administration has been demonstrated (Peier *et al.*, 2011). In this study, acute and chronic peripheral administration of NmU in wild-type mice resulted in significant suppression of food intake (85% at the first 2 h) and body weight, whilst this effect was totally absent in $NMU1^{-/-}$ mice (Peier *et al.*, 2011). These studies suggest that NmU produces its anorexigenic effect when administered centrally via NMU2 while peripheral administration evokes NmU-mediated satiety through NMU1.

1.4.3 The stress response and the hypothalamic-pituitary-adrenal axis

The stress response is regulated through a neuro-endocrine network involving the hypothalamic PVN, anterior pituitary and adrenal gland and is known as hypothalamic-pituitary (HPA) axis. Environmental or biochemical stress act as stimuli to induce synthesis of the major component of the stress-circuit, CRH in the PVN. The release of CRH from the PVN potentiates production of adrenocorticotropic hormone (ACTH) from

corticotrophs of the interior pituitary gland and this subsequently enhances the release of corticosteroids and other stress-related mediators (e.g. adrenaline) from the adrenal gland (for detailed review, (Bonfiglio *et al.*, 2011)). Thus, the hypothalamic PVN is considered as the central origin of the stress response. In addition to the distinct central distribution of NmU and NMU2 within the main stress circuit, the hypothalamic-pituitary-adrenal axis, several studies in rat and mouse have demonstrated a stimulatory effect of NmU on stress-related behavioural (e.g. grooming, locomotor activity, face washing) and biochemical (e.g. stress-related neurotransmitters and hormones) changes via both central and peripheral actions. The potential involvement of NmU in such changes has been demonstrated, for example, by ICV administration of NmU in either rat or mouse (Gartlon *et al.*, 2004; Hanada *et al.*, 2001; Kojima *et al.*, 2000; Ozaki *et al.*, 2002; Wren *et al.*, 2002). In addition to increased levels of CRH mRNA in the PVN upon ICV administration of NmU in mouse (Hanada *et al.*, 2004), the intra-PVN injection of NmU in rat elevated the levels of circulating hormones related to stress including corticosterones and ACTH (Thompson *et al.*, 2004; Wren *et al.*, 2002), thereby highlighting the critical role of the PVN. NmU-mediated stress responses were blocked by pre-treatment with anti-CRH IgG and CRH receptor antagonists in rat and mouse and were also absent in $CRH^{-/-}$ knockout mice (Hanada *et al.*, 2001). Furthermore, ICV but not peripheral administration of NmU at high dose in rat increased plasma levels of adrenaline (Sasaki *et al.*, 2008) and noradrenaline (Chu *et al.*, 2002). Taken together, these data highlight the central stimulatory role of NmU on the stress responses and its mediators.

Peripherally, the subcutaneous administration of NmU in rat elevated ACTH transiently and resulted in a prolonged increase of corticosteroids in the plasma (Malendowicz *et al.*, 1993). Further, NmU increased secretion of corticosterone from rat adrenal slices containing chromaffin cells. Removal of the medullary chromaffin cells abolished the secretory effect of NmU (Malendowicz *et al.*, 1994) indicating the specific action on the medullary area of the adrenal. The effect of NmS appears to be similar to NmU since central administration of NmS evoked a direct stimulatory effect on the HPA axis in rat via a CRH-dependent pathway (Jaszberenyi *et al.*, 2007).

NmU and NmS are likely to evoke stress-related responses through central NMU2 since distribution studies show NmU-LI and the predominant expression of NMU2 mRNA in the hypothalamus, mainly in the PVN where CRH is produced in response to stress. Recent studies in rat have shown the exclusive expression of NMU1 mRNA and protein in the medullary and cortical regions of the adrenal gland suggesting an involvement of NMU1 in the peripheral actions of NmU in the stress response (Rucinski *et al.*, 2007; Trejter *et al.*, 2008; Ziolkowska *et al.*, 2008).

1.4.4 Regulation of reproductive system hormones

Several studies investigated the regulatory effect of NmU on reproductive system hormones and also the effect of these hormones on the expression of NmU and its receptors. For example, the oestrogen derivative, E2, restores NMU expression in rat uterus after down-regulation following ovariectomy, which may suggest a regulatory effect of hormones on the NmU system during the oestrus cycle (Nandha *et al.*, 1999). Further, the reduction in hypothalamic NmU mRNA in ovariectomized rats is prevented by treatment with progesterone-E2 (Vigo *et al.*, 2007a). In female rats, hypothalamic NmU mRNA is at low levels in neonates but gradually increases to maximum levels during puberty. Further, expression levels varies during the oestrus cycle, providing further evidence of the regulatory effect of ovarian sex hormones on the expression of NmU and its receptors (Vigo *et al.*, 2007a).

1.4.5 Effects on the cardiovascular system

An early study showed a rapid and sustained increase in systemic blood pressure and heart rate in response to intravenous (IV) administration of NmU in anaesthetized rats (Minamino *et al.*, 1985a). Similarly ICV administration of NmU to conscious rats caused a similar effect, with an increase in heart rate. Notably, an increase in plasma noradrenaline was only observed at higher doses (Chu *et al.*, 2002). In contrast, IV injection of NmU to either conscious rats (Chu *et al.*, 2002) or anaesthetized dogs (Sumi *et al.*, 1987; Westfall *et al.*, 2002) showed a smaller and transitory elevation in arterial

blood pressure. These findings suggest an indirect, sympathetic effect of NmU on blood pressure following central administration. A more recent study demonstrated the involvement of the autonomic system in regulating NmU-mediated elevation of blood pressure and heart rate in the rat (Tanida *et al.*, 2009). In this study, ICV NmU increased blood pressure, heart rate and renal sympathetic nerve activity in anaesthetized rats. In addition, that study also demonstrated activation of brown adipose tissue sympathetic nerve activity, elevated brown adipose tissue temperature and inhibited gastric vagal nerve activity in conscious rats. Hypotensive effects on rat systemic blood pressure and a decrease in heart rate have been observed following microinjection of NmU in the nucleus tractus solitarius (NTS) (Tsubota *et al.*, 2003). This NmU-mediated hypotensive effect in the NTS might be via activation of the α_{2A} adrenoceptor which has a high expression in NTS (Yao, 2009). Further support of this hypothesis was provided by the detection of NmU mRNA in the catecholaminergic neurons with a similar distribution to the α_2 adrenoceptor-expressing neurons (Ivanov *et al.*, 2004). However, it seems that NmU may modulate cardiovascular tone via different mechanisms depending on the rout of administration. Spinal administration of NmU (intrathecal, IT) at high dose in rat resulted in a biphasic, initial and transient hypertensive effect with excitation of the sympathetic system lasting for 6 min, which was then followed by prolonged, 30 min hypotension (Rahman *et al.*, 2011). All of these studies highlight the important role of the autonomic nervous system in the cardiovascular effects of NmU.

In human, an *ex-vivo* vasopressor effect of NmU has been shown in coronary artery and mammary artery with similar intrinsic activity and potency to angiotensin II (Mitchell *et al.*, 2009). NmS showed a constrictor response on saphenous vein but with lower efficacy than NmU. The vasoconstrictor effect of both peptides may be via by NMU1 since ICC study showed immunoreactivity to NMU1 and mRNA were detected alongside α-actin of the medial smooth muscles layer of the blood vessels within heart (Mitchell *et al.*, 2009).

The effect of NmU on regional blood flow has been demonstrated in conscious rats, where IV administration provoked a potent vasoconstriction of the superior mesenteric artery and reduced both renal and mesenteric blood flow (Gardiner *et al.*, 1990). A similar effect has also been demonstrated in anaesthetized dogs, where IV administration resulted

in a significant reduction in blood flow of the superior mesenteric artery and portal vein but caused increased blood flow in pancreatic tissue, thereby demonstrating local and regional control of blood flow (Sumi *et al.*, 1987).

1.4.6 Effect on gastric emptying, acid secretion and ion transport

It has been shown that enhancement of the initial gastric emptying is linked to obesity (Verdich *et al.*, 2000). In conscious rats, ICV administration of NmU resulted in a maximal inhibition of gastric acid secretion and gastric emptying (Mondal *et al.*, 2003). Further, investigation showed that these effects are mediated through the CRH pathway, since pre-administration of anti-CRH IgG totally abolished the NmU effect (Mondal *et al.*, 2003). Pre-treatment with indomethacin, to inhibit prostaglandin synthesis, or removal of parasympathatic innervation by vagotomy did not interfere with the inhibitory action of NmU. Interestingly, blocking central α_2 adrenoceptors with yohimbine abolished the inhibitory effect of NmU on gastric acid secretion, which may suggest sympathetic system involvement (Mondal *et al.*, 2003). Recently, NmS has also been shown to have an inhibitory effect on gastric emptying in mice following central administration (Atsuchi *et al.*, 2010).

1.4.7 Nociception

NmU has a distinct distribution in the dorsal horn but not ventral horn of the spinal cord suggesting a sensory role (Domin *et al.*, 1987). This is supported by the expression of NMU2 mRNA in lamina I and lamina II in the dorsal horn (Yu *et al.*, 2003), which are responsible for nociception. Intrathecal administration of different NmU analogues in rat lowered the threshold to both thermal and mechanical stimuli (Yu *et al.*, 2003). In mouse, intrathecal or systemic administration of NmU increased nociception sensitivity (Cao *et al.*, 2003). Further, in $NmU^{-/-}$ mice, nociception reflexes are reduced compared to wild-type, while formalin injection to wild-type mice significantly increased NmU mRNA expression in the spinal cord (but not in the hypothalamic area), which indicates the important role of NmU in spinal cord for mediating nociception (Nakahara *et al.*, 2004b).

Recent study has shown that satiety effect, excessive locomotor activity and the pro-nociceptive effect of ICV administration of NmU observed in wild-type mice have been lost in $NMU2^{-/-}$ knockout littermates implicating a pro-nociceptive effect of NmU via NMU2 (Zeng *et al.*, 2006). Additionally, a recent study using $NMU1^{-/-}$ and $NMU2^{-/-}$ knockout mice revealed that the $NMU2^{-/-}$ knockout mice have a lower thermal nociceptive response in a hot plate test (Torres *et al.*, 2007). This study also demonstrated impaired pain responses in the $NMU2^{-/-}$ knockout mice. $NMU1^{-/-}$ knockout mice show no differences in nociceptive responses in comparison with the wild-type mice, again highlighting the involvement of NMU2 (Torres *et al.*, 2007).

1.4.8 Bone formation and remodelling

An investigation into the effects of NmU on bone formation and remodelling has demonstrated inhibitory effects on these processes (Sato *et al.*, 2007). Thus, in comparison to wild-type mice, $NmU^{-/-}$ knockout littermates showed higher bone mass formation, which was greater in males. Continuous ICV infusion of NmU reversed the increase in bone mass in the $NmU^{-/-}$ knockout mice which implicates a vital role for NmU in reducing bone mass formation and hence the regulation of bone remodelling (Sato *et al.*, 2007).

1.4.9 Insulin secretion and glucose homeostasis

An early investigation reported the expression of NmU and NMU1 mRNA in rat pancreatic tissues (Fujii *et al.*, 2000). Subsequently NMU1 but not NMU2 mRNA and protein has been demonstrated in isolated rat pancreatic islets, where NmU inhibited insulin secretion (Kaczmarek *et al.*, 2006). Furthermore, NmU potently induced the secretion of the insulinostatic hormone, somatostatin, from δ-cells of rat pancreatic islets *ex-vivo* and pre-treatment with a somatostatin antagonist blocked NmU-mediated inhibition of insulin secretion (Kaczmarek *et al.*, 2009). These data suggest the inhibitory effect of NmU on insulin secretion is somatostatin-dependent. Recently, it has also been demonstrated that acute, subcutaneous injection of NmU in mice significantly improves

glucose tolerance via NMU1, since this effect was absent in $NMU1^{-/-}$ mice (Peier *et al.*, 2011). Moreover, following 4 h of acute administration of NmU, plasma GLP-1 increased by 2-fold in fasted mice compared to vehicle treated littermates and this effect was absent in $NMU1^{-/-}$ mice (Peier *et al.*, 2011).

1.4.10 Regulation of circadian rhythm

Messenger RNA for NmU and both of its receptors are expressed in the suprachiasmatic nucleus (SCN) of the hypothalamus, which serves as the biological clock control centre (Nakahara *et al.*, 2004a). In addition to the strong c-Fos-LI in SCN neurons following ICV injection of NmU, it caused a phase shift of circadian locomotor activity and stimulated the expression of other peptides such as period 1, which is a well-characterized key-regulator of circadian rhythm (Nakahara *et al.*, 2004a). Furthermore, $NmU^{-/-}$ mice require longer time for re-entrainment than wild-type littermates following light-dark cycle shift (Nakahara *et al.*, 2004b). Interestingly, the expression of NmU within the SCN and PVN is regulated by the light-dark cycle, where the maximum expression of NmU mRNA is detected during the light phase (Graham *et al.*, 2005). The recently discovered neuromedin neuropeptide, NmS shows higher expression than NmU in the SCN, which suggests an important role in the regulation of the circadian system (Mori *et al.*, 2005). As with NmU, NmS expression seems to be regulated during the light-dark cycle with highest expression during the light phase (Moriyama *et al.*, 2005). Both, NMU1 and NMU2 are expressed in SCN with higher expression for NMU2 (Moriyama *et al.*, 2005; Nakahara *et al.*, 2004a). These Studies strongly suggest that NMU2 is involved in regulation of the circadian rhythm by both peptides as NMU2 is predominantly expressed in the SCN.

1.4.11 Inflammatory and immunological roles

Detection of NmU mRNA in human monocytes, dendritic cells and B lymphocytes cells together with the high expression of NMU1 message in NK cells, T cells and monocytes was the first evidence to suggest the involvement of NmU in the immune

system (Hedrick *et al.*, 2000). Further evidence of the immuno-regulatory effects of NmU were found in mouse Th2 cells, which express NMU1 mRNA and in which NmU increases $[Ca^{2+}]_i$ and promotes the secretion of cytokines such as interleukin 4 (IL-4), IL-5, IL-6, IL-10 and IL-13 (Johnson *et al.*, 2004). Injection of complete Freund's adjuvant (CFA) into the paws of mice caused inflammatory responses such as oedema, mast cell degranulation and neutrophil infiltration in wild-type but not in $NmU^{-/-}$ mice or mast cell knockout counterparts (Moriyama *et al.*, 2005). Peritoneal mast cells show high expression of NMU1 mRNA suggesting that NmU mediates the inflammatory response through a direct action on mast cells via NMU1 (Moriyama *et al.*, 2005). This is supported by the observation that subcutaneous injection of NmU into the paws of wild-type mice induced an inflammatory response but did not promote such a response in mast cell deficient mice (Moriyama *et al.*, 2005). The number of airway eosinophils is reduced in $NmU^{-/-}$ mice in an allergen-induced model of asthma, which implicates a role for NmU in asthma (Moriyama *et al.*, 2006b). There is also high expression of NMU1 mRNA and NmU in peritoneal macrophages. $NmU^{-/-}$ mice are resistant to the lethal effect of lipopolysaccharide-induced septic shock (LPS, endotoxin produced by gram negative bacteria), which is mediated by production of IL-6 (Moriyama *et al.*, 2006a). However, recent data has questioned the involvement of NMU1 in NmU-mediated inflammation as $NMU1^{-/-}$ mice exhibited normal inflammatory symptoms in a CFA test (Abbondanzo *et al.*, 2009). This controversy supports the need for identification of receptor subtypes at the protein level since mRNA expression levels may not reflect precisely the expression level of the protein.

1.4.12 Cancer

Investigation of gene expression by determination of their mRNA levels in both normal oral epithelial cells and oral cancer cells demonstrated changes in >600 genes associated with cancer. Among these, NmU mRNA levels were significantly down-regulated in oral cancer cells (Alevizos *et al.*, 2001). In oesophageal squamous carcinoma cells (ESCC), the NmU gene is silenced due to hypermethylation (Yamashita *et al.*, 2002). Significant growth inhibition (43%) in ESCC was observed by the expression of

recombinant NmU in these cells (Yamashita *et al.*, 2002). further, there was a 5-fold inhibition of NmU mRNA levels in K562 cells (leukemic cancer cell-line) expressing dominant negative c-myb, a proto-oncogene that promotes leukemogenesis (Shetzline *et al.*, 2004). Treatment of these cells with NmU reversed suppression of growth induced by dominant negative c-Myb (Shetzline *et al.*, 2004). Real-time PCR analysis of NmU mRNA and c-Myb in primary acute myeloid leukaemia (AML), acute lymphocytic leukaemia (ALL) and normal hematopoietic cells showed c-Myb mRNA was significantly expressed in both AML and ALL, whereas NmU message was found only in AML which suggests the participation of NmU in specific types of cancer (Shetzline *et al.*, 2004). The latter study suggested expression of NMU1 in wild type K562 cells at the protein level and functional $[Ca^{2+}]_i$ measurement. Treatment of wild type K562 cells with short interfering RNA (siRNA) against NmU caused strong inhibition of growth. Another study suggested a possible link between NmU and cancer by searching 12652 genes in 11 different ovarian cancer cells using Affymetrix GeneChip technology (Euer *et al.*, 2005). Seven ovarian cancer cell-lines exhibited up-regulation of many genes, including the NmU gene (Euer *et al.*, 2005). Furthermore, a study in non-small lung cancer (NSCLC) implicated significant expression of NmU in most lung cancers. Transfection of NSCLC cells with siRNA against NmU inhibited both NmU expression and NSCLC cell growth, while over-expression of NmU induced growth and motility (Takahashi *et al.*, 2006). NmU expression was also inversely correlated with the Rho GDP dissociation inhibitor 2 (RhoGDI2), since knocking down the latter with siRNA promoted NmU expression in human bladder, non-metastatic cancer T24 cells (Wu *et al.*, 2007). Recently, RhoGDI2 was found to be one of the metastasis suppressor genes in urinary bladder and lung metastases (Harding *et al.*, 2007). Also, over-expression of NmU in T24 cells and in poorly metastatic human bladder cancer T24T cell-lines xenografted in nude mice enhanced tumour formation (Wu *et al.*, 2007). The over-expression of NmU and its receptors, mainly NMU2 has also been shown in pancreatic cancer tissues and cell-lines (Ketterer *et al.*, 2009). Recently, microarray studies in renal cancer cells endogenously expressing NMU1 show considerable up-regulation of NmU expression in renal cancer cells lacking Von Hippel-Lindau (VHL) tumour suppressor gene functionality (Harten *et al.*, 2011). All of the above studies supported the hypothesis of the involvement NmU and

both receptors in cancer but the exact pathophysiological role is not yet defined. Further investigation is needed to clarify if NmU involvement in cancer and its potential therapeutic value in targeting the NmU system.

1.5 GPCR Signalling

1.5.1 GPCR families and structure

Both neuropeptides, NmU and NmS mediate these physiological/pathological effects via either NMU1 or NMU2, which belong to family A of the GPCRs superfamily. For future consideration of NmU and NmS as potential therapeutic targets, it is essential to understand how these receptors are activated and how the signalling by NMU1 and NMU2 are regulated depending on the earlier extensive studies of other members of GPCRs.

The seven transmembrane-domain GPCR superfamily is one of the largest human gene families comprising of approximately 800 genes (Millar *et al.*, 2010). Around half of the marketed drugs act on GPCRs and many are considered as potential therapeutic targets by pharmaceutical companies (Millar *et al.*, 2010). GPCRs are polypeptides of 300-1200 amino acids, sharing seven transmembrane α-helices (7TM) and possessing an extracellular *N*-terminus and cytoplasmic *C*-terminus. A variety of molecules, including hormones, neurotransmitters, peptides and bioactive lipids, bind specifically to one or a small number of GPCRs (Millar *et al.*, 2010). Furthermore, GPCRs are responsible for sensory perception, including vision, taste and olfaction (Pierce *et al.*, 2002).

In mammals, GPCRs are most straightforwardly classified into 3 main sub-families, A, B and C with approximately 25% amino acid homology between sub-families (Pierce *et al.*, 2002). Family A (Figure 1.3A), the largest family (673 out of 800 identified members), includes opsin receptors, olfactory receptors and adrenoceptors (Millar *et al.*, 2010). The retinal rod photoreceptor, rhodopsin was the first receptor for which a crystal structure was documented (Palczewski *et al.*, 2000). More recently the β_2 (Cherezov *et al.*, 2007) and β_1 (Warne *et al.*, 2008) adrenoceptors have also been crystallized and have allowed an appraisal of amino acid homologies, protein folding and activation mechanism

for this sub-family. On the extracellular surface, in addition to conserved cysteine residues which form a disulphide bridge, there are conserved glycosylation sites (Asn-X-Ser/Thr) within the extracellular *N*-terminus and, in some cases, the extracellular loops, which may be important in the maintenance of structural stability (Savarese *et al.*, 1992; Strader *et al.*, 1994). Furthermore, the highly conserved E/DRY motif between the boundary of the third transmembrane domain and the 2nd intracellular loop plays a key role in receptor conformation and G protein coupling following agonist binding (Rovati *et al.*, 2007; Strader *et al.*, 1994). The amino acid sequences and the predicted secondary structures (Figure 1.2) of NMU1 and NMU2 fulfil the criteria for sub-classification as family A GPCRs.

Family B (Figure 1.3B) is a much smaller (15 member) than family A with a distinct long extracellular *N*-terminus (Millar *et al.*, 2010). Most of the gastrointestinal peptides (secretin, vasoactive peptide (VIP)) corticotropin-releasing hormone (CRH) and other long peptides have receptors in family B (Pierce *et al.*, 2002). Family C (Figure 1.3C) also comprises a small number (22) of members including the $GABA_B$, metabotropic glutamate and Ca^{2+}-sensing receptors (Millar *et al.*, 2010; Pierce *et al.*, 2002). This family have a distinct "venus flytrap" module (VFM) within the large *N*-terminal domain, which is the ligand binding site (Brauner-Osborne *et al.*, 2007).

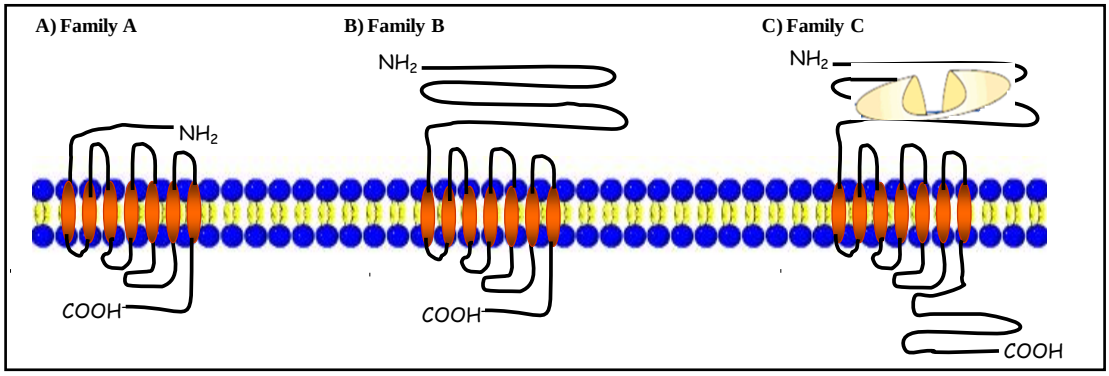

Figure 1.3 Schematic diagram representing the different GPCR families.

1.5.2 Initiation and termination of signalling by GPCRs

GPCRs are so named due to their interaction with heterotrimeric guanine nucleotide-binding proteins (abbreviated to G proteins). The heterotrimeric G proteins acts as transducers of the signal generated by the ligand-receptor complex and activate or inhibit specific signalling pathways through direct interaction with intracellular effector proteins. G proteins belong to the highly conserved GTPase superfamily and consist of three polypeptides organized into two functional units; the α-subunit and the βγ dimer. Gα and Gβγ-subunits are post-translationally lipidated and are therefore primarily localized at the surface of the inner leaflet of the plasma membrane. The α-subunit contains a binding site for a guanine nucleotide (GDP during the inactive state and GTP when activated); this domain possesses GTPase activity which facilitates GTP hydrolysis and G protein deactivation (Cabrera-Vera *et al.*, 2003). In the resting state, the G-protein exists as a heterotrimeric complex with GDP bound to the α-subunit (Figure 1.4A). Binding of ligand to receptor results in a conformational change of the receptor or alternatively binding occur to stabilize existed active conformation (Cabrera-Vera *et al.*, 2003) leading to association with Gαβγ heterodimer (Figure 1.4B). The transient agonist-receptor-G protein complex (ternary complex) facilitates activation of the G proteins through the exchange of GDP for GTP on the α-subunit (Figure 1.4C). Thus, the receptor-ligand complex acts as a guanine-nucleotide exchange factor (GEF) for the G protein heterotrimer. GTP-for-GDP exchange leads to release of α-GTP from the βγ dimer and subsequent interaction of the Gα and/or Gβγ subunits with effectors (Figure 1.4D) (Cabrera-Vera *et al.*, 2003).

Termination of effector activation or inhibition is brought about through the hydrolysis of GTP by the GTPase activity of the α-subunit. Following hydrolysis, the Gα-GDP rapidly re-associates with the Gβγ complex to re-form the inactive G protein heterotrimer. The intrinsic GTPase activity of the Gα-subunit can be facilitated by GTPase-activating proteins (GAP), particularly by members of the regulator of G protein signalling (RGS) protein family (Pierce *et al.*, 2002).

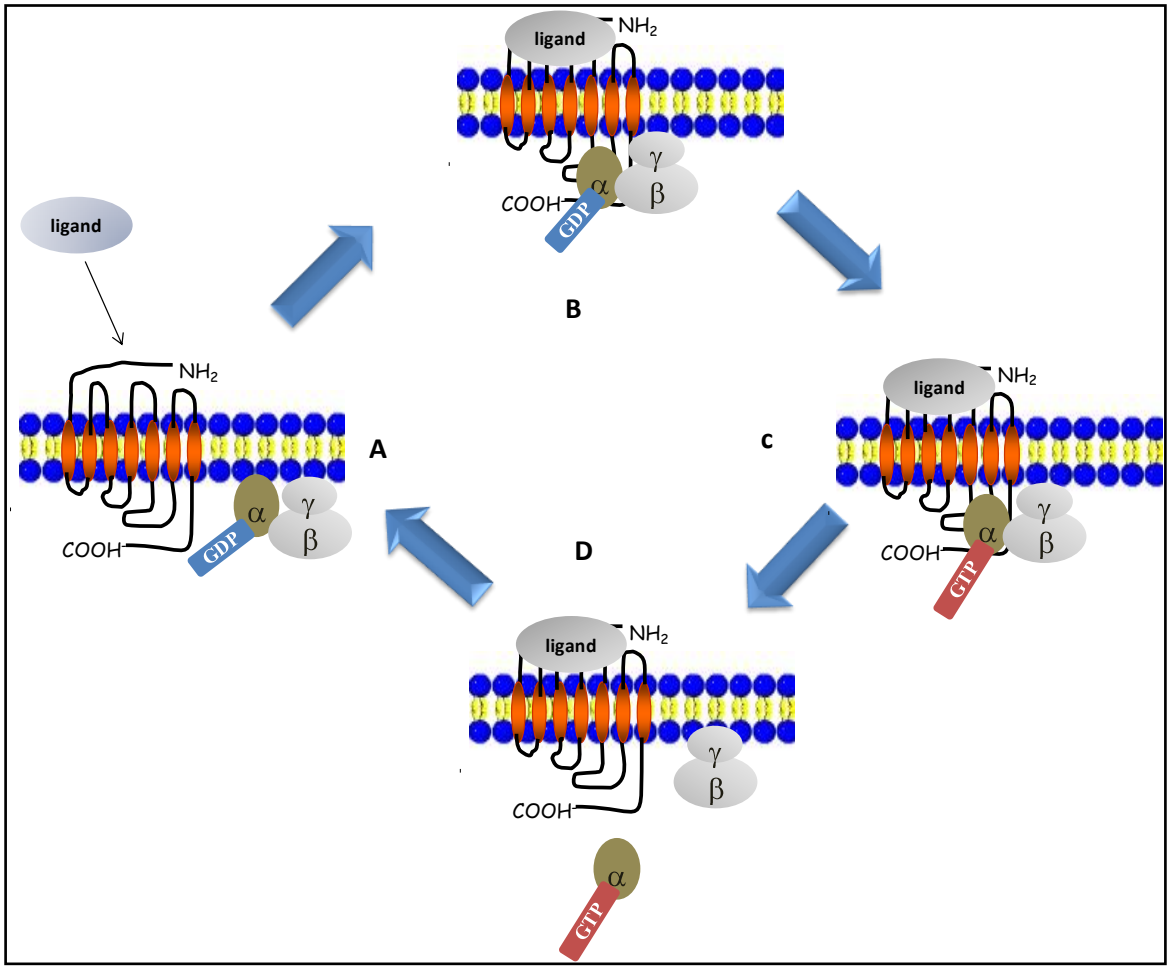

Figure 1.4. Activation-inactivation cycle of GPCRs. Schematic diagram of a GPCR in the resting state (A). Binding of ligand to the receptor promotes association of the membrane-anchored heterotrimeric G protein with the intracellular domains of the receptor (B). Formation of a ligand-receptor-G protein complex leads to the exchange of GDP for GTP on the Gα subunit (C). This results in dissociation of the Gα-GTP from the Gβγ subunit and activation/inhibition of the downstream effectors (D). Hydrolysis of the GTP to GDP by Gα subunit GTPase activity results in the rapid re-association of G protein subunits.

Heterotrimeric G proteins can also be classified according to their Gα-subunit into four main groups, $G\alpha_s$, $G\alpha_{i/o}$, $G\alpha_{q/11}$, and $G\alpha_{12/13}$. GPCRs often bind selectively to specific Gα protein family members, although more promiscuous coupling can also sometimes be seen (Hermans, 2003). It has been shown that activation of both NMU1 and NMU2 result in dual coupling to $G\alpha_{q/11}$ and $G\alpha_{i/o}$ proteins (Aiyar *et al.*, 2004; Brighton *et al.*, 2004a; Brighton *et al.*, 2008; Hosoya *et al.*, 2000).

Activation of $G\alpha_s$ (Figure 1.5) results in the activation of adenylyl cyclase (AC) triggering the synthesis of the second messenger adenosine cyclic-3',5'-monophosphate (cAMP) from ATP. The increase in intracellular cAMP activates cAMP-dependent protein kinase (PKA), which triggers many physiological events by phosphorylation of specific cellular proteins. For example, PKA-dependent phosphorylation of myosin-light chain kinase can lead to relaxation of smooth muscle. cAMP production can also be stimulated by Gβγ-subunits which increase AC activity by some, but not all isoenzymes(Clapham *et al.*, 1997). Coupling to $G\alpha_{i/o}$ (Figure 1.5) inhibits AC activity resulting in a reduction in intracellular cAMP concentration. $G\alpha_{i/o}$ protein activation can also regulate a variety of ion channels, including G protein-regulated, inwardly-rectifying K^+ channels, which is generally mediated by the Gβγ-subunits of $G\alpha_{i/o}$ and hence is PTX-sensitive (Pierce *et al.*, 2002). Members of the $G\alpha_{q/11}$ protein sub-family stimulate phosphoinositide turnover (Figure 1.5) through activation of phospholipase Cβ (PLCβ) and the hydrolysis of phosphatidylinositol-4,5-bisphosphate (PIP_2) to diacylglycerol (DAG) and inositol 1,4,5-trisphoshate (IP_3). IP_3 induces Ca^{2+} release into the cytoplasm by binding to IP_3 receptors on the endoplasmic reticulum, while DAG activates conventional and novel isoenzymes of protein kinase C (PKC) (Cordeaux *et al.*, 2002). GPCR activation of $G\alpha_{12/13}$ proteins can recruit guanine nucleotide-exchange factors for monomeric GTPases (e.g. $p115^{RhoGEF}$) facilitating GTP-for-GDP exchange (Kozasa *et al.*, 1998). In this way GPCRs can also regulate monomeric GTPases, such as Rho, to control a plethora of cellular events including cell migration, proliferation and angiogenesis (Heasman *et al.*, 2008). Following activation and dissociation of the G protein heterotrimer, Gβγ can also modulate the activity of a wide range of effectors including AC, PLC, as well as a range of ion channels (Clapham *et al.*, 1997).

The ability of GPCRs to activate mitogen-activated protein kinase (MAPK) pathways, such as extracellular signal-regulated kinase (ERK), has been demonstrated to follow both G protein-dependent and β-arrestin-dependent pathways (DeFea *et al.*, 2000b; Marinissen *et al.*, 2001).

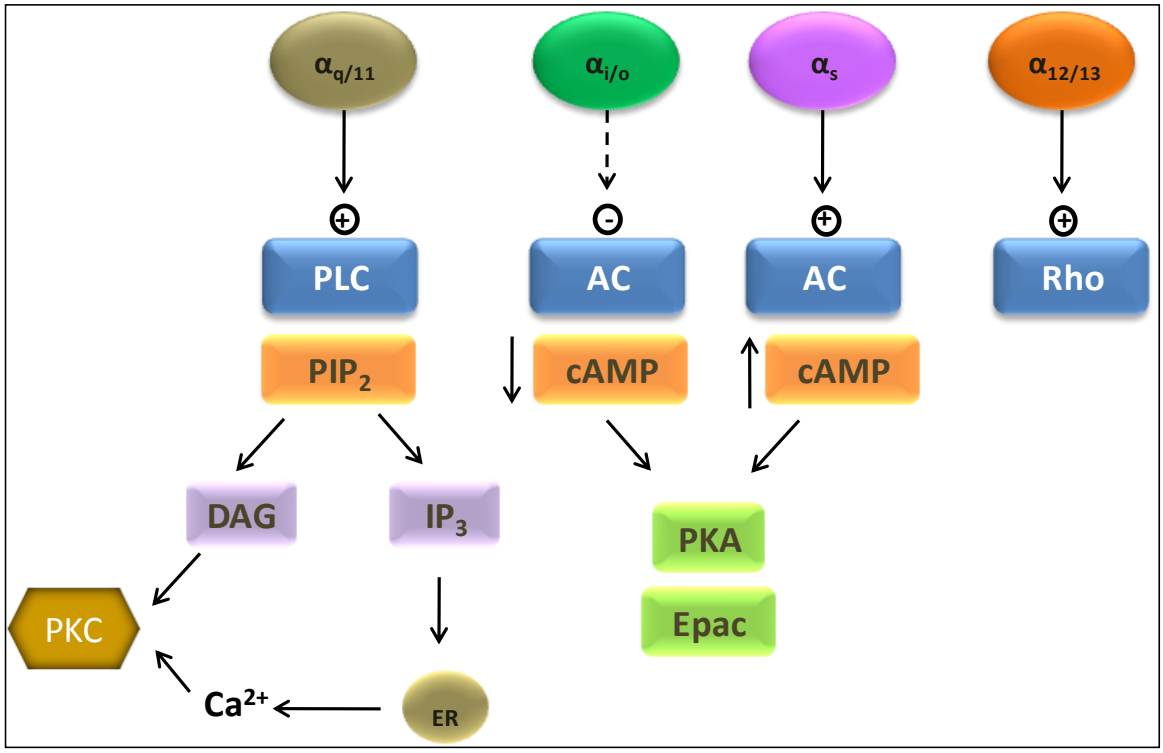

Figure 1.5 Signalling pathways by different Gα subunits. Schematic diagram showing signalling pathways regulated by different Gα subunits. Coupling to $G\alpha_{q/11}$ stimulates the PLC signalling pathway, including hydrolysis of PIP_2 and increases in $[Ca^{2+}]_i$ and PKC activity. $G\alpha_s$ and $G\alpha_{i/o}$ respectively activate and inhibit AC activity to increase or decrease cAMP synthesis from ATP. $G\alpha_{12/13}$ activates monomeric GTPase proteins including Rho.

1.5.3 NMU signal transduction

The basis by which both NMU1 and NMU2 from both human and rodent origin were identified was by their ability to increase $[Ca^{2+}]_i$ in response to NmU (Fujii *et al.*, 2000; Hedrick *et al.*, 2000; Hosoya *et al.*, 2000; Howard *et al.*, 2000; Kojima *et al.*, 2000; Raddatz *et al.*, 2000; Shan *et al.*, 2000). The increase in $[Ca^{2+}]_i$ is accompanied by a significant increase in inositol (poly)phosphate ($InsP_x$) accumulation (Aiyar *et al.*, 2004; Brighton *et al.*, 2004a; Raddatz *et al.*, 2000; Szekeres *et al.*, 2000). It has also been demonstrated that the increases in $InsP_x$ and $[Ca^{2+}]_i$ are via activation of a PLCβ-dependent pathway (Aiyar *et al.*, 2004; Brighton *et al.*, 2004a). Further, the $[Ca^{2+}]_i$ increase can be prevented by depleting intracellular Ca^{2+} stores using thapsigargin (Brighton, 2005) indicating that the increase in $[Ca^{2+}]_i$ is dependent on ER Ca^{2+} stores and is likely to be IP_3R-dependent. All of these observations suggest coupling of NMU1 and NMU2 to $G\alpha_{q/11}$.

Stimulation of NMUs also resulted in concentration-dependent inhibition of forskolin-stimulated cAMP production, suggest coupling to $G\alpha_{i/o}$ (Aiyar *et al.*, 2004; Brighton *et al.*, 2004a; Hosoya *et al.*, 2000). This inhibition was totally dependent on $G\alpha_{i/o}$ coupling since pre-treatment of the cells with pertussis toxin (PTX) abolished the inhibitory effect of NmU (Brighton *et al.*, 2004a). In contrast, increases in $InsP_x$ and $[Ca^{2+}]_i$ were PTX-insensitive. This promiscuous coupling has been demonstrated in membranes prepared from cells expressing NMU by immunoprecipitation of activated Gα-subunits ($[^{35}S]GTP\gamma S$-binding) that revealed coupling to both $G\alpha_{i/o}$ and $G\alpha_{q/11}$, but not to $G\alpha_s$ (Brighton *et al.*, 2004a). It has also been shown that stimulation of NMU1 and NMU2 by hNmU-25 results in ERK1/2 activation that is PTX-insensitive indicating involvement of $G_{q/11}$- and/or β-arrestin-dependent pathways. However, the precise mechanism linking NMUs to ERK has yet to be defined (Brighton *et al.*, 2004a).

1.5.4 Regulation of GPCR signalling

1.5.4.1 Phosphorylation and desensitization

Ligand-bound GPCR signalling can be attenuated (desensitized) by intracellular regulatory mechanisms. Receptor desensitization, which can commence simultaneously with receptor activation, allows the cell to adapt to ongoing stimulation and prevent excessive signalling (Pierce *et al.*, 2002). On agonist binding, the conformational changes induced in the receptor result in increased phosphorylation of serine/threonine residues in the intracellular loops (often the third intracellular (i3) loop) and *C*-terminal tail leading to desensitization (Pierce *et al.*, 2002). Phosphorylation of the receptor can be mediated by second messenger-kinases, such as PKC and PKA, which are activated downstream of receptor coupling to $G\alpha_{q/11}$ and $G\alpha_{s}$ respectively. This type of receptor desensitization is not specific to the activated receptor and is sometimes termed heterologous desensitization (Pierce *et al.*, 2002). It is also well-documented that receptor phosphorylation can be mediated by a family of kinases termed as G protein-coupled receptor kinases (GRKs) (Pitcher *et al.*, 1998). GRK phosphorylation is specific to the ligand-occupied receptor and is therefore termed homologous (agonist-specific) desensitization (Pierce *et al.*, 2002). Seven GRK isoenzymes had been characterized (GRK1-7), with GRK1 and GRK7 being restricted to retinal rod and cone cells. The other GRKs (except GRK4) show a ubiquitous distribution and can regulate numerous GPCRs (for a more detailed review of GRKs, please see (Pitcher *et al.*, 1998)).

Both NMU1 and NMU2 (Figure 1.2) contain putative (serine/threonine) phosphorylation sites in their intracellular domains, potentially for PKA, and PKC, (and also casein kinases I and II) (Brighton *et al.*, 2004b). The sites phosphorylated by GRKs have been characterized for a number of GPCRs. However, the actual phosphorylation status or amino acid consensus sequences for GRK phosphorylation have yet to be defined (Brighton *et al.*, 2004b).

Receptor phosphorylation by GRKs often leads to β-arrestin recruitment and termination of receptor-G protein coupling and therefore G protein dependent signalling

(Marchese *et al.*, 2008; Moore *et al.*, 2007; Pierce *et al.*, 2002). Of the four β-arrestin isoforms identified; two are non-visual, arrestin 2 (β-arrestin 1) and arrestin 3 (β-arrestin 2) which are ubiquitously expressed and fulfil crucial roles in GPCR desensitization (Pierce *et al.*, 2002). At present there is little information available regarding NMU regulation by arrestin.

1.5.4.2 Internalization and trafficking

Removal of GPCRs from the cell-surface by receptor internalization is considered an essential step in receptor desensitization, resensitization (recycling) and down-regulation (Moore *et al.*, 2007). Importantly, receptor internalization can also fulfil an intracellular signalling role. Several mechanisms have been identified for GPCR endocytosis (Hanyaloglu *et al.*, 2008; Marchese *et al.*, 2008; Moore *et al.*, 2007; Pierce *et al.*, 2002). Following GRK-mediated receptor phosphorylation and β-arrestin binding, the receptor complex can recruit essential adaptor proteins for receptor endocytosis (Marchese *et al.*, 2008; Moore *et al.*, 2007). Receptor internalization via clathrin-coated pits (CPP) is GRK- and β-arrestin-dependent and has been studied extensively (Moore *et al.*, 2007). The GPCR-β-arrestin complex binds different components of the CPP, including clathrin heavy chain and the β2-subunit of the adaptor protein-2 (AP-2). This facilitates movement of the receptor-β-arrestin complex into CPP at the surface of the cells. Dynamin, a GTPase protein which participates in the pinching of CCP from the cell-surface, is considered to be major factor in the process of clathrin-dependent endocytosis and promotes the translocation of the complex to the early endosomes.

The receptor may then be recycled either rapidly or slowly by large recycling endosomes back to the cell-surface following dephosphorylation and β-arrestin dissociation (resensitization), or β-arrestin can promote receptor ubiquitination in late endosomes and target the complex for lysosomal degradation (down-regulation) (Figure 1.6) (Hanyaloglu *et al.*, 2008; Moore *et al.*, 2007; Pierce *et al.*, 2002). Furthermore, it has been shown that a short consensus amino acid sequence at the *C*-terminus termed a tyrosine motif (Tyr-X-X-Ø, where X is any amino acid and Ø is hydrophic amino acid) binds directly to the μ2-subunit of the adaptor protein AP-2 in CCP. Binding of this sequence to AP-2 mediates

CCP-dependent GPCR internalization and trafficking and may make this process both ligand- and β-arrestin-independent (Marchese *et al.*, 2008).

NMU1 and NMU2 internalization has been demonstrated using fluorescently-tagged pNmU-8 (Cy3B-pNmU-8) (Brighton *et al.*, 2004a). Internalization can be inhibited by pre-treatment with concanavalin A highlighting the involvement of CCP-mediated internalization (Brighton, 2005). In addition, NMU2 contains a tyrosine motif (YQSF) within its *C*-terminal (see Figure 1.2), suggesting that this receptor subtype may be susceptible to AP-2-/clathrin-dependent internalization.

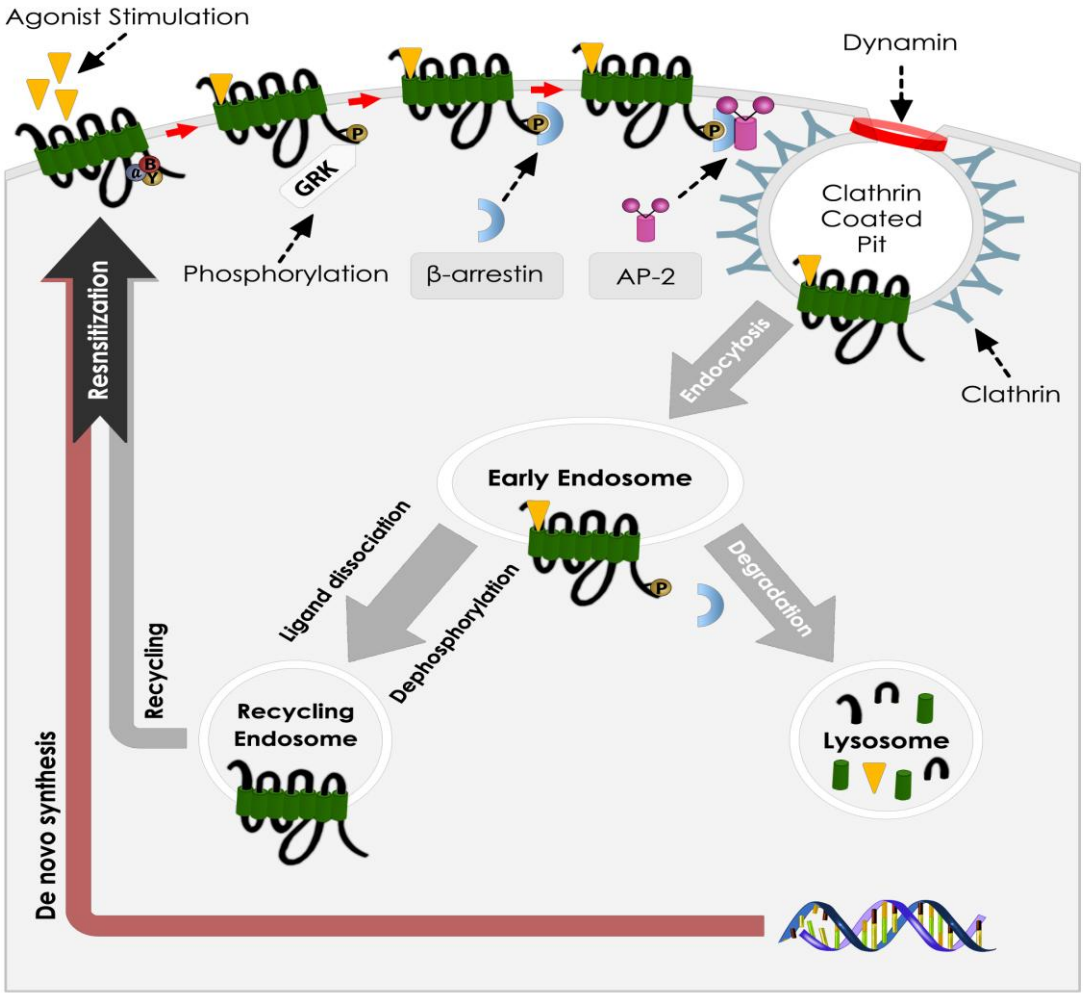

Figure 1.6 Schematic diagram of receptor internalization and trafficking. Receptor activation by ligand binding promotes G protein-dependent and independent signalling, phosphorylation of receptor intracellular domains by GRKs and β-arrestin binding. Phosphorylation and β-arrestin binding lead to the binding of CCP machinery components, AP-2 and clathrin, to the ligand-receptor-β-arrestin complex which is then directed to endocytosis with the translocation of the complex to early endosomes. Ligand dissociation and receptor dephosphorylation allow recycling and resensitization. An alternative fate is that the complex will be tagged by ubiquitin, and targeted for lysosomal degradation.

In addition to the important roles of β-arrestin in regulating rapid receptor desensitization, internalization and ubiquitination, it is now clear that β-arrestin bind to GPCRs with differing affinity and this has led to the proposal of two classes of GPCR (classes A and B) defined by their β-arrestin1/2 selectivity/affinity and longevity of interaction (Oakley *et al.*, 2000). Class A GPCRs, which include the β_2-adrenoceptor, μ-opioid receptor and D_1 dopamine receptor have higher affinity for β-arrestin-2 compared to β-arrestin-1, and the receptor-arrestin complex dissociates quite rapidly either at the cell-surface or shortly after internalization and this may account for the rapid recycling characteristic of this sub-group (Moore *et al.*, 2007; Oakley *et al.*, 2000). Class B GPCRs, which include the angiotensin II (AT_{1A}) receptor, neurotensin 1 receptor, V_2 vasopressin receptor and neurokinin-1 receptor, have a similar affinity for both β-arrestin-1 and 2, and form prolonged associations with arrestin allowing the receptor-arrestin complex to be observed within endosomes.(Moore *et al.*, 2007; Oakley *et al.*, 2000). Thus, it has been demonstrated that sustained binding of β-arrestin to V_2 vasopressin receptors results in slow recycling, with the receptor taking approximately 4 h to recycle through endosomes and back to the plasma membrane (Oakley *et al.*, 1999).

β-arrestin has also been reported to be involved in pre/post-endocytotic G-protein-independent signalling, where they serve as scaffold proteins to recruit other proteins, such as Raf/MEK/ERK and other MAPK signalling pathways to initiate signalling at the cell-surface and/or in endosomes (DeFea *et al.*, 2000a; Pierce *et al.*, 2002). In this context it is noteworthy that it has been shown that stimulation of NMU1 and NMU2 by hNmU-25 results in sustained ERK1/2 activation (for 60+ min), but the exact mechanism has yet to be explored.

1.6 Ligand-receptor pseudo-irreversible binding

Pseudo-irreversible binding has been observed between several GPCRs and their cognate peptide ligands. For example, it has been reported in KNRK cells that repetitive application of substance P, failed to evoke repetitive $[Ca^{2+}]_i$ mobilization via a neurokinin-1 receptor following washing in an attempt to remove ligand (Schmidlin *et al.*,

2001). Similarly, the endothelin receptor type A (ET_A-R) and urotensin receptor (UT-R) show high-affinity ligand-receptor binding, and it had been reported that antagonist addition fails to terminate sustained signalling by the activated receptor and displacement of agonist from the receptor is partially resistant to acid washing (pH 2.5, 10 min), even when the initial binding is performed at lower temperature to minimize internalization (Hilal-Dandan *et al.*, 1997; Qi *et al.*, 2005).

Previous studies in HEK293 cells stably expressing either NMU1 or NMU2 (HEK-NMU1 and HEK-NMU2, respectively) have revealed that robust increases in $[Ca^{2+}]_i$ seen on application of different NmU analogues did not return to basal levels even with extensive washing (Brighton *et al.*, 2004a). Furthermore, on re-application of NmU no Ca^{2+} response was seen. These data can be interpreted as either indicating a rapid and complete NMU1/2 desensitization or a pseudo-irreversibility of NmU binding. A pseudo-irreversible binding phenomenon was proposed on the basis of a failure to remove fluorescently-tagged pNmU-8 (Cy3B-pNmU-8) from the receptor with extended wash-periods, or to displace it by addition of 10-fold excess of unlabelled NmU (Brighton *et al.*, 2004a). More recent investigations of NmU signalling using cultured rat colonic myocytes also support the idea of pseudo-irreversible binding (Brighton *et al.*, 2008). In contrast, repetitive application of either rNmU-23 or hNmU-25 to strips of rat colonic smooth muscle resulted in repetitive contractile responses that were approximately equal in magnitude (Brighton *et al.*, 2008). The rapid reversibility of NmU-NMU binding in intact tissue was further emphasized by the fact that a brief 1 min wash was sufficient to allow complete relaxation and re-contraction on re-addition of agonist (Brighton *et al.*, 2008).

From these studies we can see a paradox between the ability of NmU to contract colonic smooth muscle strips repetitively and the lack of repetitive Ca^{2+} responses in cultured colonic smooth muscle cells or in recombinant system. Growing evidence suggests that proteolytic activity is needed to regulate high-affinity ligands, such as peptides. Although proteolytic activity clearly regulate extracellular concentration of a number of peptides, there is accumulating evidence that endosomes serve as a platform for peptidases to terminate GPCR signalling by cleaving and inactivating the ligand (Padilla *et al.*, 2007; Roosterman *et al.*, 2007; Roosterman *et al.*, 2008). Thus, the

necessary proteolytic activity needed to remove NmU from the receptor at the surface of the cell or after being internalized may be altered under cell culture conditions.

1.7 Aim of the project

While previous studies, particularly from this laboratory, have characterised signalling by recombinantly expressed NMU1 and NMU2, much remains to be explored including the mechanisms of receptor desensitisation, resensitisation and the functional consequences of the reported pseudo-irreversible ligand binding. The initial aim of the work described within this thesis was to further characterise the signalling pathways regulated by NmU in recombinant systems (HEK-NMU1 and HEK-NMU2). Further, given the pseudo-irreversible ligand binding, the aim was to explore the possibility of using the observed ability of low pH washes to remove receptor-bound ligand to consider the consequences of the continued presence of ligand both on receptor trafficking and desensitisation/resensitisation and on potential G-protein-independent signalling. In particular, the possibility that ligand processing is important in receptor trafficking and receptor resensitisation will be explored. It is hoped that these studies will provide insight not only into mechanisms relating to aspects of NMU regulation but also to other receptors that bind (peptide) ligands with high affinity. Further, as much of the previous characterisation of NMU signalling has been in recombinant systems, it was hoped that aspects of these studies could be taken forward into systems with native expression of NMU to compare signalling and receptor regulation in more physiologically relevant systems.

Chapter 2

Materials & Methods

2.1 Materials

2.1.1 Cell culture, chemicals, peptides and radioactive materials

Minimum essential medium (MEM), Dulbecco's modified Eagle's medium (DMEM), medium 231, smooth muscle growth supplement (SMGS), fetal bovine serum (FBS), Dulbecco's phosphate-buffered saline (D-PBS) without calcium and magnesium, Geneticin (G-418), non-essential amino acids and other cell culture reagents were from Invitrogen (Paisley, UK). Fungizone/penicillin/streptomycin (100x, composition of stock solution: amphotericin B, 25 µg/mL; penicillin, 10,000 unit/mL and streptomycin 10,000 µg/mL) was from Fisher Scientific (Loughborough, UK), RPMI-1640 medium with or without L-glutamine were purchased from Sigma-Aldrich (Poole, UK). Cell culture flasks, plates and plasticware were from NUNC (Roskidle, Denmark). Pluronic acid F-127 was from Molecular Probes (Eugene, USA). Collagenase (Type F, 1.8-2.2 FALGPA), hyaluronidase, papain, soybean trypsin inhibitor, dithiothreitol (DTT), bovine serum albumin (BSA), poly-D-lysine hydrobromide, fluo-4-acetoxymethylester (fluo-4-AM), cycloheximide, monensin, monodansyl cadaverine (MDC), dynasore hydrate, concanavalin A and phenylarsine oxide (PAO), endothelin-converting enzyme 1 (ECE-1) inhibitor, (4-chloro-N-[[(4-cyano-3-methyl-1-phenyl-1H-pyrazol-5-yl)amino]carbonyl] benzenesulfonamide, monosodium salt) (SM-19712), forskolin, dimethyl sulphoxide (DMSO), Bradford reagent, isobutylmethylxanthine (IBMX), carbachol, uridine-5'-triphosphate (UTP) were purchased from Sigma-Aldrich (Poole, UK). Greiner ELISA 96-well plates (8 well/strip) were from Scientific Laboratory Supplies Ltd. (Nottingham, UK). Human neuromedin U (hNmU-25), human neuromedin S (hNmS-33), porcine neuromedin U (pNmU-8 and pNmU-25) and rat neuromedin U (rNmU-23) were purchased from Bachem (St. Helens, UK). Fluorescently-tagged pNmU-8 (Cy3B-pNmU-8) was provided by GlaxoSmithKline (Harlow, UK). Other chemicals used routinely for laboratory experiments were purchased from either Fisher Scientific (Loughborough, UK)

or Sigma-Aldrich (Poole, UK). Safefluor, ALTIMA-FLO AF scintillation cocktails, *myo*-[^{3}H]inositol (34 Ci/mmol), 6 mL and 20 mL scintillation vials and [^{35}S]methionine (1000 Ci/mmol) were purchased from PerkinElmer LAS (UK) Ltd (Beaconsfield, UK). [2,8-^{3}H]adenosine 3',5'-cyclic monophosphate, ammonium salt ([^{3}H]cAMP, 42 Ci/mmol) was from GE Healthcare (Chalfont, UK). Water used to make solutions was distilled, de-ionized water (ddH_2O) obtained through an ELGA System (ELGA, Marlow, UK). For cell culture and molecular biology, ddH_2O was autoclaved at a temperature of 121ºC for 15 min.

2.1.2 Immunocytochemistry and immunoblotting (Western blot) reagents

Microscope glass slides, 13 and 25 mm glass coverslips were purchased from VWR International (Lutterworth, UK). ProLong® Gold antifade reagent was from Invitrogen (Paisley, UK) and paraformaldehyde was from Thermo Scientific (Loughborough, UK). Mouse monoclonal α-actin antibody and fluorescein 5-isothiocyanate (FITC)-antimouse secondary antibody generated in goat were purchased from Sigma-Aldrich (Poole, UK). Acrylamide (30%) solution was from National Diagnostic Ltd. (Hessle, UK). Pre-stained protein ladder was from Fermentas (Leon-Rot, Germany). Polyvinylidene fluoride (PVDF) membrane was purchased from Millipore (UK) Ltd. (Watford, UK). UptiLight chemiluminescent substrate solution was purchased from Cheshire Sciences (UK) Ltd. (Chester, UK). Rabbit monoclonal phospho-p44/42 mitogen-activated protein (MAP) kinases (MAPK, ERK1/2, Thr202/Tyr204) antibody, rabbit polyclonal p42 MAPK (ERK2) antibody, HRP-linked anti-rabbit IgG, secondary antibody were from New England Biolabs (UK) Ltd. (Hitchin, UK).

2.1.3 Cell-lines and primary cells

Human embryonic kidney cells (HEK293), either wild-type (HEK293-WT), or stably expressing either NMU1 or NMU2 (HEK-NMU1 and HEK-NMU2, respectively) were provided by GlaxoSmithKline (Harlow, UK). HEK-NMU1-eGFP and HEK-NMU2-eGFP stable cell-lines were generated with the help of Dr. Yan Huang, Department of Cell

Physiology and Pharmacology, University of Leicester. SU.86.86. and AsPC1 (human pancreatic cancer cell-lines) were generously provided by Dr. Knut Ketterer, Department of Surgery, Technical University of Munich, Germany. INS-1E (rat pancreatic β-cell-line), MIN6 (mouse pancreatic β-cell-line) were available in the laboratory. KYSE140 (human oesophageal cancer cell-line) was kindly provided by Dr. George DD Jones, Department of Cancer Studies & Molecular Medicine, University of Leicester, Leicester, UK.

Rat colonic smooth muscle cells were isolated from adult male Wistar rats. Cardiac myocytes were isolated from adult male Wistar rats by Dr. Nina Storey, Department of Cell Physiology and Pharmacology, University of Leicester, Leicester, UK. Pig coronary artery smooth muscle cells were isolated from dissected coronary artery from pig left ventricle hearts, which were obtained from a local abattoir.

2.1.4 Materials used for generation of NMU1-eGFP and NMU2-eGFP constructs

Vent polymerase, T_4 DNA ligase, restriction enzymes (Xho I, BamH I, Spe I, SnaB I) and all buffers were obtained from New England Biolabs (Hitchin, UK). DNA ladder (1kb plus, 100 bp-12 kp) and dNTPs for PCR were purchased from Invitrogen (Paisley, UK). Agarose powder and GelRed were purchased from Cambridge Bioscience (Cambridge, UK). DNA-gel extraction kits and plasmid midiprep kits were from QIAGEN (Crawley, UK). Primers and DH5*α* competent cells were from Invitrogen (Paisley, UK). Plasmids, pFN-hu-axor13 and PFN-cmv-hu-axor34DNA containing cDNA of NMU1 (1281 bp) and NMU2 (1248 bp), respectively were a kind gift from GlaxoSmithKline (Harlow, UK). The plasmid (pEGFP-N1) containing enhanced green fluorescent protein (eGFP), kanamycin and neomycin antibiotics resistant genes for selection during transformation in prokaryotic, *E. coli* DH5*α* competent cells and stable transfection in eukaryotic cells was purchased from Clontech (Oxford, UK).

2.2 Methods

2.2.1 Cell culture

HEK293 wild-type cells were maintained in DMEM supplemented with FBS (10% *v/v*), L-glutamine, non-essential amino acids, penicillin and streptomycin (1% *v/v* ,100x,: penicillin, 10,000 U/mL and streptomycin sulphate, 10,000 µg/mL). HEK-NMU1, HEK-NMU2, HEK-NMU1-eGFP, HEK-NMU2-eGFP were cultured in MEM supplemented with Earle's salts, FBS (10% *v/v*), non-essential amino acids, penicillin and streptomycin. All of the above cell-lines were cultured in 175 cm^2 flasks unless otherwise stated. KYSE140, SU.86.86 and AsPC1 cell-lines were maintained in RPMI-1640 containing L-glutamine, sodium hydrogen carbonate, FBS (10% *v/v*), penicillin and streptomycin and grown in 75 cm^2 flasks. INS-1E and MIN6 cell-lines were maintained in RPMI-1640 with penicillin and streptomycin and heat-inactivated FBS (10% *v/v*) and grown in either 75 cm^2 flasks or 10 cm^2 dishes. Heat inactivation of FBS was performed at 50 °C for 30 min. All cells were maintained in 95% humidified air: 5% CO_2 environment at 37 °C and passaged every 3-5 days or as required for experiments. For passaging, growth medium was aspirated and adherent cells were washed once with D-PBS, followed by addition of 5 mL (175 cm^2 flask), 3 mL (75 cm^2 flask) or 1 mL (10 cm^2 dish) trypsin-EDTA (0.05% *w/v* trypsin, 0.04% *w/v* EDTA) to dislodge cells for 2 min at room temperature (RT). The trypsin was then neutralized by addition of 15 mL, 7 mL or 9 mL growth medium to 175-cm^2 flask, 75-cm^2 flask and 10 cm^2 dishes, respectively. Cells were harvested by centrifugation (140 x*g*, 4 min) and the pellet was re-suspended in 10 mL growth medium. Cells were then re-seeded into the flask at a ratio 1:5 or counted for experimentation and cultured on 25 mm coverslips, 96-well plates or 24-well plates.

Rat colonic and pig coronary artery smooth muscle cells where grown on either uncoated, 25 mm glass coverslips or poly-D-lysine-coated 24-well plates in 231 growth medium supplemented with (SMGS 5%, *v/v*) and penicillin/streptomycin.

2.2.2 Freezing and thawing cell-lines

Two frozen stocks were maintained for all cell-lines that were used for experimentation. Long-term stocks were stored in liquid nitrogen. As an alternative, stocks were also kept in a -80 °C freezer to be used short-term (6 months). For freezing, cells were grown in 175-cm^2 flasks in antibiotic-free medium (1 week before freezing) and harvested as described earlier (see **Section 2.2.1**) during the log phase of growth (60-80% confluency). Following centrifugation and removal of the growth medium, cells were re-suspended gently, without forming bubbles, in 3 mL freezing medium (10% DMSO in FBS) and each 1 mL was transferred to a sterile cryotube and cooled-down for 1 h at -20 °C and then kept at -80 °C until used or moved to a liquid nitrogen storage bank following overnight incubation at -80 °C.

Cells were thawed by immediate transfer of the cryotube from either liquid nitrogen or -80 °C to a 37 °C water-bath for 1 min with interval shaking. The content was then transferred to a universal 30 mL tube containing 10 mL pre-warmed medium. This was followed by centrifugation of the tube (140 x*g*, 4 min) and discarding of the supernatant. The cell pellet was then re-suspended with a further 10 mL of medium and harvested again to remove any remaining DMSO. Finally the cells were suspended gently in 3 mL of medium and transferred to a suitable cell culture flask or dish, and cultured in 95% humidified air:5% CO_2 environment at 37 °C for the first week in antibiotic-free medium and then cultured as described. It is worth noting that DMSO is cytotoxic to cells at RT. Therefore, cells transferred as quickly as possible to -20 °C once they had been suspended in the freezing medium. During thawing, medium was added quickly. Freezing of the cells was always performed with the lowest possible passage number.

2.2.3 Cell counting

Cells were counted for the purpose of experimentation using a haemocytometer (Neubauer improved, with 0.100 mm depth and 0.0025 mm^2 area, Sigma-Aldrich, Poole, UK). Following re-suspension of the cells in 10 mL growth medium and gentle pipetting for appropriate mixing, a drop of cell suspension was added between the haemocytometer and the cover glass. Cells inside the large square (consisting of 16 small squares) were

counted and the average of 3-4 counts multiplied by 10^4 to give approximate cell number in 1 mL of cell suspension.

2.2.4 Surface coating for cell culture

For coating 25 mm glass coverslips, poly-D-lysine (0.1 mg/mL, 200 μL) was added to the surface for 15 min and then aspirated. The surface was then washed twice with D-PBS and left to dry for 30 min. For 24-well and 96-well plates, surfaces were coated with poly-D-lysine overnight at 4 °C then washed three times with D-PBS.

2.2.5 Isolation and culture of rat colonic smooth muscle cells and pig coronary artery smooth muscle cells

The colonic smooth muscle cell dissociation protocol used here was originally designed for isolation of pig coronary artery smooth muscle cells (Quayle *et al.*, 1996) and had been successfully used previously in our laboratory to dissociate rat colonic smooth muscle cells (Brighton *et al.*, 2008). Adult male Wistar rats (250-300 g) were killed by cervical dislocation according to Schedule 1 of The Care and Use of Laboratory Animals (Scientific Procedures Act, 1986). After opening the abdomen by a mid-line incision, 3 cm of the distal part of the colon was dissected, washed with a low Ca^{2+} physiological salt solution (low Ca^{2+} PSS, composition: NaCl, 137 mM; KCl, 5.4 mM; $CaCl_2$, 0.1 mM; HEPES, 10 mM; glucose, 10 mM; Na_2HPO_4, 0.44 mM; NaH_2PO_4, 0.4 mM; $MgCl_2$, 1 mM; pH 7.4) and transferred to ice-cold low Ca^{2+} PSS. A longitudinal incision was made to open the colon. After removal of fat and blood vessels, the mucosal layer was removed by gentle scraping with a metal spatula. The tissue was then cut into 2-3 mm segments and exposed to two enzymatic digestion steps. The first digestion was performed in 2 mL low Ca^{2+} PSS containing papain (16.5 U/mL) and DTT (3.2 mM) for 31 min at 35 °C. A second digestion step was then performed in 2 mL PSS containing collgenase F (1.65 U/mL), hyaluronidase (165 U/mL) and soybean trypsin inhibitor (0.1% *w/v*) for 30 min at 35°C. Tissue was then washed very carefully three times with low Ca^{2+} PSS (normal Ca^{2+}, 1.3 mM), which was then substituted with 2-3 mL 231 growth

medium. Dissociation of smooth muscle cells was performed by gentle mechanical sheering using trituration through a glass, fire-polished Pasteur pipette until a turbid, cell suspension formed. Cells were either plated directly onto uncoated 25 mm glass coverslips or 24-well plates coated with poly-D-lysine by adding 50-100 μL of the cell suspension. Cells were then allowed to adhere for 1-2 h in a 95% humidified air: 5% CO_2 incubator at 37 °C. Medium 231 supplemented with SMGS (5%, *v/v*) fungizone/penicillin/streptomycin (1% *v/v*) was added and changed every 48 h. For isolation of pig coronary artery smooth muscle cells, a whole pig heart was obtained from a local abattoir (Lutterworth, UK) and transferred to the laboratory in ice-cold 2 mM Ca^{2+} physiological salt solution (2 mM Ca^{2+}-PSS) (composition: NaCl, 137 mM; KCl, 5.4 mM; $CaCl_2$, 2 mM; HEPES, 10 mM; glucose, 10 mM; Na_2HPO_4, 0.44 mM; NaH_2PO_4, 0.4 mM; $MgCl_2$, 1 mM; pH 7.4). Coronary arteries were then dissected from the heart, cleaned of fat and surrounding tissues and then cut to 2-3 mm segments. Strips of the coronary artery smooth muscle were subjected to the same as those used to isolate rat colonic myocytes.

2.2.6 Isolation of cardiac myocytes

Cardiac myocytes were generously isolated and provided by the laboratory of Dr. Nina Storey, Department of Cell Physiology and Pharmacology, University of Leicester, Leicester, UK. Briefly, adult male Wistar rats (250-300 g) were killed by cervical dislocation according to Schedule 1 of The Care and Use of Laboratory Animals (Scientific Procedures Act, 1986) and single ventricular myocytes isolated by enzymatic dissociation. Hearts were excised rapidly and perfused through the aorta with Ca^{2+}-free Tyrode's solution (composition: NaCl, 137 mM; KCl, 2.7 mM; $MgCl_2$, 1.0 mM and NaH_2PO_4, 0.6 mM and pH was adjusted to 7.4), followed by a solution for enzymatic digestion of hearts, containing collagenase (type I) and protease (type XV). After digestion hearts were perfused with Ca^{2+}-Tyrode's solution (2 mM Ca_2Cl). Single myocytes were isolated by gentle agitation at 35 °C. Single ventricular myocytes were then twice washed with Ca^{2+}-Tyrode's solution prior to experimentation. Typically the yield of quiescent rod-shaped cells was 60-80%.

2.2.7 Isolation of colonic smooth muscle strips and measurement of contractile responses

Adult male Wistar rats (250-300 g) were killed by cervical dislocation according to Schedule 1 of The Care and Use of Laboratory Animals (Scientific Procedures Act, 1986). After opening the abdomen by a mid-line incision, 3 cm of the distal part of the colon was dissected, washed with 2 mM Ca^{2+} Tyrode's solution. A longitudinal opening was made and the tissue was cleaned of excessive fat and blood vessels (in some experiments, the mucosa layer was removed carefully with a metal spatula). The tissue was cut into 15 x 6 mm segments. Tissue was suspended in an organ-bath filled with 5 mL Tyrode's solution in the presence of continuous oxygenation (95% O_2:5% CO_2) under 1 g tension. The suspended tissue was allowed to equilibrate for 30 min with the organ-bath solution being replaced every 15 min. The positive control for a contractile response was achieved by addition of carbachol (1 or 100 µM). Addition of carbachol (1 or 100 µM) or rNmU-23 (1 µM in 0.1% BSA) was performed directly to the organ-bath without perfusion system.

2.2.8 Generation of cDNA for NMU1-eGFP and NMU2-eGFP

2.2.8.1 Design of primers

Primers were designed to clone the full-length NMU1 and NMU2 (see **Chapter 4, Figure 4.1**). Primers for each gene contained 13-19 bp of coding sequence for NMU1 or NMU2 including a start codon (ATG), XhoI and SpeI restriction sites, where a Kozak sequence, 'GCCACC' inserted just before ATG to enhance translation and expression in eukaryotic cells.

2.2.8.2 Polymerase chain reaction (PCR) for amplification of NMU1 and NMU2

Full-length of NMU1 (1281 bp) and NMU2 (1248 bp) were amplified from the original vectors, pFN-hu-axor13 and PFN-cmv-hu-axor34, respectively supplied by GlaxoSmithKline, Harlow, UK. Amplification was by PCR using a thermocycler (Techne

Inc., Burlington, NJ, USA). The PCR reaction consisted of 27 cycles (see **Chapter 4, Figure 4.2a**). The first cycle was a denaturation step for 1 min at 95 ºC. The subsequent 25 cycles involved three steps; denaturation (30 s, 95 ºC); annealing (1 min, 53 ºC) and; extension (3 min, 72 ºC). The last cycle was similar to the 25 cycles, but the extension step was for 10 min. The thermocycler was programmed to keep samples at 4 ºC after completion. Tubes were then collected to immediately continue cloning or kept at -20 ºC until use. Each PCR reaction was performed in a 50 µL total volume in PCR tubes. For each 50 µL reaction, either pFN-hu-axor13 (0.3 µg) or PFN-cmv-hu-axor34 plasmids (0.5 µg), thermostable buffer (10x, 5 µL), forward and reverse primers (0.5 µg/µL, 1 µL), dNTP mixture (10 mM, 1 µL), autoclaved ELGA water (complete to 49 µL) and DNA polymerase vent (2,000 U/mL, 1 µL) were included. Each tube was then gently mixed, spun down (16,500 x*g*, 2-3 s) and subjected to the PCR cycles on the thermocycler.

2.2.8.3 Preparation of agarose gel and DNA electrophoresis

The amplified DNA product of interest was detected by electrophoresis of the PCR product on an agarose gel (0.76%). Agarose powder (0.38 g) was dissolved in a 250 mL glass flask containing Tris/acetate/EDTA buffer (TAE: Tris acetate, 0.4 M; EDTA, 0.01 M, pH 8.3, 50 mL). The agarose was dissolved by heating the mixture on full power in a microwave for 40 s. The solution was then allowed to cool to approximately 50 ºC and GelRed (10,000x, 2-3 µL) added to allow visualisation of the DNA. The mixture was then transferred quickly into a horizontal casting tray with a ten-well comb and the gel was allowed to solidify at RT (approximately 30 min). After gel solidification, the comb was removed and the casting tray containing the gel was mounted in an electrophoresis chamber and covered with TAE buffer. Each of the 50 µL DNA samples were mixed with loading buffer (10x, 5 µL: glycerol, 50% *v/v*; Ficol, 2% *v/v*; EDTA, 50 mM and; bromophenol blue, 5% *w/v*). Samples were then loaded into the wells of the agarose gel alongside a DNA ladder (1.0kb Plus, 10 µL) to evaluate the DNA fragments sizes. The gel was then subjected to 140 V for 35-40 min and then removed from the chamber and visualized under UV light.

2.2.8.4 cDNA extraction and purification

Following PCR amplification of the coding sequence for NMU1 and NMU2 and visualization of both fragments at the expected size (see **Chapter 4, Figure 4.2b**), each cDNA was excised from the agarose gel under UV light (performed quickly to prevent DNA damage) using a clean scalpel blade and transferred to an autoclaved 1.5 mL pre-weighed tube. DNA was purified from the agarose gel using QIAquick gel extraction kits according to the manufacturer's instructions. Briefly, the excised gel fragment was incubated with 3x volume (e.g. for each 100 µg add 300 µL) of QG buffer and incubated for 10 min at 50 ºC with appropriate shaking every 2-3 min until a homogenous yellow colour formed. This was followed by addition of 1x volume of isopropanol (molecular biology grade) with continuous shaking and then the tube contents were transferred to a QIAquick column in a 2 mL tube. The column was then centrifuged at 16,500 x*g* for 1 min and the solution at the bottom of the tube was discarded and another 500 µL of QG buffer added to the column and centrifuged as above. The columns were washed by the addition of PE buffer (750 µL) and allowed to sit for 5 min before centrifugation (2x, 16,500 x*g*, 1 min). At this point, the tube in which the column was sitting was replaced by a fresh, autoclaved, 1.5 mL tube and the DNA was eluted from the column with water (30 µL) and further centrifugation (16,500 x*g*, 1 min). The latter step was repeated using the same 30 µL of water to ensure the entire DNA was eluted. When DNA was purified following restriction digest **(**see **Section 2.2.5.5)**, the purified DNA product was eluted using TE buffer (Tris, 10 mM; EDTA, 1 mM, pH 8.0,). The purified DNA was stored at -20 ºC until use.

2.2.8.5 XhoI-SpeI restriction digest

Restriction digest by XhoI-SpeI was performed on the purified PCR product to generate sticky ends to be ligated into the vector of interest. For a 50 µL reaction, purified PCR product (29 µL) was mixed in a PCR tube with BSA (10 mg/mL, 0.5 µL), NEB buffer 2 (suitable for both restriction enzymes according to the manufacturer's instructions, 5x, 5 µL), SpeI (10,000 U/mL, 1.2 µL), XhoI (20,000 U/mL, 0.6 µL) and water (up to 50 µL). The contents of each tube were gently mixed without vortex-mixing

and centrifuged (16,500 x*g*, 2-3 s) prior to overnight incubation at 37 ºC using a programmable thermocycler. The digested product was purified as described above, eluted using TE buffer and stored at -20 ºC until use or used immediately for ligation.

2.2.8.6 Ligation of the DNA insert to pEGFP-N1

Here, the cDNA of NMU1 or NMU2 (with XhoI and SpeI sticky ends) were ligated into a linearized pEGFP-N1 plasmid. The plasmid was prepared for ligation by restriction digest with NheI-XhoI. In a 20 µL reaction, the cDNA of NMU1 or NMU2 (4 µL) were mixed with the pEGFP-N1 (0.5 µL) vector (optimum molar ratio is 1:1-10:1 insert:vector), where the DNA insert and vector were prepared by RE digest from approximately 2 µg DNA, T_4 DNA ligase buffer (10x, 2 µL), water to 19 µL and lastly T_4 DNA ligase (1 µL). The reaction mixture was mixed by gentle tapping, centrifuged (16,500 x*g*, 2-3 s) and incubated at RT for 3-4 h. Following the ligation, the new ligated plasmids were transformed into DH5*α*, *E.coli* competent cells.

2.2.8.7 Transformation

In transformation, the plasmid containing the gene of interest is inserted into host bacterial cells (e.g. DH5*α* competent cells) to be replicated and produced in sufficient quantities for subsequent isolation and use. Due to the fact that few competent cells take up the plasmid, bacterial cells are then plated on agar growth dishes containing the antibiotic for which a gene within the plasmid confers resistance. Thus, only the transformed bacteria are able to grow and the remaining bacteria are killed. Here, DH5α competent cells (50 µL aliquot tubes stored at -80 °C) were thawed on ice for 10 min prior to transformation. The ligated product (7.5 µL) was transferred to the competent cells and incubated for 30 min on ice. This was followed by a heat-shock reaction where the tube containing the plasmid and the competent cells was incubated for 90 s at 42 ºC and then transferred immediately to ice for 2 min. The heat-shocked cells were then mixed with super optimal broth (SOC) medium (800 µL, composition: NaCl, 10 mM; KCl, 2.5 mM; $MgCl_2$, 10 mM; $MgSO_4$, 10 mM; glucose, 20 mM yeast extract, 0.5% *w/v* and; tryptone, 2% *w/v*) in a 15 mL Falcon tube and incubated for 1 h in a 37 ºC bacterial

incubator with continuous shaking at 220-230 r.p.m.. Following 1 h culture, the content was transferred to a fresh autoclaved 1.5 mL tube, centrifuged at 8500 x*g* for 2 min, 75% of the supernatant discarded and the cells suspended with the remaining 25% (approimately 100 µL). The cell suspension were then spread onto a 10 cm Lysogeny broth (LB) agar plate (tryptone, 1% *w/v*; yeast extract, 0.5% *w/v*; NaCl 1% *w/v* and agar 1.5% *w/v*) containing kanamycin antibiotic (50 µg/mL) and incubated at 37 ºC overnight. The plate was stored inverted at 4 ºC sealed with Nescofilm until miniprep isolation of plasmid from individual clones (see below).

2.2.8.8 Culture of the transformed colonies and DNA plasmid preparation

Each single transformed colony carrying DNA plasmid of interest can be then cultured, usually in one of three different scales according to the required quantity of DNA plasmid (miniprep, 20-30 µg DNA; midiprep, 100-300 µg and; maxiprep, 500-850 µg).

2.2.8.8.1 Bacterial culture and preparation of small scale DNA plasmid preparation (Miniprep)

During this stage of cloning, minipreps were used to perform diagnostic restriction digest following preliminary confirmation of the presence of the fragments of expected sizes (see **Chapter 4, Figures 4.3 and 4.4**) and for cDNA sequencing of the plasmid. Four colonies from each plate (NMU1-eGFP and NMU2-eGFP) were picked and transferred individually to sterile 15 mL Falcon tubes containing 3 mL LB medium and kanamycin (50 µg/mL). The mixture in each Falcon tube was incubated overnight in a bacterial incubator at 37 °C with continuous shaking (220-230 r.p.m.). Minipreps were performed on each culture using the QIAGEN miniprep protocol and buffers. Briefly, 1 mL of the transformed cell suspension was transferred from each tube into a clean 1.5 mL centrifuge tube. The remaining 2 mL of the cultures were sealed with Nescofilm and stored at 4 °C to allow subsequent recovery of positive clones. This was followed by centrifugation for 3 min at 4500 x*g*. The supernatant was discarded and the pellet was re-suspended and dissolved by vortexing in buffer P1 (100 µL, composition: Tris-HCl, 50

mM, pH 8.0; EDTA, 10 mM and; RNase A, 100 µg/mL) and then incubated at RT for 5-10 min. Cells were then lysed by the addition of buffer P2 (150 µL, composition: NaOH, 200 mM and SDS, 1%) to each tube with gentle shaking followed by 5 min incubation at RT to allow sufficient lysis. The reaction was then neutralized by addition of ice-cold buffer P3 (150 µL, composition: CH_3CO_2K, 3 M, pH 5.5) with gentle mixing and 5-10 min incubation on ice. The mixture was then centrifuged (16,500 x*g*, 10 min, 4 ºC) and the supernatant (~400 µL) containing DNA was carefully transferred into a new 1.5 mL centrifuge tube. Precipitation of DNA was performed by the addition of isopropanol (0.6x volume, 240 µL) and gentle mixing followed by centrifugation (16,500 xg, 30 min, 4 ºC). The supernatant was then carefully discarded and the pellet washed with ice-cold ethanol (70%, 500 µL) and gentle shaking followed by centrifugation (16,500 x*g*, 15 min 4 °C). Ethanol was then discarded and the pellet allowed to air-dry. The DNA was then dissolved in TE buffer (50 µL, composition: Tris, 10 mM and; EDTA, 1 mM, pH 8.0). DNA solution was then stored at -20 °C until use.

2.2.8.8.2 Quantitive and qualitative measurement of DNA

Quantitative measurement of the DNA product was performed by measuring the optical density (OD) of a sample (2 µL) diluted in water (500 µL), where water was used as a blank at a wavelength 260 nm. The concentration of the DNA was obtained by entering values of OD_{260nm}, dilution used and the volume of the DNA sample to the equation:

$$\text{DNA concentration}\,(\mu g/\mu L) = OD_{260} \times \text{dilution factor} \times \text{DNA stock volume}/1000$$

Furthermore the quality of the DNA preparation was checked by measuring the ratio of OD_{260nm}/OD_{280nm} where values between 1.7 and 2.0 are considered as sufficiently pure DNA (Sambrook, 2001).

2.2.8.8.3 Diagnostic restriction digest of constructs

Diagnostic restriction digests for NMU1-eGFP and NMU2-eGFP were performed in a 20 µL reaction volume. NMU1-eGFP (0.85 µg/µL, 1 µL) was incubated with BSA (10 mg/mL, 0.2 µL), XhoI (20,000 units/mL, 0.3 µL), SnaBI (5000 units/mL, 0.5 µL), NEB buffer 4 (recommended by the manufacturer for both enzymes, 2 µL) and water to 20 µL. The NMU2-eGFP construct (1.1 µg/µL, 0.8 µL) was incubated with BSA (10 mg/mL, 0.2 µL), BamHI (20,000 U/mL, 0.3 µL), BamHI buffer (10x, 2 µL) and water to 20 µL. Both reactions were carried out at 37 °C for 1.5 h followed by running the sample on an agarose gel (0.76%) stained with GelRed and visualization of the fragments bands under UV light as described earlier (see **Section 2.2.8.3**).

2.2.8.8.4 Bacterial culture and preparation of medium scale DNA plasmid preparation (Midiprep)

The rationale for culturing a transformed colony on a larger scale is to make a glycerol stock (see **Section 2.2.8.8.5**) for the clone of interest and preparation of an adequate quantity of plasmid for transfection into mammalian cells. Larger quantities of plasmid were produced using QIAGEN plasmid midi kits which can result in a yield of approximately 100 µg. For bacterial culture, one clone was chosen from five clones which had been confirmed to contain the construct of interest. In a 250 mL autoclaved flask containing 50 mL LB medium and kanamycin (50 µg/mL), 100 µL of the cell suspension (from the original culture, which was made for the miniprep and stored at 4 °C) was added and the flask covered with foil and incubated overnight in a bacterial incubator at 37 °C with continuous shaking (220-230 r.p.m.). All steps following bacterial culture were identical to the miniprep procedure and performed exactly according to the manufacturer's instructions with regards to the volumes of the buffers.

2.2.8.8.5 Glycerol stocks of transformed bacterial clones

For future use of NMU1-eGFP or NMU2-eGFP constructs, glycerol stocks of *E.coli* expressing the vectors were made. In each 2 mL cryotube, freshly made bacterial culture (600 µL) was added to glycerol (50% *v/v*, 300 µL) with gentle mixing. These stocks were

kept at -80 °C. Frozen bacterial cells could then be grown from the glycerol stock by scrapping with a sterile plastic inoculating loop and spreading onto a fresh LB agar plate containing kanamycin.

2.2.9 Transfection and generation of stable cell-lines expressing either NMU1-eGFP or NMU2-eGFP

The calcium phosphate transfection method (Graham *et al.,* 1973) was used to transfect HEK293 cells with either NMU1-eGFP or NMU2-eGFP due to the ease of transfection of this cell-type. HEK293 cells were grown for 2 weeks in antibiotic-free medium. Before performing the experiments, sterile HEPES-buffered saline (2x HBS, composition; HEPES, 50 mM; NaCl, 280 mM and; Na_2HPO_4, 1.5 mM, pH 6.95) was prepared by filtration through a 0.2 µm filter and stored at -20 °C in 500 µL aliquots.

On the day of experiments, cells were plated in a 6 cm dishes 6 h prior to transfection. Just before transfection, either the NMU1-eGFP or NMU2-eGFP construct (8 µg, 7-9 µL) was added to $CaCl_2$ (2 M, 50 µL) in sterile, autoclaved 1.5 mL microfuge tubes and water added to 400 µL. The solution was added drop-wise to 2x HBS (400 µL) with continuous gentle shaking during the addition. The mixture was then added drop-wise to the cells and the plate transferred to a 95% humidified air: 5% CO_2 incubator at 37 °C. The medium was changed 6 h following the transfection to remove dead cells and selection with Geneticin (G418, 1 µg/mL) antibiotic begun 24 h after transfection and continued for 21 days. The medium containing G418 was changed every 48-72 h. During antibiotic selection, thirteen HEK293 clones for NMU1-eGFP and 8 clones for NMU2-eGFP were obtained by plating cells at a dilution of 1 cell/well in a 96-well plate. Cells from each clone were then transferred to 24-well dishes during selection with G418. The cells were then transferred to 6-well plates for further selection. When they reached ~60% confluency, the cells were then cultured in 175 cm^2 flasks and cultured under standard conditions as described earlier (see **Section 2.2.1**) in growth medium containing G418 (200 µg/mL).

2.2.10 Buffer used to investigate NmU-mediated signalling

Unless otherwise stated for NmU-mediated signalling experiments Krebs-HEPES buffer was used (KHB, composition: NaCl, 118 mM; KCl, 4.7 mM; HEPES, 10 mM; glucose, 11.7 mM; $MgSO_4$, 1.2 mM; $NaHCO_3$, 4.2 mM; KH_2PO_4, 1.2 mM and; $CaCl_2$, 1.3 mM, pH 7.4). BSA (0.1% *w/v*) was added to KHB in all NmU signalling experiments and the solution referred to simply as 'KHB'.

2.2.11 Measurement of protein synthesis

HEK-NMU2 cells were cultured in 6-well plates for 48-72 h until 60-70% confluent. Cells were then serum-starved for 1 h in KHB. Cells were then incubated with either cycloheximide (17.5 μM) or vehicle (0.1% ethanol) for 30 min. [^{35}S]methionine (10 mCi/ml, 2 μL/mL) was added to the cells and incubated for a further 2 h. The solution was then removed from each well and the cells were washed with KHB and then lysed in ice cold lysis buffer (110 μL/well, composition; β-glycerophosphate, 10 mM; Tris-HCl, 50 mM, pH 7.5; Triton X-100, 1% *v/v*; EDTA, 1 mM; EGTA, 1 mM; Na_3VO_4, 1 mM; benzamidine-HCl, 1 mM; phenylmethylsulphonyl fluoride, 0.2 mM; leupeptin (1 μg/mL); pepstatin, (1 μg/mL); β-mercaptoethanol, 0.1% *w/v*, and NaF, 50 mM). The lysates were then centrifuged for 10 min at 16,500 x*g* and the supernatants analysed for total protein content by Bradford assay. Protein (10 μg, 5μL) from each sample was then transferred onto 3 MM Whatman paper (1 cm^2). Samples were then allowed to dry for 30 s and then boiled twice for 1 min, each time in 100 mL of trichloroacetic acid (TCA, 5%, *w/v*) containing L-methionine (0.1 g/L). Samples were then washed with ice-cold TCA (5%, *w/v*), followed by a further wash with absolute ethanol. Papers were dried at 80 °C for 1 h and transferred to 6 mL scintillation vials containing 4.2 mL ALTIMA-FLO AF scintillation cocktail and vortex-mixed for 5 s prior to determination of [^{35}S]methionine incorporation by liquid scintillation counting.

2.2.12 Bradford assay for estimation of protein concentration

Protein standards were prepared by diluting BSA (2 mg/mL) into concentrations of 0, 0.125, 0.25, 0.5, 1, and 2 mg/mL. Bradford reagent was diluted (1:5 *v/v*) with water. From each sample or standard, a 10 µL aliquot was added to a 2 mL cuvette containing 1 mL of diluted Bradford reagent (each test performed in duplicate). Following mixing of the solution by covering each cuvette with parafilm and invert slowly two times, the reactions were incubated at RT for 20 min. The absorbance was measured at 595 nm using a spectrophotometer (WPA UV 1101, Biotech Photometer, Cambridge, UK). Standard curves were fitted using GraphPad Prism (GraphPad Software Inc., San Diego, CA, USA). Protein concentrations were calculated by interpolation of the standard curve.

2.2.13 Measurement of changes in $[Ca^{2+}]_i$

Changes in $[Ca^{2+}]_i$ were monitored in single cells by confocal microscopy or in populations of cells using a NOVOstar plate reader. Cells were pre-incubated with the loading buffer, which includes BSA (0.1% *w/v*) and Fluo-4 as the fluorescent Ca^{2+} indicator. The latter is commercially available as a cell-permeant acetoxymethyl ester form (Fluo-4-AM). Once inside the cytoplasm, the acetoxymethyl ester is cleaved by cytosolic esterases and the trapped fluo-4 is available to bind Ca^{2+}. The increase in fluorescence associated with Ca^{2+} binding can be monitored using an excitation wavelength of 488 nm with detection > 500 nm. Loading buffer also included pluronic acid F-127, a non-ionic surfactant (0.036%, *w/v*) added to the loading buffer to facilitate the solubility of fluo-4 in physiological buffer. In some cell-lines, organic-anion transporters can extrude fluo-4 at a high rate, which leads to poor loading and/or high background signals. This was particularly problematic in the present study when using certain cell-lines as described below. In this case, probenecid (2.5 mM), an inhibitor of organic-anion transporters, was added to the loading buffer to inhibit dye extrusion (see **Section 2.2.1.3.1**).

2.2.13.1 Fluo-4-AM loading conditions

The concentration of fluo-4-AM, the loading time and temperature were optimized for each cell-line along with an assessment of whether or not probenecid was required (Table 2.1). The loading buffer for all cell-lines was KHB-BSA (0.1%), pluronic acid F-127 (0.036%, *w/v*) and fluo-4-AM (Table 2.1).

Table 2.1. Optimized fluo-4 loading conditions for cell-lines and primary cells and temperature for each all cell types.

Cell type	Fluo-4-AM concentration (µM)	Probenecid (2.5 mM)	Time (min)	Temperature (°C)
HEK-NMU1 **HEK-NMU2** **HEK-NMU1-eGFP** **HEK-NMU2-eGFP**	2	No	45	37
MIN6	3	Yes	30-40	25
INS-1E	3	Yes	50	25
KYSE140	2	No	45	37
SH-SY5Y	4	No	45	37
SU.86.86.	4	Yes	50	25
AsPC1	3	Yes	50	25
Rat colonic (SMC)	3	No	30	25
Rat cardiac (SMC)	5	No	30-45	37
Pig coronary artery (SMC)	3	no	45	37

2.2.13.2 Single-cell $[Ca^{2+}]_i$ imaging and $[Ca^{2+}]_i$ measurement by confocal microscopy

Cells were cultured on 25 mm coverslips for 24-48 h to reach 60% confluency. Cells were then washed once with KHB and loaded with fluo-4-AM. Cells were then washed with KHB and mounted in a chamber with the coverslip forming the base and KHB (450 µL) was added to the chamber (total chamber volume 0.5 mL). Images were taken using an Olympus inverted microscope with a 60x oil immersion lens and a PerkinElmer Ultra*VIEW* confocal imaging system (PerkinElmer LAS (UK) Ltd, Beaconsfield, UK) using a laser excitation wavelength of 488 nm and emitted light collected at wavelengths >510 nm. The desired temperature was maintained by a Peltier unit (Harvard Applications Inc, Kent, UK). Basal images were taken at least 30 s before bath addition of 50 µL (10x dilution) of the agonist. The change in fluorescence was recorded using Ultra*VIEW* 4.0 software and analyzed as an index of $[Ca^{2+}]_i$ relative to the basal levels using GraphPad Prism (GraphPad Software Inc., San Diego, CA, USA). In experiments where repetitive agonist addition was applied, washes between additions were performed by perfusion of the cells with KHB.

2.2.13.3 Measurement of Ca^{2+} signalling in cell populations using a NOVOstar plate reader

Cells were plated in poly-D-lysine coated 96-well plates (200 µL of cell suspension/well) and cultured to confluency. On the day of experiments, growth medium was aspirated and the cells were washed twice with KHB and loaded with fluo-4-AM. Cells were then washed once with KHB and incubated with 100 µL KHB at 37 °C for 5 min. Using a NOVOstar plate reader (BMG LABTECH, Offenburg, Germany), the change in fluorescence upon addition of buffer or agonist (automated addition of 20 µL at a speed of 230 µL/s from reagent plate to measurement plate, which contained 100 µL/well) was measured as an index of changes in $[Ca^{2+}]_i$. Experiments were performed at

37 °C unless otherwise stated. In desensitization protocols, challenge was performed manually using a similar volume to that used to challenge cells in the NOVOstar plate reader.

2.2.13.3.1 Chemical treatments in resensitization experiments

All of the chemical interventions in the resensitization experiments (see **Chapter 6**) were begun 30-60 min prior to the first challenge with agonist (desensitizing challenge) and continued throughout all subsequent experiments steps. Each chemical was dissolved in appropriate solvent at the desired concentration (Table 2.2) according to the manufacturer's recommendations and the cells were treated with either the chemical or buffer containing the same solvent (vehicle).

Table 2.2. Concentrations and solvents for the chemicals used in resensitization experiments.

Chemical	Solvent	Concentration
cycloheximide	ethanol	17.5 µM
monensin	ethanol	50 µM
monodansyl cadaverine	PBS	400 µM
dynasore hydrate	DMSO	80 µM
concavalin A	PBS	250 µg/mL
phenylarsine oxide	DMSO	5 µM
SM-19712	H_2O	10-100 µM

2.2.14 α-actin staining of colonic smooth muscle cells

Rat colonic smooth muscle cells were isolated through two enzymatic digestion steps as described earlier (see **Section 2.2.5**) and cultured on sterile, untreated 13 mm glass coverslips for 6 days. Cells were then washed three times with D-PBS and then fixed by addition of methanol (100%, 0.5 mL, -20 °C) and incubated at -20 °C for 10 min. Cells were then washed three times with D-PBS followed by an overnight incubation at 4 °C with monoclonal α-actin primary antibody (1:500 in D-PBS containing 10% goat serum). The next day, cells were washed three times with D-PBS, and incubated for 2 h at RT in the dark with FITC-conjugated goat anti-mouse secondary antibody (1:200, D-PBS containing 10% goat serum) followed by three washes as described above. Coverslips were then washed three times and incubated for 5 min at RT with propidium iodide (1:3000), which was then also washed three times as described above. One drop of ProLong® Gold Antifade mounting medium (Invitrogen; Oregon, USA) was then added onto a microscope glass-slide and the coverslip inverted and mounted on the glass-slide and sealed by nail varnish. The slide was stored at -20 °C protected from light until use. The glass-slides were mounted on a Nikon ECLIPSE TE2000-S fluorescence microscope (Nikon UK Limited, Surrey, UK) with a 40x objective lens. The DNA (DAPI) and α-actin (FITC) staining were viewed using different filters at excitation of 402 nm, 490 nm and emission of 455 nm and 525 nm, respectively.

2.2.15 Imaging and binding of Cy3B-pNmU-8 to cell-lines expressing NMU

Cy3B-pNmU-8 was generated and generously provided by GlaxoSmithKline. Cy3B-NHS ester (Amersham, UK) was conjugated to the *N*-terminal end of pNmU-8. Cy3B-pNmU-8 was visualized when bound to NMU using confocal microscopy with an excitation wavelength of 568 nm as described below.

HEK-NMU1 and HEK-NMU2 were cultured on 25 mm glass coverslips coated with poly-D-lysine for 24-48 h. Cells were then washed with KHB and mounted in a chamber

with the coverslip forming the base. 450 µL KHB was added to the chamber. Direct bath addition of Cy3B-pNmU-8 (100 nM, 50 µL to give 10 nM final concentration) was performed and images taken using an Olympus inverted microscope with a 60x oil immersion lens and a PerkinElmer Ultra*VIEW* confocal imaging system (PerkinElmer LAS (UK) Ltd, Beaconsfield, UK). Cells were excited using a Kr/Ar laser at a wavelength of 568 nm and emission was collected at approximately 570 nm using a red-green-blue (RGB) filter. The desired temperature was maintained at the coverslip holder by a Peltier unit (Harvard Applications Inc, Kent, UK). For experiments where long washing periods were required or a different pH used, cells were perfused (5mL/min) using KHB with either pH 7.4 or different pH values.

2.2.16 Confocal imaging of NMU2-eGFP and quantification of receptor internalization.

HEK-NMU2-eGFP were grown on 25 mm coverslips for at least 24 h. Cells were then washed with KHB at 37 ºC and mounted in a perfusion chamber containing KHB heated to 37 °C using a Peltier unit. The chamber volume was 0.5 mL and where required was perfused at 5 mL/min. Addition of hNmU-25 (30 nM, 5 min) was performed directly to the bath containing the coverslip. Following 5 min, the coverslip chamber was perfused with either pH 2.0 solution for ~20 s and then with KHB pH 7.4 for 1 min or only with normal KHB pH 7.4 for the same period. Cells were exposed to 1 min perfusion every 10 min throughout experiment period. Cells were imaged using an Ultra*VIEW* confocal microscope (PerkinElmer LAS, Beaconsfield, Bucks., U.K.) with a 60x oil-immersion objective lens and an excitation wavelength of 488 nm using Kr/Ar laser line. Emitted light was collected above 510 nm for the fluorescent emission of eGFP. The procedure for quantification of receptor internalization was adapted from previous work in the laboratory (Huang, 2011b). Images were captured at 0 min (before the ligand was added) and at 2.5, 5, 10, 20, 30, 40, 50 and 60 min following ligand addition. For at least 6 individual cells in each experiment (i.e. each coverslip), fluorescence intensity was measured at a region of the plasma membrane and within the cytosolic compartment and internalization was calculated using **equation 2.1**.

Equation 2.1

$$\text{Internalisation (\%)} = [1-(Fm_t/Fc_t)/(Fm_b/Fc_b)]\times 100\%$$

where F_m is membrane fluorescence, F_c is cytoplasmic fluorescence, t is time and b is basal (0 min). Fm_b and Fc_b represent these parameters under basal conditions at the begining of the experiment.

2.2.17 Cyclic AMP measurement

Cells were cultured on poly-D-lysine-coated 24-well plates for 48 h. In some experiments, cells were incubated in growth medium alone or with the inhibitor of $G\alpha_{i/o}$ coupling, pertussis toxin (PTX, 100 ng/mL) for a further 12 h. Cells were then washed twice with KHB (0.5 mL/well) and incubated with KHB (450 µL) containing IBMX (500 µM) for 10 min at 37 °C. IBMX was included in all cAMP experiments unless otherwise stated. Cells were then incubated for a further 10 min following addition of KHB (50 µL) alone or KHB containing different concentrations of the agonist. Following 10 min, KHB (50 µL) alone or containing forskolin (to directly stimulate adenylyl cyclase) at the required concentration was added to each well for a further 10 min at 37 °C. The reaction was terminated by aspiration of solution and the addition of ice-cold TCA (0.5 M, 400 µL). The 24-well plate was incubated on ice for at least 15 min. For cAMP extraction (Coopman *et al.*, 2010), TCA (400 µL) was transferred from each well to a 1.5 mL microfuge tube containing EDTA (10 mM, pH 7.0, 50 µL). A mixture of 1,1,1-trichlorotrifluoroethane and tri-*n*-octylamine (1:1 *v/v*, 500 µL) was then added to each tube to neutralize the acidity of the solution. Each tube was then vortex-mixed and incubated for 15 min at RT and then centrifuged at 15,700 x*g* for 2 min and 200 µL of the upper aqueous phase transferred to a fresh tube containing $NaHCO_3$ (60 mM, 50 µL). Samples were then stored at 4 °C prior to assay of the cAMP the next day. In 8 random wells, cells were lysed with NaOH (0.1 M, 500 µL) and protein concentration was

determined by Bradford assay (see **Section 2.2.12**). The level of cAMP was assessed by radio-receptor assay (BROWN *et al*, 1971), which is based on the competition between the generated cAMP and [^{3}H]cAMP for binding to the regulatory subunit of protein kinase A (PKA) which is prepared from cow adrenal glands (cAMP binding protein). A range of standard cAMP concentrations (0-10 pmol) were made in cAMP buffer (composition: Tris-HCl, 50 mM; EDTA, 4 mM; pH 7.5) to generate a standard curve. In fresh 1.5 mL microfuge tubes, 50 µL of either standard or sample was mixed with [^{3}H]cAMP (42 Ci/mmol, 100 µL) and then cAMP binding protein (150 µL) was added to each tube. Each tube was then vortexed and incubated on ice for 90 min and binding competition terminated by addition of ice-cold charcoal-BSA-cAMP buffer (250 µL, composition: cAMP buffer, 50 mL; charcoal, 0.5% (*w/v*); BSA, 2% *w/v*). The mixture was vortex-mixed and incubated for 10 min at RT, followed by additional vortex-mixing and centrifugation at 16,100 x*g*, 4 °C for 4 min. Supernatant (400 µL) from each tube was transferred to a 6 mL scintillation vial and Safefluor scintillation liquid (4.2 mL) was added. Radioactivity was then measured by liquid scintillation counting. The cAMP concentration was obtained from a standard curve generated for standard cAMP values using GraphPad Prism software 5.0 and the final cAMP concentration calculated as pmol/mg protein.

2.2.18 Cyclic AMP measurement in cardiac myocytes

Following isolation of cardiac myocytes, cells were suspended in 3 mL of oxygenated 2 mM Ca^{2+}-Tyrode's solution containing BSA (0.1%). Each 100 µL of cell suspension was transferred to a 1.5 mL microfuge tube. Tyrode's solution (100 µL) containing IBMX (500 µM) was added to each tube and incubated in a 37 °C water-bath for 10 min with gentle shaking. Cells were then incubated for a further 10 min following addition of KHB (50 µL) alone or KHB containing different concentrations of rNmU-23. After 10 min, buffer (50 µL) alone or buffer containing forskolin (10 µM) was added to each tube for a further 10 min at 37 °C. The reaction was terminated by the addition of ice-cold (1 M, 300 µL) TCA. Tubes were then kept on ice for at least 20 min followed by centrifugation at 15,700 x*g* for 2 min at 4 °C. A 400 µL aliquot of the supernatant from each sample was

then transferred to a new 1.5 mL microfuge tube to complete the cAMP extraction procedure. The extraction and assay method of cAMP used was identical to the one used for adherent cells (see **Section 2.2.16**). Each treatment was performed in triplicate.

2.2.19 Measurement of total [^{3}H]inositol phosphate generation

For each cell-line, cells were cultured in 24-well plates and incubated with *myo*-[^{3}H]inositol (2 μCi/mL) for 48 h. Growth medium was then removed and the cells were washed twice with KHB (0.5 mL) carefully and then incubated with KHB (450 μL) containing LiCl (10 mM, 10 min, 37 °C) prior to agonist addition. LiCl addition results in uncompetitive blockade of inositol monophosphatase activity (Allison *et al.*, 1976), leading to inhibition of the conversion of inositol monophosphates to inositol. This results in the accumulation of inositol (poly)phosphates ($InsP_x$). Cells were then incubated with KHB (50 μL) alone or with agonist (10x of the final concentration) for a further 15 min at 37 °C. Reactions were terminated by removal of the solution and addition of ice-cold TCA (0.5 M, 0.5 mL) followed by incubation of the plate on ice for at least 20 min. The whole 0.5 mL of TCA was transferred from each well to a new 1.5 mL microfuge tube containing EDTA (10 mM, pH 7.4, 100 μL) and neutralized by the addition of a freshly prepared mixture of 1,1,1-trichlorotrifluoroethane and tri-*n*-octylamine (50:50 *v/v*, 500 μL). Samples were incubated at RT for 15 min with vortex mixing every 5 min followed by centrifugation at 15,700 x*g* for 2 min. A 400 μL aliquot of the upper aqueous phase was then transferred to a fresh tube containing $NaHCO_3$ (62.5 mM, 100 μL). Samples were stored at 4 °C prior to separation and recovery of the [^{3}H]$InsP_x$ fraction. Anion exchange chromatography was used to extract $InsP_x$ (Challiss *et al.*, 1994) using Dowex AG1-X8 ammonium formate columns. Columns were washed with regeneration buffer (2 M ammonium formate/0.1 M formic acid, 10 mL) followed by washing with distilled water (20 mL). Samples were vortex-mixed and added to the column. Columns were then washed with distilled water (5 mL). Following full drainage, borax buffer (60 mM ammonium formate/5 mM $Na_2B_4O_7$, 10 mL) was added to each column. Fractions of [^{3}H]$InsP_x$ were eluted from the columns by addition of elution buffer (0.75 M ammonium formate/0.1 M formic acid, 10 mL). Using a 20 mL scintillation vial, 5 mL of the eluted

fraction was mixed with 8 mL of ALTIMA-FLO scintillant and [^{3}H]InsP_x were determined by liquid scintillation counting. [^{3}H]InsP_x accumulation was calculated as a percentage increase of the basal level.

2.2.20 Western blotting

2.2.20.1 Cell stimulation and sample preparation

Cell monolyers on poly-D-lysine coated 24-well plates were serum starved overnight. On the day of the experiments, growth medium was removed, and the cells were washed twice with KHB (0.5 mL). To construct concentration-response curves for agonist-stimulated increases in extracellular signal-regulated kinase phosphorylation (pERK), cells were incubated with KHB (1 mL) and challenged with KHB (110 µL) alone or containing different concentrations of hNmU-25 (0.1-100 nM) for 5 min. For investigation of the time-course activation of pERK generation, cells were incubated for 30 min with KHB (1 mL) alone or where required containing SM-19712 (10 µM). In these circumstances, chemical treatment was included in all subsequent experimental steps. Cells were then challenged with KHB (110 µL) alone or containing hNmU-25 (30 nM) for 5 min and the solution then replaced with KHB (1 mL) alone or containing SM-19712 (10 µM) for 5-180 min. Stimulation was begun at the longest time-point first, allowing all of the reactions to be terminated at the same time. At the end of the reaction, cells were washed twice with ice-cold PBS and lysed by addition of ice-cold 2x sample buffer (composition, Tri-base, 125 mM, pH 6.8; Na_3VO_4, 1 mM; SDS, 10% (*w/v*); glycerol, 50% *v/v*; bromophenol blue, 0.01% *w/v*; dithiothreitol, 250 mM (added on the day of the experiment, 110 µL) and incubated on ice for 5 min. It is worth noting here that protein measurement was assessed in each well of a 24-well plate by addition of lysis buffer only and the protein content was equal in each well (Approximately 220 µg/well). Cell lysates were collected using a cell scraper and then transferred to new 1.5 mL microfuge tubes. Samples on ice were then sonicated with a Sonifier Ultrasonic Cell Disruptor (Branson, CT, U.S.A.) for 2 s at 10% amplitude power and stored at -80 °C.

2.2.20.2 Preparation of SDS-polyacrylamide gel and electrophoresis of proteins

Due to the relatively low molecular weight of ERK, a 10% resolving gel (7 mL, composition: acrylamide, 10% *v/v*; Tris-HCl, 375 mM, pH 8.8; sodium dodecyl sulfate (SDS), 0.1% *w/v*; ammonium persulphate (APS), 0.1% *w/v*; N, N, N', N'-tetramethylethylenediamine (TEMED), 0.06% *v/v* and water to 7 mL) was mixed gently and poured in between two glass plates separated by two vertical 1.5 mm spacers of a Mini-BioRad electrophoresis system (Bio-Rad, Hemel Hempstead, UK). The top-layer of the gel was covered with water to ensure a flat edge. Following approximately 20 min, the gel was solidified and the top layer of water discarded carefully. A stacking gel (3 mL, composition: acrylamide, 5% *v/v*; Tris-HCl, 126 mM, pH 6.8; SDS, 0.1% *w/v*; APS, 0.1% *w/v*; TEMED, 0.06% *v/v* and water to 3 mL) was poured onto the top of the resolving gel and a 10-well comb inserted to form loading wells. The gels were left to solidify at RT for a further 30 min. The comb was then removed and the gel mounted into a Mini-BioRad gel electrophoresis tank. The gel tank and the upper loading tank were filled with running buffer (composition: Tris-HCl, 25 mM, pH 8.6; glycine, 192 mM and SDS 0.1% *w/v*). Samples were heated on a heat-block for 5 min at 95 °C and 10 µL of each sample loaded into each well. The first well of each gel was loaded with a pre-stained protein ladder (5 µL, Leon-Rot, Germany). Electrophoresis was performed using a POWER PAC 300 (Bio-Red, Hemel Hempstead, UK) at 140 V until the bromophenol blue dye reached the bottom of the gel (approximately 65 min).

2.2.20.3 Transfer of proteins using the semi-dry electrophoresis technique

PVDF membrane and filter papers were cut to the size of the resolving gel. The membrane was then immersed in methanol (100%) for 30 s and then in H_2O for 2 min. Membrane together with filter papers were then incubated for approx. 5-10 min in transfer buffer (composition: glycine, 40 mM; Tris, 48 mM; SDS, 0.0375% *w/v* and methanol, 20%, *v/v*). Following the removal of the stacking gel, the resolving gel was soaked in transfer buffer. A blotting sandwich was then made by firstly placing three

sheets of filter-paper cut to the size of the resolving gel on the negative plate followed by the PVDF membrane on top. The resolving gel was placed carefully on the top of the membrane and covered by a further three filter papers. The positive charged cover of the semi-dry transfer device was placed carefully on the top of the sandwich. Transfer was carried out using a POWER PAC 200 (Bio-Red, Hemel Hempstead, UK) at 15 V for 35 min.

2.2.20.4 Immunoblotting

Following transfer, membrane was immersed in methanol (100%) for 15 s and allowed to dry for 10 min. The membrane was again immersed in methanol, washed with water and transferred directly to blocking buffer (BSA, 5% in Tris buffered saline with tween (TBST), composition: Tris-base, 50 mM, pH 7.5; NaCl, 150 mM; Tween-20, 0.05% *v/v*) and incubated at RT for 1 h with gentle rocking. The membrane was then incubated in a 50 mL Falcon tube overnight at 4 ºC with TBST (BSA, 5%, 5 mL) containing either rabbit monoclonal phospho-p44/42 MAPK (ERK1/2) antibody (1:2000) or rabbit polyclonal p42 MAPK (ERK2) antibody (1:1000) with continuous rolling. Membranes were then washed three times for 10 min each with TBST (20 mL). This was followed by incubating the membrane in TBST (fat free milk, 5% *w/v*, 10 mL) containing goat anti-rabbit IgG, HRP-linked secondary antibody (1:3000) for 1 h at RT on a gently shaking platform. The membranes were then washed again three times with TBST as described above. Detection was performed by applying UptiLight™ chemiluminescent reagent (1:1 *v/*v, 2 mL/ membrane, 1 min) and exposure of membrane to X-ray film for 5-60 s, depending on the strength of the signal. Proteins of interest were identified by comparison of their size to the protein markers. The pERK signal was quantified as a relative to total ERK.

2.2.21 Data analysis

All data shown were analysed using Graphpad Prism software 4.0 or 5.0 (GraphPad Software Inc., San Diego, CA, USA) and expressed as mean ± s.e.m. Representative data shown are of at least three experiments. For Ca^{2+} response experiments, all raw data were transferred from the NOVOstar plate reader as Excel sheets and analyzed using Graphpad Prism software 4.0 or 5.0 (GraphPad Software Inc., San Diego, CA, USA). Maximal changes in fluorescence were subtracted from the basal recording and measured as an index of $[Ca^{2+}]_i$ and used to construct concentration-response curves, representative traces or columns. For measuring the recovery of either concentration-response curves or maximal Ca^{2+} responses, changes in fluorescence were expressed as a percentage of the maximum response in cells pre-exposed to buffer only (i.e. no initial agonist challenge). All statistical analyses were performed on the raw data before they were normalized. In recovery experiments, for each recovery time-point, a control response was measured to ensure that it was not significantly different from other control responses. An appropriate statistical test was chosen according to the number of the groups and variables, where the difference was considered significant at $p< 0.05$.

Chapter 3

Characterization of recombinantly-expressed NMU1 and NMU2 and pseudo-irreversible ligand binding

3.1 Introduction

Two family A GPCRs have been identified and characterized as receptors for NmU and NmS, and are designated NMU1 and NMU2 (Alexander *et al.*, 2008; Sharman *et al.*, 2011

). NMU1 (previously termed FM3 or GPR66) was firstly isolated from mouse and human cDNA due to its high homology with ghrelin and NT1 receptors (Tan *et al.*, 1998). NMU1 was de-orphanized two years later (Fujii *et al.*, 2000; Funes *et al.*, 2002; Hedrick *et al.*, 2000; Howard *et al.*, 2000; Kojima *et al.*, 2000; Raddatz *et al.*, 2000; Szekeres *et al.*, 2000) followed by NMU2 (previously termed FM-4 or TGR-1). Both NMUs share 51% identity (Howard *et al.*, 2000). This sequence homology is most evident within the transmembrane domains, while variation occurs at the extracellular *C*-terminus and within i3 loop. NMU2 possesses a shorter i3 region than NMU1, while the *C*-terminus of NMU2 is longer than NMU1. NMU1 is expressed mainly in peripheral tissues, while NMU2 is found predominantly though not exclusively in the central nervous system (see **Section 1.1.2**).

Activation of either NMU receptor by NmU resulted in an increase in $[Ca^{2+}]_i$ (Aiyar *et al.*, 2004; Brighton *et al.*, 2004a; Brighton *et al.*, 2008; Fujii *et al.*, 2000; Funes *et al.*, 2002; Gartlon *et al.*, 2004; Hedrick *et al.*, 2000; Hosoya *et al.*, 2000; Howard *et al.*, 2000; Johnson *et al.*, 2004; Kojima *et al.*, 2000; Raddatz *et al.*, 2000; Shan *et al.*, 2000), PLC activity (Aiyar *et al.*, 2004; Brighton *et al.*, 2004a), arachidonic acid release (Aiyar *et al.*, 2004; Brighton *et al.*, 2004a; Fujii *et al.*, 2000; Hosoya *et al.*, 2000), $InsP_x$ generation (Aiyar *et al.*, 2004; Brighton *et al.*, 2004a; Raddatz *et al.*, 2000; Szekeres *et al.*, 2000) and inhibition of forskolin-mediated cyclic AMP generation (Aiyar *et al.*, 2004; Brighton *et al.*, 2004a; Hosoya *et al.*, 2000). Increases in $InsP_x$ and $[Ca^{2+}]_i$ are PTX–insensitive, while inhibition of adenylyl cyclase activity is abolished by PTX pre-treatment suggesting

$G\alpha_{q/11}$ and $G\alpha_{i/o}$ coupling, respectively (Aiyar *et al.*, 2004; Brighton *et al.*, 2004a). Promiscuous coupling of both receptors has also been demonstrated using [^{35}S]GTPγS binding assays with both recombinant (Brighton *et al.*, 2004a) and endogenous (cultured rat colonic smooth muscle cells) NMU-expressing cells (Brighton *et al.*, 2008). However, others did not detect an effect of NmU on adenylyl cyclase activity in HEK293 cells transiently expressing NMU1 (Szekeres *et al.*, 2000). A recent study suggested that NMU1-mediated signalling occurs primarily via $G\alpha_{q/11}$ while NMU2 signalling preferentially occurs downstream of $G\alpha_{i/o}$ (Hsu *et al.*, 2007). Activation of NMUs by NmS had been investigated to a much lesser extent and to date an increase in $[Ca^{2+}]_i$ in Chinese hamster ovary cells recombinantly expressing NMUs has been shown (Mori *et al.*, 2005).

Previous studies have shown that NmU binds pseudo-irreversibly to either NMU1 or NMU2 in a recombinant expression system (Brighton *et al.*, 2004a) and in cultured rat colonic smooth muscle cells (Brighton *et al.*, 2008). These studies demonstrated the pseudo-irreversible binding phenomenon through lack of repetitive Ca^{2+} signalling and failure to displace fluorescently-tagged pNmU-8 (Cy3B-pNmU-8) from the receptor with extended washing or addition of high concentrations of unlabelled NmU. Interestingly, pseudo-irreversible binding of NmU was not suggested with respect to NMU-mediated contraction of strips of rat colonic smooth muscle, where a repetitive, non-desensitizing contraction could be observed even when washing time between applications was reduced to 1 min (Brighton *et al.*, 2008). A low pH buffer can be used to remove NmU, as has been shown previously for high affinity neuropeptides (Haigler *et al.*, 1980; Koenig *et al.*, 1997), but the removal NmU in order to allow rebinding of Cy3B-pNmU-8 to NMUs requires a solution of pH 2.0 (Brighton *et al.*, 2004a). In this Chapter, the effects of NmU and NmS have been explored on $[Ca^{2+}]_i$ mobilization, and forskolin-stimulated cyclic AMP generation in NMU1 or NMU2 stably expressing HEK293 cells. In addition, the effect of PTX pre-treatment on both signalling pathways has been assessed. The irreversible binding of NmU to its receptors is demonstrated here through investigating Ca^{2+} responses to repetitive agonist applications following extended buffer washes and confocal imaging of Cy3B-pNmU-8 binding. Lastly, we investigated the effect of brief pH 2.0 (15-25 s) exposure on NmU rebinding and Ca^{2+} repetitive responses.

3.2 Results

3.2.1 NMU and M_3 mACh receptor-mediated Ca^{2+} changes in cell populations

Changes in fluorescence were monitored as an index of changes in $[Ca^{2+}]_i$ in populations of adherent, fluo-4-loaded cells using a NOVOstar plate reader. Stimulation of either HEK-NMU1 or HEK-NMU2 with either hNmU-25 (Figure 3.1) or hNmS-33 (Figure 3.2) evoked concentration-dependent increases in $[Ca^{2+}]_i$. It is worth noting that untransfected HEK293 did not evoke any responses to NmU or NmS (data not shown). At higher concentrations of either hNmU-25 or hNmS-33 (Figures 3.1a, b and 3.2a, b), the rate of increase in $[Ca^{2+}]_i$ was faster, as well as being of greater amplitude, compared to lower concentrations. For example, for hNmU-25 (30 nM) or hNmS-33 (30 nM), the peak Ca^{2+} responses were achieved within 4-6 s. At lower concentrations of hNmU-25 or hNmS-33 (e.g. 3 nM), peak levels were attained after approximately 9-14 s (Figures 3.1a, b, 3.2a, b). Following the initial peak response, there was a slowly declining phase at all agonist concentrations studied (0.1 - 100 nM), which lasted until the end of the recording (40 s after agonist addition). At the end of the observation period the changes in fluorescence for hNmU-25 (30 nM) were 60 ± 1% and 65 ± 4% (n=3) of the respective peak responses in HEK-NMU1 and HEK-NMU2, while the comparable changes for hNmS-33 (30nM) were 66 ± 2% and 58 ± 1% (n=3).

Overnight pre-treatment of HEK-NMU1 and HEK-NMU2 with PTX did not significantly affect Ca^{2+} responses to either hNmU-25 (Figure 3.1c, d), or hNmS-33 (Figure 3.2c, d). By plotting maximal changes in fluorescence following agonist addition, pEC_{50} values for hNmU-25 in HEK-NMU1 in the absence or presence of PTX pre-treatment were 9.39 ± 0.24 and 9.16 ± 0.12, respectively (Figure 3.1c; n=3), and in HEK-NMU2 were 9.56 ± 0.06 and 9.31 ± 0.03 respectively (Figure 3.1d; n=3). The pEC_{50} values for hNmS-33 in HEK-NMU1 in the absence or presence of PTX pre-treatment were 8.86 ± 0.11 and 8.70 ± 0.05 (Figure 3.2c; n=3), and in HEK-NMU2 were 9.41 ± 0.05 and 8.93 ± 0.11 respectively (Figure 3.2d; n=3).

Activation of endogenously expressed M_3 mACh receptors with carbachol in either HEK-NMU1 (Figure 3.3a, c) or HEK-NMU2 (Figure 3.3b, d) also evoked concentration-dependent increases in $[Ca^{2+}]_i$. The pEC_{50} values for carbachol-evoked Ca^{2+} responses in HEK-NMU1 (Figure 3.3c) and HEK-NMU2 (Figure 3.3d) were 5.63 ± 0.06 and 5.78 ± 0.07 (n=3), respectively.

Removal of extracellular Ca^{2+} (Figure 3.4) immediately prior to stimulation of HEK-NMU2 with hNmU-25 did not affect the peak Ca^{2+} response, but markedly accelerated the rate of decline following the peak response to 35 ± 4% of the peak response at 40 s, while in the presence of extracellular Ca^{2+} the sustain plateau was 73 ± 1% (n=3).

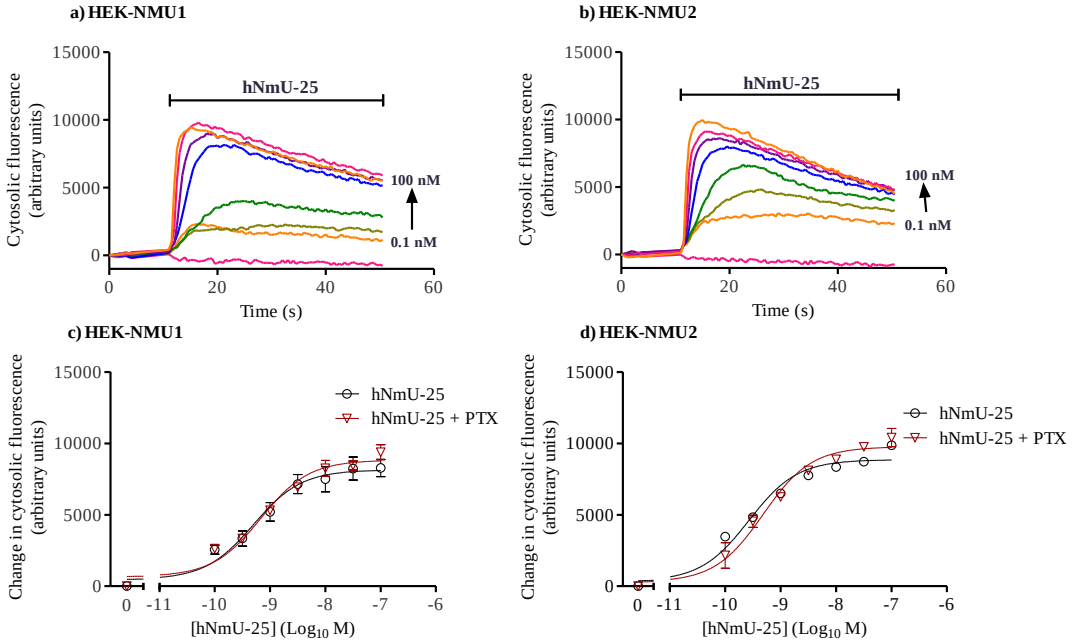

Figure 3.1. Concentration-response curves of hNmU-25-mediated Ca^{2+} responses in HEK-NMU1 or HEK-NMU2. HEK-NMU1 (a, c) or HEK-NMU2 (b, d) were cultured in 96-well plates for 48 h and a further 12 h in either medium alone or with PTX (100 ng/mL). Cells were then loaded with fluo-4-AM followed by challenge with different concentrations of hNmU-25 (0.1 to 100 nM) using a NOVOstar plate reader and changes in cytosolic fluorescence were monitored as an index of $[Ca^{2+}]_i$. Traces shown are representative of 3 experiments showing Ca^{2+} responses at different concentrations of hNmU-25 in cells expressing either NMU1 (a) or NMU2 (b). The maximal changes in fluorescence were used to construct concentration-responses curves for cells expressing either NMU1 (c) or NMU2 (d). The pEC_{50} values for hNmU-25 in HEK-NMU1 incubated with medium alone or with PTX were 9.39 ± 0.24 and 9.16 ± 0.12, respectively and in HEK-NMU2 were 9.56 ± 0.06 and 9.31 ± 0.03, respectively. Data are mean ± s.e.m., n=3.

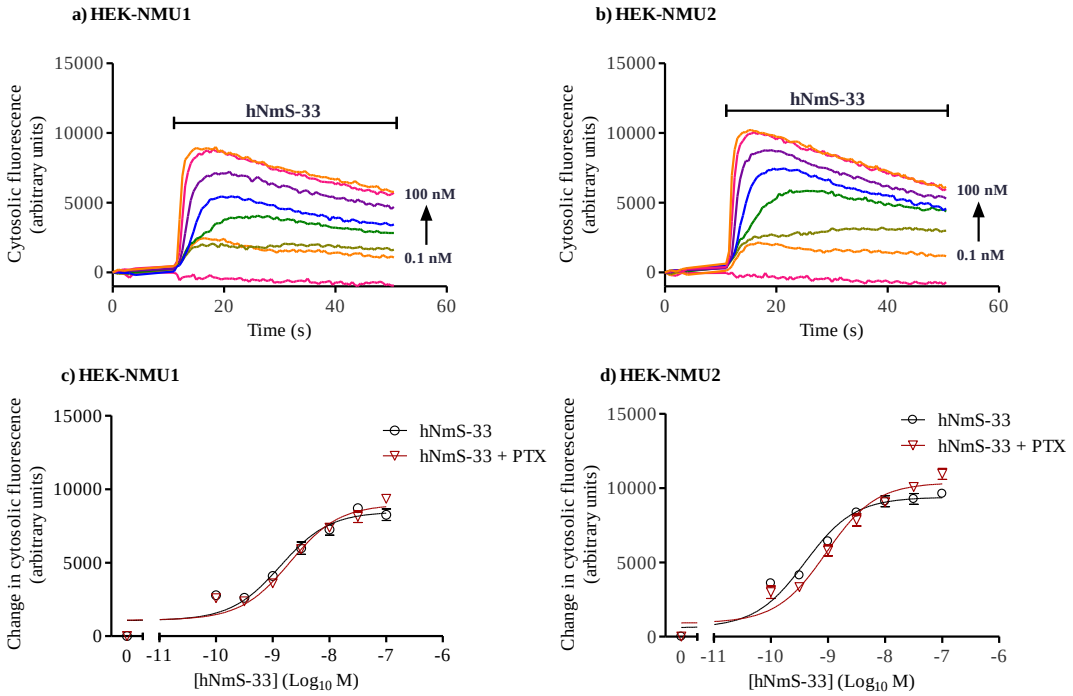

Figure 3.2. Concentration-response curves of hNmS-33-mediated Ca^{2+} responses in HEK-NMU1 or HEK-NMU2. HEK-NMU1 (a, c) or HEK-NMU2 (b, d) cells were cultured in 96-well plates for 48 h and a further 12 h with either medium alone or with PTX (100 ng/mL). Cells were then loaded with fluo-4-AM followed by challenge with different concentrations of hNmS-33 (0.1 to 100 nM) using a NOVOstar plate reader and changes in cytosolic fluorescence were monitored as an index of $[Ca^{2+}]_i$. Traces shown are representative of 3 experiments showing Ca^{2+} responses at different concentrations of hNmS-33 in cells expressing either NMU1 (a) or NMU2 (b). The maximal changes in fluorescence were used to construct concentration-responses curves for either HEK-NMU1 (c) or HEK-NMU2 (d). The pEC_{50} values for hNmS-33 in HEK-NMU1incubated with medium alone or with PTX were 8.86 ± 0.11 and 8.7 ± 0.05, respectively and in HEK-NMU2 were 9.41 ± 0.05 and 8.93 ± 0.11, respectively. Data are mean ± s.e.m., n=3.

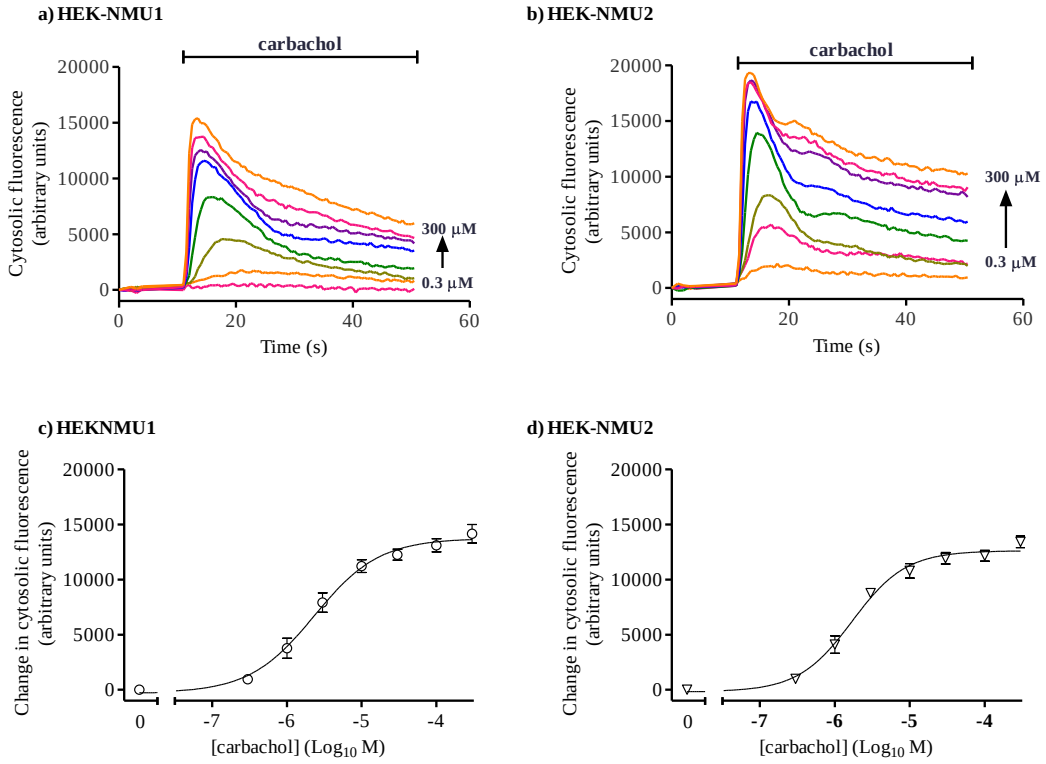

Figure 3.3. Carbachol-stimulated Ca^{2+} responses in HEK-NMU1 or HEK-NMU2. HEK-NMU1 (a, c) or HEK-NMU2 (b, d) were cultured in 96-well plates for 48-72 h. Cells were then loaded with fluo-4-AM and then challenged with different concentrations of carbachol (0.3 to 300 µM) using a NOVOstar plate reader and changes in cytosolic fluorescence were monitored as an index of $[Ca^{2+}]_i$. Traces shown are representative of 3 experiments showing Ca^{2+} responses at different concentrations of carbachol in either HEK-NMU1 (a) or HEK-NMU2 (b). Maximal changes in fluorescence were used to construct concentration-responses curves for HEK-NMU1 (c) and HEK-NMU2 (d). The pEC_{50} values for carbachol in HEK-NMU1 and HEK-NMU2 were 5.63 ± 0.06 and 5.78 ± 0.07, respectively. Data are mean ± s.e.m., n=3.

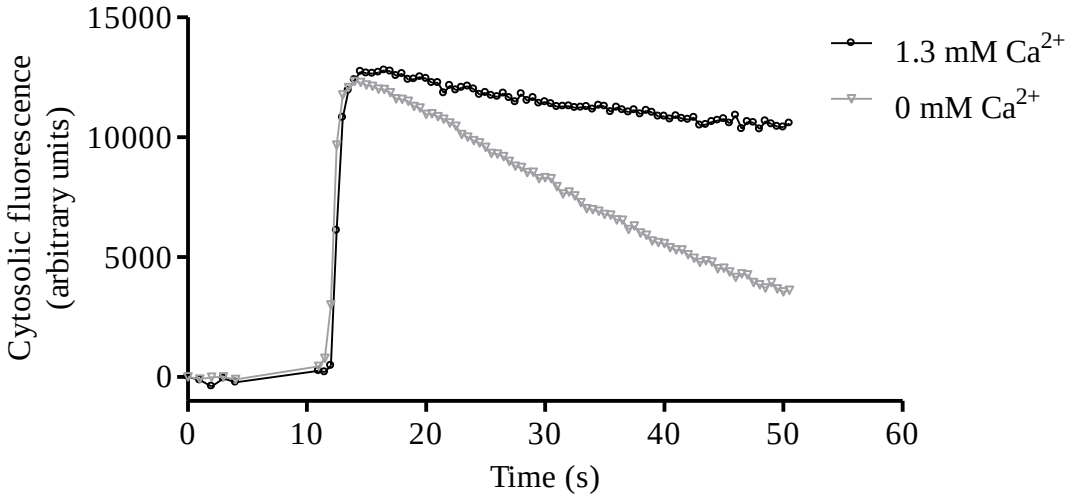

Figure 3.4. Effect of extracellular Ca^{2+} concentration on hNmU-25-mediated Ca^{2+} responses in HEK-NMU2. HEK-NMU2 were cultured in 96-well plates for 48 h. Cells were then loaded with fluo-4-AM and then challenged with hNmU-25 (30 nM) in the presence (1.3 mM) or absence of extracellular Ca^{2+} using a NOVOstar plate reader. Changes in cytosolic fluorescence were monitored as an index of $[Ca^{2+}]_i$. Traces shown are representative of 4 experiments.

3.2.2 Inhibition of forskolin-stimulated cyclic AMP generation

Incubation of HEK-NMU2 with forskolin (1 µM) did not significantly increase cyclic AMP levels (Figure 3.5) unless the non-selective phosphodiesterase inhibitor, IBMX (500 µM), to inhibit cyclic AMP degradation, was also present. In the presence of forskolin + IBMX, cyclic AMP generation increased approximately 30-fold (basal, 3 ± 0.3; +forskolin/IBMX, 90 ± 12 pmol/mg protein; n=3). Addition of hNmU-25 (0.1-100 nM) to HEK-NMU1 or HEK-NMU2 pre-incubated with IBMX (Figure 3.6a and b) 10 min prior to challenge with forskolin (1 µM, 10 min) resulted in concentration-dependent inhibition of cyclic AMP generation: pIC_{50} values were 8.12 ± 0.07 and 8.01 ± 0.09 (n=3) in HEK-NMU1 and HEK-NMU2, respectively. Similarly, pre-treatment of HEK-NMU1 or HEK-NMU2 (Figure 3.7a and b) with hNmS-33 (0.1-100 nM) for 10 min followed by forskolin (1 µM, 10 min) also caused robust inhibition: pIC_{50} values of hNmS-33 in HEK-NMU1 and HEK-NMU2 were 8.10 ± 0.06 and 7.97 ± 0.13 (n=3), respectively. Overnight incubation of the cells with PTX (100 ng/mL) abolished the inhibitory effect of either hNmU-25 or hNmS-33 (Figures 6 and 7); indeed, pre-treatment with PTX tended to increase cyclic AMP generations in response to forskolin.

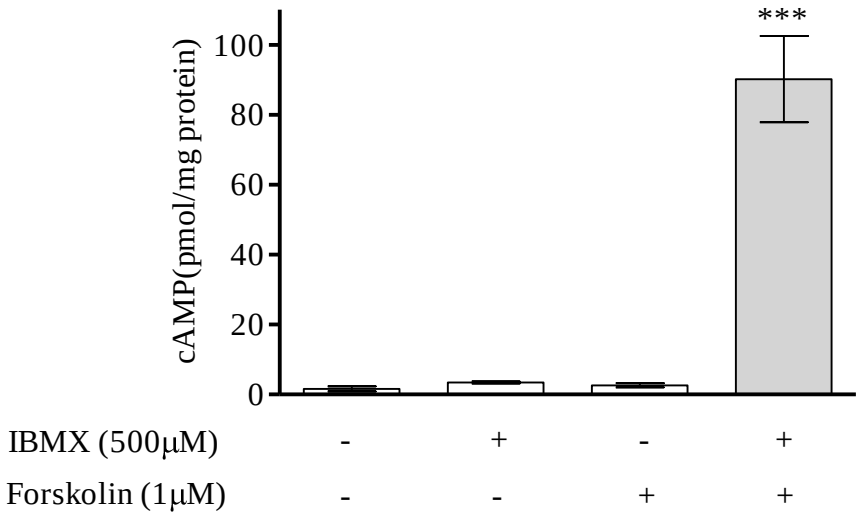

Figure 3.5. Effect of IBMX on forskolin-stimulated cyclic AMP generation in HEK-NMU2. HEK-NMU2 were cultured for 48 h in 24-well plates pre-coated with poly-D-lysine. Cells were incubated with buffer only or with forskolin (1 μM) for 10 min in the presence or absence of IBMX (500 μM) before extraction and measurement of cyclic AMP. Data are mean ± s.e.m, n=3; $^{***}P<0.001$, by Bonferroni's multiple comparison test following one-way ANOVA.

a) HEK-NMU1

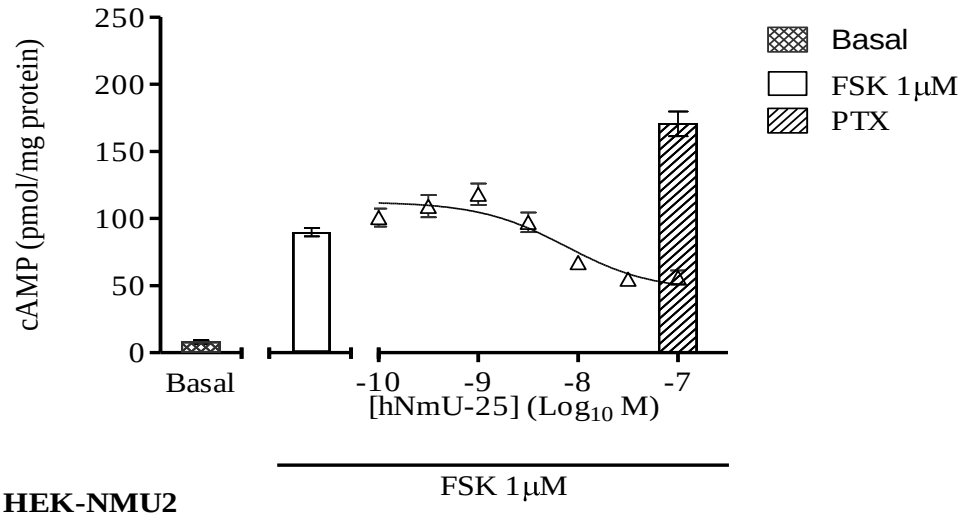

b) HEK-NMU2

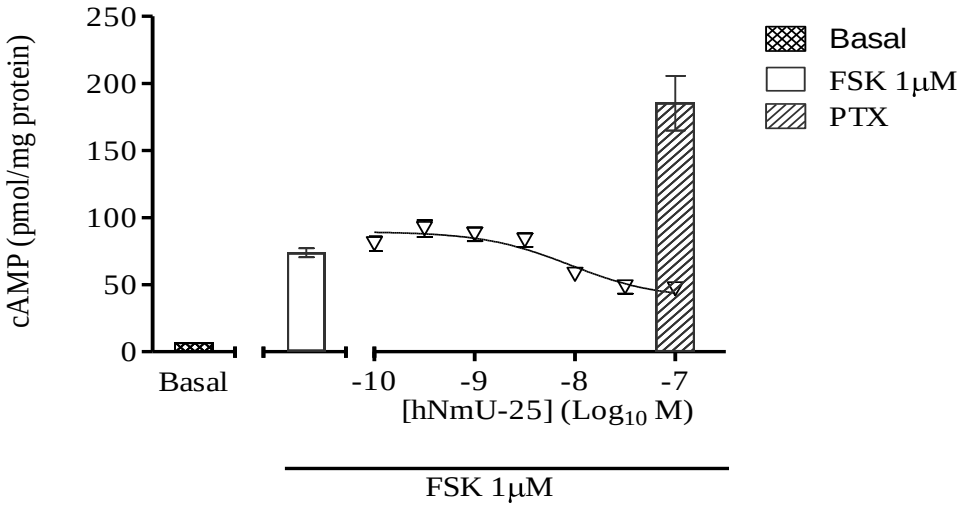

Figure 3.6. hNmU-25-mediated inhibition of forskolin-stimulated cyclic AMP generation in HEK-NMU1 or HEK-NMU2. HEK-NMU1 (a) or HEK-NMU2 (b) were cultured in 24-well plates pre-coated with poly-D-lysine for 48 h and for a further 12 h in the absence or presence of PTX (100 ng/mL. Cells were pre-incubated with IBMX (500 μM, 10 min) before addition of different concentrations of hNmU-25 (0.1-100 nM) for 10 min prior to stimulation with forskolin (FSK, 1 μM) for 10 min. Left and centre segments of each panel show basal and forskolin-stimulated cyclic AMP levels, respectively. The right segment of each panel shows concentration-dependent inhibitions of forskolin-stimulated cyclic AMP generation by hNmU-25 (pIC_{50} values of 8.12 ± 0.07 and 8.01 ± 0.09 in HEK-NMU1 and HEK-NMU2, respectively) and the effect of PTX. Data are shown as mean ± s.e.m, n=3.

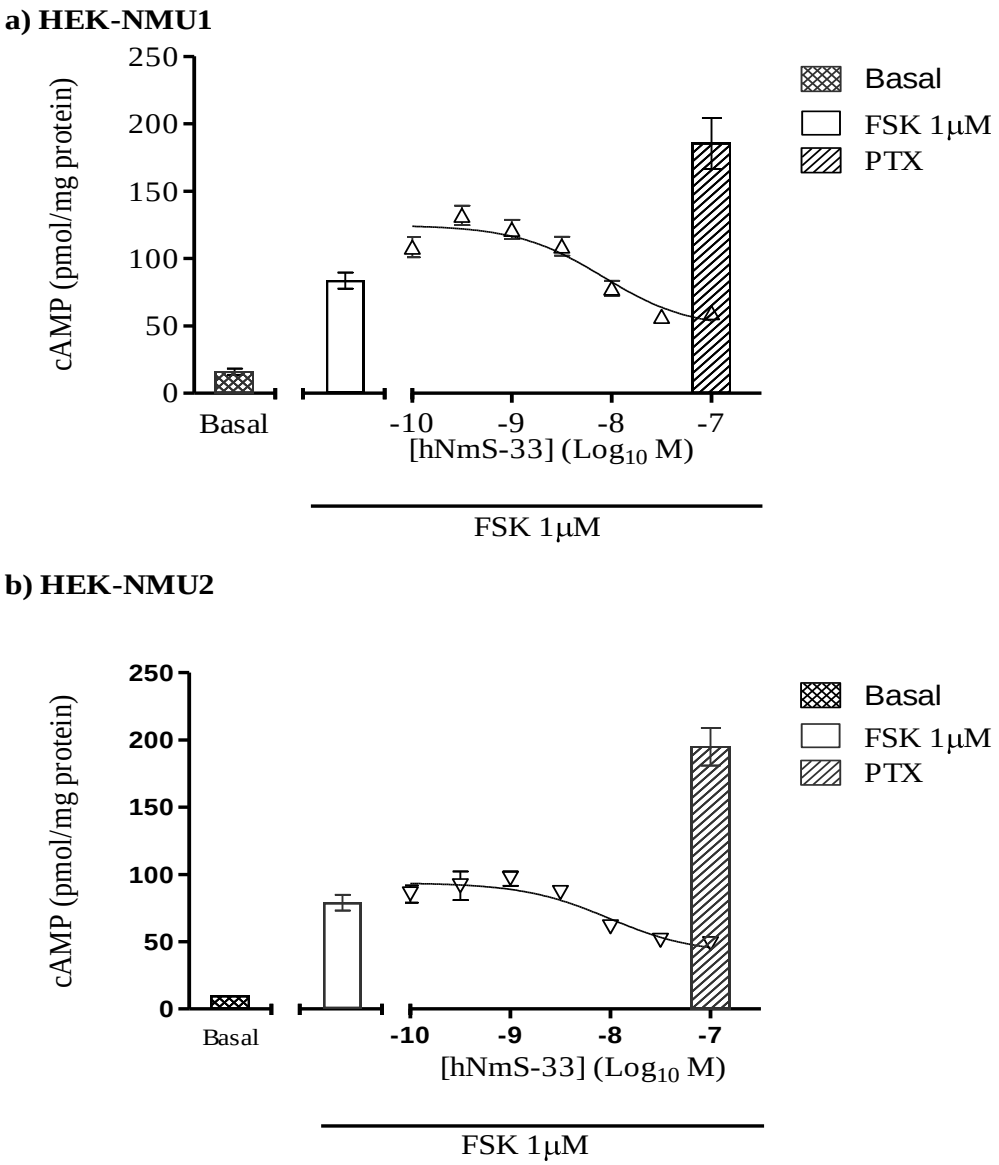

Figure 3.7. hNmS-33-mediated inhibition of forskolin-stimulated cyclic AMP generation in HEK-NMU1 or HEK-NMU2. HEK-NMU1 (a) or HEK-NMU2 (b) were cultured in 24-well plates coated with poly-D-lysine for 48 h and a further 12 h in the absence or presence of PTX (100 ng/mL). Cells were pre-incubated with IBMX (500 μM, 10 min) before addition of different concentrations of hNmS-33 (0.1-100 nM) for 10 min prior to stimulation with forskolin (FSK, 1 μM) for 10 min. Left and centre segments of each panel show basal and forskolin-stimulated cyclic AMP levels, respectively. The right segment of each panel shows concentration-dependent inhibitions of forskolin-stimulated cyclic AMP generation by hNmS-33 (pIC_{50} values of 8.10 ± 0.06 and 7.97 ± 0.13 in HEK-NMU1 and HEK-NMU2, respectively) and the effect of PTX. Data are shown as mean ± s.e.m, n=3.

3.2.3 Irreversible binding of fluorescently-labelled NmU (Cy3B-pNmU-8) to HEK-NMU1 or HEK-NMU2

Confocal imaging of cells demonstrated that addition of Cy3B-pNmU-8 (10 nM) to HEK-NMU1 or HEK-NMU2 (Figure 3.8 ia, b and iia, b) resulted in an intense membrane-localized fluorescence. Pre-incubation of HEK-NMU1 or HEK-NMU2 with unlabelled hNmU-25 (10 nM) prevented the membrane fluorescence following addition of Cy3B-pNmU-8 (Figure 3.8 ic, d and iic, d). Furthermore, addition of Cy3B-pNmU-8 (10 nM) to wild-type HEK293 cells (HEK293 WT) did not show membrane fluorescence (Figure 8 iiia, b). At 37 °C, continuous perfusion of HEK-NMU2 (Figure 3.9 i-v) with KHB (pH 7.4) for 1 min following addition of Cy3B-pNmU-8 (10 nM) did not reduce membrane fluorescence. Moreover, fluorescence began to be seen within the cytosolic compartment forming small puncta at 3 min (Figure 3.9ii). Additionally, perfusion of HEK-NMU1 (Figure 3.10 ai) or HEK-NMU2 (Figure 3.10 bi) with KHB (pH 7.4) for 5 min (performed at 12 °C to inhibit receptor internalization) did not reduce membrane fluorescence in cells challenged with Cy3B-pNmU-8 (Figure 3.10 aii, bii). Extended washing for 12 min and addition of unlabelled hNmU-25 (1 µM) in an attempt to displace bound Cy3B-pNmU-8 also did not significantly reduce membrane fluorescence (Figure 3.10 aiii, biii). In an attempt to remove bound Cy3B-pNmU-8 from HEK-NMU2 (Figure 3.11a), cells were perfused for 30 s with KHB at a range of pH values. However pH 7.4 (Figure 3.11b), pH 4.0 (Figure 3.11c), pH 3.5 (Figure 3.11d) and pH 3.0 (Figure 3.11e) failed to remove membrane fluorescence, but a pH 2.0 wash for 30 s did result in a complete loss of membrane fluorescence (Figure 3.11f). Further 5 min washes with KHB, pH 7.4 following addition of Cy3B-pNmU-8 (10 nM) and brief (15 s was sufficient) pH 2.0 wash did not restore membrane fluorescence, suggesting the removal of the fluorescent ligand rather than a quenching of fluorescence through the acid wash (Figure 3.12a, b, c). Following brief pH 2.0 wash and replacement with buffer at pH 7.4, reapplication of Cy3B-pNmU-8 (10 nM) restored membrane fluorescence (Figure 3.12d) indicating that the NMU receptor can rebind freshly added ligand.

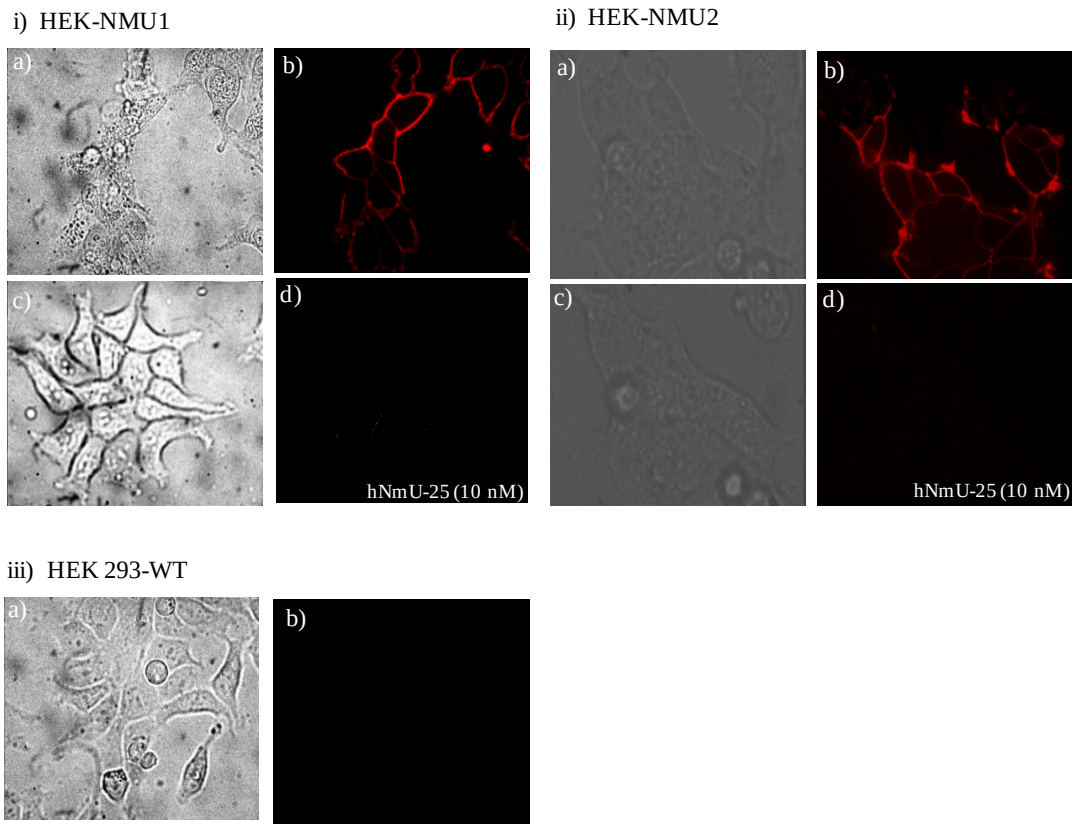

Figure 3.8. Visualization of fluorescently-tagged pNmU-8 (Cy3B-pNmU-8) binding to HEK-NMU1 or HEK-NMU2. HEK-NMU1 (i), HEK-NMU2 (ii) or HEK-293 WT cells (iii) were cultured on 25 mm glass coverslips for 24-48 h. Cells were challenged with Cy3B-pNmU-8 (10 nM) and visualized by confocal microscopy using a laser excitation wavelength of 568 nm. Representative phase images (ia and iia) and fluorescent images (ib and iib) are shown for HEK-NMU1 and HEK-NMU2 following addition of Cy3B-pNmU-8 (10 nM) for 60 s. Phase images (ic and iic) and fluorescent images (id and iid) are for HEK-NMU1 and HEK-NMU2 pre-treated with unlabelled hNmU-25 (10 nM) prior to exposure to Cy3B-pNmU-8 (10 nM). Phase image (iiia) and fluorescent image (iiib) show HEK293 WT following exposure to Cy3B-pNmU-8 (10nM). Images are representative of 3 experiments.

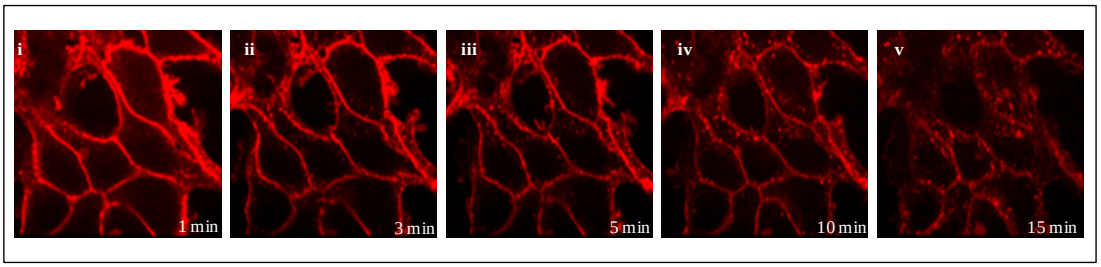

Figure 3.9. Internalization of Cy3B-pNmU-8 in HEK-NMU2. HEK-NMU2 were cultured on 25 mm glass coverslips for 24-48 h. Cells were then challenged with Cy3B-pNmU-8 (10 nM) and visualized by confocal microscopy using a laser excitation wavelength of 568 nm. Perfusion of the cells was started 60 s after addition of Cy3B-pNmU-8 and the temperature was maintained at 37 °C. Fluorescence images of HEK-NMU2 following addition of Cy3B-pNmU-8 (10 nM) at t=1 min (i), t=3 min (ii), t= 5 min (iii), 10 min (iv) and t=15 min (v). All images are representative of at least 3 experiments.

a) HEK-NMU1

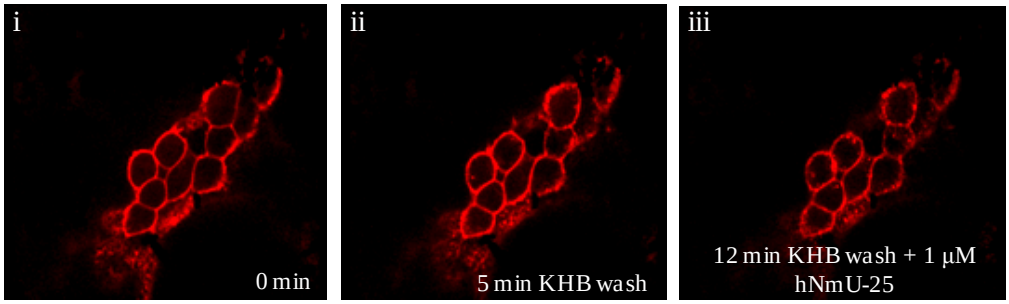

b) HEK-NMU2

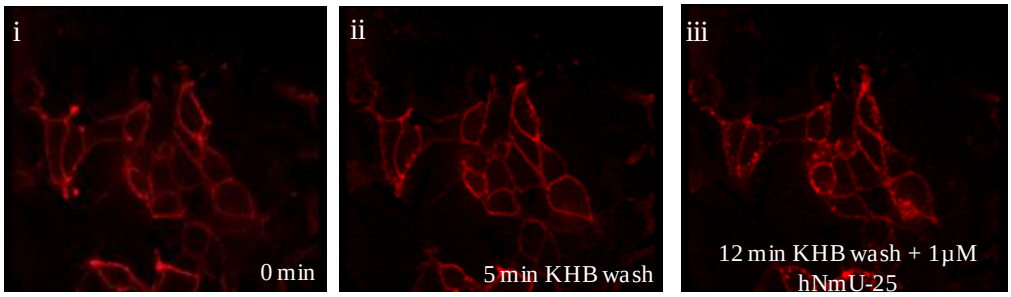

Figure 3.10. Inability to remove Cy3B-pNmU-8 from HEK-NMU1 or HEK-NMU2 by washing with normal KHB ± unlabelled ligand. HEK-NMU1 (a) or HEK-NMU2 (b) were cultured on 25 mm glass coverslips for 24-48 h. Cells were then challenged with Cy3B-pNmU-8 (10 nM) and visualized by confocal microscopy using a laser excitation wavelength of 568 nm. The temperature was maintained at 12 °C to inhibit receptor internalization. Fluorescence images for HEK-NMU1 (a) and HEK-NMU2 (b) taken following addition of Cy3B-pNmU-8 (10 nM) at t=30 s (panels ai, bi) or following perfusion of cells (KHB, pH 7.4; 5 mL/min) for 5 min (panels (aii, bii) or for 12 min with unlabelled hNmU-25 (1 µM) (panels aiii, biii). All images are representative of at least 3 experiments.

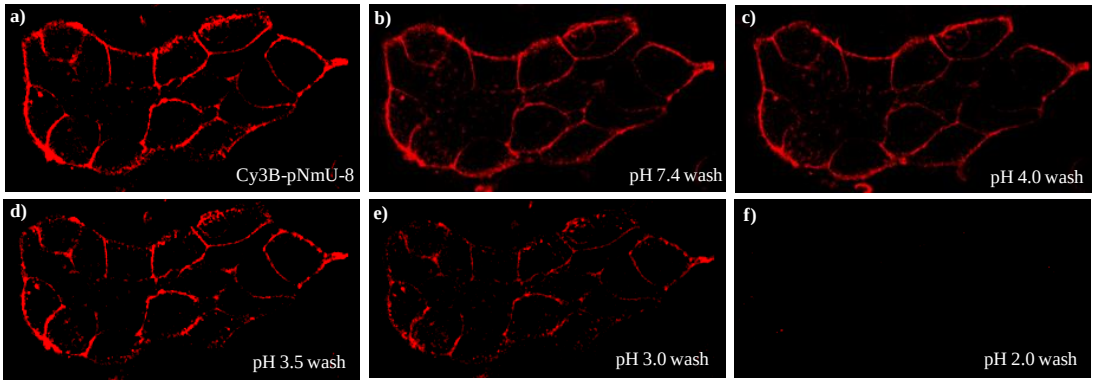

Figure 3.11. Removal of Cy3B-pNmU-8 from HEK-NMU2 by a pulse wash with low pH buffer. HEK-NMU2 were cultured on 25 mm glass coverslips for 24-48 h. Cells were then challenged with Cy3B-pNmU-8 (10 nM) and visualized by confocal microscopy using a laser excitation wavelength of 568 nm. The temperature was maintained at 12 °C to prevent receptor internalization. Panel (a) shows cell membrane fluorescence directly after exposure to Cy3B-pNmU-8 (10 nM). Cells were then washed with KHB (5 mL/min) pH 7.4 (b) followed by a brief, 30 s wash with KHB at pH 4 (c), pH 3.5 (d), pH 3.0 (e), or pH 2.0 (f). Images are representative of at least 3 experiments.

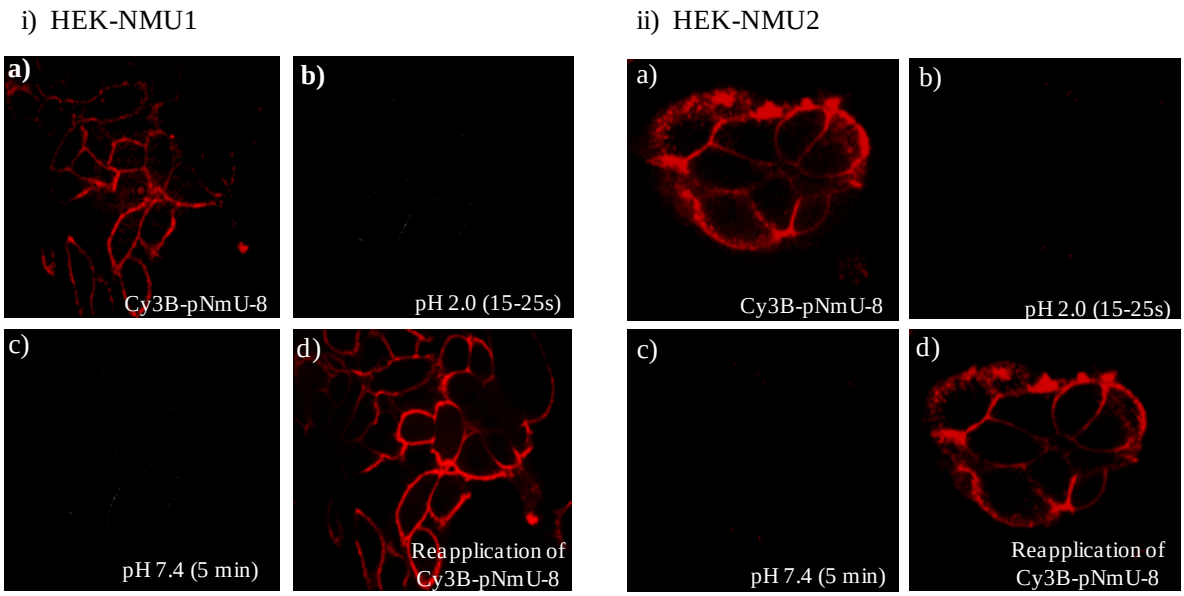

Figure 3.12. Re-binding of Cy3B-pNmU-8 to HEK-NMU1 or HEK-NMU2 following removal of Cy3B-pNmU-8 using a pulse wash with low pH buffer. HEK-NMU1 or HEK-NMU2 were cultured on 25 mm glass coverslips for 24-48 h. Cells were then challenged with Cy3B-pNmU-8 (10 nM) and visualized by confocal microscopy using a laser excitation wavelength of 568 nm. Fluorescent images (ia, b and iia, b) show HEK-NMU1 and HEK-NMU2 60 s after addition of Cy3B-pNmU-8 (10 nM) and immediately following a brief (15-25 s) wash with KHB at pH 2.0. Fluorescent images (ic and iic) taken after further perfusion with KHB, pH 7.4 (5 mL/min) for 5 min. Fluorescent images (id and iid) show membrane fluorescence of HEK-NMU1 and HEK-NMU2 after re-application of Cy3B-pNmU-8 (10 nM) following pulse pH 2.0 wash and perfusion with KHB pH 7.4. Images are representative of at least 3 experiments.

3.2.4 Effects of brief low pH wash on agonist-stimulated Ca^{2+} responses and cell viability in HEK-NMU2

To explore whether a brief acid wash affected hNmU-25-mediated Ca^{2+} responses, HEK-NMU2 cells were washed briefly (15-25 s) with buffer at either pH 2.0 or pH 7.4, followed by a 5 min recovery in pH 7.4 buffer. Following washes at pH 2.0 or pH 7.4, the pEC_{50} values for hNmU-25-mediated Ca^{2+} responses were not significantly different (control, 9.18 ± 0.10; low pH pulse-wash, 9.43 ± 0.08; n=3; Figure 3.13a). Following a longer delay (2 h) following the pH 2.0 pulse-wash, the respective pEC_{50} values were 9.16 ± 0.11 and 9.17 ± 0.02 for pH 2.0 and 7.4 pulse-washes of cells respectively (Figure 3.13b). Exclusion of trypan blue dye, as an index of cell viability, indicated good viability (92 ± 5%; n=3) following a pulse-wash at pH 2.0 (Figure 3.14 aii). Furthermore, phase images taken 30 or 60 min (Figure 3.14bi, ii) following a pulse wash at pH 2.0 confirmed the inability of trypan blue to cross the cell membrane (control, 90 ± 7%; low pH pulse-wash, 89 ± 5%; n=3). Extending the wash with pH 2.0 to 35 s (Figure 3.14 aiii) or 45 s (Figure 3.14 aiv) did cause detrimental effects on the cell viability (34 ± 5 and 28 ± 7%; n=3, respectively) where trypan blue can be seen in the cytoplasm of HEK-NMU2.

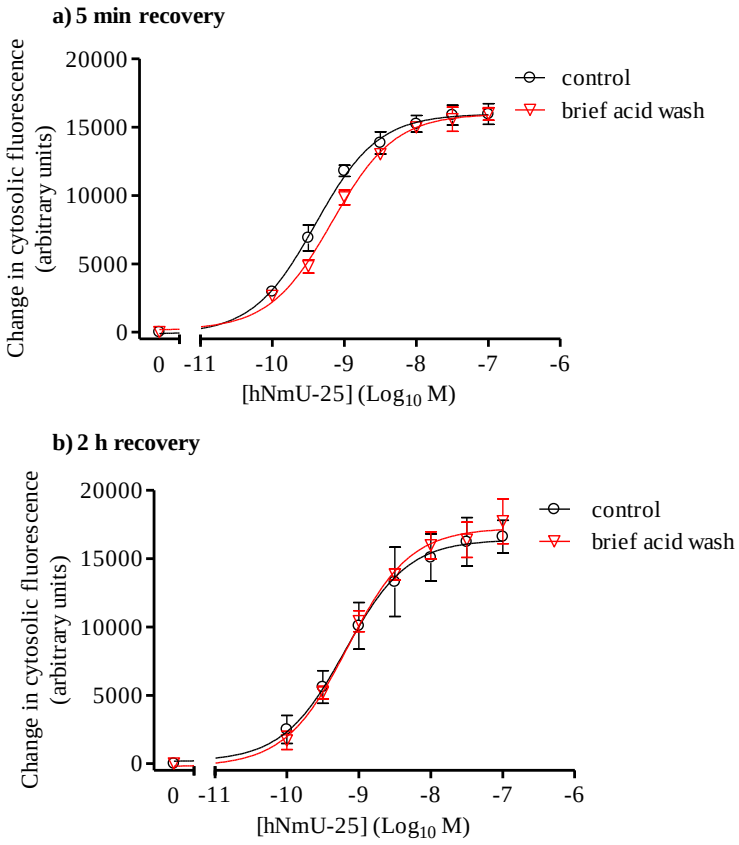

Figure 3.13. Effects of a brief, acid (pH 2.0) wash on hNmU-25-stimulated Ca^{2+} responses in HEK293-NMU2. HEK-NMU2 were cultured in 96-well plates for 48-72 h. For the 5 min recovery period (a), cells were loaded with fluo-4-AM. Cells were then exposed to a brief wash (15-25 s) with KHB pH 7.4, or KHB pH 2.0 followed by 3x KHB (pH 7.4) washes and cells were then challenged with different concentrations of hNmU-25 (0.1-100 nM) in a NOVOstar plate reader. For the 2 h recovery period (b), cells were exposed to a brief wash (15-25 s) with either KHB pH 7.4 or KHB pH 2.0 followed by 3x KHB (pH 7.4) washes. Cells were then loaded with fluo-4-AM during the last 45 min of the 2 h recovery period at 37 °C. At the end of the recovery period, cells were challenged with different concentrations of hNmU-25 (0.1-100 nM) in a NOVOstar plate reader. Changes in cytosolic fluorescence were monitored as an index of $[Ca^{2+}]_i$ and the maximal changes in fluorescence were used to construct concentration-responses curves. The pEC_{50} values 5 min after a brief buffer or acid wash were 9.43 ± 0.08 and 9.18 ± 0.10, respectively. The pEC_{50} values 2 h after a brief buffer or acid wash were 9.16 ± 0.11 and 9.17 ± 0.02, respectively. Data are mean ± s.e.m, n = 3.

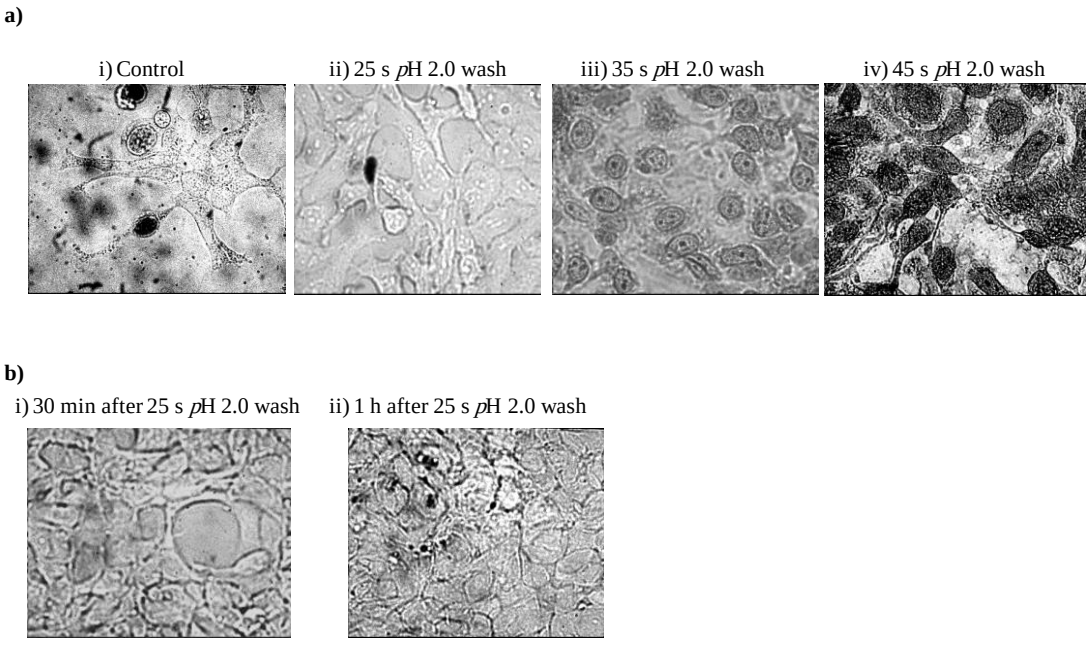

Figure 3.14. Effects of exposure to pH 2.0 buffer on cell viability. HEK-NMU2 were cultured on 25 mm glass coverslips for 24-48 h. Cells were then washed briefly with either KHB pH 7.4 (a, i) or pH 2.0 for 25 s (a, ii), 35 s (a, iii) or 45 s (a, iv) followed by 3x washes with KHB (pH 7.4) and immediately stained with 0.1% trypan blue. Cells were viewed with a 40x objective lens using an Olympus inverted microscope. Phase images (b, i, ii) show the effect of brief, 20 s pH 2.0 wash after 30 min or 1 h recovery, respectively. Images are representative of at least 3 separate experiments.

3.2.5 Ca^{2+} responses to repetitive agonist applications

In HEK-NMU2, application of a maximally-effective concentration of hNmU-25 (10 nM) evoked a rapid, transient peak Ca^{2+} response that declined despite the continued presence of hNmU-25 (Figure 3.15). Washing cells with KHB for 30 s after 60 s of the addition did not enhance the slow rate of decline. After 5 min of continuous superfusion of the cells with KHB, cells exhibited a reduction in $[Ca^{2+}]_i$ to approximately 4-9% above basal levels (Figure 3.15). Furthermore, reapplication of hNmU-25 (10 nM) at t=375 s did not affect the $[Ca^{2+}]_i$ (n=5-7 cells for each experiment in 5 independent experiments). Activation of endogenously expressed M_3 muscarinic receptors in HEK-NMU2 by carbachol (Cch, 300 µM) after 30 s of basal recording (Figure 3.16) induce a fast (6-9 s) peak of Ca^{2+} followed by a fall for 10-20 s and then a more sustained phase. Superfusion of the cells at 90 s with KHB caused a comparatively rapid reduction in $[Ca^{2+}]_i$ over the next 20-30 s of recording. By 300 s of superfusion, 85% of the cells had returned to basal levels. Images were not taken between t=100 s and t=275 s and the rate of decline during this period cannot be assessed. A further challenge of HEK-NMU2 with carbachol (300 µM) following this period at t=375s evoked a second Ca^{2+} responses in all cells and that was 40 ± 2% (n=6-7 cells for each experiment in 3 independent experiments) of the initial peaks.

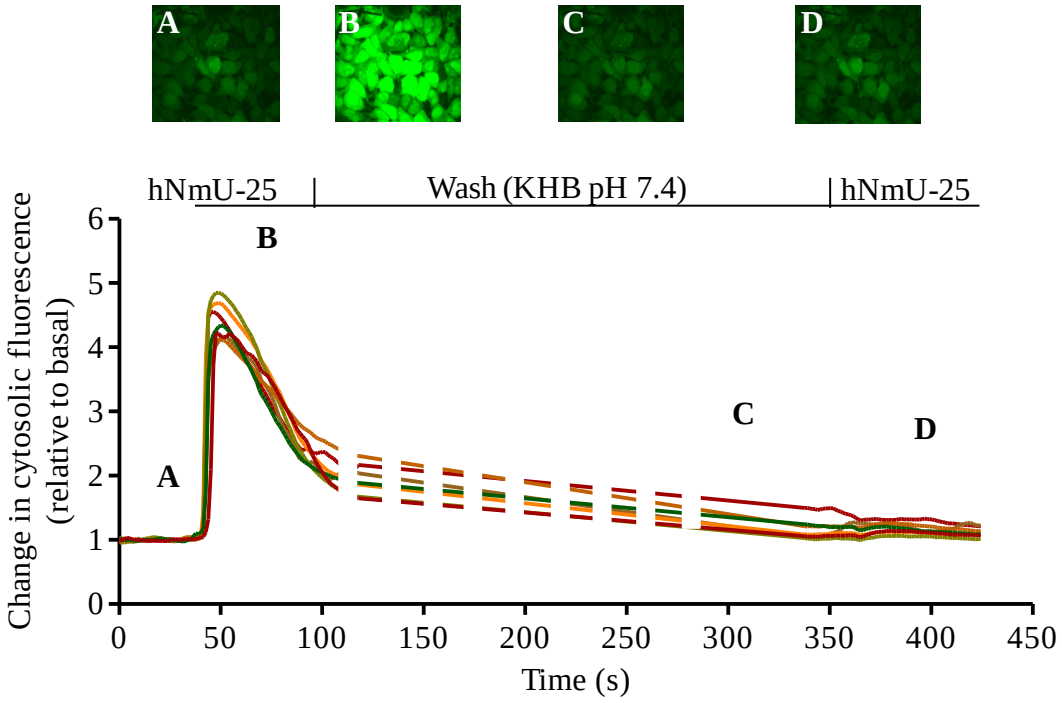

Figure 3.15. Ca^{2+} responses to repeated application of hNmU-25 in HEK-NMU2. Cells were cultured on 25 mm glass coverslips for 24-48 h, loaded with fluo-4-AM and changes in cytosolic fluorescence intensity were measured as an index of $[Ca^{2+}]_i$ using confocal microscopy. Following recording of basal fluorescence, cells were challenged with hNmU-25 (10 nM) at t=30s for 60 s. Cells were then perfused with KHB (pH 7.4) for 5 min before a second addition of hNmU-25 (10 nM). Changes in cytosolic fluorescence were calculated relative to the basal level. The dotted lines indicate that data were not collected between t=100 s and t=275 s. Each line represents $[Ca^{2+}]_i$ recorded in a single cell; representative images were taken at the points indicated by capital letters on the main trace. Data are representative of 5 experiments, with at least 6-7 cells observed in each experiment.

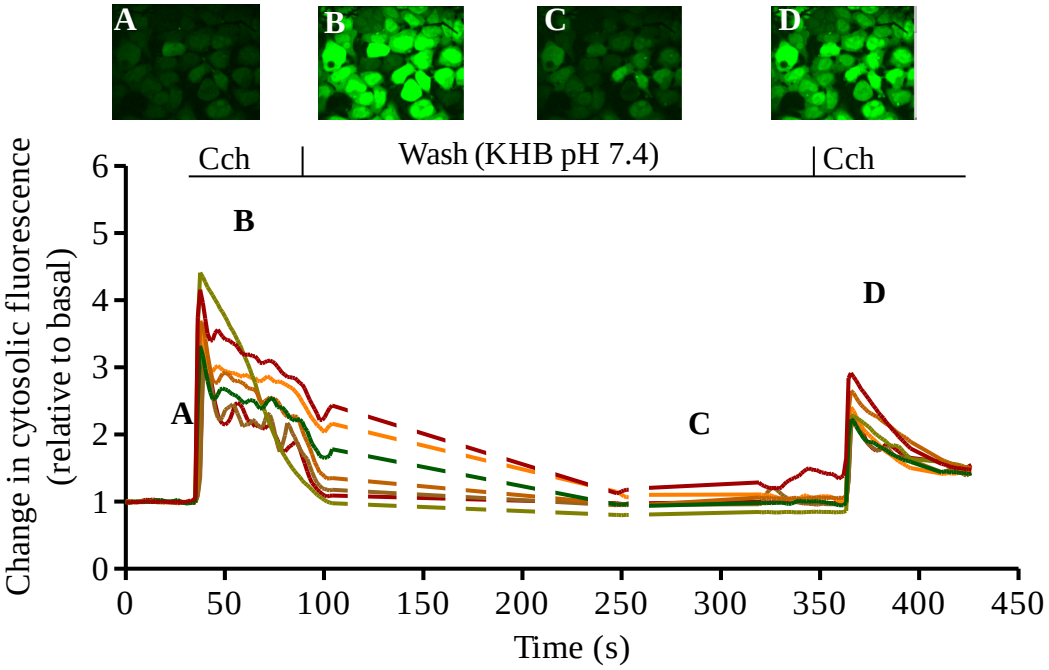

Figure 3.16. Ca^{2+} responses to repeated application of carbachol in HEK-NMU2. Cells were cultured on 25 mm glass coverslips for 24-48 h, loaded with fluo-4-AM and changes in cytosolic fluorescence intensity were measured as an index of $[Ca^{2+}]_i$ using confocal microscopy. Cells were challenged with carbachol (Cch, 300 μM) at t=30 s for 60 s. Cells were then perfused with KHB (pH 7.4) and after 5 min, Cch (300 μM) was reapplied. Changes in cytosolic fluorescence were calculated relative to the basal level. The dotted lines indicate that data were not collected between t=90 s and t=275 s. Each line represents data from a single cell and each representative image was taken at the points indicated by capital letters. Data are representative of 3 experiments, with at least 6-7 cells observed in each experiment.

3.2.6 Ca^{2+} responses to repetitive application of agonist in HEK-NMU2 including a brief acid wash

As previously observed, Ca^{2+} imaging using confocal microscopy demonstrated that stimulation of HEK-NMU2 with hNmU-25 (10 nM) induced a rapid peak increase in $[Ca^{2+}]_i$ which had declined to 67-83% of the peak before washing (Figure 3.17). After 60 s exposure to hNmU-25, cells were briefly (15-25 s) washed with KHB pH 2.0 and perfused with KHB pH 7.4 for 5-6 min by which time $[Ca^{2+}]_i$ had returned to close to pre-stimulation levels. Re-application of hNmU-25 (10 nM) now resulted in a detectable Ca^{2+} response in all cells, which was 56 ± 8% (n=5-7 cells for each experiment in 5 independent experiments) of the earlier hNmU-25 response of naïve cells. The same experiment was carried out using carbachol (300 µM) to activate the endogenous M_3 mACh receptor population in HEK-NMU2 (Figure 3.18). After 60 s exposure to Cch, cells were briefly (for 15-25 s) washed with KHB, pH 2.0 and then perfused with KHB, pH 7.4 for 5-6 min. At this time $[Ca^{2+}]_i$ had returned to basal levels in all cells. Re-application of carbachol (300 µM) resulted in a robust increase in $[Ca^{2+}]_i$ in all cells, which was 39 ± 8% (n=5-7 cells for each experiment in 3 independent experiments) of the earlier Cch response of naïve cells.

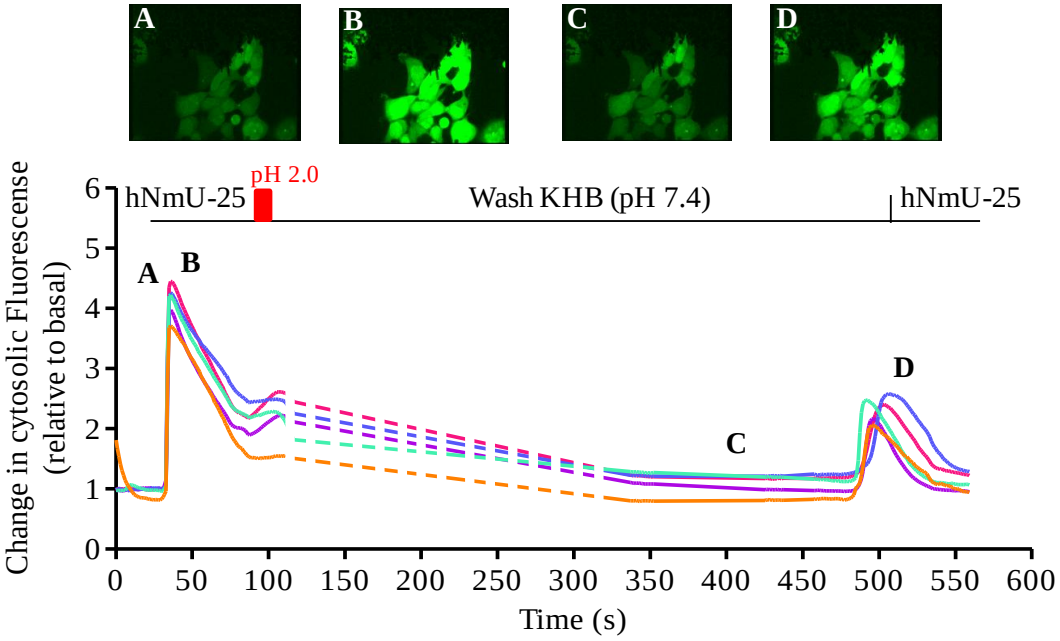

Figure 3.17. Ca^{2+} responses to repeated application of hNmU-25 in HEK-NMU2 after a brief pH 2.0 wash. Cells were cultured on 25 mm glass coverslips for 24-48 h, loaded with fluo-4-AM and changes in cytosolic fluorescence intensity were measured as an index of $[Ca^{2+}]_i$ using confocal microscopy. Following recording of basal fluorescence, cells were challenged with hNmU-25 (10 nM) for 60 s. Cells were then briefly perfused KHB (pH 2.0) for 15-25 s followed by a wash with KHB (pH 7.4). After a further 5-6 min, hNmU-25 (10 nM) was re-applied. Changes in cytosolic fluorescence were calculated relative to the basal level. The dotted lines indicate that data were not collected between t=100 s and t=325 s. Each line represents data from a single cell and representative images are shown for time-points indicated by capital letters. Data are representative of 5 experiments, with at least 5 cells observed in each experiment.

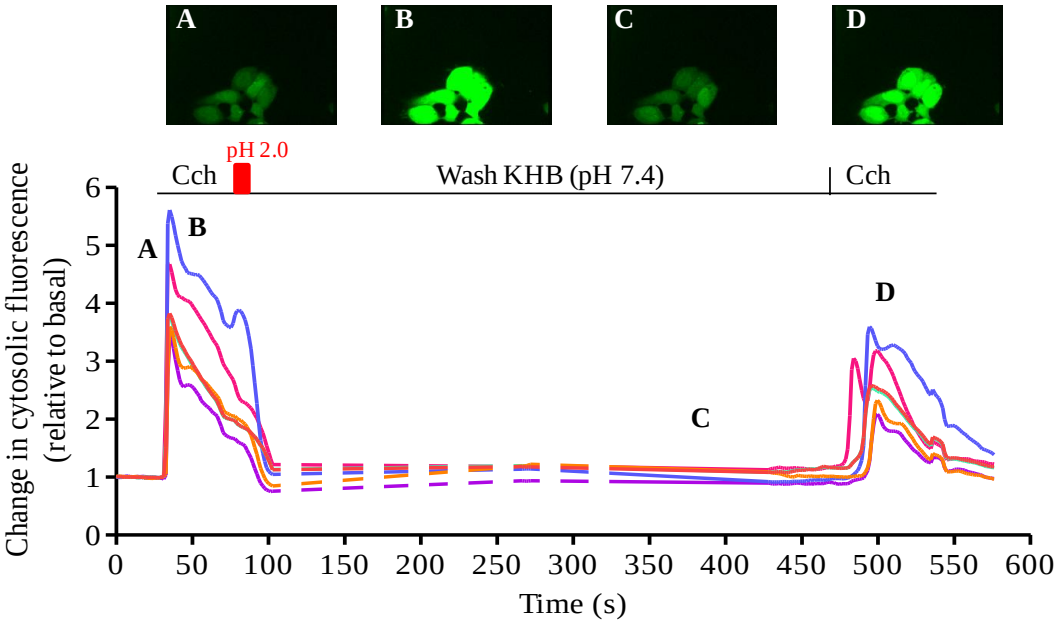

Figure 3.18. Ca^{2+} responses to repeated application of carbachol in HEK-NMU2 after brief low pH wash. Cells were cultured on 25 mm glass coverslips for 24-48 h, loaded with fluo-4-AM and changes in cytosolic fluorescence intensity were measured as an index of $[Ca^{2+}]_i$ using confocal microscopy. Following recording of basal fluorescence, cells were challenged with carbachol (Cch, 300 µM) for 60 s. Cells were then perfused with KHB (pH 2.0) followed washing with KHB (pH 7.4). After 5-6 min, Cch (300 µM) was re-applied**.** Changes in cytosolic fluorescence were calculated relative to the basal level. The dotted lines indicate that data were not collected between t=100 s and t=325 s. Each line represents data from a single cell and representative images are shown for the time-points indicated by capital letters. Data are representative of 3 experiments, with at least 5-7 cells observed in each experiment.

3.3 Discussion

3.3.1 Dual coupling of NMU receptors in recombinant systems

Stimulation of HEK-NMU1 or HEK-NMU2 by NmU (hNmU-25) or NmS (hNmS-33) neuropeptides result in concentration-dependent and PTX-insensitive peak-plateau increases in $[Ca^{2+}]_i$. The $G\alpha_{q/11}$ coupling and intracellular Ca^{2+} increase on stimulation of NMUs by either NmU or NmS has been characterized previously in recombinant systems (Aiyar *et al.*, 2004; Brighton *et al.*, 2004a; Mori *et al.*, 2005; Raddatz *et al.*, 2000; Shan *et al.*, 2000; Szekeres *et al.*, 2000), as well as in endogenous NMU-expressing cell-types (Brighton *et al.*, 2008; Johnson *et al.*, 2004; Moriyama *et al.*, 2006b). As has been shown for numerous other $G\alpha_{q/11}$-coupled GPCRs, such as the endogenously expressed M_3 muscarinic receptor in HEK293 cells, the peak Ca^{2+} response is likely to be primarily mediated through activation of PLC and generation of inositol 1,4,5-trisphosphate (IP_3), which results in IP_3 receptor-dependent Ca^{2+} mobilization (Tong *et al.*, 1999; Zhu *et al.*, 1998). On the other hand, the plateau phase is more dependent on Ca^{2+} influx across the cell membrane, since removal of Ca^{2+} from the extracellular environment did not abolish the initial peak, but prevented the plateau phase. This finding is consistent with previous work in the same cell-lines where pre-treatment with thapsigargin abolished NmU-mediated $[Ca^{2+}]_i$ increases, and in the absence of extracellular Ca^{2+} the sustained phase of the Ca^{2+} response was lost (Brighton, 2005). Thapsigargin is an irreversible inhibitor of the sarcoplasmic/endoplasmic reticulum Ca^{2+}-ATPase (SERCA) pump, which increases cytosolic Ca^{2+} by inhibiting the re-uptake mechanism that refills the store opposing the continuous, agonist-independent leak of Ca^{2+} from endoplasmic reticulum (ER) stores (Cahalan, 2009). Several mechanisms have been suggested for the entry of Ca^{2+} from the extracellular space to refill intracellular stores and maintain the sustained phase of $[Ca^{2+}]_i$ elevation. This mechanism is generally termed store-operated Ca^{2+} entry (SOCE), or capacitative Ca^{2+} entry (CCE). The mechanisms responsible for this have been an area of intense investigation and although some questions still remain, recent work has elucidated some of the mechanisms and molecules involved, including STIM, Orai and TRPC proteins (for more detail see (Cahalan, 2009)). Mammalian ER membranes contain the STIM (STIM1 and STIM2) protein, which is found as a dimer. STIM contains an EF-

hand motif which serves as Ca^{2+} sensor localized at the *N*-terminus of STIM in the lumen of the ER. In the resting state, intracellular Ca^{2+} stores are replete (~400 μM) with Ca^{2+} bound to the STIM-EF-hand motif. Depletion of ER Ca^{2+} stores (<300 μM) results in dissociation of bound Ca^{2+} from the low affinity EF-hand motif, STIM then forms oligomeric clusters and translocates to the ER-plasma membrane junction. The physical interaction of STIM clusters with plasma membrane Orai dimers leads to the formation of a Ca^{2+} release-activating Ca^{2+} (CRAC) channel and Ca^{2+} influx. CRAC channel closure occurs through the rebinding of Ca^{2+} to the STIM EF-hand motif leading to disassembly of STIM clusters (Cahalan, 2009). In addition to activation of Ca^{2+} influx through CRAC channels, it has been shown that STIM1 can induce Ca^{2+} entry via the activation of multiple types of transient receptor potential cation (TRPC) channels (Cahalan, 2009).

Both NmU (hNmU-25) and NmS (hNmS-33) caused concentration-dependent and PTX-sensitive inhibitions of cyclic AMP generation in HEK-NMU1 and HEK-NMU2 cells. NmU and NmS were essentially equipotent and responses were indistinguishable between NMU1- and NMU2-expressing HEK cells. However, the measured potencies of these neuropeptides were 6-36 fold greater for stimulating a $[Ca^{2+}]_i$ response compared to inhibiting adenylyl cyclase activity. This is in contrast to previously published work with these cells (Brighton *et al.*, 2004a), where NMU receptor activation led to a marginally more potent inhibition of forskolin-stimulated cAMP generation than was observed for phosphoinositide hydrolysis and $[Ca^{2+}]_i$ increases. This variation may be due to differences in the experimental procedures used. It is noteworthy that a previous study reported NMU2, transiently expressed in CHO cells, to inhibit partially adenylyl cyclase activity (Hosoya *et al.*, 2000), while activation of NMU1 transiently transfected in HEK293 has been reported not to affect cAMP levels (Szekeres *et al.*, 2000).

Dual coupling to $G\alpha_q$ and $G\alpha_{i/o}$ has been demonstrated for many recombinantly expressed GPCRs, such as M_1 and M_3 mACh receptors (Offermanns *et al.*, 1994) and the A_3 adenosine receptor (Palmer *et al.*, 1995) (for detailed review see (Hermans, 2003)). This multiplicity in G protein coupling might, for example, be due to receptor over-expression in the recombinant system, which could lead to "promiscuous" coupling to the most abundant G proteins, primarily $G\alpha_{i/o}$ (Gudermann *et al.*, 1997). However, it seems that promiscuous coupling is not restricted to recombinantly expressed receptors. For

example, dual coupling to $G\alpha_{q/11}$ and $G\alpha_{i/o}$ has been reported for the ET_A receptor in cardiac myocytes (Hilal-Dandan *et al.*, 1994; Hilal-Dandan *et al.*, 1992) and NMUs in the cultured colonic myocytes (Brighton *et al.*, 2008). The report that NMU1-mediated signalling occurs primarily via $G\alpha_{q/11}$, while NMU2 signalling preferentially occurs downstream of $G\alpha_{i/o}$ has also been proposed (Hsu *et al.*, 2007), although the present data clearly contrast with such an assertion. There is a clear need to investigate the dual coupling of NMUs in native systems: more studies are required to assess whether promiscuous coupling of NMUs is tissue/cell-specific and whether this plays any physiological or pathological role in NmU/NmS signalling.

3.3.2 Pseudo-irreversible binding of NmU

NmU demonstrates high-affinity binding to both NMU1 and NMU2, which has been shown by radioligand binding, where dissociation constants (K_d) of [^{125}I]hNmU-25 at NMU1 and NMU2 are in the sub-nanomolar range (135-290 and 110-230 pM, respectively) (Aiyar *et al.*, 2004; Brighton *et al.*, 2004a). Pseudo-irreversible binding has been demonstrated by a failure of high concentrations of unlabelled hNmU-25 to displace [^{125}I]hNmU-25 binding, the continuous generation of [^{3}H]$InsP_x$ for 60 min even after attempts to remove hNmU-25, and the lack of repetitive Ca^{2+} signalling on re-application of hNmU-25 following washes in an attempt to remove bound ligand (Brighton, 2005; Brighton *et al.*, 2004a). The availability of a fluorescently-tagged form of NmU (Cy3B-pNmU-8) has facilitated the visualization of ligand-receptor interactions in living cells and provided further evidence supporting NmU-NMU pseudo-irreversible binding. Thus, confocal imaging demonstrated a failure to remove bound Cy3B-pNmU-8 even with extended washes (Brighton *et al.*, 2004a). In the current study, two approaches were applied to investigate pseudo-irreversible binding of NmU in HEK-NMU1 and HEK-NMU2. Firstly, Cy3B-pNmU-8 was used to monitor NmU binding and secondly single-cell NmU-mediated $[Ca^{2+}]_i$ mobilization was used to investigate the consequences of pseudo-irreversible binding on functional responses. Cy3B-pNmU-8 binds specifically and essentially irreversibly to NMUs, since pre-addition of unlabelled NmU to HEK-NMU1 or HEK-NMU2 prevented fluorescence at the cell membrane on subsequent

addition of Cy3B-pNmU-8. Further, no membrane fluorescence was seen following application of Cy3B-pNmU-8 to untransfected HEK293 cells. The membrane fluorescence observed on addition of Cy3B-pNmU-8 (10 nM) was not displaced by unlabelled NmU (1 µM), which confirmed irreversible binding of NmU to its receptors. Different washing times with normal buffer (pH 7.4) failed to decrease the intensity of the fluorescence which indicates the inability to remove NmU-8-Cy3B from NMU receptors. These observations support previous reports either in recombinant systems (Brighton *et al.*, 2004a), or with endogenously expressed NMUs in cultured colonic smooth muscle cells (Brighton *et al.*, 2008).

Single-cell Ca^{2+} measurement of fluo-4 loaded HEK-NMU2 demonstrated that after the initial Ca^{2+} response to NmU, washing the cells with standard buffer for up to 5 min followed by a second addition of hNmU-25 did not induce a second Ca^{2+} response. In contrast, following an application of carbachol to stimulate endogenously M_3 mACh receptors and subsequent washing, carbachol was able to evoke a second Ca^{2+} response. When the second addition was 5 min after the first challenge, the second response was ~40% of the initial one. Extending the washing time between the two additions of NmU in HEK-NMU2 did not restore the response to the second addition, which provides further evidence of pseudo-irreversible binding.

There remains the possibility that these data may simply result from a rapid and full desensitization of the NMUs. However, pseudo-irreversible binding has been observed between several GPCRs and their cognate peptide ligands. For example, it has been reported that in KNRK cells, repetitive application of substance P failed to evoke repetitive $[Ca^{2+}]_i$ mobilization via the neurokinin 1 (NK1) receptor following an attempt to remove ligand by washing and a 5 min resensitization period (Schmidlin *et al.*, 2001). In fact, this study demonstrated that the NK1 receptor required approximately 3 h to show full recovery of Ca^{2+} responses to substance P (Schmidlin *et al.*, 2001). Furthermore, following exposure of ET_A receptor to endothelin for 5 min in neonatal cardiac myocytes, BQ123 (ET_A-R antagonist) failed to antagonize the $[^3H]InsP_x$ generation or inhibition of adenylyl cyclase activity (Hilal-Dandan *et al.*, 1997).

3.3.3 Removal of NmU by brief acid wash and receptor desensitization

Low pH solutions have been successfully used to remove high-affinity peptide ligands from their receptors at the cell-surface (Haigler *et al.*, 1980; Koenig *et al.*, 1997). However, other studies have demonstrated ligand-receptor complexes where even acidic conditions result in only partial dissociation. For example, only 50% of bound [^{125}I]ET-1 was removed from the cell-surface of cardiac myocytes in an attempt to strip bound ET-1 by acid washing (pH 2.5, 10 min). This occurred when binding was performed at 37 °C or 4 °C, the latter temperature being used to minimize internalization (Hilal-Dandan *et al.*, 1997). Similarly, following radioligand binding of urotensin II ([^{125}I]U-II) to its receptor in human skeletal muscle cells at 37 °C, 4 °C, or in the presence of 0.45 M sucrose (to inhibit endocytosis), stripping of the ligand with pH 2.5 for 10 min only dissociated approximately half of the bound [^{125}I]U-II (Qi *et al.*, 2005).

Previous work demonstrated the possibility of removing receptor-bound Cy3B-pNmU-8 by washing cells with low pH solution (Brighton *et al.*, 2004a). The current dataset demonstrated that washing with pH 7.4, 4, 3.5, or 3 for 30 s failed to remove the fluorescent NmU analogue from the cell membrane, while a pH 2.0 wash removes the ligand. Rapid washing (15-25 s) at pH 2.0 was sufficient to completely displace Cy3B-pNmU-8 from the cell membrane. Such harsh conditions could clearly have serious effects on the integrity of the cell and its ability to respond to agonist re-challenge. However, removal of Cy3B-pNmU-8 with pH 2.0 solution (15-25 s) followed by a return to pH 7.4 buffer and reapplication of NmU-8-Cy3B (10 nM) restored fluorescence at the surface of the cell membrane. This showed that the receptor was still able to bind ligand and the loss of fluorescence following acid washing was not due to any pH-sensitivity of the fluorophore. It is noteworthy that Cy3B is acid-insensitive even at very low pH (see Amersham Bioscience, Fluorescence Screening Guide). In order to assess the impact of pH 2.0 on receptor/cell function, a brief pH 2.0 wash followed by pH 7.4 washes was applied and NMU2-mediated $[Ca^{2+}]_i$ mobilization assessed in cell populations. This treatment did not significantly change the EC_{50} compared to that observed in HEK-NMU2 subjected to standard buffer wash. Together with the apparently minimal effect of the pH 2.0 wash protocol on the cell viability, even after 60 min, this protocol provided the opportunity to further investigate the desensitization profile of NMUs in a manner

distinguishable from pseudo-irreversible ligand binding. When the same washing procedure was used to investigate Ca^{2+} signalling using single-cell confocal imaging, a second Ca^{2+} response was generated by reapplication of NmU that was ~57% of the initial one. A similar result was obtained for carbachol, which was used as a positive control due to the relatively low affinity of carbachol for muscarinic receptor (i.e. µM). This result was similar for the carbachol responses with standard (pH 7.4) washing, thereby highlighting the lack of effect of the acid wash on Ca^{2+} signalling. The acid wash duration seemed to be crucial, since any extension of the wash-period even by 5-10 s, resulted in significant detrimental effects on the viability of the cells and the absence of a further Ca^{2+} response. These findings allow us to further investigate the desensitization-resensitization profiles of NMUs and whether they undergo recycling and resensitization, or are targeted to lysosomes to be degraded. This theme will be pursued in a later thesis Chapter.

Chapter 4

Generation and characterization of HEK-NMU1-eGFP and HEK-NMU2-eGFP cell-lines

4.1 Introduction

Activation of GPCRs on the cell surface by ligand binding promotes functional signalling via G protein-dependent and -independent pathways (Pierce *et al.*, 2002). Ligand binding to GPCRs also induces phosphorylation of intracellular domains within receptors, the binding of β-arrestins and internalization of the ligand-receptor-β-arrestin complex into intracellular compartments for signal termination, signal propagation and/or receptor resensitization (Marchese *et al.*, 2008; Moore *et al.*, 2007). Internalization is followed by trafficking of the complex to early endosomes and then the receptor recycles either rapidly or slowly through large recycling endosomes back to the plasma membrane, or alternatively is targeted to lysosomes to be degraded (Marchese *et al.*, 2008; Moore *et al.*, 2007). Initially, GPCR activation, trafficking and interactions with other proteins have been studied using a variety of methods, including the use of radiolabelled ligands, enzyme-linked immunosorbent assay (ELISA), co-immunoprecipitation assays, Western-blotting analysis, as well as an array of functional responses (Bohme *et al.*, 2009). However, these techniques have several limitations and potential for artefacts that may contribute to misleading findings (Bohme *et al.*, 2009).

The generation of fluorescent molecules that can be incorporated into either ligand or receptor without affecting normal ligand-receptor interactions, signalling and/or trafficking can provide invaluable tools for monitoring GPCR activation and regulation at the molecular level in living cells and in real-time using methods including fluorescence-activated cell-sorting (FACS) and single-cell imaging systems (Bohme *et al.*, 2009; Huang *et al.*, 2011a). Several GPCR ligands have been tagged with low molecular weight molecules, including fluorescein, rhodamine and cyanine dyes (Bohme *et al.*, 2009). For

example, the fluorescently tagged pNmU-8 (Cy3B-pNmU-8) allowed visualization of NmU binding to the plasma membrane of HEK-NMU1 and HEK-NMU2 and its internalization (see **Chapter 3, Section3.2.3**). In addition to ligand-tagging, short amino acid sequences have been generated as epitope tags, which can be incorporated into the GPCR of interest without affecting normal receptor behaviour (Huang *et al.*, 2011a). The antigenicity of the epitope tag can be used with, for example, commercially-available antibodies to allow monitoring of ligand-receptor co-localization and trafficking.

Fluorescent tags, such as mutated and enhanced version of the green fluorescent protein (eGFP) allow visualization of the receptor in live cells without the need for antibodies. Furthermore, eGFP is brighter, has a higher expression in eukaryotic cells than many other fluorescent tags, and also has stable fluorescence allowing its use for immunocytochemistry (ICC) as well as live-cell imaging (Huang *et al.*, 2011a). The possibility to visualize eGFP directly without the need of fluorescent antibodies or reagents can also reduce the potential for cytotoxicity (Huang *et al.*, 2011a). Additionally, the availability of good-quality antibodies against eGFP provides useful tools for some GPCRs, where appropriate antibodies are unavailable. It has also been reported that eGFP cDNA can often be inserted into the *C*-terminal domain of GPCRs without altering the binding, signalling or trafficking properties of the receptor (Huang *et al.*, 2011a). This Chapter reported an attempt to clone and express *C*-terminus epitope-tagged human neuromedin U receptors, NMU1-eGFP and NMU2-eGFP in order to monitor the trafficking of hNMU1 and hNMU2. cDNAs encoding the fusion proteins NMU1-eGFP and NMU2-eGFP were transfected stably into HEK293 cells (HEK-NMU1-eGFP and HEK-NMU2-eGFP). Furthermore, binding of Cy3B-pNmU-8 to NMU1-eGFP and NMU2-eGFP and functional coupling of each receptor to $G\alpha_{q/11}$ and $G\alpha_{i/o}$ has been assessed.

4.2 Results

4.2.1 Generation of NMUR1-eGFP and NMUR2-eGFP constructs and establishment of stable HEK cell-lines

Full-length of NMU1 gene (NMUR1) and NMU2 gene NMUR2 were amplified from pFN-hu-axor13 and PFN-cmv-hu-axor34 plasmids, respectively through PCR using forward and reverse primers which contained Spe I and Xho I restriction sites, respectively (Figure 4.1). The PCR products were run on 0.76% agarose gel containing GelRed (0.005% *v/v*) and visualized under UV light. Both NMUR1 and NMUR2 products were detected at the expected sizes (Figure 4.2). The amplified fragments were purified from the agarose gel, subjected to overnight restriction digests with Xho I and Spe I and purified using Qiagen DNA purification kits before ligation into the pEGFP-N1 plasmid. Diagnostic digestion following ligation of each insert with Xho I and Sna B I for NMUR1-eGFP and BamH I for NMUR2-eGFP resulted in fragments of the expected sizes (Figures 4.3 and 4.4). Confocal images following 48 h of transfection of each construct separately into HEK293 cells showed plasma membrane fluorescence in both NMU1-eGFP- and NMU2-eGFP-transfected cells (Figure 4.5). Furthermore, confocal images after 21 days of transfection of NMUR1-eGFP or NMUR2-eGFP constructs into HEK293 cells and selection with geneticin (G418, 1 µg) and addition of Cy3B-pNmU-8 (10 nM) demonstrated receptor-ligand co-localization, either at the cell-surface or in the cytosolic compartment (Figure 4.6).

Primers for NMUR1 (Full-length 1281bp), without a stop codon for generation of NMU1 tagged with eGFP at the *C*-terminus

5'primer (30 bp), to introduce restriction site of SpeI:

5'- G**AC TAG T** GCC ACC ATG GC TTG CAA TGG CAG-3' (labelled Nmur115)

3'primer (28 bp), to introduce restriction site of XhoI:

5'-CCG **CTC GAG** GGA TGG ATC GGT CTC TTG C -3' (labelled Nmur112)

Primers for NMUR2 (1248bp), without a stop codon for generation of NMU2 tagged with eGFP at the *C*-terminus

5'primer (26 bp), to introduce restriction site of SpeI:

5'-G**AC TAG T** GCC ACC ATG TCA GGG ATG G-3' (labelled Nmur211)

3'primer (25 bp), to introduce restriction site of XhoI:

5'-CCG **CTC GAG** GGT TTT GTT AAA GTG G-3' (labelled Nmur212)

Figure 4.1. Primers for cloning and amplification (PCR) of NMUR1 and NMUR2.

Restriction enzyme sites are indicated in the box while underlined letters represent the start codon. The Kozak sequence introduced before the start codon is indicated by the shaded box.

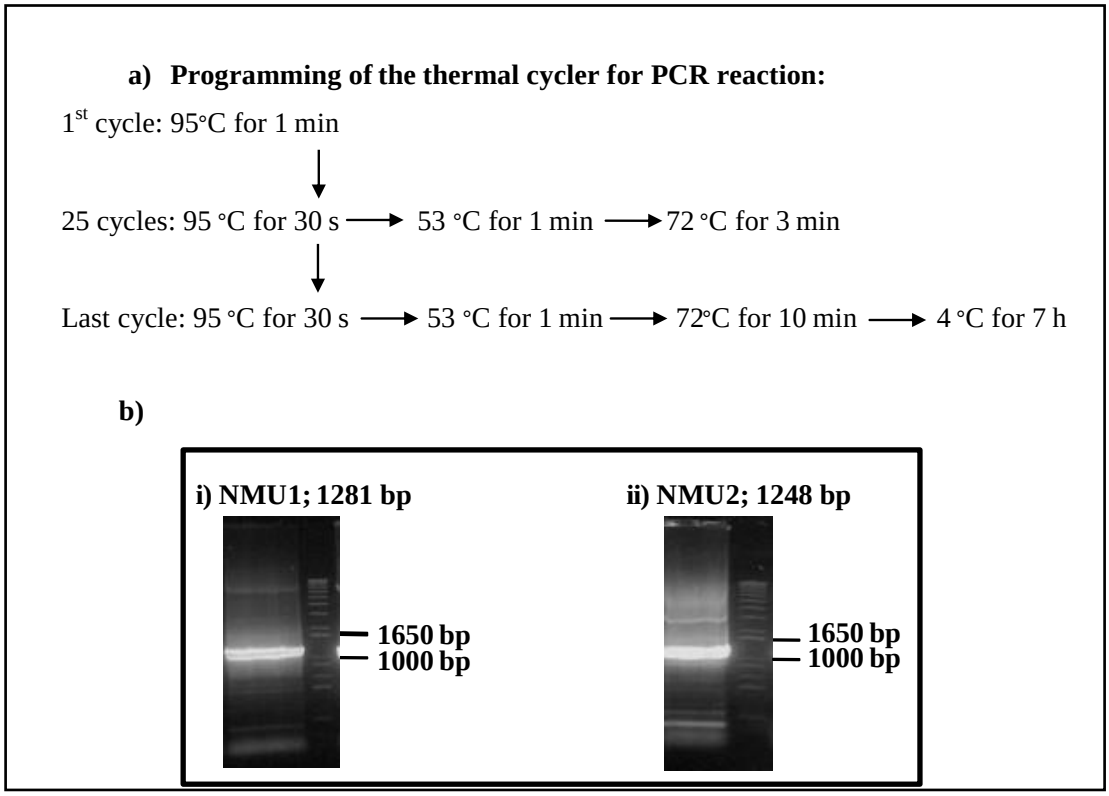

Figure 4.2. Amplification of NMUR1 and NMUR2 cDNA from pFN-hu-axor13 and PFN-cmv-hu-axor34 plasmids, respectively. Full-length NMUR1 and NMUR2 were amplified by mixing pFN-hu-axor13 (0.3 μg) or PFN-cmv-hu-axor34 (0.4 μg) plasmids with primers. The PCR products were run on an agarose gel (0.76%) containing GelRed (0.005% *v/v*). NMUR1 (bi) and NMUR2 (bii) PCR products were then visualized and imaged under UV light.

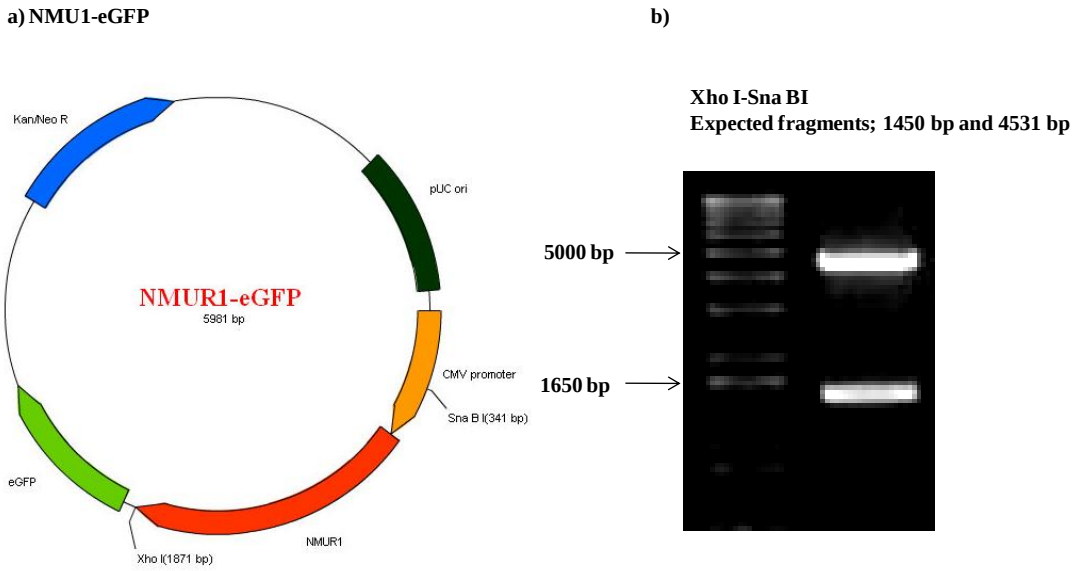

Figure 4.3. NMUR1-eGFP construct map and diagnostic digestion by the restriction enzymes Xho I and Sna BI. Diagram (a) represents plasmid map of pEGFP-N1 containing NMUR1. Image (b) shows the result of digestion of the construct with Xho I and Sna BI restriction enzymes. The DNA fragments were separated by agarose gel electrophoresis with GelRed and viewed under UV light.

a) NMUR2-eGFP

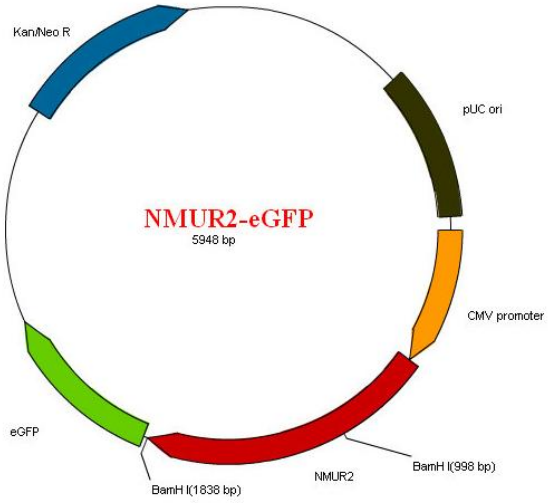

b)

BamH I
Expected fragments; 840 bp and 5090 bp

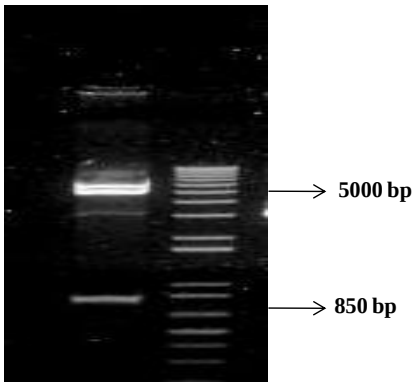

Figure 4.4. NMUR2-eGFP construct map and diagnostic digestion by the restriction enzyme BamH I. Diagram (a) represents plasmid map of pEGFP-N1 containing NMUR2. Image (b) shows digestion of the construct with BamHI restriction enzyme. The DNA fragments were separated by agarose gel electrophoresis with GelRed and viewed under UV light.

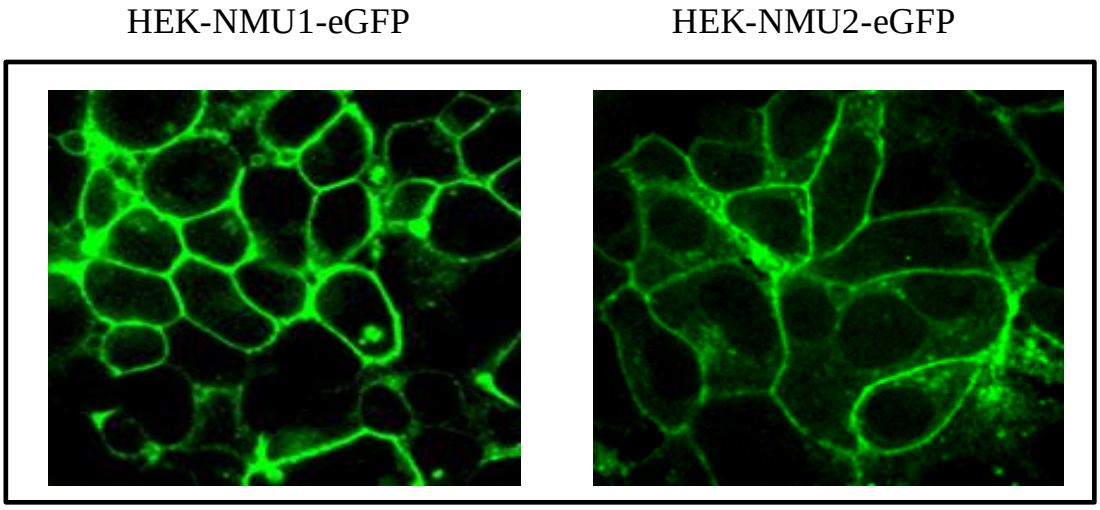

Figure 4.5. Confocal images of HEK-NMU1-eGFP and NMU2-eGFP expressed in HEK293 cells. Following 48 h of transfecting HEK293 cells with plasmid containing either NMU1-eGFP or NMU2-eGFP, cells grown on 25 mm glass coverslips were viewed using confocal microscopy with a laser excitation wavelength of 488 nm. Images are representative of 3 different experiments for each cell line showing eGFP-fluorescence appropriate cell membrane localization.

a) HEK-NMU1-eGFP

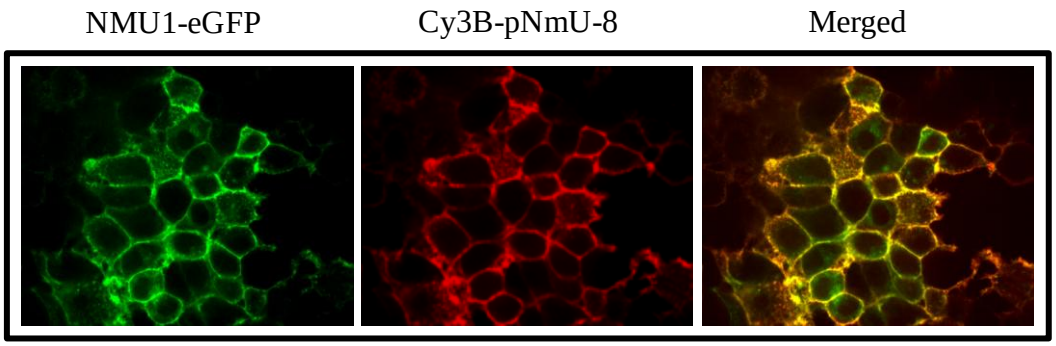

b) HEK-NMU2-eGFP

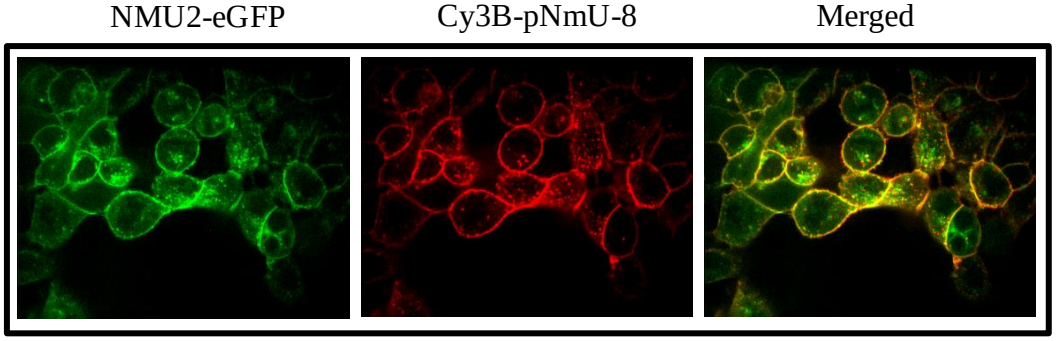

Figure 4.6. Binding of fluorescently-tagged pNmU-8 (Cy3B-pNmU-8) to either HEK-NMU1-eGFP or HEK-NMU2-eGFP. Following transfection of HEK293 cells with plasmid containing either NMUR1-eGFP or NMUR2-eGFP, cells were selected with Geneticin (1 µg/mL) for 21 days. HEK-NMU1-eGFP (a) or HEK-NMU2-eGFP (b) were cultured on 25 mm glass coverslips for 24 h, exposed to Cy3B-pNmU-8 (10 nM) and then visualized following 10 min of the addition by confocal microscopy using laser excitation wavelengths of 488 nm and 568 nm for green fluorescent protein and Cy3B, respectively. Images are representative of 5 separate experiments.

4.2.2 Functional characterization of HEK-NMU1-eGFP and HEK-NMU2-eGFP

Investigation of Ca^{2+} responses ($G\alpha_{q/11}$ coupling) to hNmU-25 in populations of fluo-4-loaded HEK-NMU1-eGFP and HEK-NMU2-eGFP cells demonstrated concentration-dependent increases in $[Ca^{2+}]_i$ followed by a slow declines similar to the response observed in HEK-NMU1 and HEK-NMU2. However, in cells expressing the eGFP-tagged receptors, maximal responses were reduced by 2-3 folds compared to cells expressing the untagged receptors (Figure 4.7).

Carbachol-mediated Ca^{2+} signalling was also studied in cells expressing either NMU2 or NMU2-eGFP to determine whether these reductions were due to interference by the eGFP either in receptor coupling or in the $[Ca^{2+}]_i$ measurement technique itself. The magnitude of Ca^{2+} responses to carbachol were also reduced in HEK-NMU2-eGFP compared to HEK-NMU2 with a slight (insignificant) reduction in potency (Figure 4.8). This might suggest that the higher basal fluorescence in HEK-NMU2-eGFP cells influences the measurement technique.

Another approach was taken to confirm the effect of eGFP fluorescence rather than interference in receptor coupling. Thus, PLC activity in response to receptor activation was determined by measurement of agonist-stimulated $[^3H]InsP_x$ accumulation against a LiCl block of inositol monophosphatase (Allison *et al.*, 1976). Incubation of HEK-NMU1, HEK-NMU1-eGFP, HEK-NMU2 or HEK-NMU2-eGFP with increasing concentrations of hNmU-25 (0.01-100 nM) for 15 min following a 10 min pre-incubation with LiCl (10 mM) resulted in concentration-dependent increases in $[^3H]InsP_x$ accumulation. Responses to hNmU-25 were similar in all cell-lines (Figure 4.9).

Coupling to $G\alpha_{i/o}$ in HEK-NMU1-eGFP and HEK-NMU2-eGFP in comparison to HEK-NMU1 and HEK-NMU2 was investigated using a cAMP assay (Figure 4.10). These studies demonstrated the ability of forskolin (1 μM) to evoke a significant increase in cAMP accumulation in all cell-lines. Pre-addition of hNmU-25 (0.01-100 nM) failed to inhibit forskolin-stimulated cAMP elevation in either HEK-NMU1-eGFP or HEK-NMU2-eGFP. In contrast, hNmU-25 caused concentration-dependent inhibitions of

forskolin-stimulated cAMP accumulation with pIC_{50} values of 8.23 ± 0.20 for HEK-NMU1 and 8.31 ± 0.20 for HEK-NMU2.

Real-time monitoring of NMU2-eGFP internalization in HEK-NMU2 was performed using confocal microscopy and following challenge with hNmU-25 (30 nM, 5 min) revealed gradual translocation of NMU2-eGFP fluorescence from plasma membrane to the cytosol, where internalization was observable after 2.5 min and maximum internalization (30-40% of receptors) was observed after 20-30 min (Figure 4.11). Following 2.5-10 min of initial exposure to hNmU-25, NMU2-eGFP fluorescence formed aggregates at the plasma membrane or just underneath the cell surface. Interestingly, removal of the ligand by brief acid wash did not inhibit the rate of internalization and indeed enhanced receptor sequestration particularly after 20 min post ligand exposure.

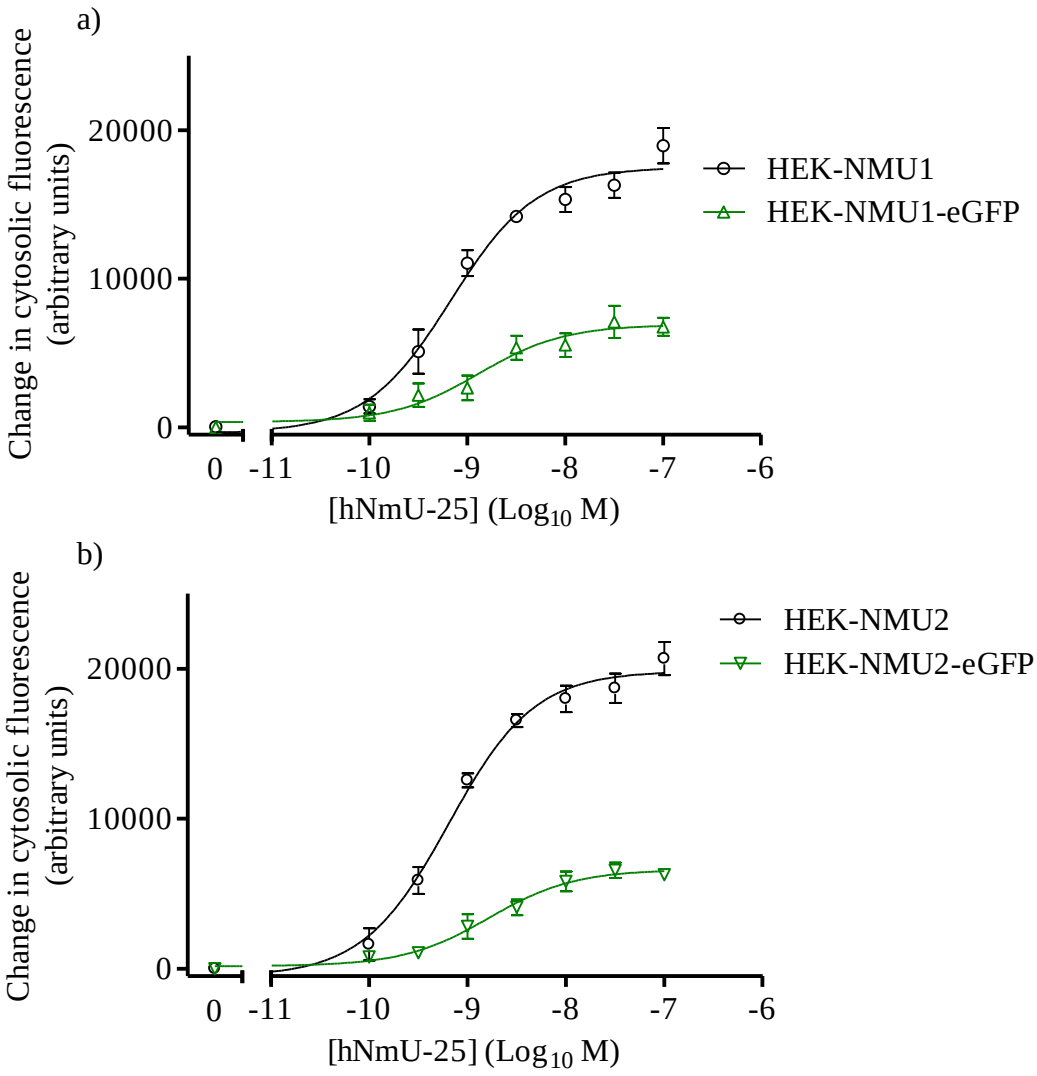

Figure 4.7. Concentration-response curves for hNmU-25-mediated changes in $[Ca^{2+}]_i$ in NMU1- or NMU2-expressing cell-lines. HEK-NMU1 or HEK-NMU1-eGFP (a) and HEK-NMU2 or HEK-NMU2-eGFP (b) were cultured on 96-well plates, loaded with fluo-4-AM and challenged with different concentrations of hNmU-25 using a NOVOstar plate reader. Changes in fluorescence were monitored as an index of $[Ca^{2+}]_i$. The maximal changes in fluorescence were used to construct concentration-response curves for cells expressing NMU1 and NMU1-eGFP (a) or NMU2 and NMU2-eGFP. The pEC_{50} values for hNmU-25 in HEK-NMU1 and HEK-NMU1-eGFP were 9.18 ± 0.05 and 8.86 ± 0.15, respectively while in HEK-NMU2 and HEK-NMU2-eGFP values were 9.20 ± 0.10 and 8.77 ± 0.15, respectively. Data are mean ± s.e.m., n=3.

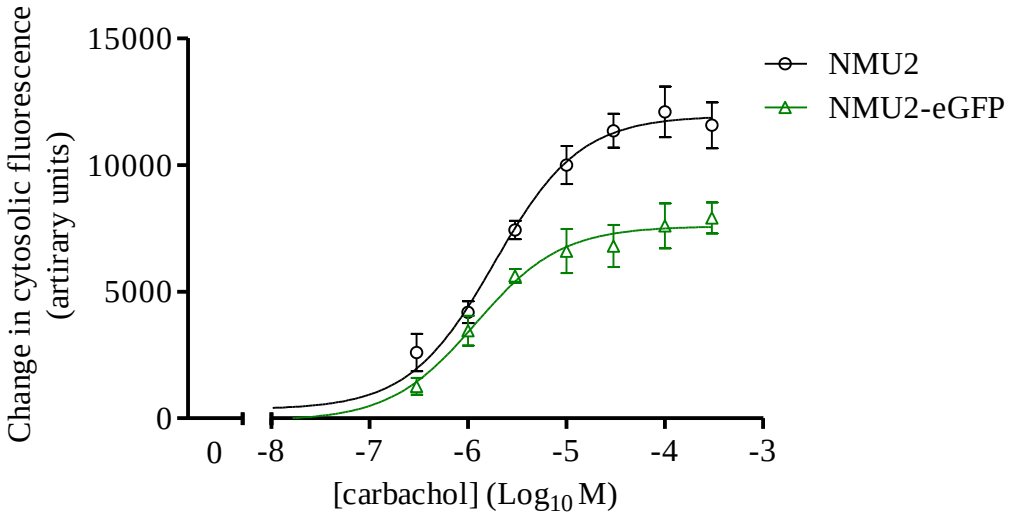

Figure 4.8. Carbachol-stimulated changes in $[Ca^{2+}]_i$ in NMU2-expressing cell-lines. HEK-NMU2 or HEK-NMU2-eGFP were cultured on 96-well plates, loaded with fluo-4-AM and challenged with different concentrations of carbachol using a NOVOstar plate reader. Fluo-4-AM fluorescence was monitored as an index of $[Ca^{2+}]_i$ and the difference in fluorescence was calculated relative to the basal level. The maximal changes in fluorescence were used to construct concentration-response curves. The pEC_{50} values were 5.70 ± 0.10 and 5.87 ± 0.19 for HEK-NMU2 and HEK-NMU2-eGFP, respectively. Data are mean ± s.e.m., n=3.

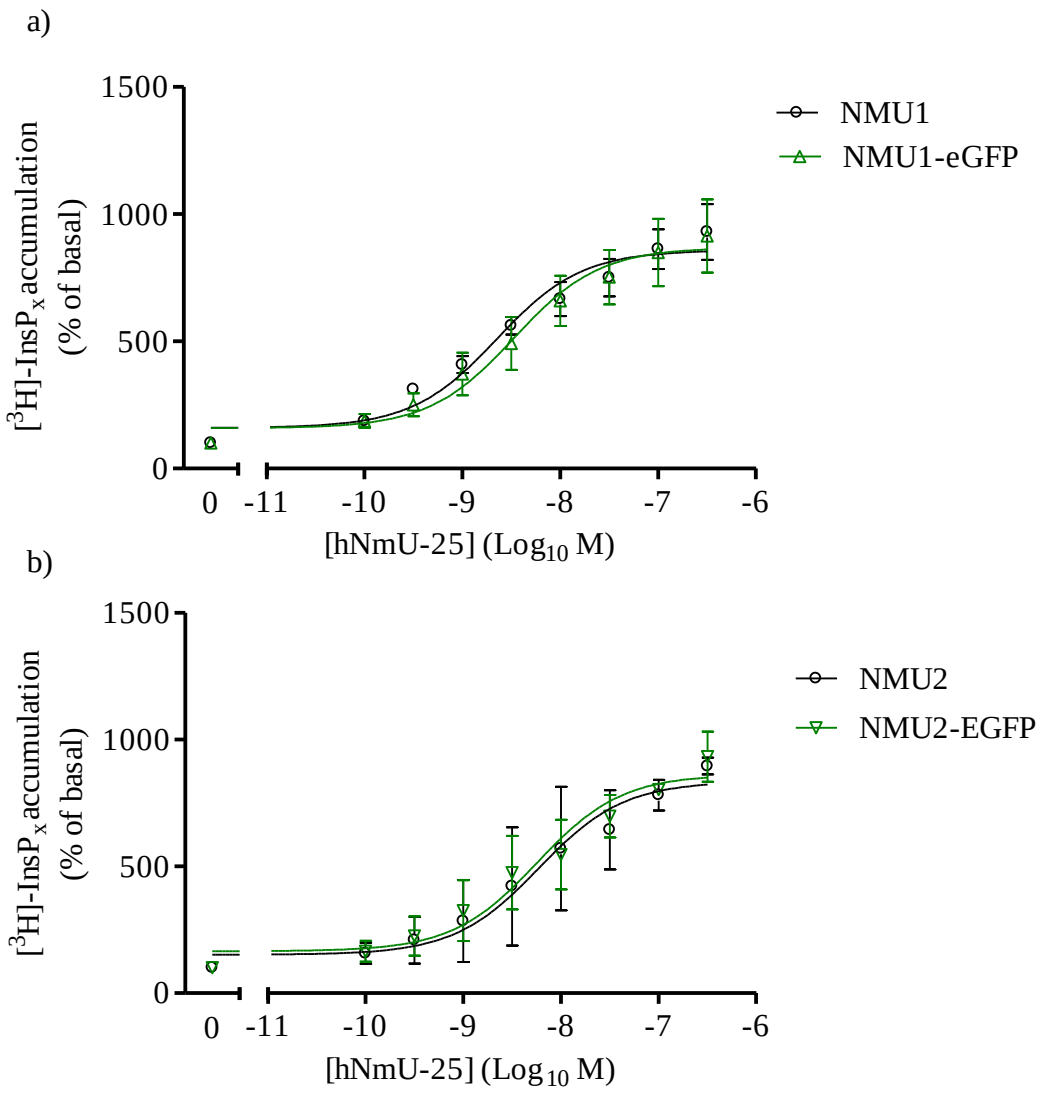

Figure 4.9. Concentration-response curves for hNmU-25-stimulated [^{3}H]InsP$_x$ accumulation in NMU1 or NMU2-expressing cell-lines. For each cell-line, cells were grown in 24-well plates and incubated with myo-[^{3}H]inositol for 48 h and then incubated with LiCl (10 mM) for 10 min prior to agonist addition. Cells were then challenged with different concentrations of hNmU-25 for 15 min. [^{3}H]InsP$_x$ accumulation is expressed as a percentage increase over respective basal levels. The pEC$_{50}$ values for hNmU-25 in HEK-NMU1 and HEK-NMU1-eGFP were 8.83 ± 0.15 and 8.65 ± 0.21, respectively while in HEK-NMU2 and HEK-NMU2-eGFP values were 8.23 ± 0.11 and 8.25 ± 0.21, respectively. Data are mean ± s.e.m., n=3.

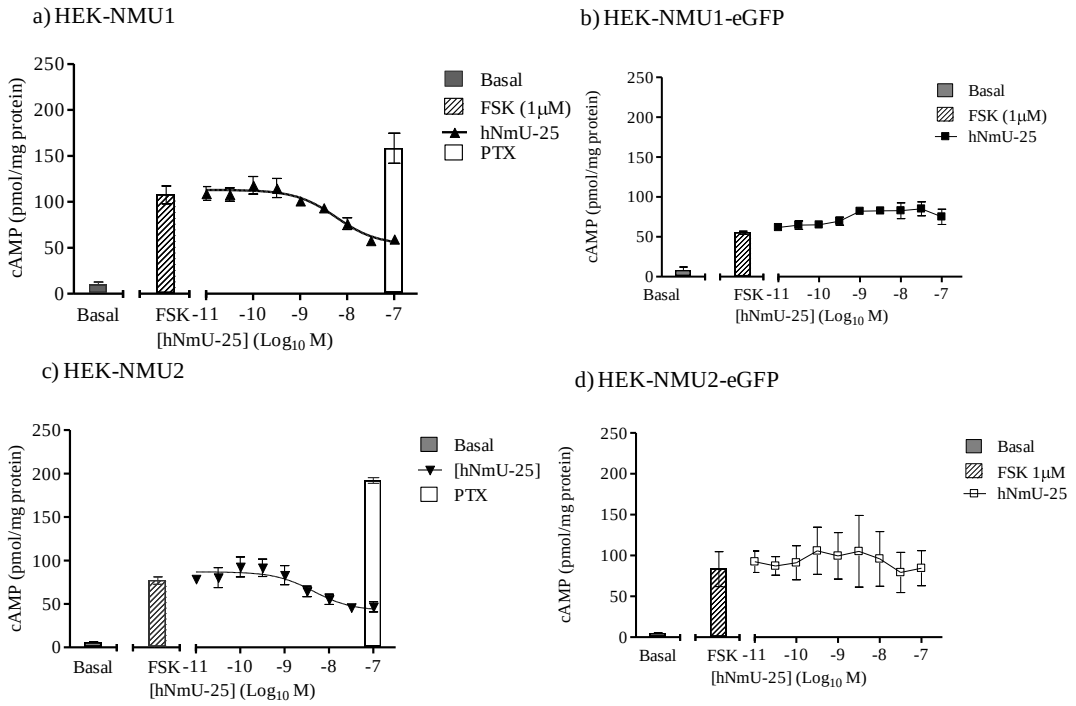

Figure 4.10. Effect of hNmU-25 on forskolin-stimulated cAMP accumulation in HEK-NMU1, HEK-NMU1-eGFP, HEK-NMU2 and HEK-NMU2-eGFP. Each cell-line was plated for 48 h in 24-well plates coated with poly-D-lysine. Cells were incubated for 10 min with hNmU-25 (0.01-100 nM) and then stimulated with forskolin (FSK, 1 μM) for a further 10 min before extraction and measurement of cAMP. In each graph, left and centre segments show basal and forskolin-stimulated cAMP levels, respectively. The right segment of each panel shows the influence of increasing concentrations of hNmU-25 on forskolin-stimulated cAMP accumulation. The pIC_{50} values were 8.23 ± 0.20 for HEK-NMU1 and 8.31 ± 0.20 for HEK-NMU2, while hNmU-25 did not significantly inhibit forskolin-stimulated cAMP accumulation in HEK-NMU1-eGFP or HEK-NMU2-eGFP. Data are mean ± s.e.m., n=3.

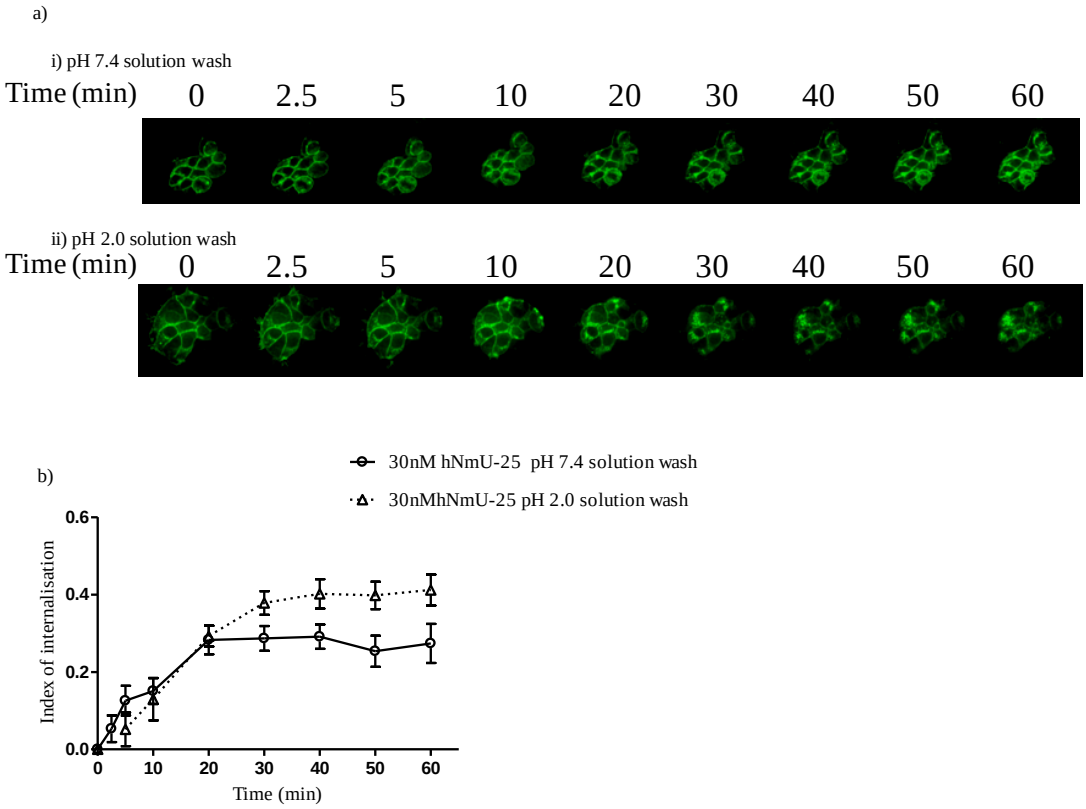

Figure 4.11. Confocal imaging and quantification of hNmU-25-mediated internalization of NMU2 following washes with buffer at either pH7.4 or pH2.0. HEK-NMU2-eGFP were cultured on 25 mm glass coverslips for 24 h. Cells were then challenged with hNmU-25 (30 nM) for 5 min followed by perfusion with KHB (pH 7.4, ai) or subjected to a brief (20s) pH 2.0 wash followed by KHB (pH 7.4) perfusion for 1 min (aii). Cells were exposed to 1 min perfusion every 10 min throughout duration of the experiments. Internalization was visualized and captured using confocal microscopy at excitation an wavelength of 488 nm (ai, aii) at 0 (before ligand addition, basal), 2.5, 5, 10, 20, 30, 40, 50 and 60 min. Experiments were performed at 37 °C and images are representative of 3 experiments. The index of internalization was calculated in each experiment by choosing 6 cells randomly and measuring the ratio of plasma membrane and cytosolic fluorescence as described in Methods. Data are mean ± s.e.m., n=18 cells from three separate experiments.

4.3 Discussion

Two constructs were generated by inserting full-length NMU1 or NMU2 into the pEGFP-N1 plasmid (whereby eGFP is attached to the *C*-terminus of the inserted protein) using a method that has been used previously to epitope-tag other GPCRs, such as the GLP-1 receptor (Huang, 2011b). Sequencing analysis revealed that the NMU1 of NMU1-eGFP has an identical sequence to NMU1 with accession number NM 006056, while NMU2 of NMU2-eGFP has the identity of hNMU2 with accession number NM 020167. In stably transfected HEK293 cells, confocal images of NMU1-eGFP and NMU2-eGFP showed intense plasma membrane fluorescence, typical of the localization of GPCRs (Millar *et al.*, 2010). However, NMU1-eGFP also exhibited localization to small subcellular compartments, while NMU2-eGFP showed a similar distribution as well as some cytosolic fluorescence. The dense subcellular localization in both stable cell-lines might indicate the existence of these receptors in specialized compartments, such as the endoplasmic reticulum and Golgi complex; organelles responsible for the synthesis of the proteins and transportation to the cell-surface. Thus, the fusion protein may simply recapitulate the physiological synthesis and transport of the receptor (Tarasova *et al.*, 1997). However, it must also be considered that the presence of such a large (30 KDa) epitope-tag could theoretically affect the processing and the trafficking of the receptor (McLean *et al.*, 2000).

Cell phenotype plays an essential role in the pattern of receptor expression (Bohme *et al.*, 2009). The presence of cytosolic fluorescence in HEK-NMU2 has also been observed in HEK293 cells expressing other GPCRs tagged with eGFP at the *C*-terminus, such as the GLP-1 receptor (Huang, 2011b; Syme *et al.*, 2006). This might be due to the fact that NMU2 has a short sequence of amino acids at the *C*-terminus known as a tyrosine motif, Tyr-X-X-Ø (YQSF, Figure 1.2). This has been shown to be involved in constitutive, clathrin-dependent internalization of other GPCRs, including the protease-activated receptor-1 (PAR-1) (Marchese *et al.*, 2008). Furthermore, it has been reported recently using immunocytochemistry that in human pancreatic ductal adenocarcinoma (PDAC), endogenously expressed NMU2 shows cell-surface, cytoplasmic and nuclear localizations (Ketterer *et al.*, 2009).

Addition of Cy3B-pNmU-8 (10 nM) to either cell-line revealed that both NMU1-eGFP and NMU2-eGFP are able to bind to their cognate ligand. Further, binding was pseudo-irreversible, as perfusion of the cells with KHB following agonist addition for 1 min did not decrease the intensity of the fluorescence. This is consistent with the previously observed irreversible binding of Cy3B-pNmU-8 to unlabelled NMUs recombinantly expressed in HEK293 cells (see **Chapter 3**, (Brighton *et al.*, 2004a)).

Following ligand addition for 10 min, each construct exhibited a different degree of internalization and intracellular localization of ligand/receptor. For example, NMU1-eGFP and Cy3B-pNmU-8 co-localized mainly at the cell membrane or just underneath the plasma membrane. In HEK-NMU2, merged images showed strong co-localization of NMU2-eGFP/Cy3B-pNmU-8 at the cell membrane and a heterogeneous population of receptor, ligand or ligand/receptor within the cytosol. Although both receptors share 51% homology (Howard *et al.*, 2000) and show comparable ligand affinity and pseudo-irreversible binding, the trafficking compartments for each receptor subtype might be distinct. This is supported by the differences between NMU1 and NMU2 within the *C*-terminus and intracellular domains, and is also supported by the fact that GPCR subtypes often exhibit different subcellular localization and trafficking (Bohme *et al.*, 2009). However, careful comparisons are needed using hNmU-25/Cy3B-pNmU-8 and unlabelled receptors using imaging as well as functional studies to support this finding, since it has been reported that tagging GPCRs at either *N*- or *C*-termini may affect binding, coupling and/or trafficking of the receptor (Bohme *et al.*, 2009).

The marked (2-3 fold) reductions in hNmU-25-mediated Ca^{2+} responses observed in fluo-4-loaded NMU-eGFP cell-lines in comparison to the untagged NMU-expressing cell-lines may be due to the overlap of spectral range of eGFP and fluo-4-AM, rather than an altered coupling efficiency. Indeed, a similar reduction was observed for carbachol-mediated Ca^{2+} responses in fluo-4-loaded HEK-NMU2-eGFP cells compared to the responses in cells expressing unlabelled NMU2. Several suggestions have been put forward to overcome the problem of spectral overlapping of eGFP and calcium-sensitive fluorophores. For example, the use of red-shifted fluorescent Ca^{2+} indicators, such as Rhod-2, x-Rhod 1 or GFP-Certified™ FluoForte™ dye, which have different excitation

and emission wavelengths (> 530 nm) compared to eGFP (Bolsover *et al.*, 2001) has been suggested. Furthermore, it has been shown that this problem can be solved by combining the use fura-2 and "long pass emission filtering", where emission of fura-2 is collected at >560 nM (Berkova *et al.*, 2003).

The functional output of NmU-mediated $G\alpha_{q/11}$ coupling of the eGFP- and non-tagged receptors was also compared by determining hNmU-25-mediated [^{3}H]$InsP_x$ accumulation. Stimulation of HEK-NMU1-eGFP and HEK-NMU2-eGFP with hNmU-25 resulted in concentration-dependent accumulations of [^{3}H]$InsP_x$ with no significant differences in potency and efficacy being seen compared to cells expressing wild-type NMUs. This finding indicates that tagging NMUs with eGFP has no detrimental effect on NMU activation of the $G\alpha_{q/11}$-PLC signalling pathway and the differences in the magnitude of the $[Ca^{2+}]_i$ response observed earlier is most likely due to the presence of eGFP and fluorescence interference. In contrast, inhibition of forskolin-stimulated cAMP accumulation on hNmU-25 addition was not observed in HEK-NMU1- or NMU2-eGFP cell-lines. Although some studies have reported partial or no adenylyl cyclase inhibitory effects of NMU activation (Hosoya *et al.*, 2000; Szekeres *et al.*, 2000), whether this is dependent on cell-type or the level of receptor expression is unclear. Since the intracellular loops and *C*-terminus of GPCRs play essential roles in G protein coupling, activation and trafficking (Marchese *et al.*, 2008; Rasmussen *et al.*, 2007; Strader *et al.*, 1994), eGFP might selectively hinder coupling to $G\alpha_{i/o}$. It is still a topic of debate whether eGFP should be inserted at the *C*- or *N*- terminus of GPCRs (Huang, 2011b). For example, it has been shown that tagging the *N*-terminus, but not the *C*-terminus, of the receptor affects ligand binding and functionality of rat olfactory I7 receptor (Ivic *et al.*, 2002). In contrast, other reports have demonstrated that *C*-terminal tagging interferes with ligand binding and trafficking of several GPCRs, including β_1 and β_2 adrenoceptors, the μ-opioid receptor and bradykinin B_2 receptor (Kalatskaya *et al.*, 2006; McLean *et al.*, 2000; Perret *et al.*, 2003).

The level of NMU2-eGFP internalization was comparable to the level of [^{125}I]hNmU-25 internalization in HEK-NMU2 observed in earlier work (Brighton, 2005). However, maximum internalization here was achieved after approximately 30 min, while the previous study showed maximum internalization within 10 min. This is may be due to the

difference in measurement technique or tagging NMU2 with eGFP at the *C*-terminus affect the kinetics of NMU2 internalization. Alternatively the previous study used [^{125}I]hNmU-25 to assess internalisation and thus measured accumulation of ligand rather that receptor internalisation directly. In the present study, the rate of internalization was not slowed by the removal of the bound-ligand by brief acid wash indicating that the first challenge with hNmU-25 was adequate to induce internalization. The reasons for the apparent increase in receptor internalisation following the acid wash are unclear. Although the eGFP-tagged receptors have allowed measurement of receptor internalization, it must be noted that the G protein coupling may differ from that of the untagged receptors. The potential effect of such a difference on receptor trafficking is unclear. Both eGFP-tagged NMU cell-lines will need to be further characterized in comparison to unlabelled NMU-expressing cells in order to be used with confidence for monitoring NMU1 and NMU2 trafficking.

Chapter 5

Screening for endogenous cellular responses to NmU

5.1 Introduction

Characterization of NMU signalling via $G\alpha_{q/11}$ and/or $G\alpha_{i/o}$ pathways has mainly been conducted in recombinant systems (Aiyar *et al.*, 2004; Brighton *et al.*, 2004a; Hosoya *et al.*, 2000; Hsu *et al.*, 2007; Szekeres *et al.*, 2000). The data presented in Chapter 3 are consistent with the previous reports of NMU1/2-mediated increases in $[Ca^{2+}]_i$ via activation of $G\alpha_q$-PLC signalling, and inhibition of cAMP accumulation via $G\alpha_i$-AC signalling. However, absolute and relative differences in NMU1 and NMU2 coupling in different recombinant backgrounds have been found (Brighton *et al.*, 2004a). In recombinant systems, receptors are generally expressed at supra-physiological levels giving rise to an increased risk of promiscuous coupling (Cordeaux *et al.*, 2000; Zhu *et al.*, 1994).

To date, only one study has investigated potential dual $G_{q/11}/G_{i/o}$ coupling and pseudo-irreversibility of NmU binding of endogenously expressed NMUs in cultured rat colonic myocytes (Brighton *et al.*, 2008). This study demonstrated that rNmU-23 (10 nM) activates both $G\alpha_q$ and $G\alpha_i$ in membranes of rat colonic myocytes (cultured for 7-9 days before membrane preparation) using $[^{35}S]GTP\gamma S$ binding/Gα-specific immunoprecipitation assays, and that rNmU-23 and hNmU-25 cause equipotent concentration-dependent elevations of $[Ca^{2+}]_i$ in cultured intact colonic myocytes. Furthermore, the pseudo-irreversibility of binding was also demonstrated by single-cell confocal imaging using the fluorescent ligand, Cy3B-pNmU-8, with 10-fold higher concentrations of unlabelled hNmU-25 being unable to displace Cy3B-pNmU-8, even when experiments were performed at 12 °C to minimize internalization (Brighton *et al.*, 2008). Interestingly, strips of rat colonic smooth muscle could be contracted repetitively by repeated additions of rNmU-23, even when the washing time between additions was shortened from 30 min to 1 min (Brighton *et al.*, 2008). In contrast, single-cell Ca^{2+} imaging of cultured rat colonic myocytes showed a lack of repetitive Ca^{2+} signalling on re-addition of either rNmU-23 or hNmU-25 even with extended 5 min wash-periods

between applications (Brighton *et al.*, 2008). A number of studies have shown the natural expression of NMUs and/or the ability of NmU to evoke NMU-mediated $[Ca^{2+}]_i$ mobilization in a range of cells endogenously expressing NMU (see **Chapter 1, section 1.2.2**), such as K562 cells (Shetzline *et al.*, 2004), mouse Th2 cells (Johnson *et al.*, 2004), primary mast cells (Moriyama *et al.*, 2005), human pancreatic cancer cell-lines (Ketterer *et al.*, 2009), pancreatic β-cells (Kaczmarek *et al.*, 2006) and eosinophils (Moriyama *et al.*, 2006b). Based on these data and studies that have shown previously a significant expression of either NMU1 or NMU2, several isolated primary cells and cell-lines have been investigated here to assess their responsiveness to NmU addition. Different approaches have been applied in this initial screening exercise, including organ-bath assays, assessment of $[Ca^{2+}]_i$ mobilization in single-cells by confocal imaging and cell populations using a NOVOstar plate-reader, $[^3H]InsP_x$ assays and inhibition of forskolin-stimulated cAMP generation assays.

5.2 Results

5.2.1 Screening of tissues and primary cells for NmU-mediated responses

A previous study established the ability of rat NmU (rNmU-23) to contract the distal segment of the rat colon and evoke Ca^{2+} responses in cultured colonic myocytes (Brighton *et* a*l*., 2008). Furthermore, that study also demonstrated the ability of rat NMU to couple to both $G\alpha_{q/11}$ and $G\alpha_{i/o}$. In the present study, segments of rat colon were prepared to study NmU-mediated signalling by endogenously expressed NMU at either a tissue or cellular level. Enzymatic digestion of the distal part of rat colon resulted in isolation of cells with a morphological shape resembling smooth muscle cells (Figure 5.1a). A smooth muscle cell phenotype was confirmed on the day of experiments (day 6 in culture) by immunocytochemical identification of α-actin, a smooth muscle cell marker, which is found mainly in the cytosolic microfilament bundles (Skalli *et al.*, 1989). Staining was evident as fluorescent strands within the cytoplasmic region in all of the cells (Figure 5.1b).

Confocal Ca^{2+} imaging of rat colonic myocytes cultured for 6 days and fluo-4-loaded, revealed that addition of rNmU-23 (100 nM-1 μM) following 30 s of basal recording did not evoke a Ca^{2+} response (Figure 5.2). In contrast, application of UTP (100 μM) to the same cells approximately 3 min after addition of rNmU-23 (t=230 s) resulted in a robust Ca^{2+} response that was 0.5-2.5 fold (n=10) above basal levels (Figure 5.2). In these experiments, rNmU-23 was not removed by perfusion of the chamber to avoid detachment of the cells from the coverslip. Modifications of the cell isolation technique, culture of the cells and the experimental conditions were tried, but did not result in consistent Ca^{2+} responses to rNmU-23.

In order to assess whether rNmU-23 altered cAMP levels in cultured colonic myocytes, cells that had been cultured for 6 days were challenged with forskolin (10 μM, 10 min), which resulted in a significant increase in cAMP levels (168 ± 5 pmol/mg protein compared to basal levels of 26 ± 3 pmol/mg protein, n=3, Figure 5.2). The ability of NmU to inhibit forskolin-stimulated cAMP accumulation (see **Chapter 2, section 2.2.15**) in these cells was assessed by incubation with one of a range of concentrations of rNmU-23 (1-100 nM) added 10 min prior to incubation of the cells with forskolin (10

μM, 10 min). Pre-addition of rNmU-23 to the cells did not cause any significant inhibition of forskolin-stimulated cAMP accumulation (Figure 5.3).

The contractile response to NmU in strips of colonic smooth muscle was also examined (Figure 5.4). As a positive control, rat colonic smooth muscle strips were challenged with carbachol (1 μM) following 30 min pre-equilibrium in organ-baths supplied with oxygenated Tyrode's solution. Carbachol evoked a robust contractile peak response followed by a decline towards pre-contraction levels. Addition of rNmU-23 (1 μM) after 30 min of carbachol challenge did not cause a contractile response. Moreover, 15 min following addition of rNmU-23, re-challenge of colonic strips with carbachol (1 μM) resulted in a second contractile response which was equal to the initial response (Figure 5.4). The contractile response to NmU was also assessed in strips of mouse colonic smooth muscle in which carbachol (100 μM) but not rNmU-23 evoked a contractile response (Figure 5.5). The batches of rNmU-23 used here were shown in parallel experiments to evoke Ca^{2+} responses in HEK-NMU2.

Expression of NmU and its receptors (principally NMU1) has been reported in human left ventricle and coronary artery (Mitchell *et al.*, 2009). Thus, pig coronary artery smooth muscle cells (pCASMC) were isolated using a similar enzymatic digestion to that used for rat colonic myocytes and cells were cultured on 25 mm glass-coverslips or in 24-well plates to be screened for responses to NmU. Confocal Ca^{2+} imaging of pCASMC cultured for 5-7 days and then loaded with fluo-4-AM demonstrated no change in $[Ca^{2+}]_i$ on addition of pNmU-25 (1 μM) following 30 s of basal recording (Figure 5.6). In contrast, subsequent challenge with UTP (100 μM) (150 s following addition of pNmU-25) resulted in a Ca^{2+} response with a fast peak and slower decline back towards the basal levels in the majority of cells (Figure 5.6). Furthermore, the robust increase in cAMP accumulation in response to forskolin (10 μM, 10 min) was not significantly affected by pre-addition of pNmU-25 (1 μM, 10 min; Figure 5.7).

In freshly isolated rat cardiac myocytes (kindly prepared by Dr. Nina Storey, Department of Cell Physiology and Pharmacology, University of Leicester), rNmU-23 inhibited forskolin-stimulated cAMP accumulation in a concentration-dependent manner (pIC_{50} = 8.43 ± 0.15; n=3; Figure 5.8). Pre-incubation of cardiac myocytes with PTX (200 ng/mL) for 4 h prior to rNmU-23 (100 nM) challenge significantly reduced the inhibitory

effect of rNmU-23 on forskolin-stimulated cAMP accumulation (Figure 5.9). Confocal Ca^{2+} imaging demonstrated a robust, transient Ca^{2+} response to caffeine (15 mM), but no Ca^{2+} response to rNmU-23 (100 nM) in these cells (Figure 5.10).

a)

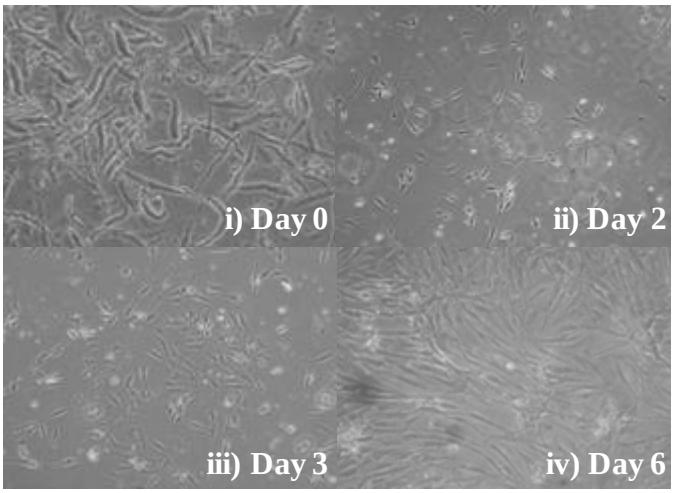

b)

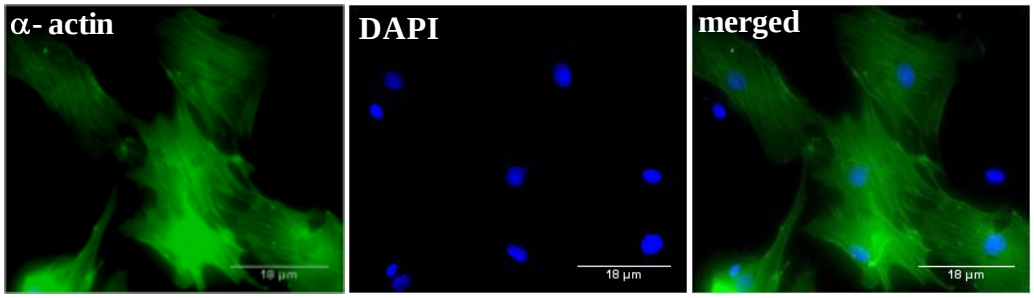

Figure 5.1. Immunocytochemical staining of α-actin in cultured rat colonic smooth muscle cells. Rat colonic smooth muscle cells were isolated by enzymatic digestion and cultured on glass coverslips up to 6 days. Phase images (a) show representative cultures of freshly isolated rat colonic smooth muscle (ai), 2 days in culture (aii), 3 days in culture (aiii) or 6 days in culture (aiv). For α-actin staining, cells were cultured for 6 days, permeabilized, fixed and probed using an α-actin primary antibody and FITC-labelled secondary antibody; nuclei were stained with DAPI (4',6-diamidino-2-phenylindole). The α-actin and nuclei staining were viewed with a 40X objective lens using a Nikon ECLIPSE TE2000-S fluorescence microscope at excitation wavelengths of 488 nm and 350 nm, respectively.

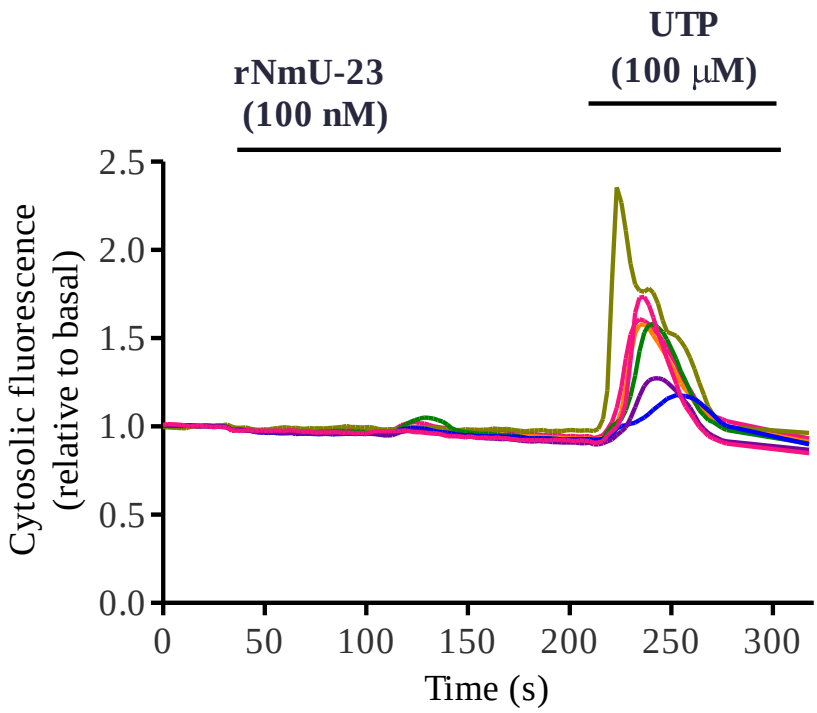

Figure 5.2. Ca^{2+} responses to sequential additions of rNmU-23 and UTP in cultured colonic smooth muscle cells. Cells were isolated and cultured on 25 mm glass coverslips for 6 days before loading with fluo-4-AM. Cells were then challenged with either rNmU-23 (100 nM) or UTP (100 μM) as indicated and cytosolic fluorescence was measured as an index of $[Ca^{2+}]_i$ using confocal microscopy. Changes in fluorescence were calculated relative to the basal level. Each line represents data from a single cell. Data are representative of 10 separate experiments, where each experiment was performed on cells from a different preparation.

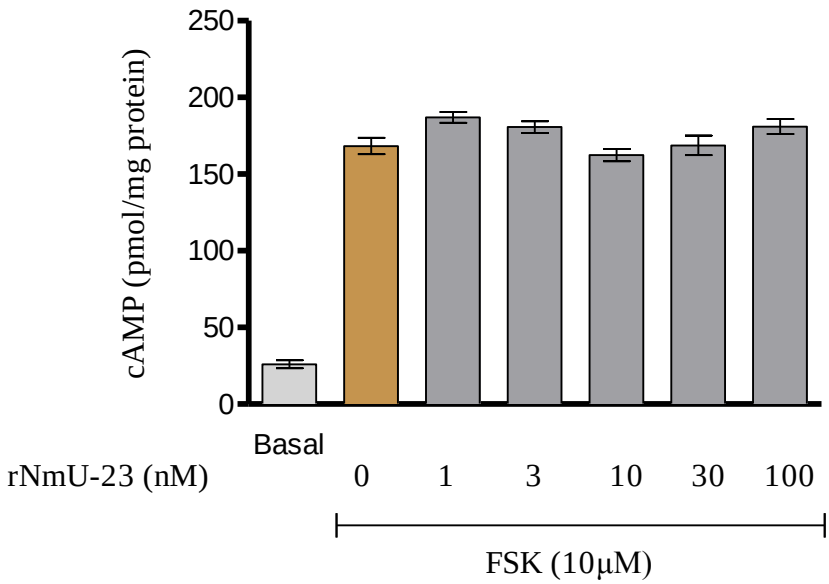

Figure 5.3. Lack of effect of rNmU-23 on forskolin-stimulated cAMP accumulation in colonic smooth muscle cells. Colonic smooth muscle cells were cultured in 24 well plates for 7 days. Cells were incubated in the presence of IBMX (500 μM) and rNmU-23, at the concentrations indicated for 10 min prior to the addition of forskolin (FSK, 10 μM, 10 min). cAMP was then extracted and measured. Data are mean ± s.e.m., n=3.

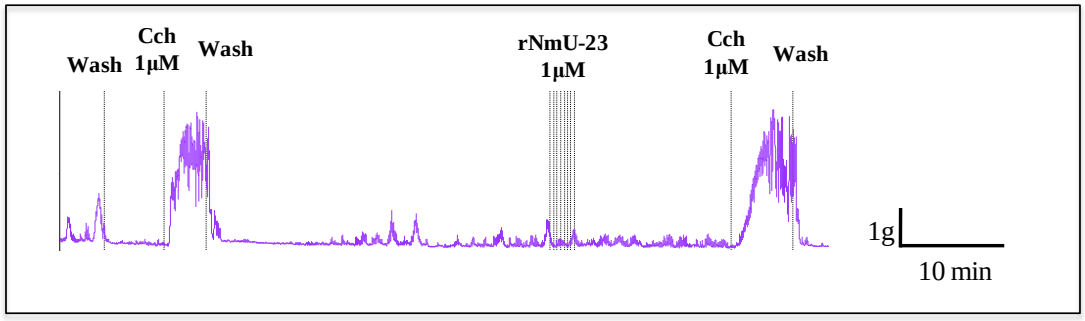

Figure 5.4. Effect of carbachol and rNmU-23 on contraction of rat colonic smooth muscle strips. Rat colonic smooth muscle strips were prepared and suspended under 1 *g* tension in an organ-bath containing oxygenated Tyrode's solution. After a 30 min equilibriation period, strips were challenged with carbachol (Cch, 1 µM) as indicated by the vertical lines followed by washing with buffer as indicated. Strips were challenged 30 min later with rNmU-23 (1 µM), then washed and left for 15 min before re-challenge with carbachol (1 µM). Data shown are representative of 8 experiments performed using tissue from different animals.

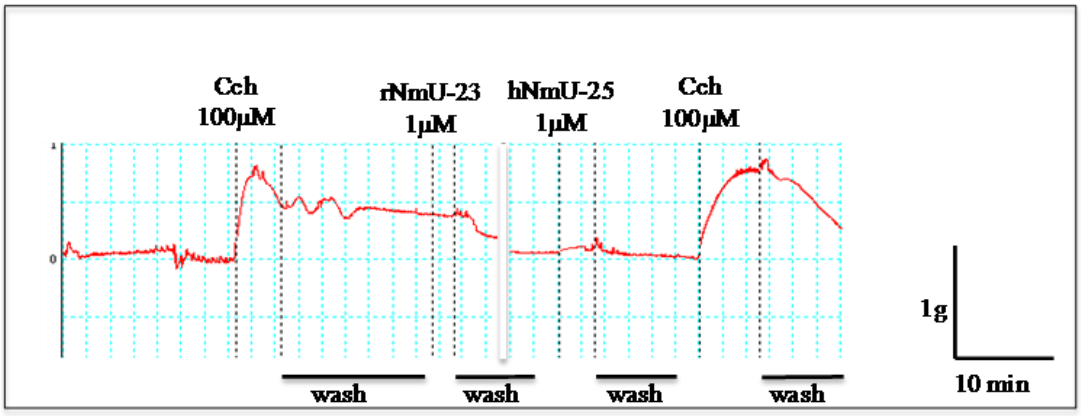

Figure 5.5. Effects of carbachol, rNmU-23 or hNmU-25 on contraction of mouse colonic smooth muscle strips. Mouse colonic smooth muscle strips were prepared and suspended under 1 *g* tension in an organ-bath containing oxygenated Tyrode's solution. After a 20 min equilibration period, strips were challenged with carbachol (Cch, 100 µM) followed by washing with buffer. After a further 30 min, strips were challenged rNmU-23 (1 µM) as indicated by vertical dotted lines, followed by washing with buffer for 20-30 min before challenge with hNmU-25 (1 µM). After further washing, strips were rechallenged with carbachol (100 µM). Data shown are representative of 3 experiments performed using tissue from different animals.

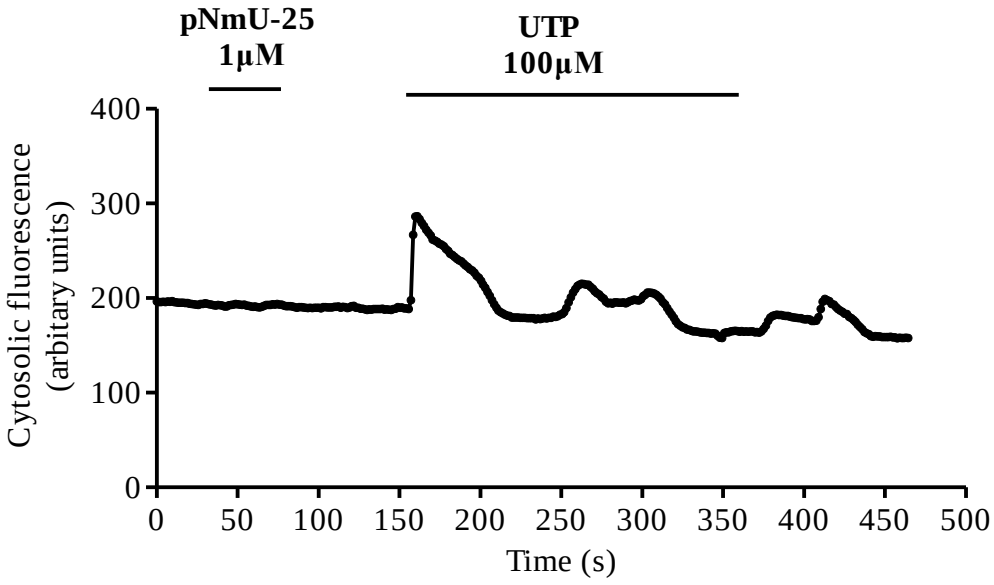

Figure 5.6. Ca^{2+} responses to rNmU-23 or UTP in cultured pig coronary artery smooth muscle cells. Cells were cultured on 25 mm glass coverslips for 5-7 days and then loaded with fluo-4-AM. Cells were challenged sequentially with rNmU-23 (1 µM) followed by UTP (100 µM). Changes in cytosolic fluorescence intensity were measured as an index of $[Ca^{2+}]_i$ using confocal microscopy. Data shown here are representative of 7 separate experiments from three different preparations.

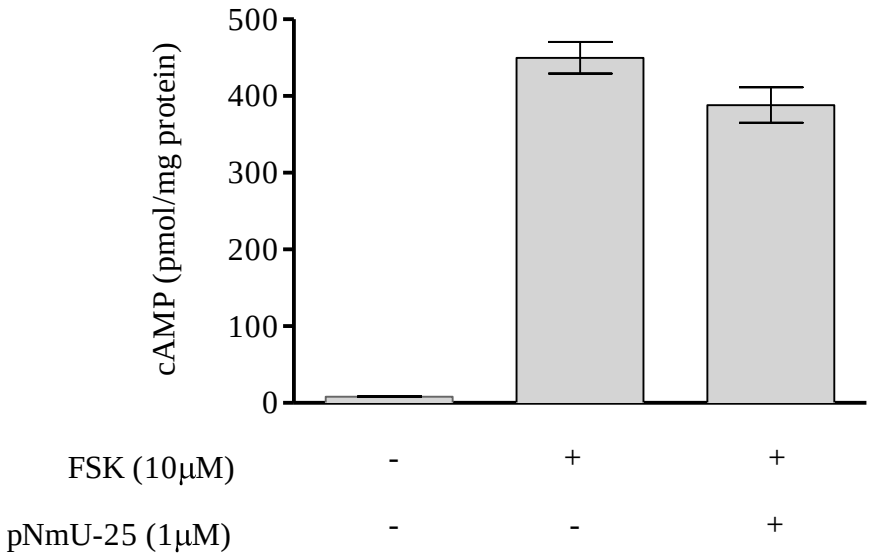

Figure 5.7. Lack of effect of pNmU-25 on forskolin-stimulated cAMP accumulation in pig coronary artery smooth muscle cells. Pig coronary artery smooth muscle cells were isolated by enzymatic digestion and cultured in 24-well plates for 5 days. Cells were incubated in the presence of IBMX (500 μM) and pNmU-25 (1 μM) prior to addition of forskolin (FSK, 10 μM) for 10 min. cAMP was then extracted and measured. Data are mean ± s.e.m., n=3.

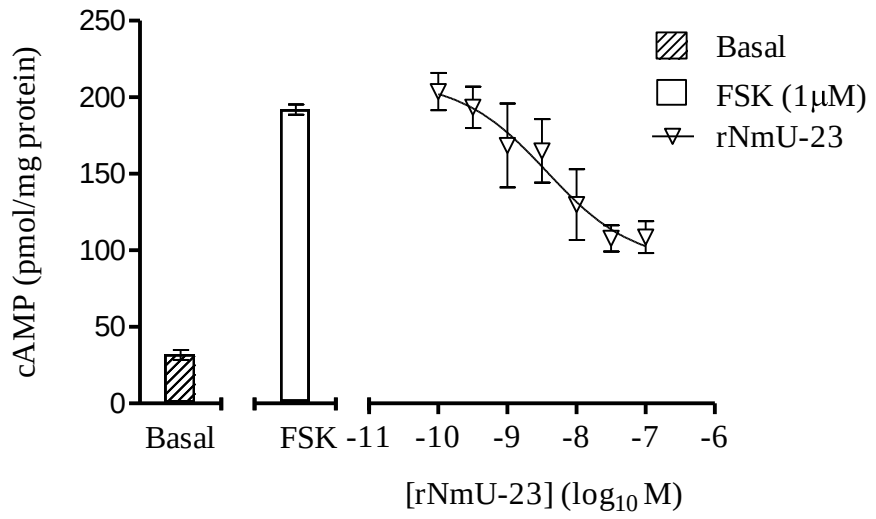

Figure 5.8. Inhibition of forskolin-stimulated cAMP accumulation in rat cardiac myocytes by rNmU-23. Freshly isolated rat cardiac myocytes were suspended in oxygenated Tyrode's solution containing IBMX (500 μM) and equilibrated for 10 min. rNmU-23, at the concentrations indicated was then added for 10 min followed by addition of forskolin (FSK, 10 μM) for a further 10 min. cAMP was then extracted and measured. The pIC_{50} value for inhibition of FSK-stimulated cAMP accumulation by rNmU-23 was 8.43 ± 0.15. Data are shown as mean ± s.e.m., n=3.

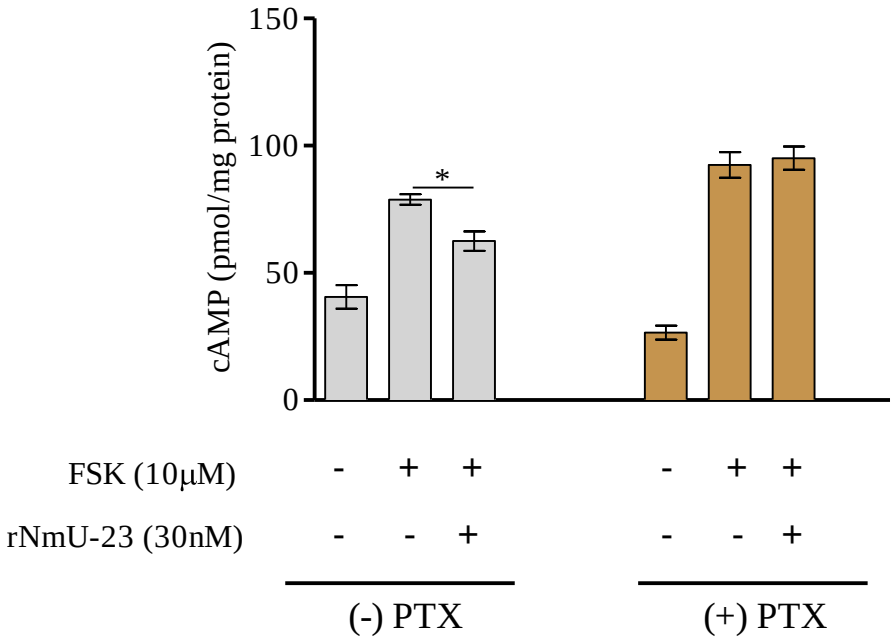

Figure 5.9. Effect of PTX on rNmU-23-mediated inhibition of forskolin-stimulated cAMP accumulation in rat cardiac myocytes. Freshly isolated rat cardiac myocytes were suspended in oxygenated Tyrode's solution and incubated in the absence or presence of PTX (200 ng/mL) for 4 h. Cells were then washed and then equilibrated in fresh Tyrode's solution containing IBMX (500 μM) for 10 min. rNmU-23 (30 nM) was then added for 10 min followed by addition of forskolin (FSK, 10 μM) for a further 10 min. cAMP was then extracted and measured. Data are shown as mean ± s.e.m., n=4; **P*<0.05.

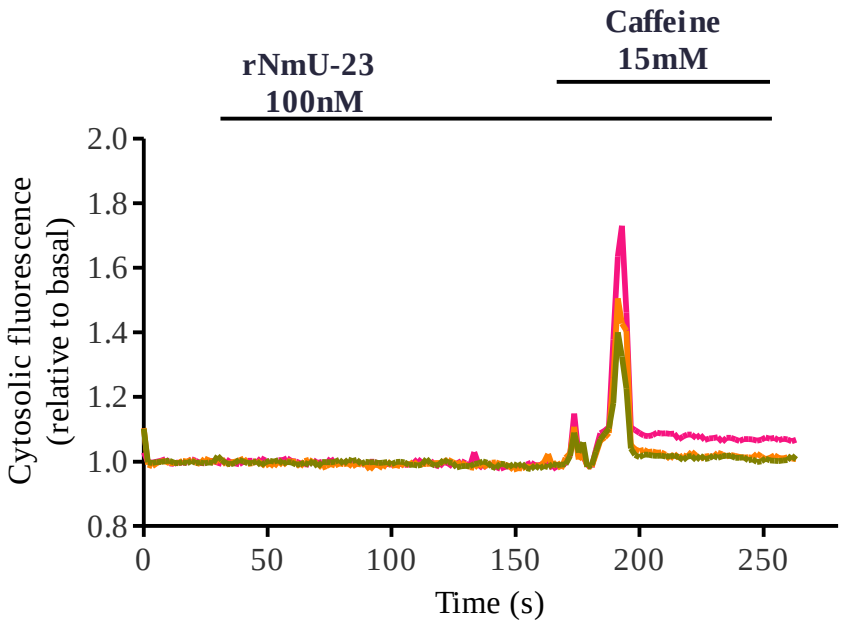

Figure 5.10. Ca^{2+} responses to sequential additions of rNmU-23 and caffeine in freshly isolated rat cardiac myocytes. Freshly isolated rat cardiac myocytes were loaded with fluo-4-AM and encouraged to adhere onto 25 mm glass coverslips coated with poly-D-lysine for 30-45 min at 37 °C. Cells were challenged sequentially with rNmU-23 (100 nM) followed by caffeine (15 mM) and changes in cytosolic fluorescence were measured as an index of $[Ca^{2+}]_i$ using confocal microscopy. Changes in fluorescence were calculated relative to the basal levels. Each trace represents data from a single cell. Data shown are representative of 3 separate experiments each from a different myocyte preparation.

5.2.2 Screening for NmU-mediated responses in different cell-lines

On the basis of recent literature, several cell-lines were selected for screening for endogenous expression of NMU. For example, recent reports suggested the expression of NMU1 in rat pancreatic islets (Kaczmarek *et al*., 2006) and the over-expression of NMU2 in pancreatic cancer cell-lines (Ketterer *et al*., 2008). Dr. Ketterer generously provided two pancreatic cancer cell-lines that showed the highest expression of NMU2 by qRT-PCR, SU.86.86 and AsPC1. Single-cell confocal microscopy (data not shown), or cell population (NOVOstar plate reader) measurement of $[Ca^{2+}]_i$ did not suggest any consistent responses to hNmU-25 (1 μM), whereas carbachol (1 mM) produce robust Ca^{2+} responses in both cell-lines (Figures 5.11 and 5.12). Similarly, hNmU-25 (1 μM) did not significantly inhibit forskolin-stimulated cAMP elevation in either cell-line (Figures 5.13 and 5.14). In an assay of phosphoinositide turnover ($[^3H]InsP_x$ accumulation in the presence of LiCl), incubation of HEK-NMU2 with hNmU-25 (1 μM) for 15 min resulted in aprox. 3.5 fold increase in $[^3H]InsP_x$ accumulation compared to cells incubated with buffer only, while no significant increase of $[^3H]InsP_x$ was observed in either pancreatic cancer cell-line (Figure 5.15).

INS-1E (rat pancreatic β-cell-line) and MIN6 (mouse pancreatic β-cell-line) were also examined by measuring changes in $[Ca^{2+}]_i$ in cell populations using a NOVOstar plate reader. In both MIN6 and INS-1E, carbachol (100 μM) induced robust Ca^{2+} responses. In contrast, Ca^{2+} responses to different concentrations of rNmU-23 (30 nM-1 μM) were not significantly different compared to responses seen on buffer-only additions (Figures 5.16 and 5.17).

The responses to NmU were also examined in KYSE140 cells (a human oesophageal cancer cell-line) as NmU and its receptors have been reported to be up-regulated (Yamashita *et al.*, 2002). No response could be detected on addition of hNmU-25 (1 μM). In contrast, carbachol (100 μM) evoked Ca^{2+} responses in the KYSE140 cell-line (Figure 5.18).

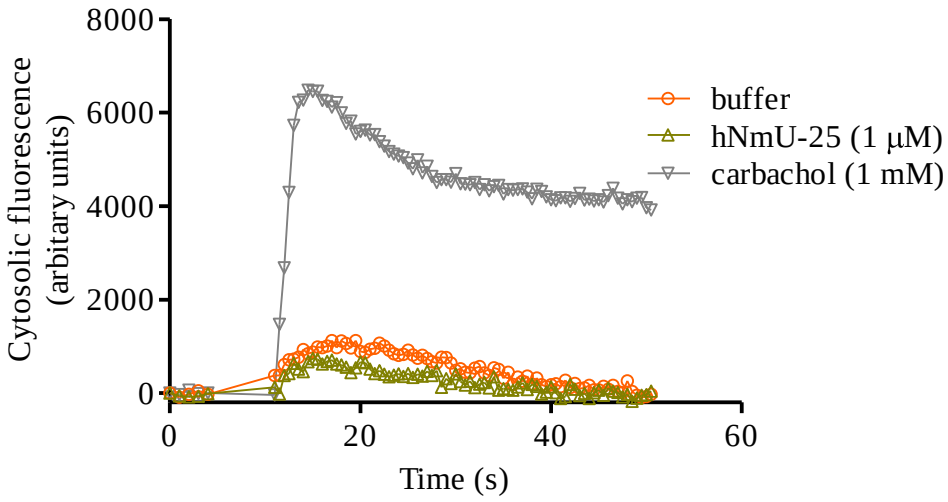

Figure 5.11. Ca^{2+} responses to carbachol or hNmU-25 in SU.86.86 cells (a human pancreatic cancer cell-line). Cells were cultured in 96-well plates for 2-3 days, and then loaded with fluo-4-AM. Cells were then challenged after 11 s of basal recording with carbachol (1 mM), hNmU-25 (1 μM), or buffer only using a NOVOstar plate reader. Cytosolic fluorescence was monitored as an index of $[Ca^{2+}]_i$. Traces shown are representative of 7 separate experiments.

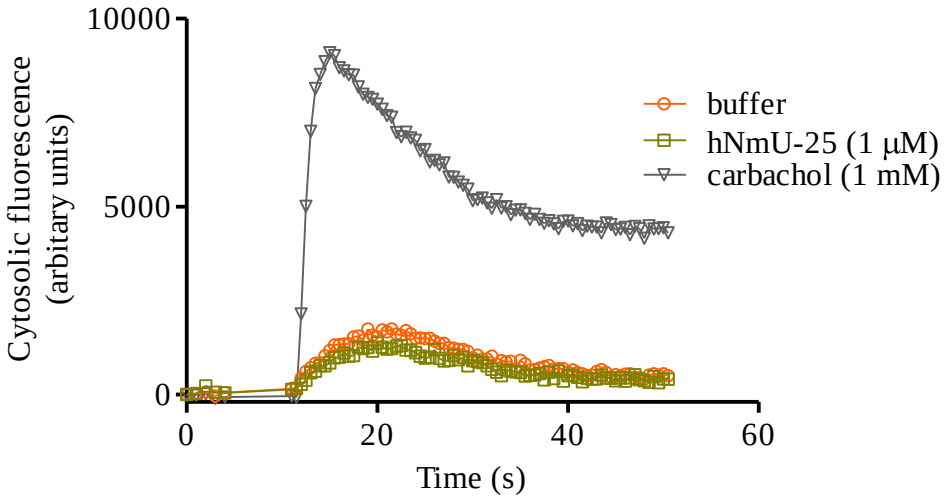

Figure 5.12. Ca^{2+} responses to carbachol or hNmU-25 in AsPC1 cells (a human pancreatic cancer cell-line). AsPC1 cells were cultured in 96-well plates for 5 days, before loading with fluo-4-AM. Cells were then challenged after 11 s of basal recording with carbachol (1 mM), hNmU-25 (1 μM), or buffer-only using a NOVOstar plate reader. Cytosolic fluorescence was monitored as an index of $[Ca^{2+}]_i$. Traces shown are representative of 3 separate experiments.

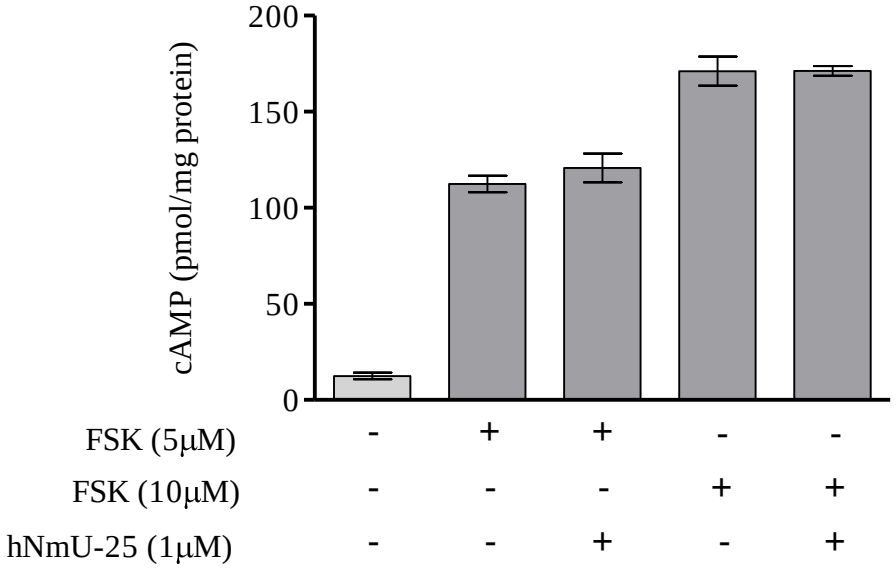

Figure 5.13. Lack of effect of hNmU-25 pre-addition on forskolin-stimulated cAMP accumulation in SU.86.86. cells. Cells were cultured on poly-D-lysine-coated 24-well plates for 48 h. In the presence of IBMX (500 μM), hNmU-25 (1μM) was added for 10 min prior to forskolin (FSK, 5 or10 μM) addition for a further 10 min. cAMP was then extracted and measured. Data are shown as mean ± s.e.m., n=3.

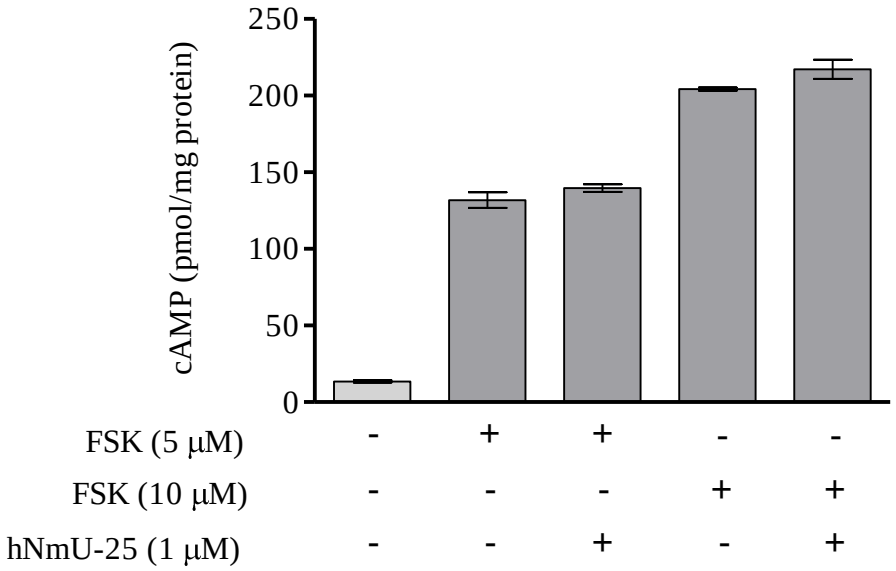

Figure 5.14. Lack of effect of hNmU-25 on forskolin-stimulated cAMP accumulation in AsPC1 cells. Cells were cultured on poly-D-lysine-coated 24-well plates for 3-4 days. In the presence of IBMX (500 μM), hNmU-25 (1μM) was added for 10 min prior to forskolin (FSK, 10 μM) addition for a further 10 min. cAMP was then extracted and measured. Data are shown as mean ± s.e.m., n=3.

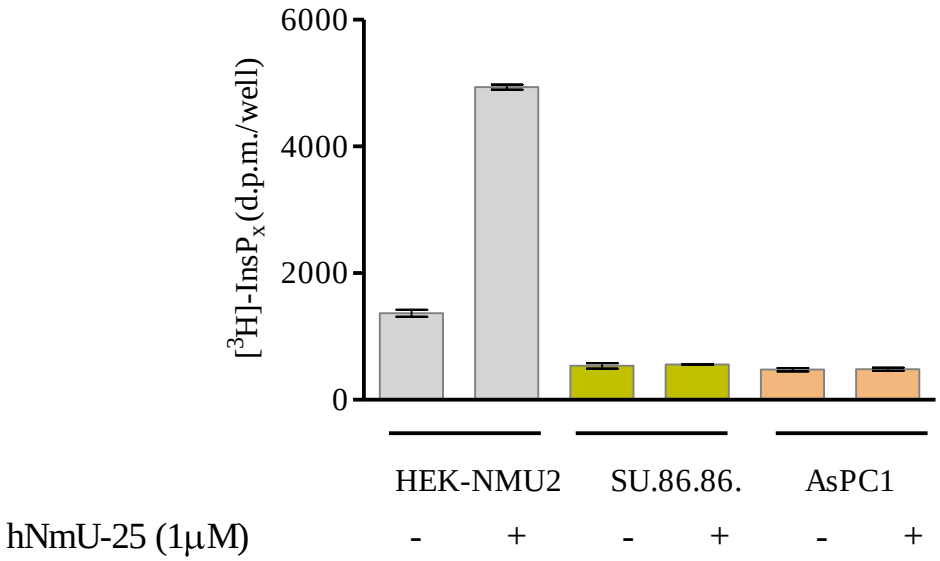

Figure 5.15. Lack of effect of hNmU-25 on [^{3}H]InsP$_x$ accumulation in HEK-NMU2, SU.86.86. and AsPC1 cell-lines. For each cell-line, cells were grown in 24-well plates and incubated with *myo*-[^{3}H]inositol (2 μCi/ml) for 48 h. Cells were then incubated with 10 mM LiCl for 10 min before addition of hNmU-25 (1 μM) or vehicle for 15 min. The [^{3}H]InsP$_x$ fraction was recovered and counted. Data are shown as mean ± s.e.m., n=3.

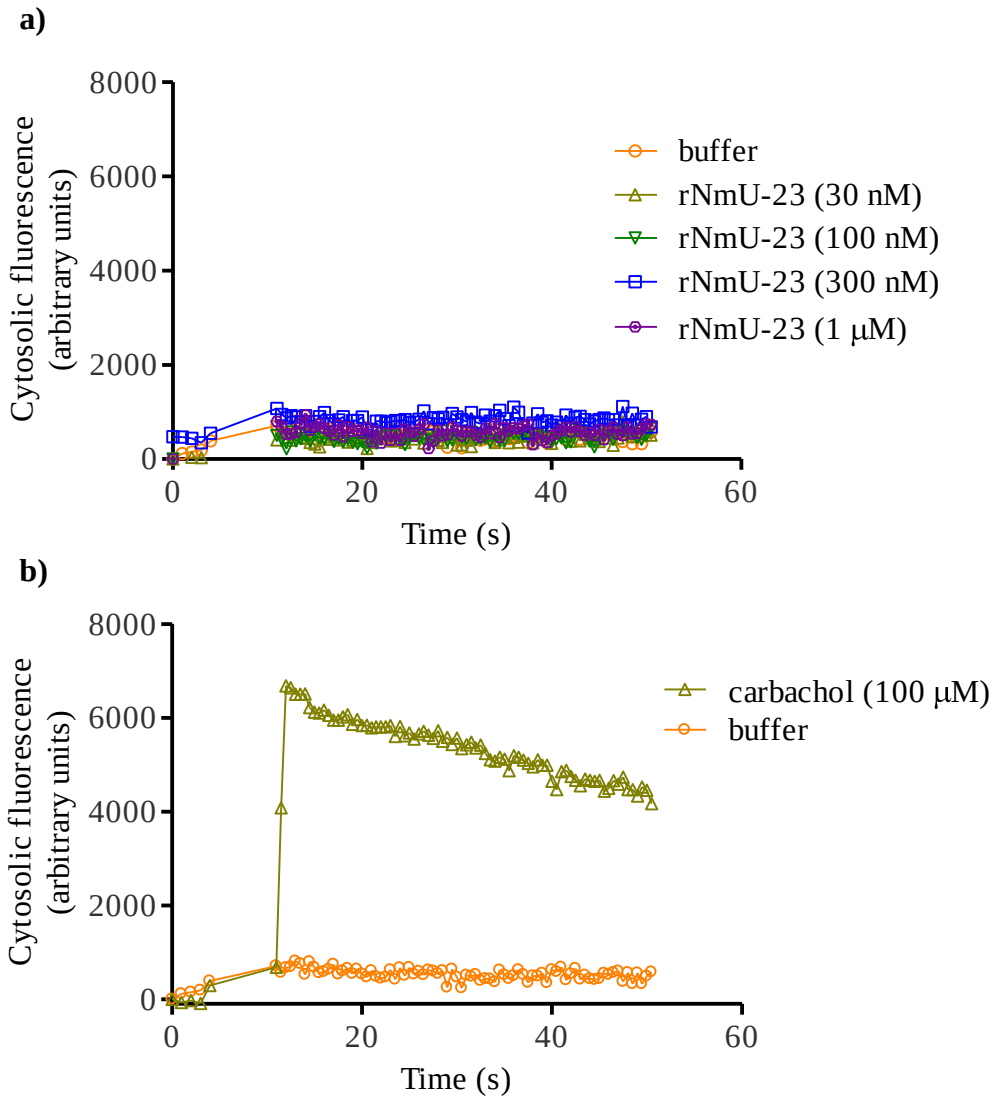

Figure 5.16. Ca^{2+} responses to addition of rNmU-23 or carbachol in MIN6 cells (a mouse pancreatic β-cell line). Cells were cultured in 96-well plates for 3-4 days and then loaded with fluo-4-AM. Cells were then challenged after 11 s of basal recording with (a) buffer or different concentrations of rNmU-23, or (b) buffer or carbachol (100 μM), using a NOVOstar plate reader. Cytosolic fluorescence was monitored as an index of $[Ca^{2+}]_i$. Traces shown are representative of 4 separate experiments.

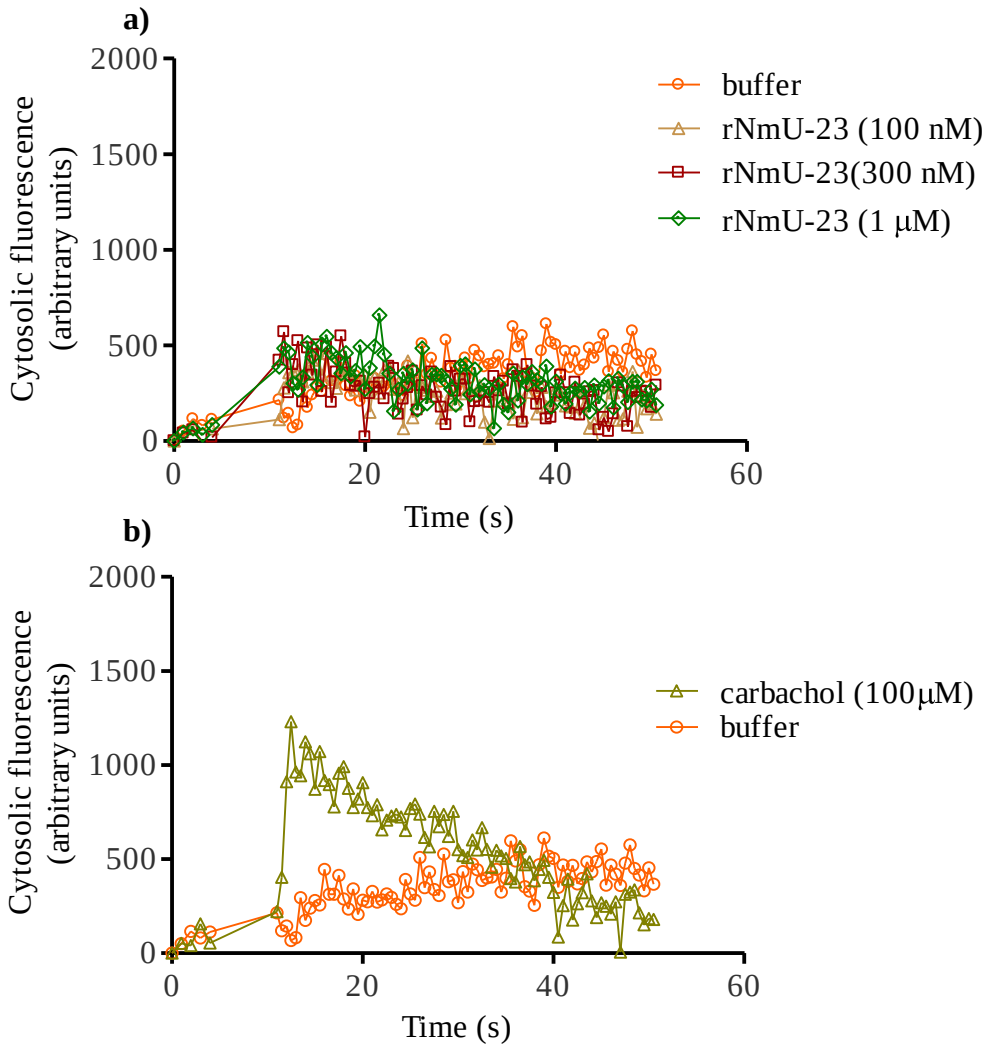

Figure 5.17. Ca^{2+} responses to addition of rNmU-23 or carbachol in INS-1E cells (a rat pancreatic β-cell-line). Cells were cultured in 96-well plates for 5 days and then loaded with fluo-4-AM. Cells were then challenged after 11 s of basal recording with (a) buffer or different concentrations of rNmU-23, or (b) buffer or carbachol (100 μM) using a NOVOstar plate reader. Cytosolic fluorescence was monitored as an index of $[Ca^{2+}]_i$. Traces shown are representative of 3 separate experiments.

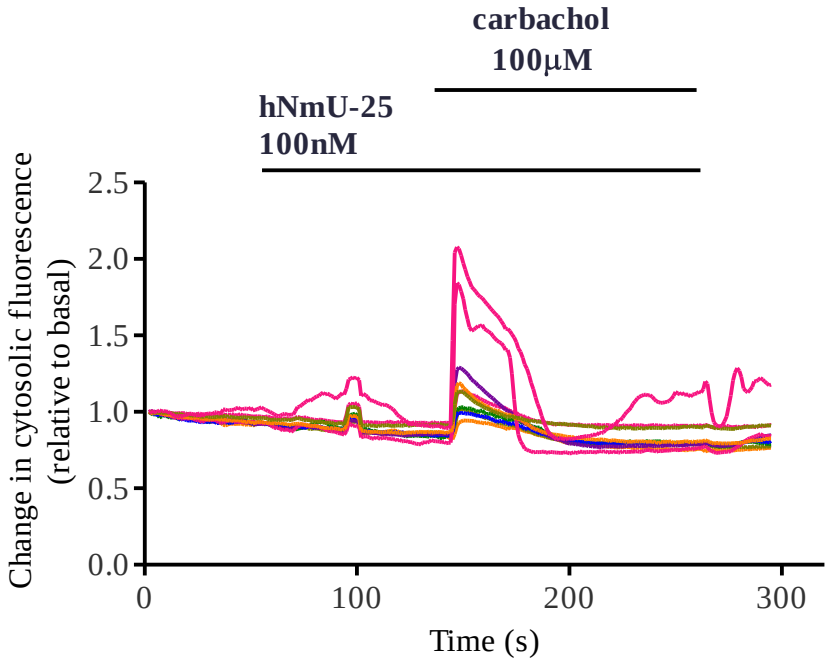

Figure 5.18. Ca^{2+} responses to addition of hNmU-25 or carbachol in KYSE140 cells (a human oesophageal cancer cell-line). Cells were cultured on 25 mm glass coverslips for 2-3 days and then loaded with fluo-4-AM. Cells were challenged with hNmU-25 (100 nM) and, following washout, carbachol (100 μM). Cytosolic fluorescence was measured as an index of $[Ca^{2+}]_i$ using confocal microscopy. Changes in fluorescence were calculated relative to the basal level. Each trace represents data from a single cell. Data shown are representative of 5 separate experiments.

5.3 Discussion

In human and rodents, NMU1 is expressed primarily in peripheral tissues, including pancreas, adipose tissue, gastrointestinal tract (stomach, intestine, duodenum and colon), lymphocytes, kidney, spleen, lung, cardiovascular blood vessels, testes, uterus and prostate (Hsu *et al.*, 2007; Mitchell *et al.*, 2009; Raddatz *et al.*, 2000; Szekeres *et al.*, 2000). On the other hand, NMU2 is mainly expressed in the CNS (pontine reticular formation, thalamus, hypothalamus, medulla oblongata and spinal cord), pituitary gland, lung, testes, ovary and uterus (Hsu *et al.*, 2007; Raddatz *et al.*, 2000; Shan *et al.*, 2000).

A wide range of physiological roles for NmU have been reported (see **Chapter 1, section 1.3**) and are consistent with NMU distribution. For example, early *in vivo* studies showing the increase in blood pressure upon central or peripheral administration of NmU is consistent with the presence of NMU in blood vessels and in the CNS (Minamino *et al.*, 1985a; Mitchell *et al.*, 2009; Westfall *et al.*, 2002). *In vitro* studies have also demonstrated that the existence of both NMU isoforms in human and rodent uterus is consistent with the uterine contractile effects of NmU observed in different species (Minamino *et al.*, 1985a; Prendergast *et al.*, 2006). Furthermore, expression of NMU1 mainly in human and rat colon (Hsu *et al.*, 2007; Jones *et al.*, 2006) is in agreement with the contractile effect of NmU on strips of rat colonic smooth muscle and Ca^{2+} responses in cultured smooth muscle cells isolated from rat colon (Brighton *et al.*, 2008).

Attempts to reproduce earlier work with cultured rat colonic myocytes failed to demonstrate any NmU-linked signalling via $G_{q/11}$ (Ca^{2+}) or $G_{i/o}$ (adenylyl cyclase inhibition). In contrast, stimulation with UTP, which is known to elevate $[Ca^{2+}]_i$ via activation of a purinergic P2Y receptor-$G\alpha_{q/11}$ signalling pathway (Jacobson *et al.*, 2010), provoked consistent Ca^{2+} responses in the same cells. The technique used to isolate rat colonic myocytes was identical to that used in earlier work and has been transferred successfully to isolate rat tracheal smooth muscle cells that respond to adrenaline and methacholine through α-adrenoceptors and M_3 mACh receptors, respectively (Hall, 2011). Furthermore, the cells used in experiments exhibit morphological and biochemical (α-actin staining) characteristics of smooth muscle cells (Brighton *et al.*, 2008; Skalli *et al.*, 1989). It is worth noting here that following the failure to detect responses, several protocol modifications were explored, such as trying different isolation techniques, using

different segments of colon, along with alteration to digestive enzymes, incubation times and temperature. In addition, Ca^{2+} indicator dye loading conditions, as well as the type of dye used, were also varied (data not shown). It has been reported that culturing smooth muscle cells leads to down-regulation of some GPCRs, such as the M_3 mACh receptor (Boselli *et al.*, 2002; Widdop *et al.*, 1993) and that withdrawal of serum could at least partially restore M_3 mACh receptor expression (Singer *et al.*, 2002); however, serum-withdrawal from cultured rat colonic smooth muscle cells did nothing to restore NmU responsiveness (data not shown). To avoid the possibility that primary colonic smooth muscle cells cultured here are different to those prepared previously, NmU-mediated contractile responses were also examined in native tissue. Inexplicably, strips of rat colonic smooth muscle that had been dissected from distal colon as close to of the region detailed in (Brighton *et al.*, 2008) as possible, failed to respond to NmU (rNmU-23) despite the same strips showing potent contractile responses to carbachol. I performed contraction assays both in our laboratory at Leicester and also at GSK (Harlow, UK) with the kind help of GSK staff, but without any success. Furthermore, strips of mouse colonic smooth muscle showed contractile responses to carbachol, but not rNmU-23 or hNmu-25. The present findings are consistent with several previous reports, where no direct contractile effect for NmU was detected in the colon of rat, mouse or guinea-pig, with the exception of potentiating the effects of electrical-field stimulation (EFS) in mouse colon (Benito-Orfila *et al.*, 1991; Dass *et al.*, 2007; Prendergast *et al.*, 2006).

Following an earlier study, which reported the presence of NmU and the expression NMU1 in human left ventricle and coronary artery (Mitchell *et al.*, 2009), two other primary cell-types were screened for NmU-evoked responses, porcine coronary artery smooth muscle cells (pCASMCs) and rat cardiac myocytes. Successfully isolated pCASMC showed Ca^{2+} responses to UTP, which used as positive control, while there was no evidence of NMU-linked $G_{q/11}$ (Ca^{2+}) or $G_{i/o}$ (adenylyl cyclase inhibition) signalling. On the other hand, stimulation of cardiac myocytes with rNmU-23 resulted in inhibition of AC activity that was concentration-dependent and PTX-sensitive, while evidence for NMU-$G\alpha_q$-PLC coupling was not detected. It has been shown that $G\alpha_q$-PLC-mediated increases in $[Ca^{2+}]_i$ are not evident in excitable cells, such as cardiac myocytes under normal physiological conditions, however, substantial activation of this pathway has been

observed in ischemia, as well as other heart pathologies (Woodcock *et al.*, 2005). Although PTX-sensitive, NmU-mediated inhibition of forskolin-stimulated cAMP accumulation could be demonstrated, this response was highly variable between different preparations. Indeed, often forskolin itself failed to evoke an increase in cAMP or evoked only a small increase. This might suggest that the variability was attributable to preparation conditions (e.g. digestive enzyme composition/exposure time) for the cardiomyocytes.

Screening of responses to NmU was also performed in a number of cell-lines, where endogenously expressed NMUs and/or responses to NmU have been reported in the literature (see **Chapter 1, Section 1.2.2**). For example, NMU2 mRNA and protein has been reported in several human pancreatic cancer cell-lines, including AsPC1 and SU.86.86 (Ketterer *et al.*, 2009). Carbachol, which has been demonstrated to have an effect in these cell-lines (Pahl *et al.*, 1993), induced a robust Ca^{2+} increase while hNmU-25 did not evoke any $G_{q/11}$ (Ca^{2+} and [^{3}H]$InsP_x$ increase) or $G_{i/o}$ (AC inhibition)-linked signalling. To ensure bioactivity of hNmU-25, parallel experiments were performed in HEK-NMU2, where agonist addition resulted in substantial [^{3}H]$InsP_x$ accumulation. It has also been shown that isolated rat pancreatic islets express mRNA and protein of rNMU1 (Kaczmarek *et al.*, 2006). Again, no responses were detected for rNmU-23 in MIN6 or INS-1E cells (mouse and rat pancreatic β-cell-lines, respectively), while carbachol evoked Ca^{2+} responses in both cell-lines. Finally, the human oesophageal cancer cell-line, KYSE140, which has been shown to respond to hNmU-25 (Yamashita *et al.*, 2002) also exhibited Ca^{2+} responses to carbachol while no responses were detected to hNmU-25.

The reason(s) for the lack of responses to NmU is unclear. While some of the reports of native NMU were based on expression rather than function, other laboratories have clearly had more success in observing NMU-dependent cell/tissue responses. Several questions could be posed; for example, is NMU receptor expression lost or down-regulated in culture? Does co-expression of NmU and NMUs result in an autocrine/paracrine action of NmU which silences responses to exogenous NmU due to receptor down-regulation and/or irreversible binding of endogenous ligand? Alternatively, receptors could be present, but not at the cell-surface. Previous studies have provided

some insights that should be considered in future screening for NmU-mediated responses in native systems. For instance, high expression of NMU2 has been demonstrated by immunocytochemistry at the cell-surface, but also in the cytoplasm and nucleus of pancreatic ductal adenocarcinoma (PDAC) cells, indicating partial intracellular expression of NMU2 (Ketterer *et al.*, 2009). Additionally, NmU and mNMU1 are co-expressed in mouse peritoneal macrophages (Moriyama *et al.*, 2006a). However, the expression of NMU1 is much higher in NmU-knockout mice than wild-type counterpart, perhaps illustrating the ability of the endogenous NmU to down-regulate its receptors (Moriyama *et al.*, 2006a).

Having invested a great deal of time and effort into finding a suitable endogenous NMU1 or NMU2-expressing cell-type, this approach was reluctantly abandoned and attention re-focused on the recombinant HEK-NMU1/HEK-NMU2 models. However, in the future the availability of endogenously expressing NMUs will be needed to provide essential information allowing us to ask whether the findings that are observed in the recombinant systems accurately recapitulate native systems, including irreversible NmU-NMU binding and receptor desensitization/trafficking/resensitization profiles.

Chapter 6

NMU regulation: desensitization, internalization and resensitization

6.1 Introduction

The pseudo-irreversible binding of NmU to its receptors, NMU1 and NMU2, has been demonstrated in both endogenous and recombinant expression systems (Brighton *et al.*, 2004a). Work described in this Thesis (see **Chapter 3**) has confirmed the irreversible binding of NmU to NMUs through the lack of repetitive Ca^{2+} responses on re-application of NmU and an inability of normal washing protocols to reduce membrane fluorescence following addition of Cy3B-pNmU-8. The data showed that it was necessary to apply a brief acid wash (15-25 s at pH 2.0) protocol to achieve displacement of Cy3B-pNmU-8 from NMU1- or NMU2-expressing cells (see **Chapter 3, Figure 3.12**) and to allow a second (diminished) Ca^{2+} response to be seen on re-application of NmU (see **Chapter 3, Figure 3.17**). The brevity of the exposure to pH 2.0 medium meant that cell viability and pEC_{50} values determined for NmU-mediated Ca^{2+} responses on NmU-naïve cells were not different to those of cells not exposed to the acid wash (see **Chapter 3, Section 3.2.4**).

The cellular consequences of this pseudo-irreversible binding between NmU and its receptors are unclear. Internalization of eGFP-tagged NMU1 and NMU2 can be detected within 10 min of ligand addition (see **Chapter 4, Figure 4.6 and 4.11**) and it has been shown that NMU internalization is likely to be clathrin-dependent in these cells, since it is inhibited by concanavalin A (Brighton, 2005). Like the majority of GPCRs, desensitization/internalization of NMU1 and NMU2 is also likely to be β-arrestin-dependent and essential for signal termination and/or receptor resensitization (Marchese *et al.*, 2008; Moore *et al.*, 2007). The accepted model of GPCR regulation suggests that following GPCR internalization, the ligand-receptor-β-arrestin complex translocates to early endosomes, where β-arrestin might also serve as a scaffold assembling an active

MAP kinase signalling complex (DeFea *et al.*, 2000a; Pierce *et al.*, 2002). The GPCR is trafficked via specific pathways towards either lysosomal degradation (e.g. as occurs for the protease-activated (PAR1) or chemokine 4 (CXCR4) receptors), or towards recycling/resensitization (e.g. as occurs for the β_2-adrenoceptor (fast recycling) and NK_1 receptor (slow), at least with short-term exposures to agonist) (Marchese *et al.*, 2008; Roosterman *et al.*, 2007). The decision between fast and slow recycling pathways followed has been shown to be at least partially dependent on the affinity of the GPCR for β-arrestin. On this basis, GPCRs have been classified into two classes, A and B (Marchese *et al.*, 2008; Moore *et al.*, 2007; Oakley *et al.*, 2000). Class A GPCRs, including the β_2-adrenoceptor and μ-opioid receptor (MOR), show transient association with β-arrestin (favouring β-arrestin-2 over β-arrestin-1), dissociating at the cell-surface or directly following internalization, and resulting in rapid recycling/ resensitization (Moore *et al.*, 2007). In contrast, class B GPCRs, including angiotensin II (AT_1), neurotensin, vasopressin 2 (V_2) and NK_1 receptors, associate tightly with β-arrestins (binding with equal affinity to β-arrestin-1 and β-arrestin-2), resulting in slow recycling/resensitization (Marchese *et al.*, 2008; Moore *et al.*, 2007).

While the acid wash allows removal of the ligand from NMU at the plasma membrane, thereby allowing aspects of receptor desensitization independent of continued ligand binding to be examined. High-affinity, pseudo-irreversible binding may well be the physiological reality for these receptors. Thus, in this Chapter the consequences of either allowing ongoing ligand-receptor interaction or experimental removal of ligand from NMU (through the pH 2.0 wash protocol) on the time-courses of desensitization/resensitization have been investigated. In addition, a number of pharmacological approaches have been used to delineate the pathways followed by the ligand-receptor complex in the physiologically-relevant desensitization/resensitization process.

The acidification of endosomes is essential for dissociation of ligands from GPCRs as well as recycling, as ligand dissociation is thought to cause the receptor to assume a conformation favourable for dephosphorylation. For example, inhibition of endosomal acidification attenuates β_2-adrenoceptor dephosphorylation and markedly delays recycling (Krueger *et al.*, 1997). A potential additional role of endosomal acidification for receptors

with high-affinity ligands suggested in several recent studies, involves peptidases that facilitate receptor recycling by degrading peptide agonists, specifically at acidic endosomal pH (Murphy *et al.*, 2011; Roosterman *et al.*, 2007). The work described here focuses on a potential role for endothelin-converting enzyme-1 (ECE-1) in regulating NmU/NmS-NMU interactions. There are a number of reasons for proposing a role for this metalloendopeptidase in signalling by neuromedins. ECE-1 can process a wide range of peptides with vasoactive properties, including bradykinin, angiotensin II, neurotensin, substance P, calcitonin, atrial natriuretic peptide, as well as amyloid-β peptide (Eckman *et al.*, 2001; Hoang *et al.*, 1997; Johnson *et al.*, 1999). ECE-1-mediated, *in-vitro* degradation of at least some of these peptides, including bradykinin and substance P, requires an acidic environment, resembling endosomal pH (Fahnoe *et al.*, 2000). Indeed, endosomal ECE-1 has recently been shown to be essential for the recycling of the neurokinin-1 receptor, the heterodimer of calcitonin receptor-like receptor/receptor activity-modifying protein (CLR/RAMP1) and the somatostatin type 2A (sst2A) receptor by degrading receptor-bound peptide ligands (substance P, calcitonin gene-related peptide and somatostatin-14, respectively) within acidic endosomes (Padilla *et al.*, 2007; Roosterman *et al.*, 2007; Roosterman *et al.*, 2008). Degradation of these ligands disrupts ligand-receptor-β-arrestin binding, leading to translocation of β-arrestin back to the cytosol and the subsequent recycling of the receptor back to the cell-surface (Roosterman *et al.*, 2007). Recycling and resensitization of NK_1 receptor and CLR/RAMP1 are significantly reduced by inhibition of endosomal acidification, the expression of NK_1 receptor in cells lacking ECE-1 activity (such as the KNRK cell-line), inhibition of ECE-1 activity or knocking-down ECE-1; in contrast, over-expression of ECE-1 markedly accelerates their trafficking and resensitization (Padilla *et al.*, 2007; Roosterman *et al.*, 2007). The work described in this Chapter also addressed the question of whether the resensitization of Ca^{2+} responses to hNmU-25, pNmU-8 and hNmS-33 are affected by ECE-1 activity in NMU1- and NMU2-transfected HEK293, as HEK293 cells are reported to express both ECE-1 mRNA and protein (Padilla *et al.*, 2007; Roosterman *et al.*, 2007).

6.2 Results

6.2.1 Effect of the duration of pre-exposure to hNmU-25 on homologous desensitization of NMU2-mediated Ca^{2+} responses

Having established that a brief, 20 s, pH 2.0 washing protocol could be applied to remove receptor-bound NmU, this protocol was used to investigate desensitization of hNmU-25-mediated Ca^{2+} signalling that occurs independently of irreversible NmU binding. Briefly, HEK-NMU2 were pre-exposed to a maximal concentration of hNmU-25 (30 nM) for 1, 3, 5 or 30 min followed by brief (15-25 s) wash with pH 2.0 buffer and two washes with KHB, pH 7.4. Cells were then allowed a 5 min recovery period before re-challenging with the same concentration of hNmU-25 (Figure 6.1a, b). Ca^{2+} responses to hNmU-25 (30 nM) following 1, 3, 5 or 30 min of initial exposure to hNmU-25 showed similar profiles of an initial peak and slow decline. However, the magnitude of the responses was different (Figure 6.1c). Pre-exposure of HEK-NMU2 to a maximal concentration of hNmU-25 (30 nM) for 1 min prior to a brief, acid wash did not result in significant desensitization (91 ± 4% (n=3) of the Ca^{2+} response observed in cells initially challenged with vehicle rather than hNmU-25). Following a 3 min pre-exposure to hNmU-25, Ca^{2+} responses were 74 ± 6% (n=3) of the vehicle-control response. Pre-incubation of the cells with hNmU-25 for 5 and 30 min significantly desensitized subsequent hNmU-25-mediated Ca^{2+} responses (to 42 ± 5% (n=3) and 45 ± 3% (n=3) of the vehicle-control response, respectively). The extent of desensitization following 5 and 30 min pre-exposures to hNmU-25 (30 nM) was not significantly different (Figure 6.1d).

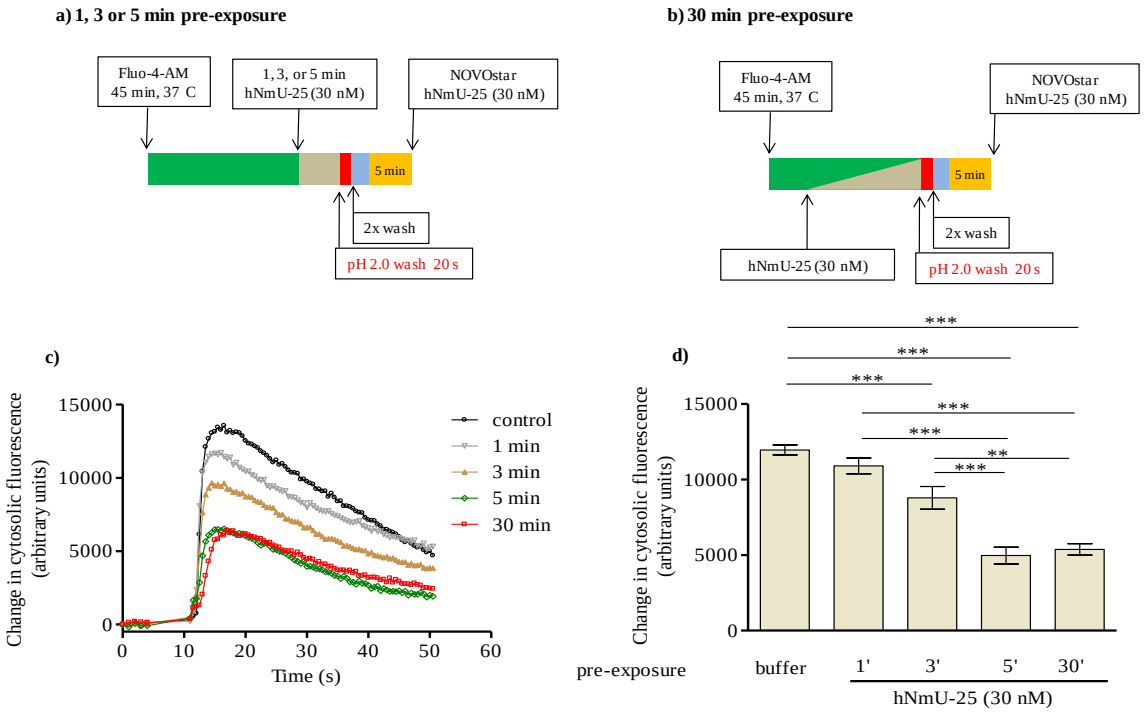

Figure 6.1. Effect of the duration of pre-exposure to hNmU-25 on homologous desensitization in HEK-NMU2. Cells were cultured in 96-well plates, loaded with fluo-4-AM and then challenged with either buffer, or a maximal concentration of hNmU-25 (30 nM) for 1, 3 or 5 min (a). To achieve the 30 min pre-incubation time-point (b), cells were challenged with either buffer or hNmU-25 (30 nM) during the last 30 min of loading with fluo-4-AM. Following challenges with buffer or hNmU-25, cells were briefly (20 s) washed with acidified KHB (pH 2.0) and washed twice with KHB, pH 7.4 before a 5 min recovery period in normal KHB. Cells were then stimulated with hNmU-25 (30 nM) using a NOVOstar plate reader. Traces (c) are representative of Ca^{2+} responses to hNmU-25 (30 nM) in HEK-NMU2 pre-exposed to buffer only (control) for 5 min or hNmU-25 (30 nM) for 1, 3, 5 or 30 min. The maximal changes in cytosolic fluorescence following the second hNmU-25 challenge are shown in panel (d). Data are mean ± s.e.m, n=3; $^{**}P<0.01$, $^{***}P<0.001$, by Bonferroni's multiple comparison test following one-way ANOVA.

6.2.2 Time-course of resensitization of the hNmU-25-mediated Ca^{2+} response in HEK-NMU2

Earlier data looking at the effect of stimulus duration on the extent of desensitization used (by necessity) an acid wash to remove ligand. Having established that 5 min pre-exposure to hNmU-25 (30 nM) caused a significant desensitization following 5 min recovery, this desensitizing challenge was used to investigate the time-course of any subsequent resensitization. The protocol used to investigate the time-course of recovery of hNmU-25-mediated Ca^{2+} signalling is shown in Figure 6.2a, b. Briefly, cells were pre-exposed to hNmU-25 (30 nM, 5 min) followed by a brief (20 s) KHB, pH 2.0 wash and two KHB, pH 7.4 washes immediately. This was followed by a 5 min to 2 h recovery period after which the cells were stimulated with different concentrations of hNmU-25 (0.1-100 nM) (Figure 6.2a, b). Challenge with a maximally-effective concentration of hNmU-25 after 5 min recovery evoked 35 ± 3% (n=6) of the peak Ca^{2+} response in cells not subjected to initial hNmU-25 pre-exposure, while this response had recovered to 75 ± 5% (n=6) after a 1 h recovery period and had almost fully recovered by 2 h (Figure 6.2c, d).

To understand resensitization/recovery of NmU-mediated Ca^{2+} responses in a more physiological context, an identical protocol was then used with the exception that acid wash was not used (without removing ligand) and a recovery period of 5 min to 6 h (Figure 6.2a, b). Removal of a brief low pH wash resulted in a slower recovery rate of hNmU-25-mediated Ca^{2+} signalling (compare data in Figure 6.3c with Figure 6.2c). for example, pre-exposure to hNmU-25 (30 nM, 5 min) followed by 5 min recovery resulted in a near-total loss of the agonist-stimulated Ca^{2+} response, which gradually recovered over time, such that full resensitization was observed after 6 h recovery (Figure 6.3c). Recovery of responsiveness occurred slowly, with 27 ± 4% (n=4) and 69 ± 3% (n=4) recovery compared to control responses at 2 and 3 h, respectively (Figure 6.2c, d).

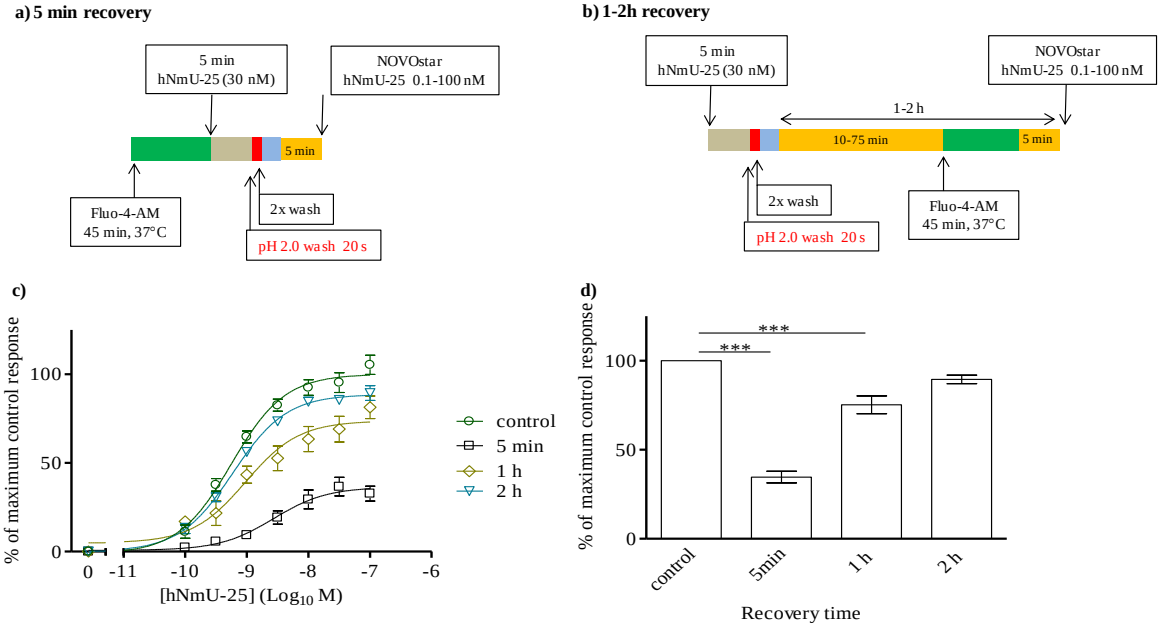

Figure 6.2. Effect of brief acid washing on the time-course of resensitization of hNmU-25-mediated Ca^{2+} responses in HEK-NMU2. Cells were cultured in 96-well plates for 48-72 h. For the 5 min recovery protocol (a), cells were loaded with fluo-4-AM and then challenged with either buffer or hNmU-25 (30 nM) for 5 min. This was followed by a brief wash (20 s; KHB, pH 2.0) and two washes with KHB, pH 7.4 and a 5 min recovery period in KHB. For the 1-2 h recovery protocol (b), cells were challenged with buffer or hNmU-25 (30 nM) for 5 min followed by a brief (20 s; KHB, pH 2.0) wash and two washes with KHB, pH 7.4 as described above. This was followed by a 1-2 h recovery period. Cells were loaded with fluo-4-AM during the last 45 min of the recovery period. Cells were then challenged with different concentrations of hNmU-25 (0.1-100 nM) using a NOVOstar plate reader. Concentration-response curves were constructed based on maximal changes in fluorescence as an index of $[Ca^{2+}]_i$ and expressed as a percentage of the maximum response in HEK-NMU2 pre-exposed to buffer only (i.e. no initial hNmU-25 challenge) (panel c). The control concentration-response curve (c) represents Ca^{2+} responses in HEK-NMU2 loaded with fluo-4-AM followed by brief (20 s) pH 2.0 wash and two pH7.4 washes prior to challenge with different concentrations of hNmU-25 (0.1-100 nM). Data are mean ± s.e.m., n=5-6; $^{***}P<0.001$, by Dunnett's multiple comparison test following one-way ANOVA.

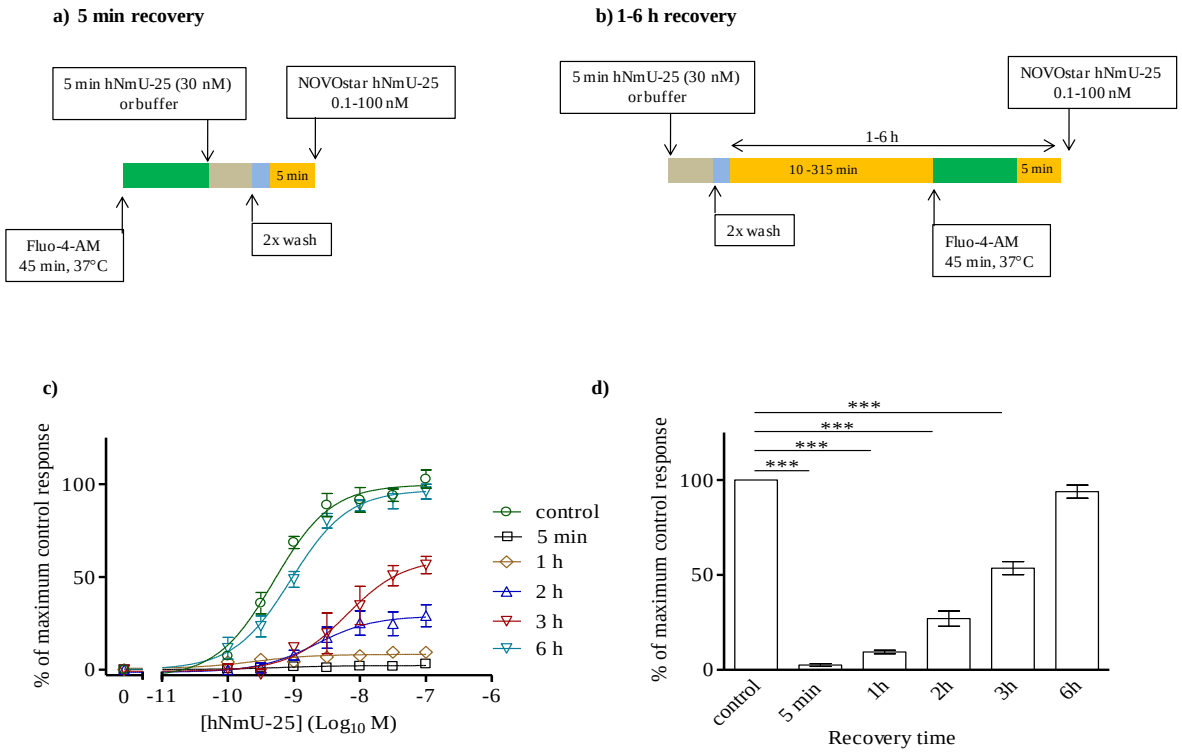

Figure 6.3. Time-course of resensitization of the hNmU-25-mediated Ca^{2+} response in HEK-NMU2. Cells were cultured in 96-well plates for 48-72 h. For the 5 min recovery protocol (a), cells were loaded with fluo-4-AM and then challenged with either buffer or hNmU-25 (30 nM) for 5 min followed by two KHB washes and a 5 min recovery period. For the 1-6 h recovery protocol (b), cells were challenged with either buffer or hNmU-25 (30 nM) for 5 min followed by two KHB washes and 1-6 h recovery period in KHB (5 min-3 h), or serum-free medium (6 h recovery). During the last 45 min of the recovery period, cells were loaded with fluo-4-AM. After an appropriate period of incubation, cells were challenged with different concentrations of hNmU-25 (0.1-100 nM) using a NOVOstar plate reader. Concentration-response curves were constructed based on the maximal changes in fluorescence observed and expressed as a percentage of the maximum Ca^{2+} response in HEK-NMU2 pre-exposed to buffer only (i.e. no initial hNmU-25 challenge) (panel c). It should be noted that control concentration-response curves were generated for each time-point and were not significantly different from each other. Data are mean ± s.e.m., n=3-4; $^{***}P<0.001$, by Dunnett's multiple comparison test following one-way ANOVA.

Table 6.1. pEC_{50} values for the time-course of hNmU-25mediated Ca^{2+} resensitization response in the presence or absence of brief acid-wash.

Recovery time	normal wash	brief acid-wash
Control	9.30 ± 0.08	9.21 ± 0.09
5 min	Not applicable (R^2= 0.1)	8.40 ± 0.06
1 h	Not applicable (R^2= 0.1)	8.73 ± 0.26
2 h	8.60 ± 0.26	9.30 ± 0.06
3 h	8.41 ± 0.07	Not performed
6 h	9.10 ± 0.07	Not performed

6.2.3 Effects of internalization inhibitors on the resensitization of hNmU-25-mediated Ca^{2+} signalling

The protocol used to explore the effects of inhibitors of GPCR internalization on the recovery of hNmU-25-mediated Ca^{2+} responses is described in Materials & Methods **(section 2.2.13.3)**. Before examining the effect of inhibitors of GPCR internalization on the recovery of hNmU-25-mediated Ca^{2+} responses, potential effects on initial hNmU-25-mediated Ca^{2+} signalling were investigated. In these studies, concanavalin A (250 µg/mL, 60 min) pre-incubation significantly inhibited the initial hNmU-25-mediated Ca^{2+} responses (to 65 ± 5% (n=3) of the control peak responses (Figure 6.4a). Similarly, a range of the putative inhibitors of receptor internalization, such as monodansyl cadaverine (MDC, 400 µM), phenylarsine oxide (PAO, 5 µM) and sucrose (0.45 M) were investigated and all were found to significantly affect hNmU-25-mediated Ca^{2+} signalling in naïve cells (Figure 6.4a). Furthermore, extending the incubation time to 3 h with concanavalin A (250 µg/mL), MDC (400 µM), PAO (5 µM), or sucrose (0.45 M) resulted in near complete loss of hNmU-25-mediated Ca^{2+} responses in naïve HEK-NMU2 (Figure 6.4b). In contrast, pre-treatment of HEK-NMU2 with the dynamin-dependent internalization inhibitor, dynasore (80 µM) for 3 h did not significantly affect hNmU-25-mediated Ca^{2+} responses in naïve cells compared to vehicle-treated cells (Figure 6.5). Moreover, after 3 h recovery, following the initial 5 min exposure to hNmU-25 (30 nM), Ca^{2+} responses in cells treated with dynasore (80 µM) were significantly inhibited to 17 ± 2% (n=7) of control Ca^{2+} responses to a hNmU-25 re-challenge; in contrast, re-challenging vehicle-treated cells with hNmU-25 (30 nM) after 3 h recovery evoked 69 ± 1% (n=7) of the control Ca^{2+} responses (Figure 6.6). These data indicate that dynasore significantly impairs the recovery of NMU2-mediated responses.

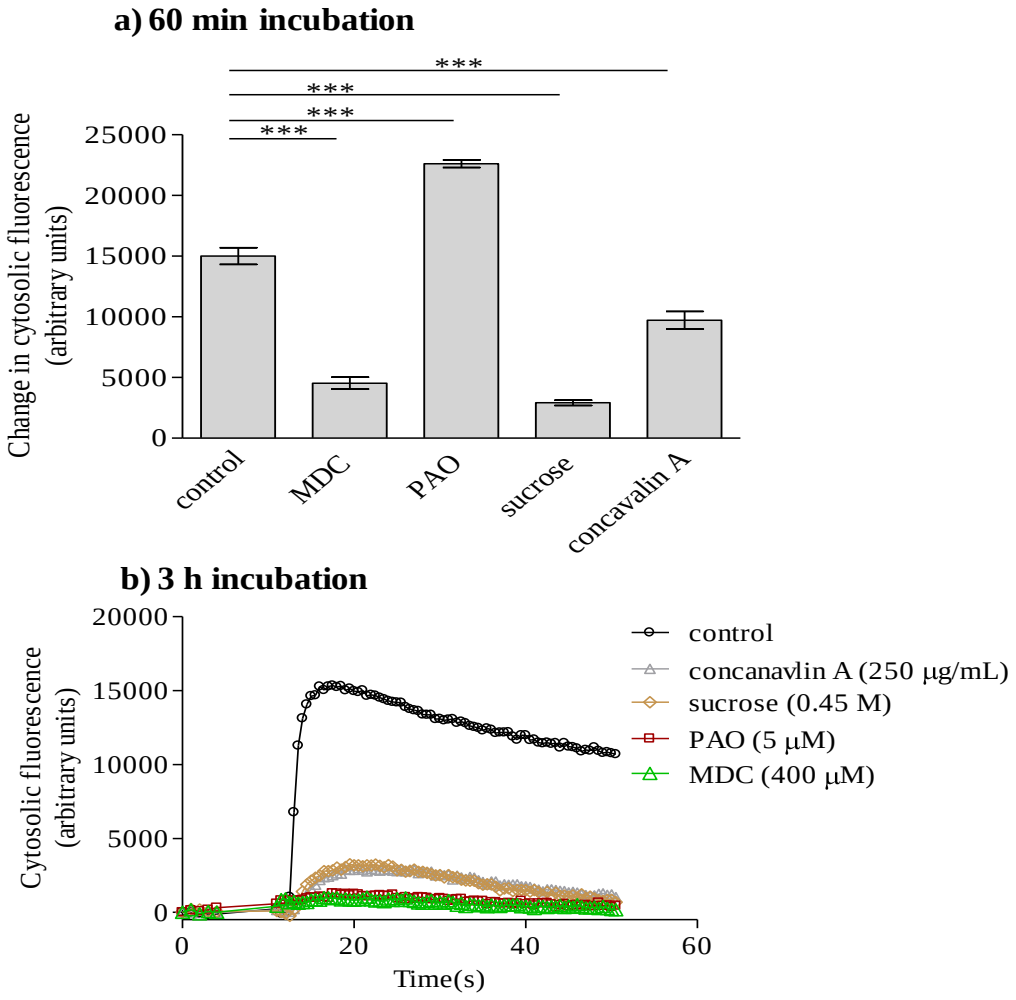

Figure 6.4. Effect of internalization inhibitors on the initial hNmU-25-mediated Ca^{2+} responses in HEK-NMU2. Cells were cultured in 96-well plates for 48 h and loaded with fluo-4-AM in KHB (control) alone, or with monodansylcadaverine (MDC, 400 µM), phenylarsine oxide (PAO, 5 µM), sucrose (0.45 M) or concanavalin A (250 µg/mL). Cells were challenged with hNmU-25 (30 nM) using a NOVOstar plate reader and changes in cytosolic fluorescence were recorded as an index of changes in $[Ca^{2+}]_i$ (a). Data are mean ± s.e.m., n=3, with each experiment performed in duplicate; $^{***}P<0.001$, by Dunnett's multiple comparison test following one-way ANOVA. Traces (b) are representative of 3 experiments for hNmU-25-mediated Ca^{2+} responses following 3 h incubation in KHB alone or with the various inhibitors. During the last 45 min of the incubation, cells were loaded with fluo-4-AM alone or with the inhibitor compounds and then challenged with hNmU-25 (30 nM) (b).

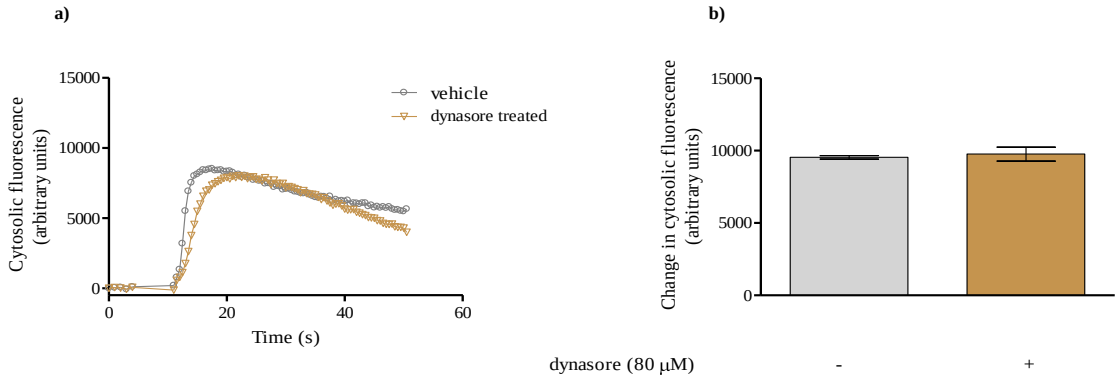

Figure 6.5. Effect of the internalization inhibitor, dynasore, on the initial hNmU-25-mediated Ca^{2+} responses in HEK-NMU2. Cells were cultured in 96-well plates for 48 h. Cells were then pre-treated for 3 h with either vehicle (0.8% DMSO), or dynasore (80 μM). During the last 45 min cells were loaded with fluo-4-AM containing dynasore (80μM) or vehicle. Cells were then challenged with hNmU-25 (30 nM) using a NOVOstar plate reader and changes in cytosolic fluorescence were recorded as an index of changes in $[Ca^{2+}]_i$. Traces (a) are representative of hNmU-25-mediated Ca^{2+} responses in cells pre-treated with either dynasore (80 μM) or vehicle for 3 h. Data are mean ± s.e.m., n=6 with each experiment performed in duplicate; no significant difference ±dynasore was shown by unpaired Student's *t*-test (b).

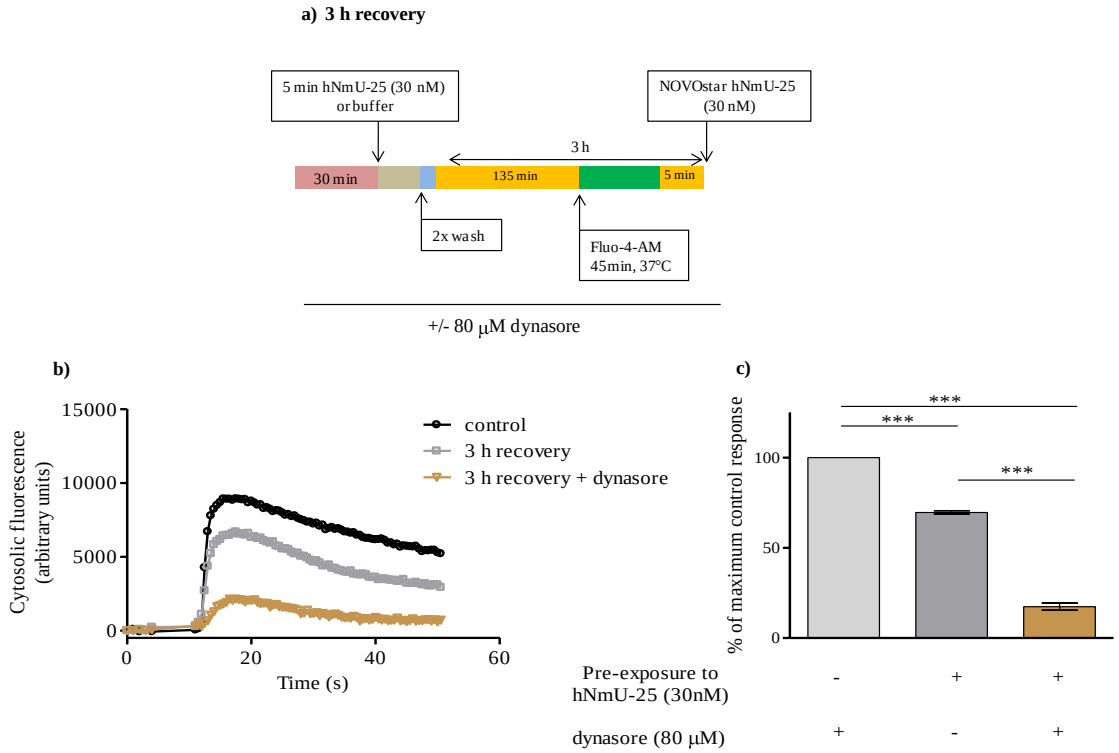

Figure 6.6. Effect of the internalization inhibitor, dynasore, on the recovery of hNmU-25-mediated Ca^{2+} responses in HEK-NMU2. Cells were cultured in 96-well plates for 48-72 h. Dynasore (80 μM) was present or absent throughout all subsequent experimental steps. For the 3 h recovery protocol (a), cells were pre-treated with either dynasore (80 μM) or vehicle (0.8% DMSO) for 30 min then challenged with either hNmU-25 (30 nM) or buffer for 5 min followed by two KHB washes. During the 3 h recovery period in KHB cells were with fluo-4-AM during the last 45 min. Cells were re-challenged with hNmU-25 (30 nM) using a NOVOstar plate reader and changes in cytosolic fluorescence were recorded as an index of changes in $[Ca^{2+}]_i$. Traces (b) are representative of Ca^{2+} responses to hNmU-25 (30 nM) in cells pre-challenged with buffer(control) or hNmU-25 (30 nM) followed by 3 h recovery period ±dynasore and then re-challenge with hNmU-25 (30 nM). Data are expressed as a percentage of the maximum response in HEK-NMU2 pre-challenged with buffer only (c). Data are mean ± s.e.m., n=7 with each experiment performed in duplicate; $^{***}P<0.001$, by Bonferroni's multiple comparison test following one-way ANOVA.

6.2.4 Effect of inhibiting de novo protein synthesis on NMU2 resensitization

To investigate the role of protein synthesis in the recovery of Ca^{2+} signalling following exposure to hNmU-25, the protein synthesis inhibitor, cycloheximide, was used. Cycloheximide concentration used here, has been used previously by other group and showed 95% inhibition of protein synthesis in HEK293 cells (Yu *et al.*, 1997). Incubation of HEK-NMU2 with cycloheximide (17.5 µM) for 2 h resulted in a significant inhibition of [^{35}S]methionine incorporation (Figure 6.7), establishing its ability to inhibit protein synthesis in these cells. To investigate the effect of cycloheximide on the recovery of hNmU-25-mediated Ca^{2+} responses, cells were pre-treated for 30 min with vehicle (0.1% ethanol) or cycloheximide (17.5 µM) and then pre-exposed to buffer or hNmU-25 (30 nM) for 5 min. This was followed by two KHB washes and a 5 min to 6 h recovery period prior to stimulation with hNmU-25 (30 nM) in the continued absence or presence of cycloheximide (Figures 6.8a, b). The resensitization profile of hNmU-25-mediated Ca^{2+} signalling in HEK-NMU2 was not significantly affected by cycloheximide treatment at any time-point (Figure 6.8c). Moreover, the hNmU-25 Ca^{2+} response in naïve cells treated with cycloheximide was not significantly different from cells treated with vehicle only at any time-point (Figure 6. 8d). Introduction of a brief (20 s) KHB, pH 2.0 wash to the resensitization protocol (Figures 6.8a, b) also showed that hNmU-25-mediated Ca^{2+} signalling and the time-course of recovery were not significantly different in HEK-NMU2 treated with either vehicle or cycloheximide (Figure 6.9c). After 3 h recovery, in vehicle- and cycloheximide-treated cells, hNmU-25-mediated Ca^{2+} responses were almost entirely restored (99 ± 5% (n=4) and 98 ± 7% (n=4) of initial peak response in vehicle and cycloheximide-treated cells, respectively).

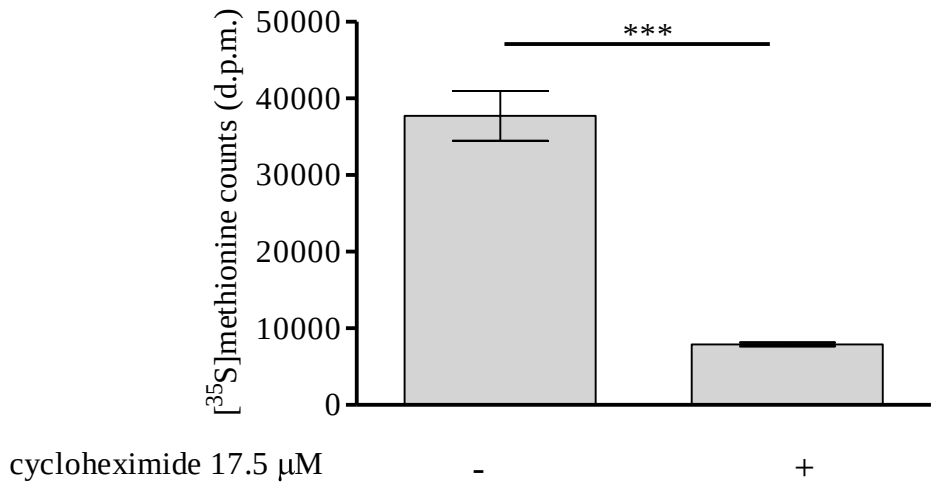

Figure 6.7. Effect of cycloheximide on protein synthesis in HEK-NMU2. Cells were cultured in 6-well plates for 48-72 h and serum-starved for 1 h in KHB. Cells were then pre-incubated with vehicle alone (0.1% ethanol) or with cycloheximide (17.5 μM) for 30 min. Cells were incubated for a further 2 h at 37°C after addition of [^{35}S]methionine. Cells were then lysed and [^{35}S]methionine incorporation into protein determined (see Methods). Data are shown as mean ± s.e.m, n=4 with each experiment performed in triplicate; $^{***}P<0.001$, unpaired, two-tailed Student's *t*-test.

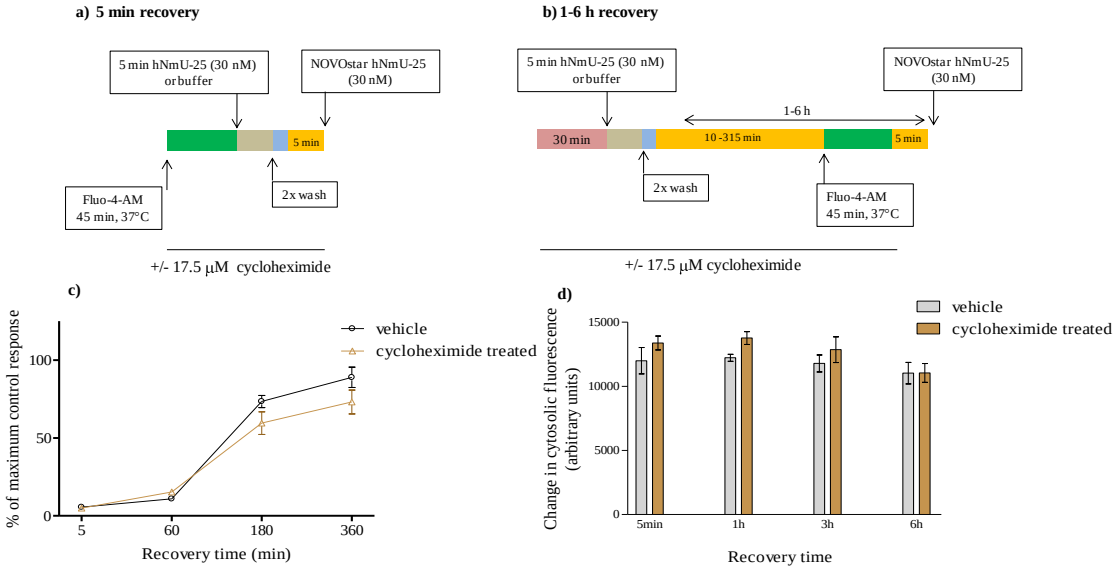

Figure 6.8. Effect of protein synthesis inhibition on the recovery of hNmU-25-mediated Ca^{2+} responses in HEK-NMU2. Cells were cultured in 96-well plates for 48-72 h. Cycloheximide (17.5 µM) was present or absent throughout all subsequent experimental steps. For the 5 min recovery protocol (a), cells were loaded with fluo-4-AM, and then challenged with buffer or hNmU-25 (30 nM) for 5 min followed by two KHB washes and a 5 min recovery period in KHB. For the 1-6 h recovery protocol (b), cells were pre-treated with vehicle (0.1% ethanol) or cycloheximide (17.5 µM) for 30 min and then challenged with buffer or hNmU-25 (30 nM) for 5 min followed by two KHB washes. This was followed by a recovery period of 1-6 h. During the last 45 min of the recovery period, cells were loaded with fluo-4-AM before challenge with hNmU-25 (30 nM) using a NOVOstar plate reader and changes in cytosolic fluorescence were recorded as an index of changes in $[Ca^{2+}]_i$. Data are expressed as a percentage of the maximum response in HEK-NMU2 pre-challenged with buffer only (i.e. no initial hNmU-25 challenge) (c). The effect of cycloheximide on the initial Ca^{2+} responses to hNmU-25 (30 nM) in comparison to untreated cells was also investigated at all time-points (d). Data are mean ± s.e.m., n=4 with each experiment performed in duplicate; Bonferroni's multiple comparison test following two-way ANOVA (c) and one-way ANOVA (d). The two-way ANOVA showed a significant effect of time but not treatment.

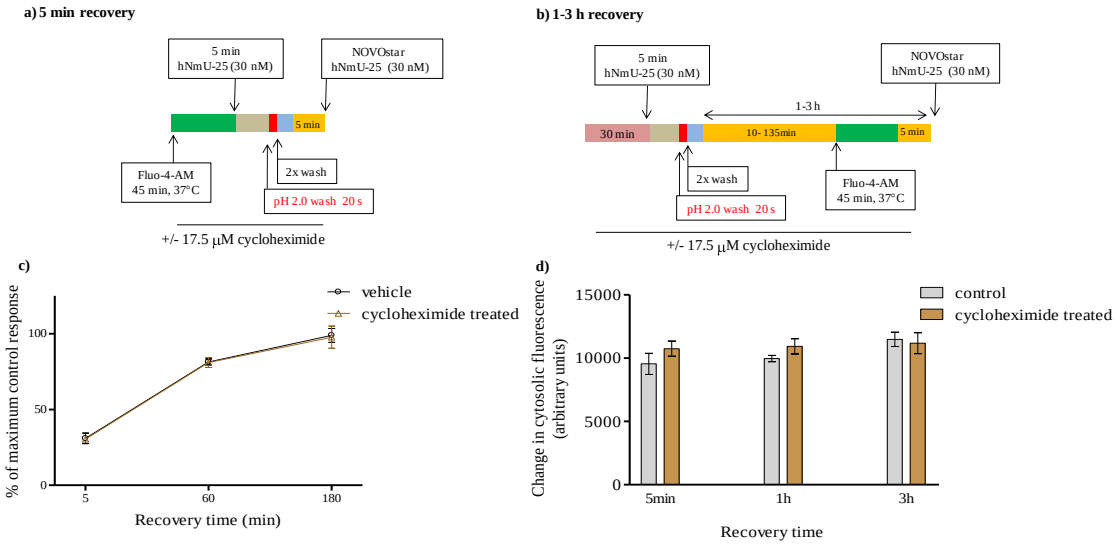

Figure 6.9. Effect of protein synthesis inhibition on the recovery of hNmU-25-mediated Ca^{2+} responses in HEK-NMU2 after a brief acid wash. Cells were cultured in 96-well plates for 48-72 h. Cycloheximide (17.5 μM) was present or absent throughout all subsequent experimental steps. For the 5 min recovery protocol (a), cells were loaded with fluo-4-AM (2 μM) and then challenged with either buffer or hNmU-25 (30 nM) for 5 min followed by a brief acid wash (KHB pH 2.0; 20 s) and two pH 7.4 KHB washes. This was followed by a 5 min recovery period in KHB. For the 1-3 h recovery protocol (b), cells were pre-treated with vehicle or cycloheximide (17.5 μM, 30 min) then challenged and washed as in protocol (a). This was followed by a 1-3 h recovery period. During the last 45 min of recovery, cells were loaded with fluo-4-AM before challenge with hNmU-25 (30 nM) using a NOVOstar plate reader and changes in cytosolic fluorescence were recorded as an index of changes in $[Ca^{2+}]_i$. Data are expressed as a percentage of the maximum response in HEK-NMU2 pre-challenged with buffer (i.e. no initial hNmU-25 challenge) (c). The effect of cycloheximide on the initial Ca^{2+} responses to hNmU-25 (30 nM) in comparison to untreated cells was also investigated at all time-points (d). Data are mean ± s.e.m., n=4 with each experiment performed in duplicate; Bonferroni's multiple comparison test following two-way ANOVA (c) and one-way ANOVA (d). The two-way ANOVA showed a significant effect of time but not treatment.

6.2.5 Effect of inhibiting endosomal acidification on NMU2 resensitization

Chemical inhibition of endosomal acidification by monensin or bafilomycin A has been widely used to study the role of endosomal acidification in recycling and resensitization of many GPCRs. Using a protocol similar to that used to study the effect of protein synthesis inhibition **(Section 6.2.4)**, monensin was used to examine the effect of preventing endosomal acidification on resensitization of hNmU-25-mediated Ca^{2+} signalling (Figure 6.10a, b). Treatment of HEK-NMU2 with monensin (50 μM) resulted in a significant inhibition of resensitization of hNmU-25-mediated Ca^{2+} responses. For example, vehicle-treated (0.1% ethanol) cells recovered essentially completely (98 ± 4% (n=4) of the control peak levels) within 6 h, while monensin-treated cells recovered very poorly (11 ± 5% (n=4) of the control Ca^{2+} peaks) (Figure 6.10c). Initial hNmU-25-mediated Ca^{2+} responses were not significantly affected by monensin pre-treatment (Figure 6.10d).

Removal of bound hNmU-25 by incorporating a brief acid wash to the resensitization protocol (Figure 6.11a, b), did not prevent monensin significantly inhibiting the recovery of hNmU-25-mediated Ca^{2+} responses. For example, after 3 h recovery following pre-exposure to hNmU-25, challenging monensin-treated cells with hNmU-25 (30 nM) evoked 70 ± 2% (n=4) of the peak control responses, while vehicle-treated cells exhibited complete, (99 ± 5%; n=4) recovery. Again, monensin pre-treatment could be shown not to affect initial Ca^{2+} responses to hNmU-25 in naïve cells at all time-points studied (Figure 6.11d).

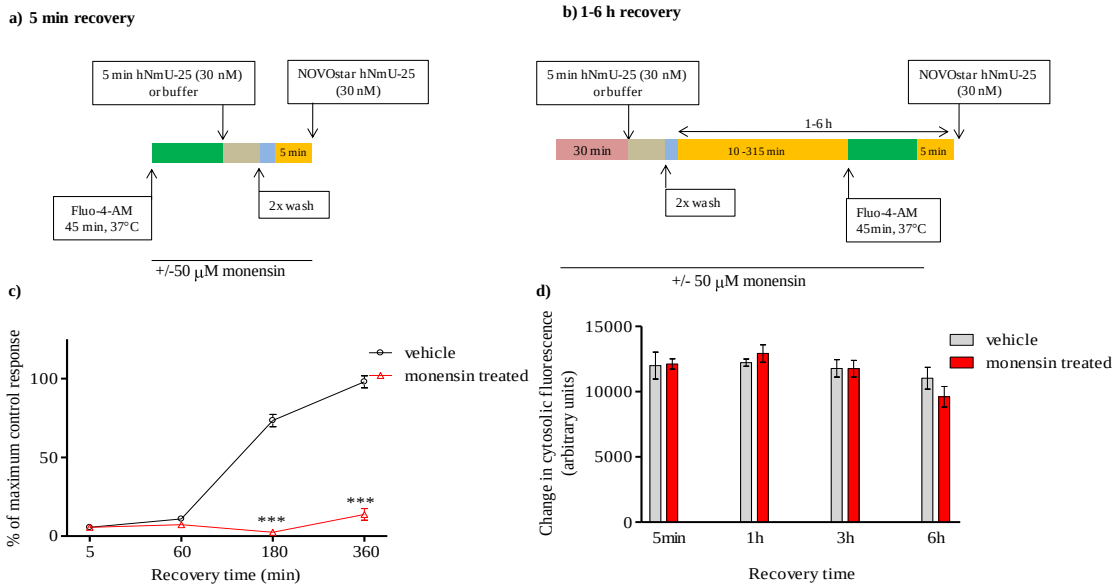

Figure 6.10. Effect of inhibition of endosomal acidification by monensin on the resensitization of hNmU-25-mediated Ca^{2+} responses in HEK-NMU2. Cells were cultured in 96-well plates for 48-72 h. Monensin (50 μM) was present or absent throughout all subsequent experimental steps. For the 5 min recovery protocol (a), cells were loaded with fluo-4-AM. Cells were then challenged with either hNmU-25 (30 nM) or buffer for 5 min followed by two KHB washes and a 5 min recovery period in KHB. For the 1-6 h recovery protocol (b), cells were pre-treated with either vehicle (0.1% ethanol) or monensin (50 μM) for 30 min then challenged with either hNmU-25 (30 nM) or buffer for 5 min followed by two KHB washes. During the last 45 min of the recovery period cells were loaded with fluo-4-AM. Following the recovery period, cells were challenged with hNmU-25 (30 nM) using a NOVOstar plate reader and changes in cytosolic fluorescence were recorded as an index of changes in $[Ca^{2+}]_i$. Data are expressed as a percentage of the maximum response in HEK-NMU2 pre-challenged with buffer only (i.e. no initial hNmU-25 challenge) (c). The effect of monensin on the initial Ca^{2+} responses to hNmU-25 (30 nM) in comparison to untreated cells was also assessed at all time-points (d). Data are mean ± s.e.m.; n=4; $^{***}P<0.001$, Bonferroni's multiple comparison test following two-way ANOVA (c) and one-way ANOVA (d). Significant differences indicated in (c) are between ± monensin at that time point.

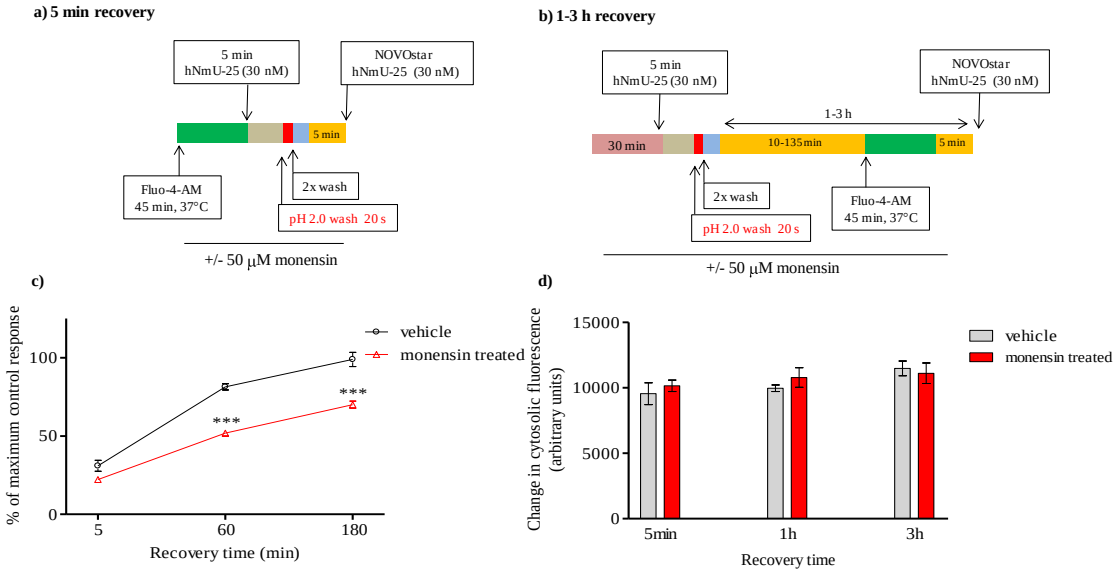

Figure 6.11. Effect of inhibition of endosomal acidification by monensin on resensitization of hNmU-25-mediated Ca^{2+} responses in HEK-NMU2 incorporating a brief acid wash. Cells were cultured in 96-well plates for 48-72 h. Monensin (50 μM) was present or absent throughout all subsequent experimental steps. For the 5 min recovery protocol (a), cells were loaded with fluo-4-AM and then challenged with either hNmU-25 (30 nM) or buffer for 5 min followed by a brief (20 s) wash with KHB, pH 2.0 and then two KHB, pH 7.4 washes. This was followed by a 5 min recovery period in KHB. For the 1-3 h recovery protocol (b), cells were pre-treated with either vehicle (0.1% ethanol) or monensin (50 μM) for 30 min then challenged with either hNmU-25 (30 nM) or buffer for 5 min followed by a brief wash with KHB, pH 2.0 and then two pH 7.4 KHB washes. During the last 45 min of the recovery period, cells were loaded with fluo-4-AM. Following the recovery period, cells were challenged with hNmU-25 (30 nM) using a NOVOstar plate reader and changes in cytosolic fluorescence were recorded as an index of changes in $[Ca^{2+}]_i$. Data are expressed as a percentage of the maximum response in HEK-NMU2 pre-exposed to buffer only (i.e. no initial hNmU-25 challenge) (c). The effect of monensin on the initial Ca^{2+} responses to hNmU-25 (30 nM) in comparison to untreated cells was also assessed at all time-points (d). Data are mean ± s.e.m., n=4; $^{***}P<0.001$, Bonferroni's multiple comparison test following two-way ANOVA (c) and one-way ANOVA (d). Significant differences indicated in (c) are between ± monensin at that time point.

6.2.6 Effects of the ECE-1 inhibitor, SM-19712, on the recovery of hNmU-25-mediated Ca^{2+} signalling in HEK-NMU2

To examine the potential effect of inhibiting ECE-1 activity on the resensitization profile of hNmU-25-mediated Ca^{2+} responses, a treatment of HEK-NMU2 cells with the ECE-1 inhibitor, SM-19712 (10 μM), was incorporated into the resensitization protocol (Figure 6.12a, b). The initial loss of Ca^{2+} response to (desensitization) hNmU-25 (30 nM) was similar in the absence and presence of SM-19712 treatment. However, SM-19712 treatment significantly inhibited the recovery of hNmU-25 Ca^{2+} responsiveness compared to vehicle-treated cells at 1-6 h recovery times (Figure 6.12c). For example, SM-19712 significantly inhibited the recovery of Ca^{2+} responses after 3 h recovery to 17 ± 3% (n=6) of the control peak level compared to 69 ± 4% (n=6) recovery in vehicle-treated cells. Moreover, in the absence of SM-19712, cells fully recovered after 6 h, whereas cells treated with SM-19712 only recovered to 63 ± 2% (n=6) of the control response (Figure 6.12c). Treatment of HEK-NMU2 with SM-19712 (10-100 μM) did not affect initial Ca^{2+} responses to hNmU-25 (30 nM) compared to cells treated with vehicle only (Figure 6.12d).

To assess the ligand/receptor specificity of SM-19712 effect, the time-course of resensitization of carbachol-mediated Ca^{2+} signalling at the endogenously expressed muscarinic M_3 receptors was also assessed in the presence or absence of SM-19712 (Figure 6.13a, b). Pre-exposure of HEK-NMU2 to carbachol (100 μM) for 5 min followed by 5 min recovery resulted in approximately 40% inhibition of the Ca^{2+} responses to carbachol re-challenge with full resensitization occurring by 30 min (Figure 6.13c). The time-course of recovery of carbachol-mediated Ca^{2+} responses was not significantly altered by the presence of SM-19712 (10 μM) (Figure 6.13c).

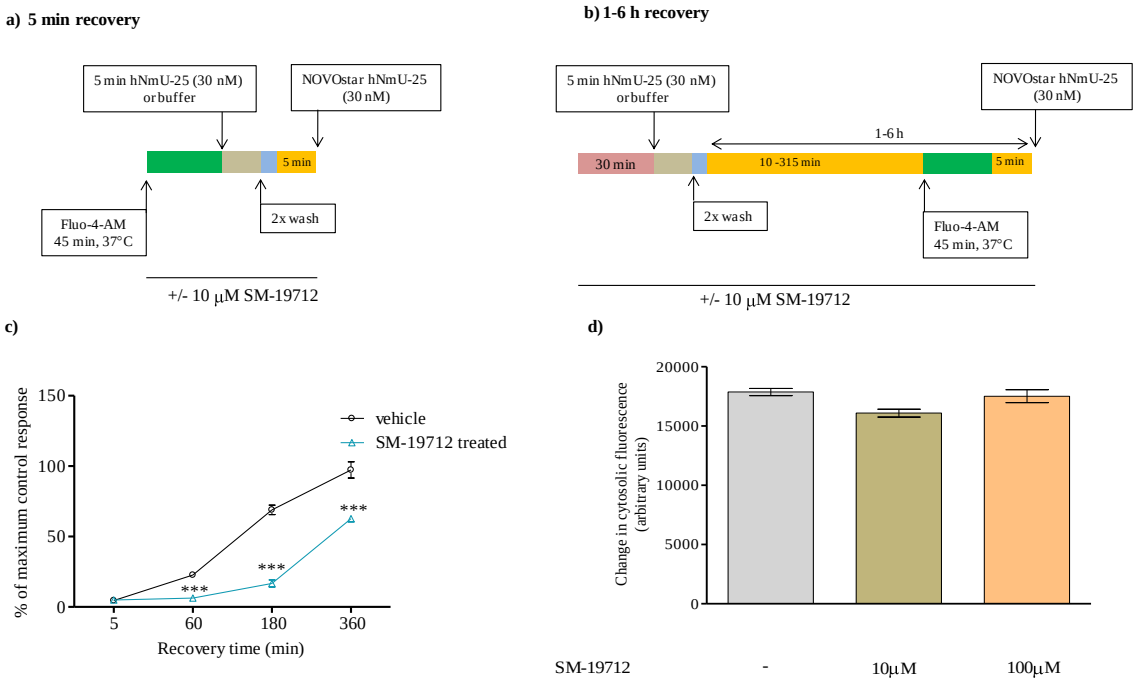

Figure 6.12. Effect of the ECE-1 inhibitor, SM-19712, on the recovery of hNmU-25-mediated Ca^{2+} responses in HEK-NMU2. Cells were cultured in 96-well plates for 48-72 h. SM-19712 (10 µM) was present or absent throughout all subsequent experimental steps. For the 5 min recovery protocol (a), cells were loaded with fluo-4-AM and then challenged with hNmU-25 (30 nM) or buffer for 5 min followed by two KHB washes and a 5 min recovery period in KHB. For the 1-6 h recovery protocol (b), cells were pre-treated with SM-19712 (10 µM) or vehicle for 30 min and then challenged with hNmU-25 (30 nM) or buffer for 5 min followed by two KHB washes. During the last 45 min of the recovery period, cells were loaded with fluo-4-AM. Cells were re-challenged with hNmU-25 (30 nM) using a NOVOstar plate reader and changes in cytosolic fluorescence were recorded as an index of changes in $[Ca^{2+}]_i$. Data are expressed as a percentage of the maximum response in HEK-NMU2 pre-challenged with buffer only (i.e. no initial hNmU-25 challenge) (c). The effect of SM-19712 (10-100 µM) on the initial Ca^{2+} responses to hNmU-25 (30 nM) in comparison to vehicle-treated cells was also assessed (d). Data are mean ± s.e.m., n = 6 in duplicate; $^{***}P<0.001$, Bonferroni's multiple comparison test following two-way ANOVA (c) and one-way ANOVA (d). Significant differences indicated in (c) are between ± SM-19712 at that time point.

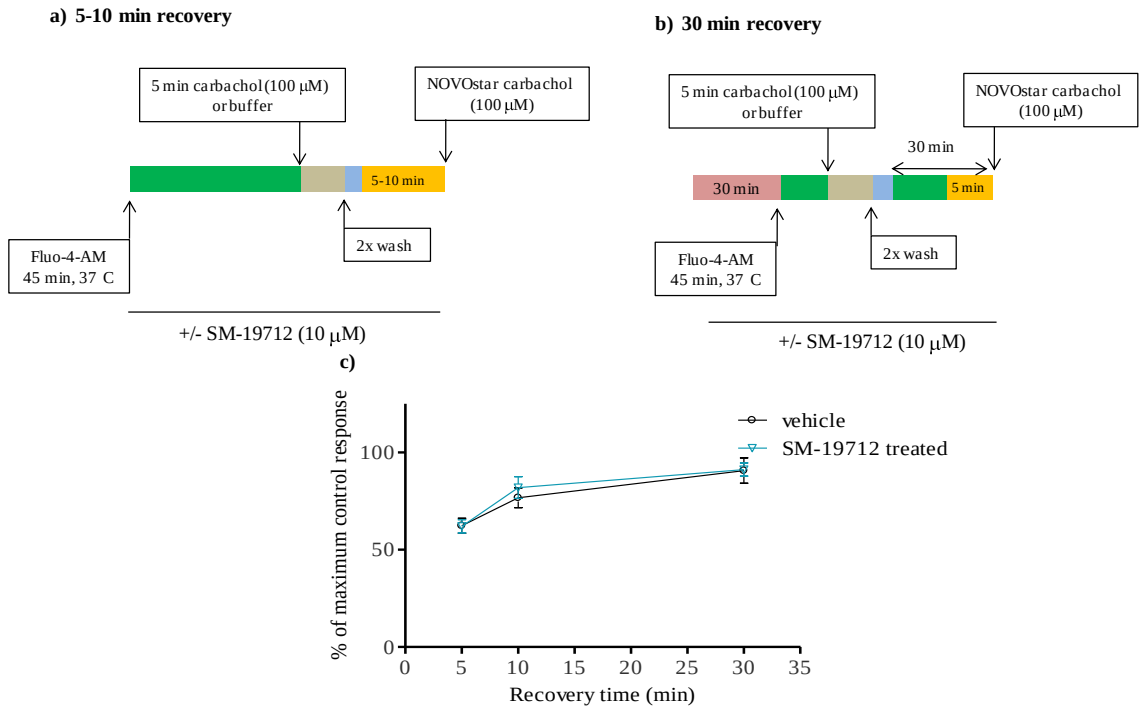

Figure 6.13. Effect of the ECE-1 inhibitor, SM-19712, on resensitization of carbachol-mediated Ca^{2+} responses in HEK-NMU2. Cells were cultured in 96-well plates for 48-72 h. SM-19712 (10 µM) was present or absent throughout all subsequent experimental steps. For the 5-10 min recovery protocol (a), cells were loaded with fluo-4-AM and then challenged with carbachol (100 µM) or buffer for 5 min followed by two washes with KHB and a 5 min recovery period in KHB. For the 30 min recovery protocol (b), cells were pre-treated with SM-19712 (10 µM) or vehicle for 30 min and then loaded with fluo-4-AM. Stimulation with either carbachol (100 µM) or buffer for 5 min occurred after 15 min of the loading period followed by two washes with KHB and then continued loading for a further 25 min. Cells were re-challenged with carbachol (100 µM) using a NOVOstar plate reader and changes in cytosolic fluorescence were recorded as an index of changes in $[Ca^{2+}]_i$. Data are expressed as a percentage of the maximum response in HEK-NMU2 pre-challenged with buffer only (i.e. no initial carbachol challenge) (c). Data are mean ± s.e.m., n=3 with each experiment performed in duplicate; Bonferroni's multiple comparison test followingtwo-way ANOVA. The two-way ANOVA showed a significant effect of time but not treatment.

6.2.7 NMU2-mediated activation of ERK and the effect of the ECE-1 inhibitor, SM-19712

Stimulation of HEK-NMU2 with hNmU-25 resulted in an increase of pERK signals (as an index of ERK activation) in a concentration-dependent manner with a pEC_{50} value of 9.51 ± 0.17 (Figure 6.14b, n=3). The peak of ERK activation upon stimulation of vehicle treated HEK-NMU2 with a maximum concentration of hNmU-25 (30 nM) was achieved within 5 min followed by a slow decline which returned to the basal level after approximately 60 min (Figure 6.14ci). Similarly, stimulation of SM-19712 treated cells with hNmU-25 30 nM evoked an increase in the pERK signal, which reached a peak after 5 min. However, elevation of pERK in cells treated with the ECE-1 inhibitor was prolonged with peak activation being observed from 5-30 min and then gradually declining but at a rate much slower than vehicle treated cells. Indeed, the pERK signal was clearly observed up to 2 h in the presence of SM-19712 but only apparent up to 1 h in the absence of SM-19712 (Figure 6.14cii). Furthermore, the magnitude of ERK activation was higher in SM-19712 treated cells at all time points (Figure 6.14d). For example, the peak signal in SM-19712 cells was 1.5-2.5 fold stronger than vehicle treated cells at 5-60 min and 5-6 fold stronger at 90-120 min (Figure 6.14d).

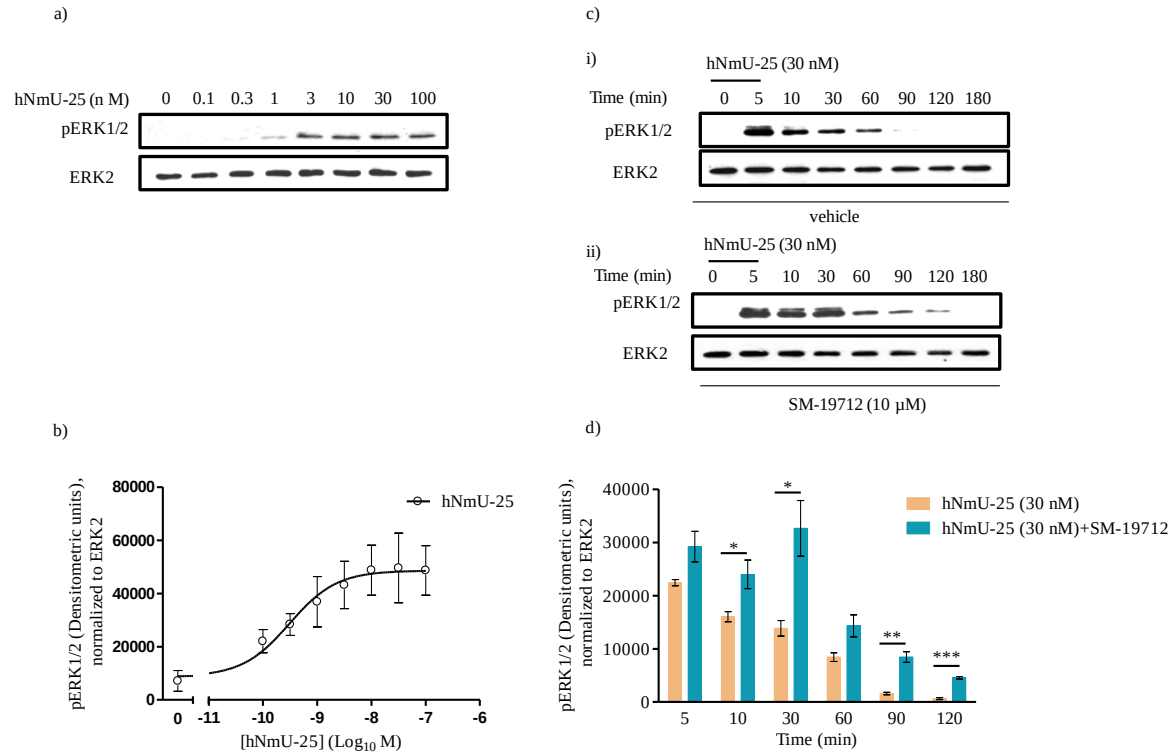

Figure 6.14. Concentration-response curve and time-course of hNmU-25-mediated ERK activation and the effect of the ECE-1 inhibitor, SM-19712. HEK-NMU2 cultured on 24-well plates for 48 h were serum starved overnight. To construct concentration-response curves (a, b) for agonist-stimulated increases in extracellular signal-regulated kinase phosphorylation (pERK), cells were washed twice with KHB (0.5 mL), incubated with KHB (1 mL, 10 min) and challenged with KHB alone or KHB containing different concentrations of hNmU-25 (0.1-100 nM, 5 min). For investigation of the time-course of pERK generation (c), cells were pre-incubated with KHB (1 mL, 30 min) alone, or where required SM-19712 (10 µM). In this latter circumstance, treatment was included in all subsequent experimental steps. Cells were then challenged with KHB alone or KHB containing hNmU-25 (30 nM) for 5 min and the solution then replaced with KHB alone or containing SM-19712 (10 µM) for 5-180 min. The pERK and ERK was estimated in 20 µg protein by Western blotting (a and c) and the signal density of each were quantified using ImageJ software. The level of pERK was calculated as relative to ERK (b, d). Data are representative blots or mean ± s.e.m., n=3, **P*<0.05, ***P*<0.01, ****P*<0.001; Bonferroni's multiple comparison test following two-way ANOVA.

6.2.8 Effect of incubation under high-glucose culture conditions on the recovery of hNmU-25-mediated Ca^{2+} signalling

High-glucose exposure of cells can increase the expression of ECE-1 (Jafri *et al.*, 2006; Keynan *et al.*, 2004). Together with the effect of the ECE-1 inhibitor, SM-19712 on the recovery of hNmU-25-mediated Ca^{2+} responses that was observed earlier, the effect of high-glucose exposure of HEK-NMU2 was assessed against the recovery of NMU-2-mediated Ca^{2+} signalling at 1 h following an initial challenge (Figure 6.15a). Incubation of HEK-NMU2 for 24, 48 or 72 h in medium containing high glucose (25 mM), significantly increased the recovery of the Ca^{2+} response at 1 h (to 56 ± 1% (n=3) at 24 h, 70 ± 3% (n=3) at 48 h and 87 ± 3% (n=3) at 72 h of high glucose exposure, compared to 22 ± 2% (n=3) in cells incubated in normal (5.5 mM glucose) medium (Figure 6.15b). The greater recovery of the hNmU-25-stimulated Ca^{2+} response observed in cells incubated in high-glucose medium was lost if cells were treated with the ECE-1 inhibitor, SM-19712 (10 μM) (Figure 6.16a, b).

It has been suggested previously that protein kinase C (PKC) activity is involved in the up-regulation of ECE-1 expression seen in cells exposed to high-glucose medium (Khamisi *et al.*, 2009). Experiments were therefore designed to examine whether inhibition of PKC would inhibit the ability of high glucose to enhance the recovery of NMU2-mediated Ca^{2+} signalling. HEK-NMU2 were incubated in high-glucose (25 mM) medium for 48 h followed by a further 12 h in the same medium in the absence or presence of the PKC inhibitor, Ro 31-8220 (10 μM). Cells were then challenged with hNmU-25 (30 nM) or vehicle and after washing and a 1 h recovery period were re-challenged with hNmU-25 (Figure 6.17a). The extent of recovery of the hNmU-25-stimulated Ca^{2+} response was not significantly affected by the presence of Ro 31-8220 in cells incubated in normal glucose medium, whereas the presence of the PKC inhibitor significantly reduced the recovery of responsiveness in cells incubated in high-glucose medium (89 ± 3% (n=4) versus 54 ± 3% (n=4) of the control Ca^{2+} responses in high-glucose-exposed cells in the respective absence and presence of Ro 31-8220 (10 μM (Figure 6.17b).

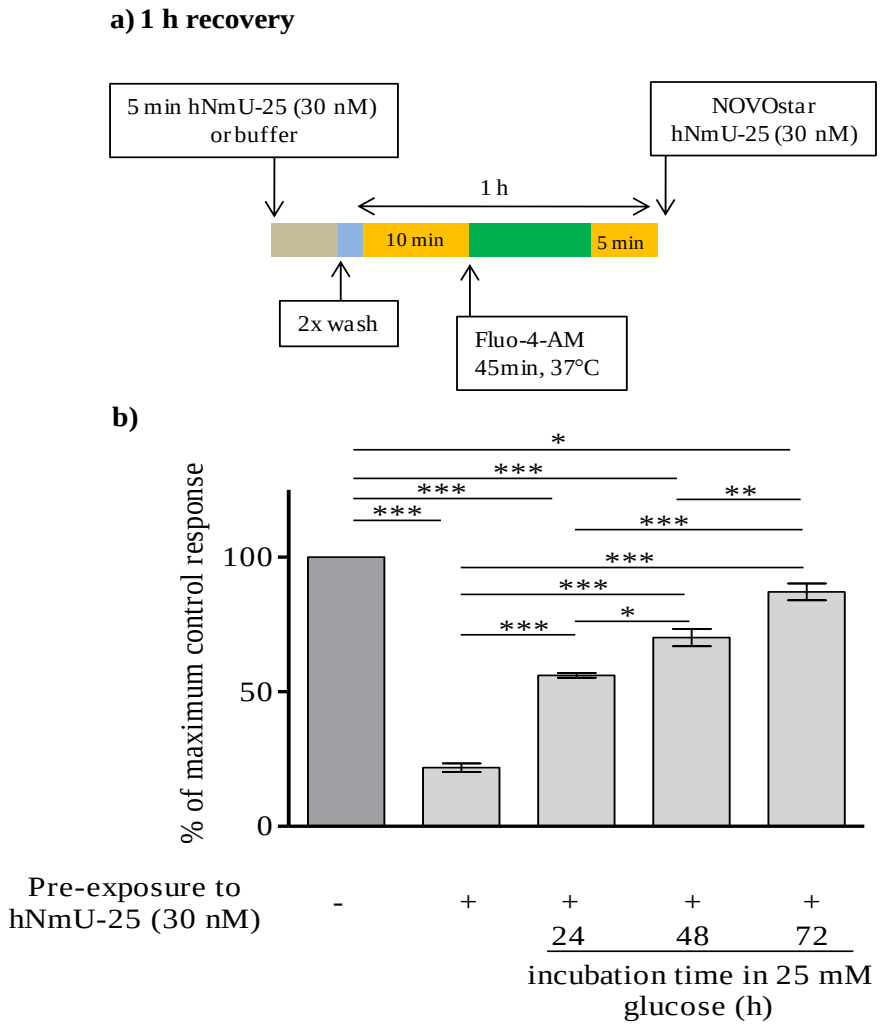

Figure 6.15. Effect of high glucose on resensitization of hNmU-25-mediated Ca^{2+} signalling in HEK-NMU2. Cells were cultured in 96-well plates with medium containing either normal (5.5 mM) or high (25 mM) glucose for 24-72 h. For the 1 h recovery protocol (a), cells were challenged with either hNmU-25 (30 nM) or buffer for 5 min followed by two KHB washes. Cells were loaded with fluo-4-AM during the last 45 min of the recovery period. Cells were re-challenged with hNmU-25 (30 nM) using a NOVOstar plate reader and changes in cytosolic fluorescence were recorded as an index of changes in $[Ca^{2+}]_i$. Data are expressed as a percentage of the maximum response in HEK-NMU2 pre-challenged with buffer (i.e. no initial hNmU-25 challenge) (b). Data are mean ± s.e.m., n=3, each experiment performed in duplicate; **P*<0.05, ***P*<0.01, ****P*<0.001, Bonferroni's multiple comparison test following one-way ANOVA.

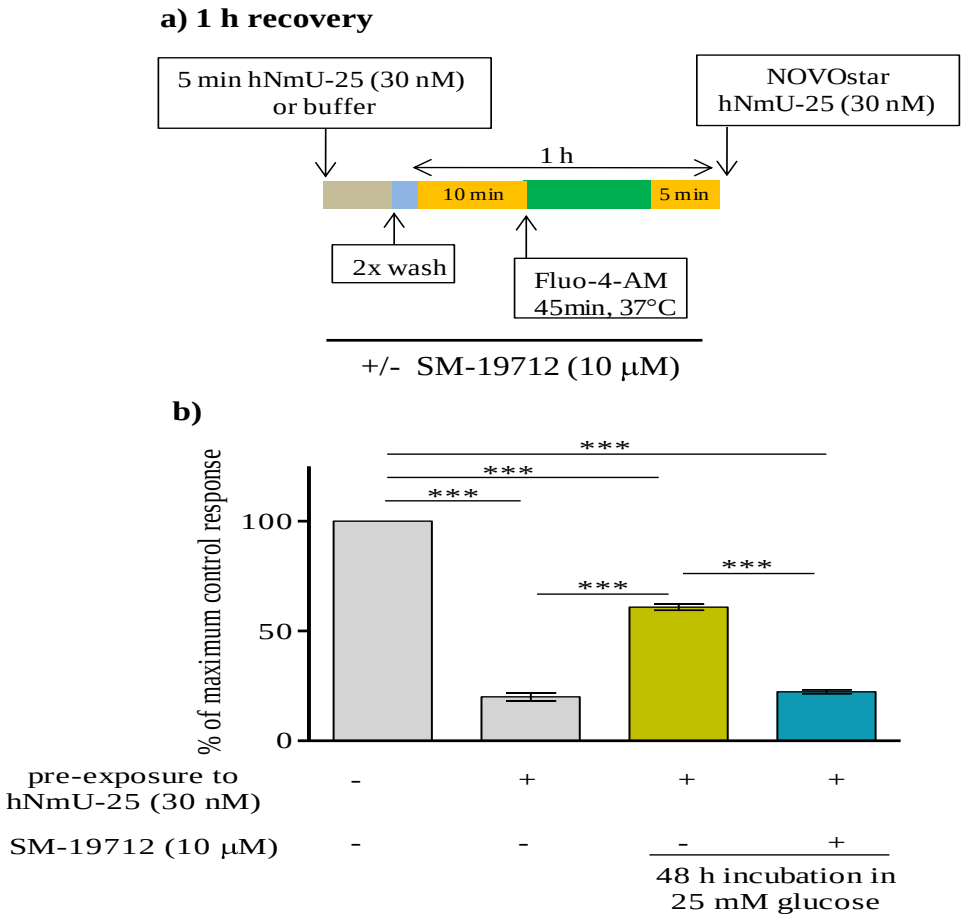

Figure 6.16. Effect of high glucose and ECE-1 inhibition on resensitization of hNmU-25-mediated Ca^{2+} signalling in HEK-NMU2. Cells were cultured in 96-well plates in medium containing normal (5.5 mM) or high (25 mM) glucose for 48 h. SM-19712 (10 µM) was present or absent throughout all subsequent experimental steps. For the 1 h recovery protocol (a), cells were pre-treated with either vehicle or SM-19712 (10 µM) for 30 min and then challenged with hNmU-25 (30 nM) or buffer for 5 min followed by two KHB washes. Cells were loaded with fluo-4-AM during the last 45 min of the recovery period. Cells were challenged with hNmU-25 (30 nM) using a NOVOstar plate reader and changes in cytosolic fluorescence were recorded as an index of changes in $[Ca^{2+}]_i$. Data are expressed as a percentage of the maximum response in HEK-NMU2 pre-challenged with buffer only (b). Data are mean ± s.e.m., n=5, each experiment performed in duplicate; ***P<0.001, Bonferroni's multiple comparison test following one-way ANOVA.

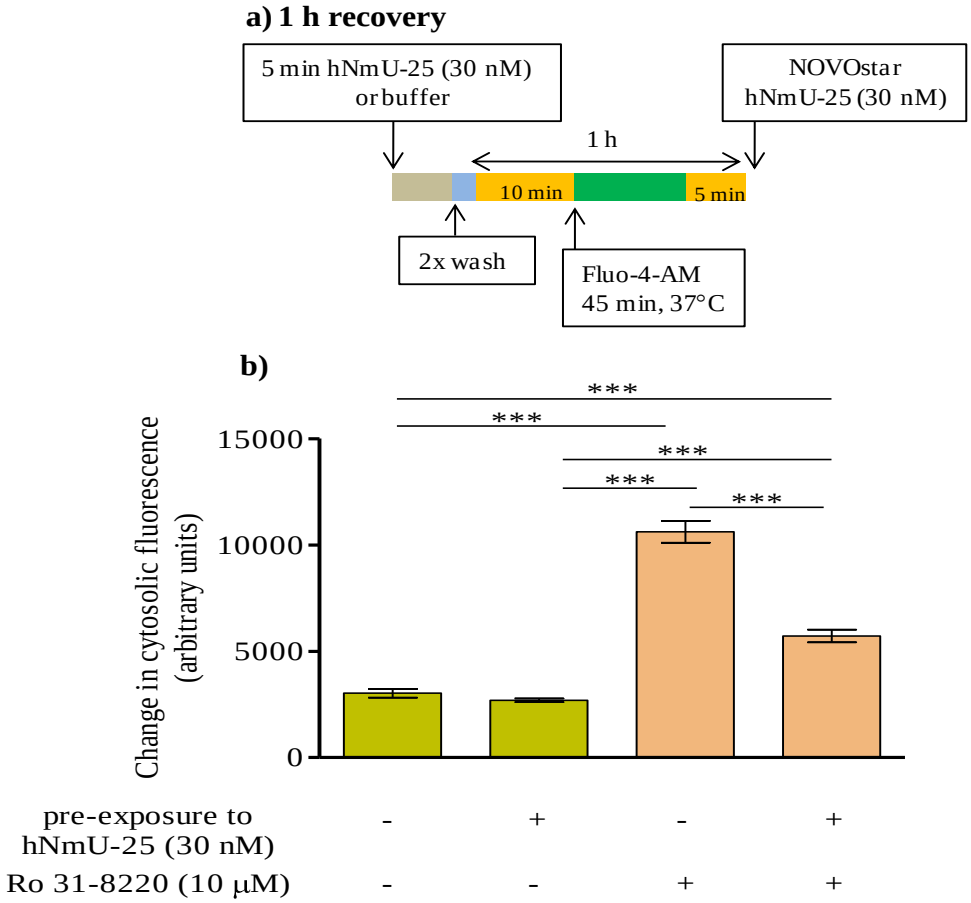

Figure 6.17. Effect of the PKC inhibitor, Ro 31-8220, on resensitization of hNmU-25-mediated Ca^{2+} responses in HEK-NMU2 cultured in high-glucose medium. Cells were cultured in 96-well plates with medium containing high (25 mM) glucose for 48 h and then incubated for a further 12 h with the same medium either alone, or with the PKC inhibitor, Ro 31-8220 (10 μM). Cells were challenged with hNmU-25 (30 nM) or buffer for 5 min followed by two KHB washes followed by a recovery period of 1 h in KHB. Cells were loaded with fluo-4-AM during the last 45 min of the recovery period (a). Cells were then challenged with hNmU-25 (30 nM) using a NOVOstar plate reader and changes in cytosolic fluorescence were recorded as an index of changes in $[Ca^{2+}]_i$. Data are mean ± s.e.m., n=4 with each experiment performed in duplicate (b); ***P<0.001, Bonferroni's multiple comparison test following one-way ANOVA;.

6.2.9 Time-course of resensitization of hNmS-33-mediated Ca^{2+} signalling and the effect of SM-19712 and dynasore in HEK-NMU2

So far, hNmU-25 has been used exclusively as the ligand to stimulate NMU2. However, other endogenous (and synthetic) ligands also can activate NMU2 and it was considered important to examine whether alternate ligands interact with the receptor in an identical manner to hNmU-25. Thus, the recently discovered endogenous peptide, hNmS-33, were used here to examine whether alternate ligands have similar or contrasting pharmacodynamic properties at NMU2.

In populations of adherent, fluo-4-loaded HEK-NMU2 Ca^{2+} responses were measured to varying concentrations of either hNmS-33 or hNmU-25 (Figure 6.18). These agonists stimulated Ca^{2+} responses that were not significantly different either in terms of the maximum Ca^{2+} response or the concentration of agonist necessary to stimulate 50% of the maximal response (pEC_{50} values, 9.42 ± 0.08 and 9.34 ± 0.05 for hNmU-25 and hNmS-33, respectively). The aim of repeated Ca^{2+} measurement for the two peptides here is to insure that both are not degraded and fully bioactive at the time of experiments.

To assess the resensitization profile of hNmS-33-mediated Ca^{2+} signalling in HEK-NMU2, a protocol corresponding to that used to assess the recovery of hNmU-25-mediated Ca^{2+} signalling was used (Figure 6.19a, b). The recovery rate of hNmS-33-mediated Ca^{2+} responses was significantly slower than that observed for hNmU-25. For instance, after 6 h recovery, hNmU-25-mediated Ca^{2+} responses had fully recovered, whereas challenge with hNmS-33 (30 nM) at the same time point evoked only 68 ± 2 % (n=3) of the control response (Figure 6.19c). Furthermore, inclusion of the ECE-1 inhibitor, SM-19712 (10 μM), throughout the recovery period did not significantly affect recovery of hNmS-33-mediated Ca^{2+} signalling (Figure 6.20a, b); thus, at the 6 h recovery time-point, stimulation of vehicle-treated and SM-19712-treated HEK-NMU2 exhibited 66 ± 4% (n=3) and 67 ± 2% (n=6) recoveries relative to control responses, respectively (Figure 6.20c).

To examine the effect of inhibiting dynamin-dependent internalization on the recovery of Ca^{2+} responses to hNmS-33, HEK-NMU2 were exposed to hNmS-33 (30 nM, 5 min) and allowed to recover for 6 h in the absence or presence of dynasore (80 μM)

prior to a second challenge with a similar concentration of hNmS-33 (Figure 6.21a). At 6 h after the initial hNmS-33 (30 nM) exposure, the recovery of the Ca^{2+} response was significantly inhibited in cells treated with dynasore compared to agonist treatment and time-matched control cells re-challenged with hNmS-33 (30 nM) (recoveries of 56 ± 4% (n=4) versus 29 ± 3% (n=4) in the respective absence and presence of dynasore; Figure 6.21b, c).

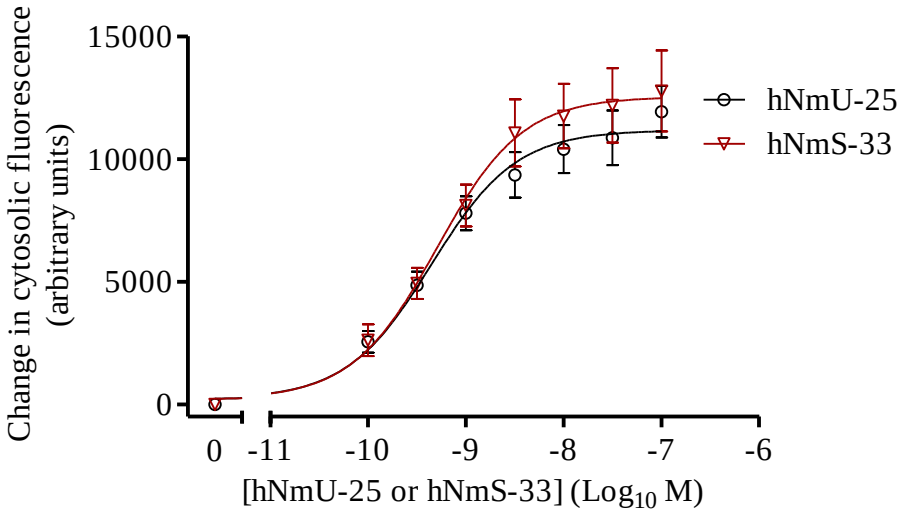

Figure 6.18. Concentration-dependent Ca^{2+} responses to hNmU-25 or hNmS-33 in HEK-NMU2. Cells were cultured in 96-well plates for 48-72 h. Cells were then loaded with fluo-4-AM and challenged with different concentrations of either hNmU-25 (0.1 to 100 nM) or hNmS-33 (0.1 to 100 nM) using a NOVOstar plate reader. Changes in cytosolic fluorescence were monitored as an index of $[Ca^{2+}]_i$. Maximal changes in fluorescence were used to construct concentration-response curves (b). The pEC_{50} values for hNmU-25 and hNmS-33 in HEK-NMU2 were 9.42 ± 0.08 and 9.34 ± 0.05, respectively. Data are mean ± s.e.m.; n=4.

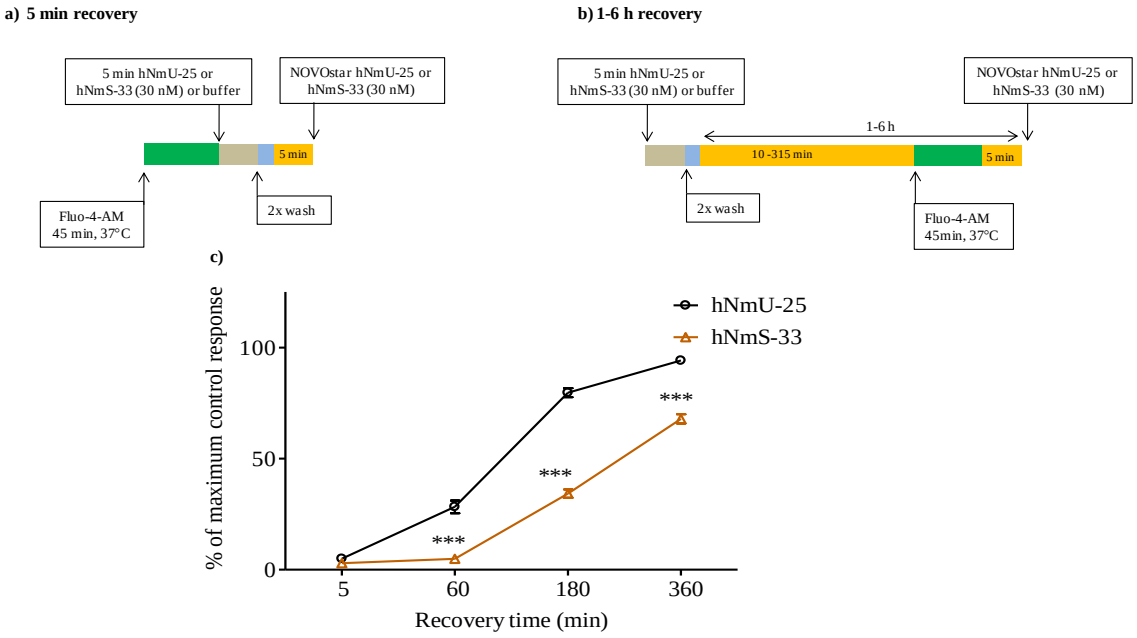

Figure 6.19. Time-course of resensitization of either hNmU-25- or hNmS-33-mediated Ca^{2+} responses in HEK-NMU2. Cells were cultured in 96-well plates for 48-72 h. For the 5 min recovery protocol (a), cells were loaded with fluo-4-AM, challenged with hNmU-25 (30 nM), hNmS-33 (30 nM) or buffer, for 5 min followed by two KHB washes and a 5 min recovery period in KHB. For the 1-6 h recovery protocol (b), cells were challenged with hNmU-25 (30 nM), hNmS-33 (30 nM) or buffer for 5 min followed by two KHB washes. During the last 45 min of the recovery period, cells were loaded with fluo-4-AM. Cells were then challenged with hNmU-25 (30 nM) or hNmS-33 (30 nM) using a NOVOstar plate reader and changes in cytosolic fluorescence were recorded as an index of changes in $[Ca^{2+}]_i$. Data are expressed as a percentage of the maximum response in HEK-NMU2 pre-challenged with buffer only (i.e. no initial hNmU-25 or hNmS-33 challenge) (c). Data are mean ± s.e.m.; n=3 with each experiment performed in duplicate; $^{***}P<0.001$, Bonferroni's multiple comparison test following two-way ANOVA.

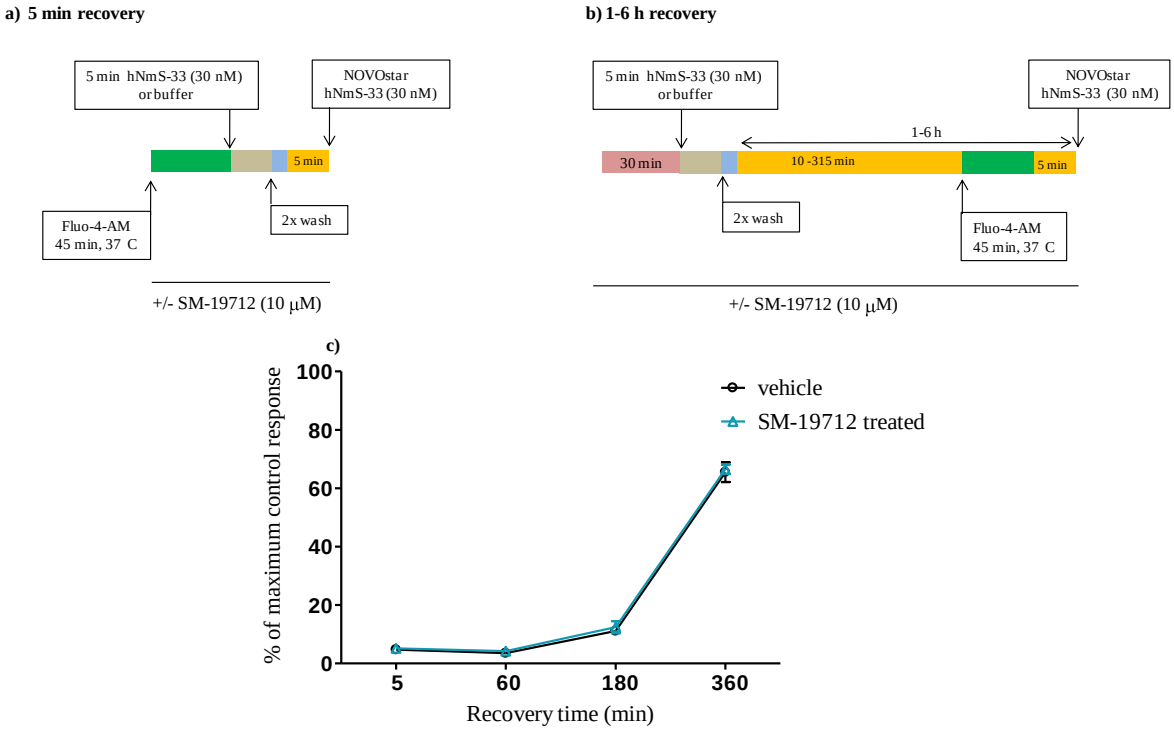

Figure 6.20. Effect of the ECE-1 inhibitor, SM-19712, on the resensitization of hNmS-33-mediated Ca^{2+} responses in HEK-NMU2. Cells were cultured in 96-well plates for 48-72 h. SM-19712 (10 μM) was present or absent throughout all subsequent experimental steps. For the 5 min recovery protocol (a), cells were loaded with fluo-4-AM and then challenged with either hNmS-33 (30 nM) or buffer for 5 min followed by two KHB washes and a 5 min recovery period in KHB. For the 1-6 h recovery protocol (b), cells were pre-treated with vehicle or SM-19712 (10 μM) for 30 min then challenged with either hNmS-33 (30 nM) or buffer for 5 min followed by two KHB washes. During the last 45 min of the recovery period, cells were loaded with fluo-4-AM. Cells were then challenged with hNmS-33 (30 nM) using a NOVOstar plate reader and changes in cytosolic fluorescence were recorded as an index of changes in $[Ca^{2+}]_i$. Data are expressed as a percentage of the maximum response in HEK-NMU2 pre-challenged with buffer only (c). Data are mean ± s.e.m.; n=3 for vehicle-treated cells and n=6 for SM-19712-treated cells with each experiment performed in duplicate; $^{***}P<0.001$, Bonferroni's multiple comparison test following two-way ANOVA. The two-way ANOVA showed a significant effect of time but not treatment.

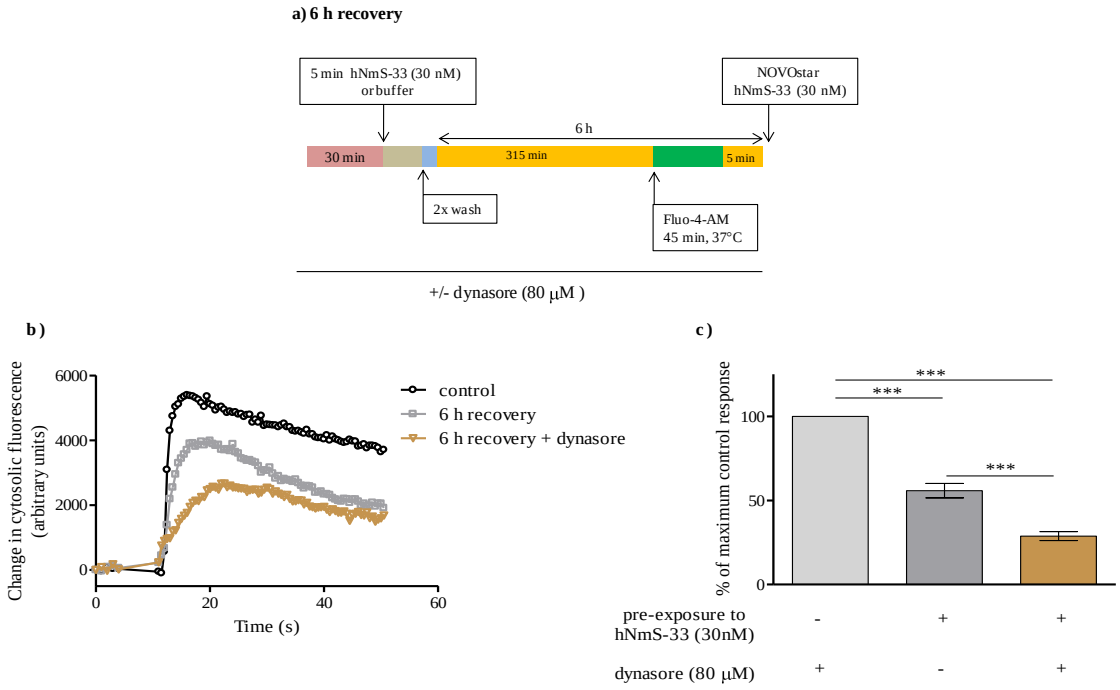

Figure 6.21. Effect of the internalization inhibitor, dynasore, on the recovery of hNmS-33-mediated Ca^{2+} responses in HEK-NMU2. Cells were cultured in 96-well plates for 48-72 h. For the 6 h recovery protocol (a), cells were pre-treated with dynasore (80 μM) or vehicle for 30 min and then challenged with hNmS-33 (30 nM) or buffer for 5 min followed by two KHB washes. This was followed by a 6 h recovery period in serum-free medium. Cells were loaded with fluo-4-AM during the last 45 min of this period. Cells were re-challenged with hNmS-33 (30 nM) using a NOVOstar plate reader and changes in cytosolic fluorescence were recorded as an index of changes in $[Ca^{2+}]_i$. Traces (b) are representative of Ca^{2+} responses to hNmS-33 (30 nM) in cells pre-challenged with buffer (control) or hNmS-33 (30 nM) followed by a 6 h recovery period ± dynasore followed by challenge with hNmS-33 (30 nM). Data are expressed as a percentage of the maximum response in HEK-NMU2 initially challenged with buffer only (c). Data are mean ± s.e.m., n=4, each experiment performed in duplicate; ***P<0.001, Bonferroni's multiple comparison test following one-way ANOVA.

6.2.10 Time-course of resensitization of Ca^{2+} signalling in HEK-NMU2 stimulated by pNmU-8 and SM-19712 dynasore

Ca^{2+} responses in populations of adherent, fluo-4-loaded HEK-NMU2 revealed that pNmU-8 and hNmU-25 have similar potency and magnitude of Ca^{2+} responses to hNmU-25 and pNmU-8 (Figure 6.22). To compare the recovery profile of pNmU-8- and hNmU-25-mediated Ca^{2+} signalling in HEK-NMU2, a similar protocol to that used earlier (Figure 6.19a, b) was employed, although the 6 h time-point was not used as pNmU-8-mediated Ca^{2+} responses recovered in a shorter time. Briefly, cells were pre-exposed to pNmU-8 (30 nM), hNmU-25 (30 nM) or buffer for 5 min followed by washing (pH 7.4 buffer) and a recovery period of 5 min-3 h and then re-challenge with the same concentration of pNmU-8 or hNmU-25 (Figure 6.23a, b). At the 1 h recovery time-point, pNmU-8-treated cells showed a significantly greater recovery compared to those challenged with hNmU-25 (44 ± 4% (n=6) versus 21 ± 2% (n=6) recovery of Ca^{2+} responses, respectively). This difference was also seen at the 3 h time-point (pNmU-8, 86 ± 2 % (n=7) versus hNmU-25, 60 ± 3% (n=7): Figure 6.23c). Treatment of HEK-NMU2 with SM-19712 (10 μM) did not significantly affect the recovery of the Ca^{2+} response at 3 h in pNmU-8-treated HEK-NMU2. For example, after 3 h recovery, stimulation of pNmU-8-treated cells resulted in a Ca^{2+} response that was 81 ± 2% (n=4) or 84 ± 3% (n=4) of the control peak level in the absence and presence of SM-19712 respectively (Figure 6.24a-c).

The effect of the dynamin-dependent internalization inhibitor, dynasore (80 μM) on the recovery of pNmU-8-mediated Ca^{2+} signalling was also assessed using the 3 h recovery protocol (Figure 6.25a). After 3 h recovery, Ca^{2+} responses to pNmU-8 (30 nM) were significantly inhibited by dynasore (12 ± 1% (n=4) of the control response compared to 83 ± 3% (n=4) recovery in the absence of inhibitor (Figure 6.25b, c)).

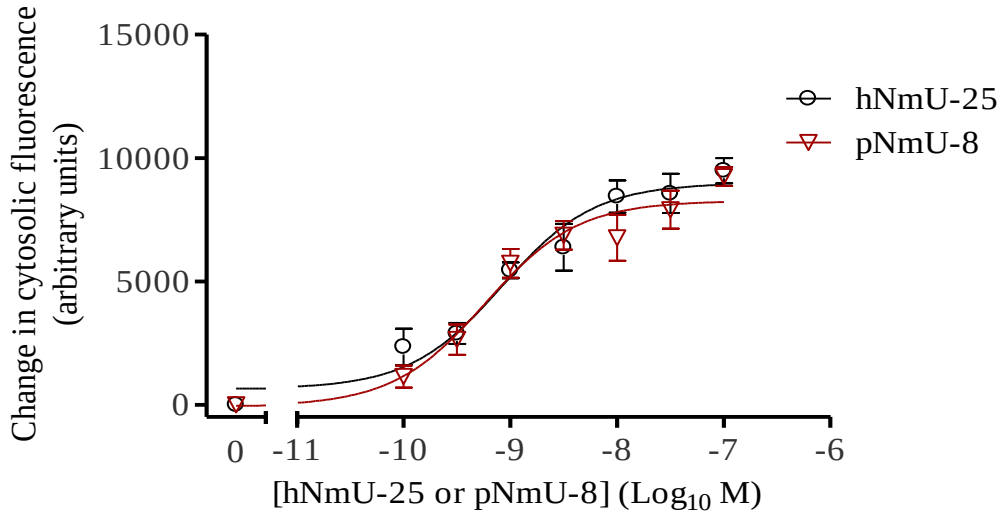

Figure 6.22. Ca^{2+} responses to hNmU-25 and pNmU-8 in HEK-NMU2. Cells were cultured in 96-well plates for 48-72 h**.** Cells were then loaded with fluo-4-AM followed by challenge with different concentrations of hNmU-25 (0.1 to 100 nM) or pNmU-8 (0.1 to 100 nM) using a NOVOstar plate reader. Changes in cytosolic fluorescence were monitored as an index of $[Ca^{2+}]_i$. Maximal changes in fluorescence were used to construct concentration-response curves. The pEC_{50} values for hNmU-25 and pNmU-8 in HEK-NMU2 were 9.14 ± 0.10 and 9.23 ± 0.13, respectively. Data are mean ± s.e.m.; n=4.

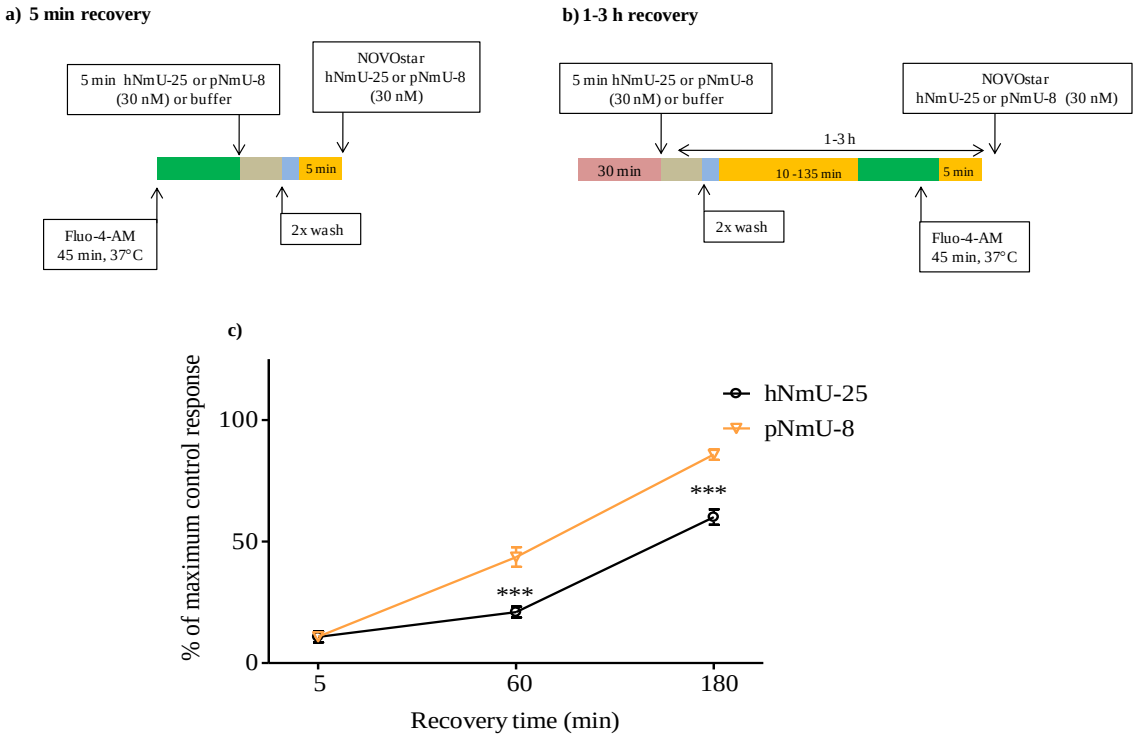

Figure 6.23. Time-courses of resensitization of hNmU-25- or pNmU-8-mediated Ca^{2+} responses in HEK-NMU2. Cells were cultured in 96-well plates for 48-72 h. For the 5 min recovery protocol (a), cells were loaded with fluo-4-AM and then challenged with hNmU-25 (30 nM), pNmU-8 (30 nM) or buffer for 5 min followed by two KHB washes and a 5 min recovery period in KHB. For the 1-3 h recovery protocol (b), cells were challenged with hNmU-25 (30 nM), pNmU-8 (30 nM) or buffer for 5 min followed by two KHB washes. Cells were loaded with fluo-4-AM during the last 45 min the recovery period. Cells were then challenged with hNmU-25 (30 nM) or pNmU-8 (30 nM) using a NOVOstar plate reader and changes in cytosolic fluorescence were recorded as an index of changes in $[Ca^{2+}]_i$. Data are expressed as a percentage of the maximum response in HEK-NMU2 pre-challenged with buffer only (c). Data are mean ± s.e.m.; n=3 (5 min time-point), n=6 (1 h time-point) or n=7 (3 h time-point) with each experiment performed in duplicate; $^{***}P<0.001$, Bonferroni's multiple comparison test following two-way ANOVA.

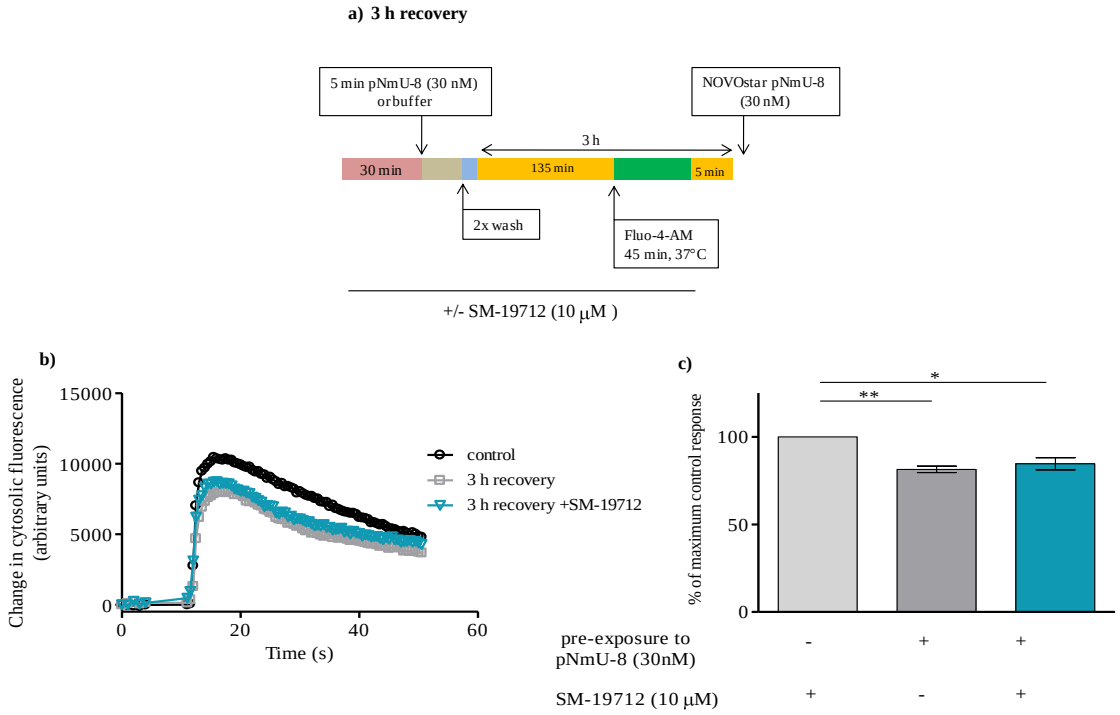

Figure 6.24. Effect of the ECE-1 inhibitor, SM-19712, on resensitization of pNmU-8-mediated Ca^{2+} response in HEK-NMU2. Cells were cultured in 96-well plates for 48-72 h. For the 3 h recovery protocol (a), cells were pre-treated with vehicle or SM-19712 (10 μM) for 30 min and then challenged with either pNmU-8 (30 nM) or buffer for 5 min followed by two KHB washes. Cells were loaded with fluo-4-AM during the last 45 min of the recovery period. Cells were then challenged with pNmU-8 (30 nM) using a NOVOstar plate reader and changes in cytosolic fluorescence were recorded as an index of changes in $[Ca^{2+}]_i$. Traces (b) are representative of Ca^{2+} responses to pNmU-25 (30 nM) in cells challenged with buffer only (control) followed by recovery for 3 h and then re-challenged with pNmU-8 (30 nM), or pre-challenged with pNmU-8 (30 nM) followed by 3 h recovery ±SM-19712 and then re-challenged with pNmU-8 (30 nM). Data are expressed as a percentage of the maximum response in HEK-NMU2 pre-challenged with buffer only (c). Data are mean ± s.e.m., n=4 with each experiment performed in duplicate; **P*<0.05, ***P*<0.01, Bonferroni's multiple comparison test following one-way ANOVA.

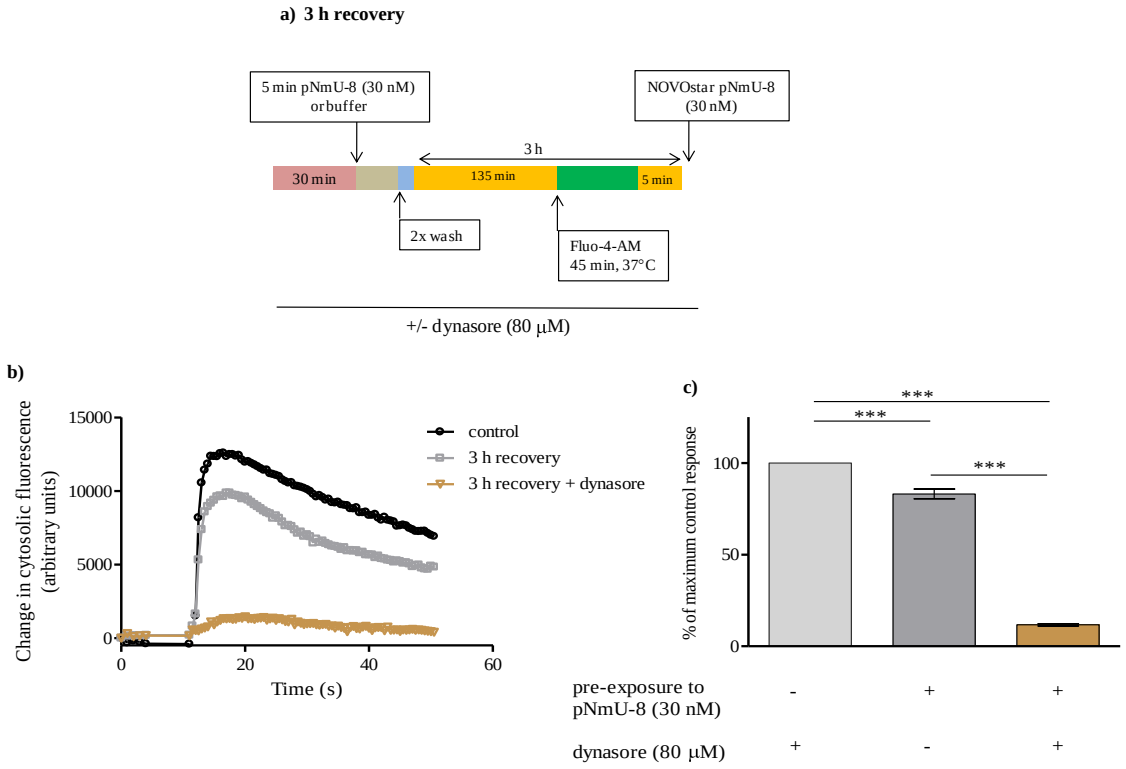

Figure 6.25. Effect of the internalization inhibitor, dynasore, on resensitization of pNmU-8-mediated Ca^{2+} responses in HEK-NMU2. Cells were cultured in 96-well plates for 48-72 h. For the 3 h recovery protocol (a), cells were pre-treated with dynasore (80 µM) or vehicle for 30 min then challenged with pNmU-8 (30 nM) or buffer for 5 min followed by two KHB washes. Cells were loaded with fluo-4-AM during the last 45 min of the recovery period. Cells were then re-challenged with pNmU-8 (30 nM) using a NOVOstar plate reader and changes in cytosolic fluorescence were recorded as an index of changes in $[Ca^{2+}]_i$. Traces (b) are representative of Ca^{2+} responses to pNmU-8 (30 nM) in cells either pre-challenged with buffer (control) followed by 3 h recovery and then challenged with pNmU-8 (30 nM), or pre-challenged with pNmU-8 (30 nM) followed by 3 h recovery period ±dynasore (80 µM) and then challenged with pNmU-8 (30 nM). Data are expressed as a percentage of the maximum response in HEK-NMU2 pre-challenged with buffer only (c). Data are mean ± s.e.m.; n=4 with each experiment performed in duplicate; ***P<0.001, Bonferroni's multiple comparison test following one-way ANOVA.

6.2.11 Effect of high-glucose on resensitization of the pNmU-8- mediated Ca^{2+} response in HEK-NMU2

Given that culture of cells in high-glucose medium was able to increase the rate of recovery of hNmU-25-mediated Ca^{2+} responses following an initial desensitizing exposure to this ligand (Figure 6.15), the effect of culture in high-glucose on the recovery of Ca^{2+} responses to pNmU-8 in HEK-NMU2 was assessed together with the sensitivity of these responses to the ECE-1 inhibitor, SM-19712 (Figure 6.26a). Culturing HEK-NMU2 in high-glucose (25 mM) medium for 48 h resulted in a significantly greater recovery of Ca^{2+} responses to pNmU-8 (30 nM) after 1h (5.5 mM glucose medium, 56 ± 2% (n=3); 25 mM glucose medium, 77 ± 4% (n=3) compared to control responses; Figure 6.26b). In addition, SM-19712 (10 μM) had no significant effect on the recovery of Ca^{2+} responses at 1 h in HEK-NMU2 cultured in high-glucose medium (71 ± 3%, n=3; Figure 6.26b).

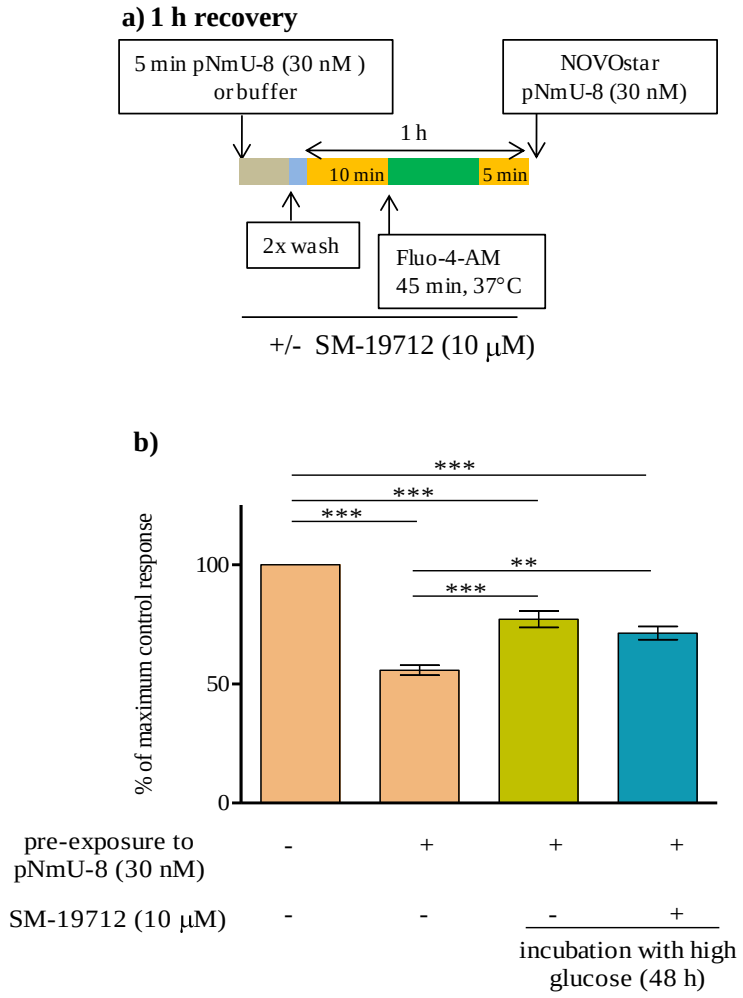

Figure 6.26. Effects of high-glucose and the ECE-1 inhibitor, SM-19712, on resensitization of pNmU-8-mediated Ca^{2+} responses in HEK-NMU2. Cells were cultured in 96-well plates with medium containing normal (5.5 mM) or high (25 mM) glucose for 48 h. For the 1 h recovery protocol (a), cells were pre-treated with SM-19712 (10 μM) or vehicle for 30 min and then challenged with pNmU-8 (30 nM) or buffer for 5 min followed by two KHB washes. Cells were loaded with fluo-4-AM during the last 45 min of the recovery period. Cells were then challenged with pNmU-8 (30 nM) using a NOVOstar plate reader and changes in cytosolic fluorescence were recorded as an index of changes in $[Ca^{2+}]_i$. Data are expressed as a percentage of the maximum response in HEK-NMU2 pre-challenged with buffer only (b). Data are mean ± s.e.m., n=3, each experiment in duplicate; $^{**}P<0.01$, $^{***}P<0.001$, Bonferroni's multiple comparison test following one-way ANOVA.

6.2.12 Time-course of resensitization of hNmU-25-mediated Ca^{2+} responses and the effects of SM-19712 and dynasore in HEK-NMU1

Earlier results (see **Chapter 3**) highlighted the ability of hNmU-25 to evoke increases in $[Ca^{2+}]_i$ in either HEK-NMU1 or -NMU2 in a concentration-dependent, PTX-insensitive manner (Figure 3.1). Furthermore, NMU1- and NMU2-stimulated Ca^{2+} responses to hNmU-25 were not significantly different in this HEK cell background in terms of either magnitude or potency (Figure 3.1). In addition, the data demonstrated that the both NMU1 and NMU2 receptors bind Cy3B-pNmU-8 essentially irreversibly as this ligand could not be displaced by exhaustive washing or addition of unlabeled ligand (Figures 3.8, 3.10, 3.12).

Therefore, a similar protocol to that used above to explore the recovery of Ca^{2+} responses in HEK-NMU2 was applied to study the time-course of the recovery of hNmU-25-mediated Ca^{2+} signalling in HEK-NMU1 in the absence or presence of SM-19712 (Figure 6.27a, b). Exposure of HEK-NMU1 to hNmU-25 (30 nM) for 5 min followed by 5 min recovery resulted in approximately 90% (n=3) loss of the hNmU-25 (30 nM) response in both the absence and presence of SM-19712 (Figure 6.27c). After 1 h recovery, Ca^{2+} responses in vehicle-treated cells demonstrated a recovery to 51 ± 9% (n=3) of the control response, whereas cells treated with SM-19712 exhibited little recovery (13 ± 1% (n=3); Figure 6.27c). Furthermore, whereas in the absence of SM-19712, Ca^{2+} responses gradually recovered over time towards full restoration by 6 h (Figure 6.27c), in the presence of the ECE-1 inhibitor only a 56 ± 2% (n=3) recovery was observed at 6 h after the initial hNmU-25 challenge (Figure 6.27c).

The effect dynasore (80 μM) was assessed in HEK-NMU1 exposed to hNmU-25 (30 nM) for 5 min and then allowed to recover for 3 h (Figure 6.28a). At this recovery time-point, Ca^{2+} responses to the rechallenge with hNmU-25 (30 nM) were markedly suppressed by the presence of dynasore; thus, in the absence of the inhibitor an 80 ± 4% (n=3) recovery compared to the control response was observed, whereas dynasore-treated HEK-NMU1 only recovered to 21 ± 3% (n=3) (Figure 6.28b, c).

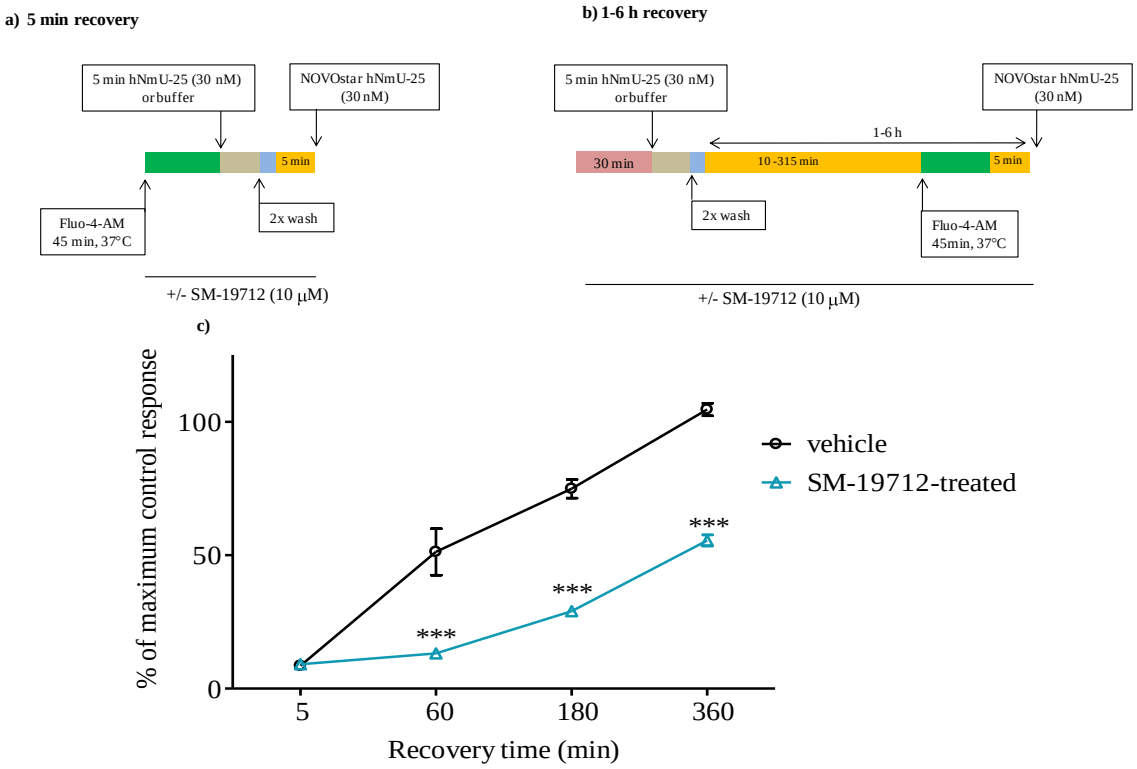

Figure 6.27. Effect of the ECE-1 inhibitor, SM-19712, on the recovery of hNmU-25-mediated Ca^{2+} responses in HEK-NMU1. Cells were cultured in 96-well plates for 48-72 h. SM-19712 (10 µM) was absent or present throughout all subsequent experimental steps. For the 5 min recovery protocol (a), cells were loaded with fluo-4-AM and then challenged with either hNmU-25 (30 nM) or buffer for 5 min followed by two KHB washes and a 5 min recovery period in KHB. For the 1-6 h recovery protocol (b), cells were pre-treated with SM-19712 (10 µM) or vehicle for 30 min then challenged with hNmU-25 (30 nM) or buffer for 5 min followed by two KHB washes. During the last 45 min of the recovery period, cells were loaded with fluo-4-AM. Cells were then challenged with hNmU-25 (30 nM) using a NOVOstar plate reader and changes in cytosolic fluorescence were recorded as an index of changes in $[Ca^{2+}]_i$. Data are expressed as a percentage of the maximum response in HEK-NMU1 pre-challenged with buffer only (c). Data are mean ± s.e.m., n=3 with each experiment in duplicate; $^{***}P<0.001$, Bonferroni's multiple comparison test following two-way ANOVA. Significant differences indicated in (c) are between ± SM-19712 at that time point.

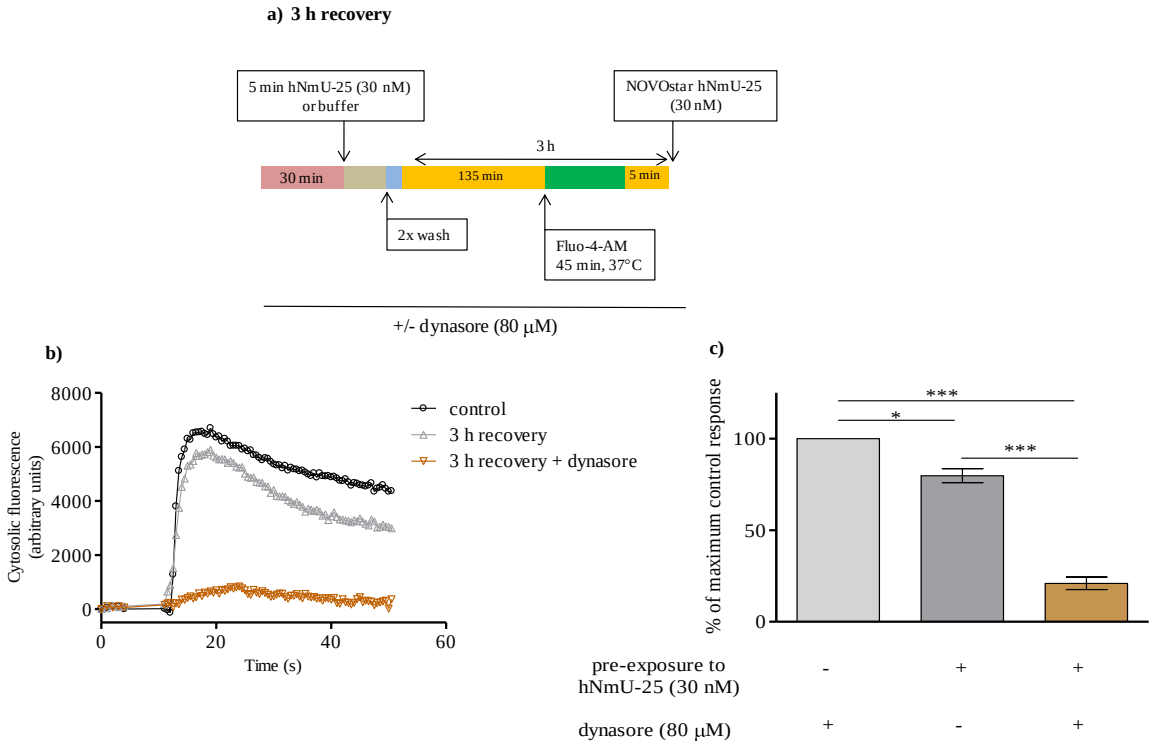

Figure 6.28. Effect of the internalization inhibitor, dynasore, on the recovery of hNmU-25-mediated Ca^{2+} responses in HEK-NMU1. Cells were cultured in 96-well plates for 48-72 h. For the 3 h recovery protocol (a), cells were pre-treated with dynasore (80 µM) or vehicle (0.8% DMSO) for 30 min then challenged with either hNmU-25 (30 nM) or buffer for 5 min followed by two KHB washes. During the recovery period cells were incubated with fluo-4-AM during the last 45 min. Cells were re-challenged with hNmU-25 (30 nM) using a NOVOstar plate reader and changes in cytosolic fluorescence were recorded as an index of changes in $[Ca^{2+}]_i$. Traces (b) are representative of Ca^{2+} responses to hNmU-25 (30 nM) in cells pre-challenged with buffer (control) or hNmU-25 (30 nM) followed by 3 h recovery period ±dynasore and then re-challenge with hNmU-25 (30 nM). Data are expressed as a percentage of the maximum response in HEK-NMU1 pre-challenged with buffer only (c). Data are mean ± s.e.m., n=3 with each experiment performed in duplicate; $^{***}P<0.001$, Bonferroni's multiple comparison test following one-way ANOVA.

6.2.13 Effects of SM-19712 and dynasore on resensitization of the hNmS33-mediated Ca^{2+} response in HEK-NMU1

Ca^{2+} responses to hNmU-25 or hNmS-33 in populations of HEK-NMU1 were essentially identical in terms of both potency and magnitude (Figure 6.29). To study the time-course of recovery of Ca^{2+} responses to hNmS-33 in HEK-NMU1, the protocol corresponding to the recovery of hNmS-33-mediated Ca^{2+} signalling in HEK-NMU2 was used and the effects of the ECE-1 inhibitor SM-19712 were also assessed (Figure 6.30a, b). Treatment of HEK-NMU1 with SM-19712 (10 μM) caused a significant inhibition in the recovery of hNmS-33-mediated Ca^{2+} responses (Figure 6. 30c); thus, after 6 h recoveries were 76 ± 1% (n=3) and 59 ± 1% (n=3) compared to control responses in the absence and presence of SM-19712 respectively (Figure 6.30c). Ca^{2+} responses to hNmS-33 (30 nM) in HEK-NMU1 were also assessed following 5 min initial exposure to hNmS-33 (30 nM) and 6 h recovery in the continued presence or absence of the dynamin-dependent internalization inhibitor, dynasore (80 μM) (Figure 6.30a). Similar to previous findings in HEK-NMU2, the recovery rates for the Ca^{2+} response were significantly inhibited from 74 ± 4% (n=4) to 31 ± 2% (n=4) of the control Ca^{2+} response in the absence and presence of dynasore (Figure 6.31b, c).

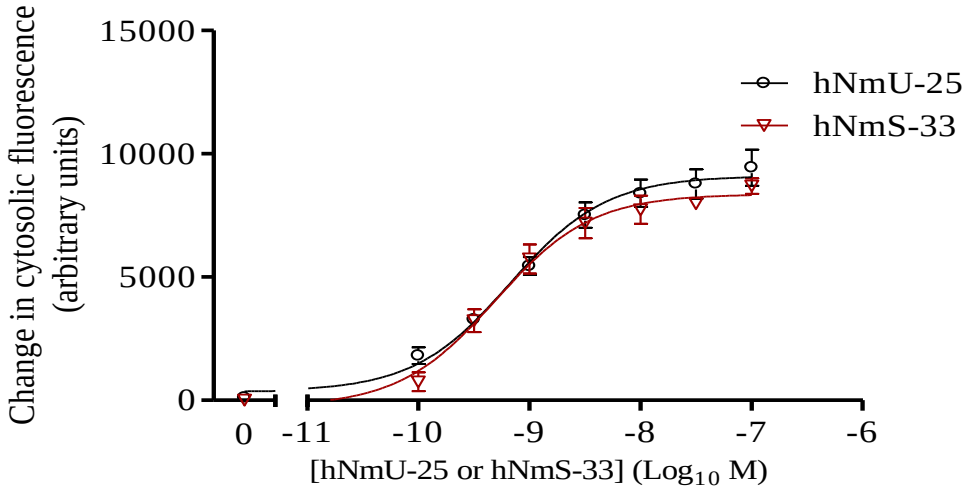

Figure 6.29. Concentration-dependent Ca^{2+} responses to hNmU-25 or hNmS-33 in HEK-NMU1. Cells were cultured in 96-well plates for 48-72 h. Cells were loaded with fluo-4-AM and then challenged with different concentrations of either hNmU-25 (0.1 to 100 nM) or hNmS-33 (0.1 to 100 nM) using a NOVOstar plate reader. Changes in cytosolic fluorescence were monitored as an index of $[Ca^{2+}]_i$. The maximal change in fluorescence at each agonist concentration was used to construct the concentration-response curves for HEK-NMU1. The pEC_{50} values for hNmU-25 and hNmS-33 in HEK-NMU1 cells were 9.18 ± 0.05 and 9.30 ± 0.10, respectively. Data are mean ± s.e.m.; n=4.

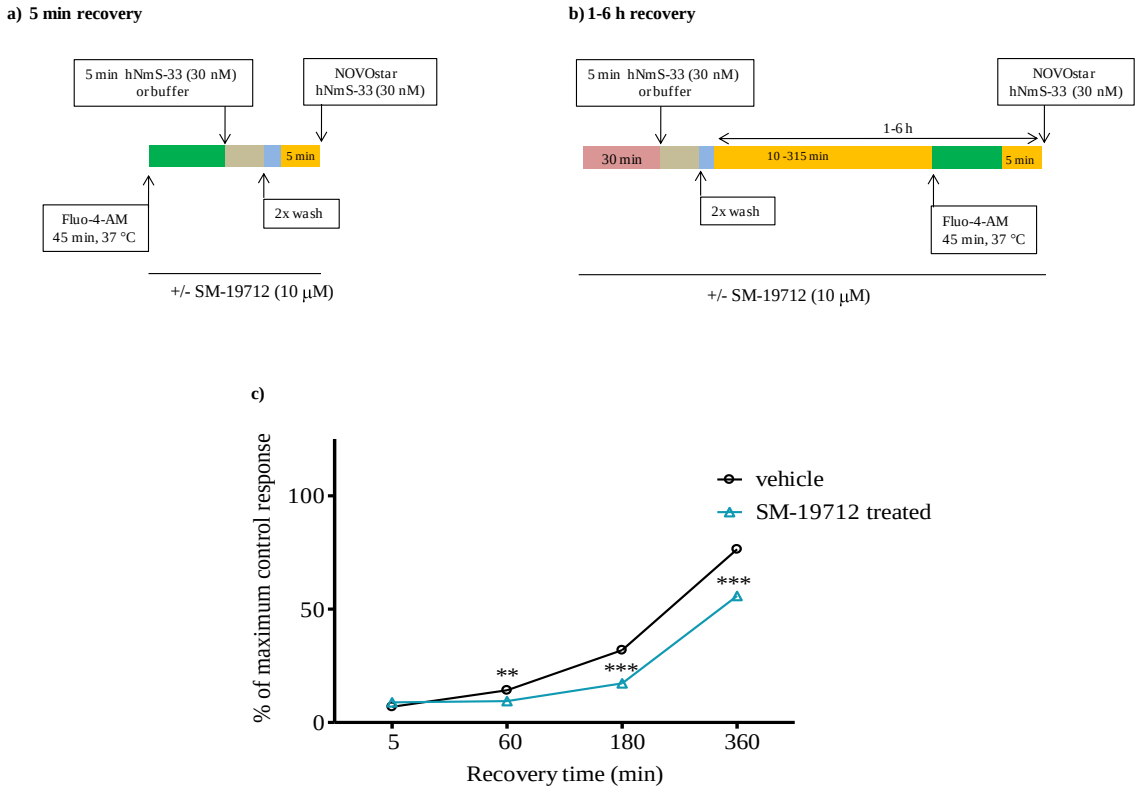

Figure 6.30. Effect of the ECE-1 inhibitor, SM-19712, on the resensitization of hNmS-33-mediated Ca2+ responses in HEK-NMU1. Cells were cultured in 96-well plates for 48-72 h. SM-19712 (10 µM) was absent or present throughout all subsequent experimental steps. For the 5 min recovery protocol (a), cells were loaded with fluo-4-AM. Cells were then challenged with either hNmS-33 (30 nM) or buffer for 5 min followed by two KHB washes and a 5 min recovery period in KHB. For the 1-6 h recovery protocol (b), cells were pre-treated with either SM-19712 (10 µM) or vehicle for 30 min then challenged with either hNmS-33 (30 nM) or buffer for 5 min followed by two KHB washes. During the last 45 min of the recovery period, cells were loaded with fluo-4-AM. Cells were then challenged with hNmS-33 (30 nM) using a NOVOstar plate reader and changes in cytosolic fluorescence were recorded as an index of changes in $[Ca^{2+}]_i$. Data are expressed as a percentage of the maximum response in HEK-NMU1 pre-challenged with buffer only (c). Data are mean ± s.e.m.; n=3 with each experiment performed in duplicate; $^{**}P<0.01$, $^{***}P<0.001$, Bonferroni's multiple comparison test following two-way ANOVA.

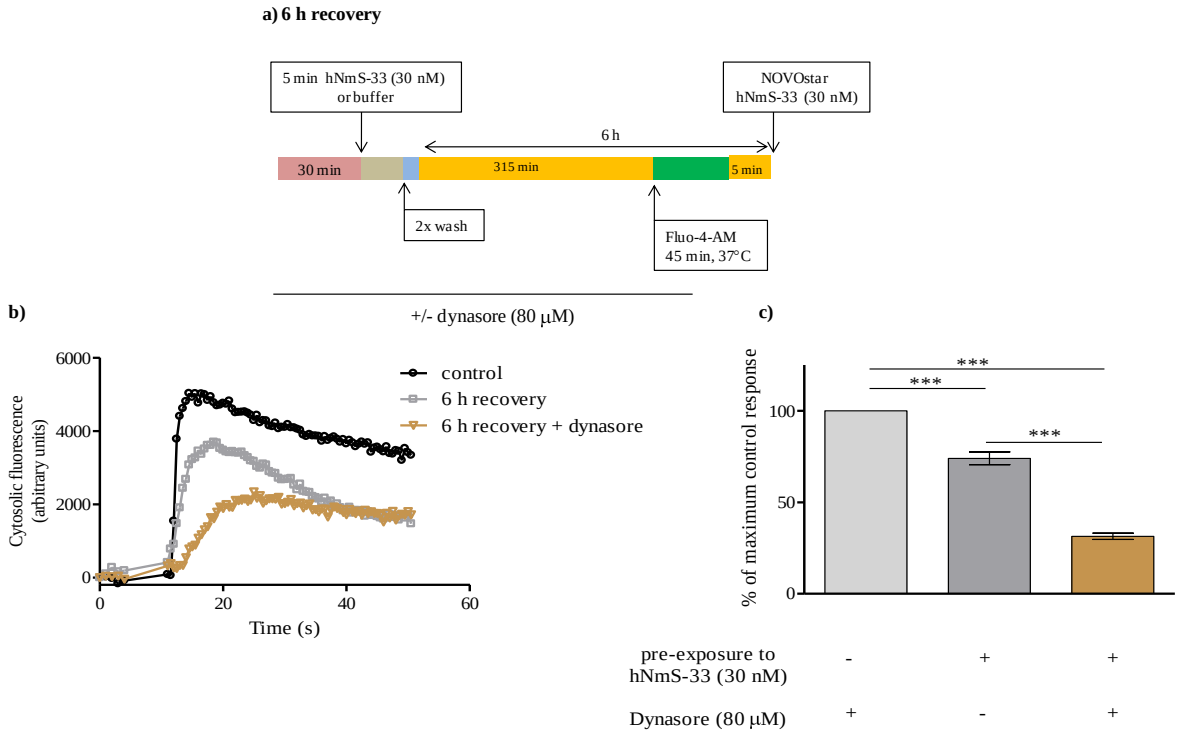

Figure 6.31 Effect of the internalization inhibitor, dynasore, on the recovery of hNmS-33-mediated Ca^{2+} responses in HEK-NMU1. Cells were cultured in 96-well plates for 48-72 h. For the 6 h recovery protocol (a), cells were pre-treated with dynasore (80 µM) or vehicle for 30 min and then challenged with either buffer or hNmS-33 (30 nM) for 5 min followed by two KHB washes. Cells were maintained in serum-free medium during the recovery period. Cells were loaded with fluo-4-AM during the last 45 min of the recovery period and then challenged with hNmS-33 (30 nM) using a NOVOstar plate reader and changes in cytosolic fluorescence were recorded as an index of changes in $[Ca^{2+}]_i$. Traces (b) are representative of Ca^{2+} responses to hNmS-33 (30 nM) in cells pre-challenged with buffer (control) or hNmS-33 (30 nM) followed by 3 h recovery period ±dynasore and re-challenged with hNmS-33 (30 nM). Data are expressed as a percentage of the maximum response in HEK-NMU1 pre-challenged with buffer only (c). Data are mean ± s.e.m., n=4, each experiment performed in duplicate; ***P<0.001, Bonferroni's multiple comparison test following one-way ANOVA.

6.3 Discussion

6.3.1 Characteristics of NMU2 desensitization

In addition to the diversity of regulation of GPCR signalling, pseudo-irreversible binding of NmU to NMUs (see **Chapter 3**) adds a further complication to understanding the regulation of NMU-mediated signalling. The use of the brief acid wash, post-agonist exposure, allowed the regulation of NMU2 desensitization to be assessed without the additional complication of the pseudo-irreversibility of NmU-NMU binding at least to plasma membrane-located receptors. In contrast to the recovery of hNmU-25-mediated Ca^{2+} responses observed in single-cell Ca^{2+} assays following 1 min pre-exposure to hNmU-25 (30 nM), which was approximately 56% (see **Chapter 3, Figure 3.17**), Ca^{2+} responses to hNmU-25 in populations of cells using a NOVOstar plate reader showed almost full recovery (~ 91%). Enhancement of the recovery in the latter experiments may be due to a difference in washing technique, where in the confocal imaging experiments, the pH 2.0 brief wash was applied via a perfusion system, which may lead to mixing with pH 7.4 buffer in the chamber and a reduction in the efficiency of the wash. Thus, there may have been a reduced ability to remove ligand compared to the manual application of the brief acid wash protocol in the current study. Under these conditions, 5 min exposure to hNmU-25 (30 nM) was sufficient to cause an apparently maximal NMU2 desensitization with the Ca^{2+} response to hNmU-25 re-challenge being reduced by 50-60%, which was not significantly different from 30 min pre-exposure to the same concentration of hNmU-25. As with desensitization of other GPCRs, desensitization of NMU2 may include GRK-dependent phosphorylation, β-arrestin binding, dynamin/CCP-dependent or -independent endocytosis, translocation to endosomes followed by either receptor recycling back to the cell-surface (resensitization) or lysosomal degradation (downregulation). In the latter case, new receptor would need to be synthesized to allow full resensitization. Although the extent of desensitization was similar between 5 min and 30 min exposure, the mechanism of desensitization/resensitization or the recovery time might be different, since several GPCRs including β_2-adrenoceptors and CLR/RAMP1 resensitize via recycling mechanisms after short exposure to agonist while prolonged

exposure directs these receptors to lysosomal degradation and down-regulation (Cottrell *et al.*, 2007; Marchese *et al.*, 2008).

Regulation of GPCRs is essential in physiological systems to limit persistent signalling (desensitization) and to enhance signalling when required. Receptor trafficking is critical for receptor resensitization (through recycling) and the insertion of newly synthesized receptors into the plasma membrane (Marchese *et al.*, 2008). The time required for receptors to be fully resensitized differs among different GPCRs and ranges from minutes, as for the β_2-adrenoceptor, to hours for some receptors including and V_2 vasopressin receptor. This extended resensitization time is a consequence of a variety of factors, including the affinity for β-arrestin binding (Oakley *et al.*, 1999; Pierce *et al.*, 2002). For example, for class A GPCRs, which bind to β-arrestin-2 more favourably than β-arrestin-1 but still with low affinity, the receptor-β-arrestin complex dissociates rapidly at the cell-surface or directly after internalization resulting in fast recycling/resensitization (Moore *et al.*, 2007). Class B GPCRs on the other hand bind with high affinity to either β-arrestin-1 or β-arrestin-2 which internalize together with the receptor to endosomes and dissociate at a slow rate, delaying recycling and resensitization (Moore *et al.*, 2007).

Data presented in this Chapter show that, in the absence of the acid wash, the apparent resensitization of the Ca^{2+} response following 5 min pre-exposure to hNmU-25 (30 nM) in NMU2 expressing cells required at least 6 h. With the inclusion of an acid wash, resensitization was substantially hastened, perhaps by as much as 5-10 fold. For example, resensitization of Ca^{2+} responses following 1 h recovery was 75% in cells subjected to a brief acid wash in contrast to ≤10% recovery in HEK-NMU2 exposed only to normal buffer washing. Furthermore, in the presence of hNmU-25 bound to cell-surface NMU2 (no acid wash), a more pronounced recovery (60%) was observed only after 2-3 h, while under conditions where hNmU-25 was stripped off from the cell-surface receptors by brief acid wash, the majority of the recovery occurred within 60 min. These data suggest full desensitization (without acid wash) or partial desensitization of NMU2 (after stripping ligand by brief acid wash) can be achieved without the need for receptor internalization, since removal of bound hNmU-25 from cell-surface NMU2 after 5 min pre-exposure followed by 5 min recovery (10 min from addition of agonist) resulted in

restoration of ~35% of the original Ca^{2+} response (i.e. active receptors available at the cell-surface).

Although full desensitization of NMU-mediated signalling was still apparent after 5 min recovery following a buffer wash, the 35% of the response attained by stripping off ligand by acid wash indicates that some NMU2 was still available at the cell-surface (not internalized). This is supported by earlier work in the lab, where incubation of NMUs expressing cells with [^{125}I]hNmU-25 at 37°C resulted in instant loss of ligand from the cell-surface and maximum internalization (50-60%) of radiolabelled hNmU-25 was seen after 10 min and continued unchanged up to 60 min (Brighton, 2005). It has also been shown that full desensitization of substance P-mediated Ca^{2+} responses following stimulation of HEK293 cells expressing the NK_1 receptor occurs with only 25% of NK_1 receptors internalized (Bennett *et al.*, 2002). This also suggests either that partial resensitization is due to signalling mediated by partially desensitized receptors still at the cell-surface, or that some cell-surface receptors are resensitized possibly independently of internalization. The possibility that the desensitized response could be driven by phosphorylated, partially desensitized receptors that have been desensitized by ligand binding, but had not had time to internalize, recycle and resensitize is supported by previous reports (Willars *et al.*, 1995; Wojcikiewicz *et al.*, 1994)**.**

Although previous evidence supports the idea that the apparently resensitized response could be through partially desensitized receptors, there also exists the possibility that following ligand removal by acid washing, there is resensitization of a sufficient proportion of receptors to mediate a reduced response. This could theoretically occur through dephosphorylation and resensitization of NMU2 at the cell-surface without the requirement of internalization-dependent resensitization, or be dependent on the fast recycling/resensitization of a small distinct pool of receptors. For instance, full resensitization of the NK_1 receptor was achieved before all internalized receptors trafficked back to the cell-surface and this resensitization was inhibited by protein phosphatase inhibitors (Bennett *et al.*, 2002; Murphy *et al.*, 2011). Alternatively, the rest of NMU2 on the cell-surface may internalize slowly. Further studies are needed to explore these possibilities.

The slow resensitization of NMU2 in the absence of an acid wash is a typical characteristic of class B GPCRs which exhibit stable associations with β-arrestins (Oakley *et al.*, 2000). For instance, Ca^{2+} responses mediated via the NK1 receptor required approximately 3 h to fully recover following challenge with a maximum concentration of substance P, while the CLR/RAMP1 needed 4-6 h for full resensitization of CGRP-mediated Ca^{2+} signalling (Padilla *et al.*, 2007; Schmidlin *et al.*, 2001). This suggests that NMU2 might similarly behave as class B GPCR. Further investigation is needed to ask whether NMU2 has high-affinity for β-arrestin-1/-2 as other class B GPCRs (Moore *et al.*, 2007). Certainly the high-affinity binding of ligand and the pseudo-irreversibility of its dissociation would be consistent with the prolonged existence of a ligand/receptor/β-arrestin complex, which would then require time to dissociate and recycle.

6.3.2 Pharmacological interrogation of the role of internalization in NMU2 resensitization

To ask whether internalization is essential for NMU2 resensitization, a number of approaches were used to interfere pharmacologically with NMU2 internalization. Several studies have demonstrated the ability of concanavalin A, high sucrose, phenylarsine oxide and monodansylcadaverine to block internalization of a number of GPCRs in HEK293 cells (Gray *et al.*, 2001; Kim *et al.*, 2004; Law *et al.*, 2000). However, since the present study focused on functional Ca^{2+} assays to assess desensitization/resensitization, it was initially essential to examine the effects of each of these agents on control responses in naïve cells to ensure some specificity of action. All of these agents proved to be unsatisfactory as they interfered with this assay readout (NmU-stimulated increases in $[Ca^{2+}]_i$), most likely independently of any effect on receptor trafficking. Furthermore, prolonged, 3 h incubation with these agents resulted in a total disappearance of the initial hNmU-25-mediated Ca^{2+} response. The novel inhibitor of the GTPase activity of dynamin, dynasore, has also been used successfully to assess dynamin-dependent internalization of several GPCRs in HEK293 cells (Garcia Lopez *et al.*, 2009; Lalo *et al.*, 2010; Macia *et al.*, 2006; Magnan *et al.*, 2010). In contrast with other agents, Ca^{2+} responses in agonist-naïve HEK-NMU2 were not compromised by inclusion of dynasore.

Further, dynasore has been recently used to investigate resensitization of Ca^{2+} responses of purinoceptors ($P2Y_1$ and $P2Y_{12}$) without altering initial responses (Mundell *et al.*, 2008). The highly significant inhibitory effect of dynasore on the recovery of response to hNmU-25 suggests internalization of the hNmU-25-NMU2 complex occurs via a dynamin-dependent mechanism and that the internalization process is a critical component of the resensitization mechanism.

6.3.3 Resensitization of Ca^{2+} responses by NMU2 is dependent on recycling rather than de novo synthesis of new receptors

Although apparent full resensitization, observed following 6 h recovery, is achieved at least with respect to the Ca^{2+} response, it is not clear if NMU2 is resensitized via recycling to the cell-surface, or whether the NmU-NMU2 complex is targeted for lysosomal degradation and there is a requirement for significant *de novo* synthesis of NMU2. Cycloheximide, has been shown to block protein synthesis and has also been used to assess Ca^{2+} resensitization and/or the trafficking pathway of many GPCRs in HEK293 cells (Bohm *et al.*, 1996; Cottrell *et al.*, 2007; Gray *et al.*, 2001; Lalo *et al.*, 2010; Ubl *et al.*, 2000). Cycloheximide was used in the present study to assess the role of *de novo* receptor synthesis on the resensitization process. Inclusion of cycloheximide at a concentration titrated to inhibit substantially whole-cell *de novo* protein synthesis, did not affect control Ca^{2+} responses in naïve cells. Furthermore, treatment with cycloheximide had a small and statistically insignificant effect on NMU2 resensitization and no effect when ligand was removed from NMU2 by a brief acid wash. These data suggest that NMU2 is likely to be substantially resensitized/recycled, at least in the HEK293 cell background. It should be noted here that the observed *de novo* protein synthesis-independent resensitization in the present study applies to transient, 5 min pre-exposure to the ligand. Prolonged exposure of receptors to ligand can redirect receptors to lysosomal degradation rather than endosomal recycling. For example, rapidly recycling β_2-adrenoceptors or slowly recycling CLR/RAMP1 are redirected to lysosomes for degradation (down-regulation) following prolonged exposure to agonist (Cottrell *et al.*, 2007; Marchese *et al.*, 2008).

Endosomal acidification is thought to be a key driver in inducing conformational changes that promote ligand-receptor dissociation. Endosomal pH ranges from 6.0-6.8 (in early endosomes) to 4.8-6.0 (in late endosomes) and is highly regulated by the vacuolar H^+-ATPase-pump (Huotari *et al.*, 2011). Monensin, a monovalent ionophore, bafilomycin A, a vacuolar H^+-ATPase inhibitor, and weak bases, such as NH_4Cl, have been widely used to investigate endosomal-mediated resensitization/recycling of GPCRs since interrupting endosomal acidification potentially disrupts endosomal function and may disrupt receptor-ligand dissociation and/or receptor dephosphorylation (Bennett *et al.*, 2002; Krueger *et al.*, 1997; Mollenhauer *et al.*, 1990; Mundell *et al.*, 2008; Padilla *et al.*, 2007). Whereas monensin had no effect on the initial responses in naïve cells, it essentially prevented NMU2 resensitization. Furthermore, monensin-treated, acid-washed cells showed a significant decrease in the rate of resensitization, but with greater recovery than seen for monensin-treated cells washed with normal buffer. Thus, NMU2 resensitization is dependent on endosomal acidification. This is consistent with studies on other receptors, where resensitization of NK_1, $P2Y_1$ and $P2Y_{12}$ receptors was inhibited by monensin ((Bennett *et al.*, 2002; Mundell *et al.*, 2008). The precise mechanisms by which the inhibition of endosomal acidification inhibits NMU2 resensitization are unclear. One possibility is that the reduced acidification interferes with the rate of hNmU-25-NMU2 dissociation as such acidification is often thought to be a key determinant of ligand-receptor dissociation (Mellman *et al.*, 1986). It is also possible that reduced acidification reduces NMU2 dephosphorylation or that endosomal trafficking is more generally impaired by monensin (Krueger *et al.*, 1997; Mollenhauer *et al.*, 1990). For ligands which bind with very high-affinity, resulting in pseudo-irreversible binding, it is also unclear if endosomal acidity (pH 4.8-6.0) is sufficient to terminate ligand-receptor interaction. Indeed, the present work (see **Chapter 3**) has already demonstrated the need of a pH much lower than endosomal acidity to dissociate the ligand-receptor complex. Since these data show that resensitization of NMU2 is mediated via an internalization/recycling pathway (endosomal trafficking), either prolonged exposure of the ligand-receptor complex within acidified endosomes, or other unidentified factors present in the intracellular compartments may be needed to free ligand from receptor.

6.3.4 Potential role of proteases in regulation NMU2 signalling

Accumulating evidence implicates ECE-1 in the processing of a variety of peptide hormones. ECE-1 converts big endothelin to bioactive endothelin-1 at physiological pH. However, ECE-1 has substrates other than big endothelin, especially at acidic pH (Bunnett *et al.*, 2010; Fahnoe *et al.*, 2000; Johnson *et al.*, 1999; Roosterman *et al.*, 2007). Thus, the next question was to ask whether pharmacological inhibition of this peptidase could affect any aspect of NMU turnover. Inclusion of SM-19712 substantially delayed NMU2 resensitization by approximately 40% after 6 h recovery. The high selectivity of SM-19712 toward ECE-1 among other peptidases, even at supramaximal concentrations (Umekawa *et al.*, 2000) and its lack of effect on the resensitization of Ca^{2+} responses to a non-peptide, small molecule ligand (carbachol at the M_3 muscarinic receptor) suggests a specific involvement of ECE-1 in resensitization of hNmU-25-mediated Ca^{2+} responses.

Interestingly, a previous study showed that SM-19712 did not affect resensitization of Ca^{2+} responses to other peptides, such as angiotensin II, which exerts its effects via a class B GPCR, the AT_{1A} receptor, highlighting that the ability of ECE-1 to enhance ligand dissociation/degradation and recycling is not general across all class B GPCRs (Padilla *et al.*, 2007). It has also been shown that ECE-1 degrades its substrates including substance P, CGRP and somatostatin-14 at acidic pH, either bound to its cognate receptor or not (Padilla *et al.*, 2007; Roosterman *et al.*, 2007; Roosterman *et al.*, 2008). Although we know that ECE-1 can degrade neuropeptide ligands, we do not know whether it degrades free or receptor-bound ligand. However, the effects on the recovery of Ca^{2+} responses seen here and in other reports in the presence of ECE-1 inhibition may suggest an effect on bound ligand.

Previous work has demonstrated that hNmU-25 activates ERK1/2 via a $G\alpha_{q/11}$-PTX-insensitive pathway (Brighton *et al.*, 2004a). The present work showed that stimulation of HEK-NMU2 results in a concentration-dependent activation of ERK1/2. Furthermore, stimulation of NMU2 by hNmU-25 resulted in rapid and sustained ERK1/2 activation, with a peak observed at 5 min, followed by a decline up to 60 min. These data suggest that at least the rapid activation of ERK via NMU2 occurred at the cell-surface. $G\alpha_{q/11}$ can activate the MAP kinase pathway by several routes. For example, activation of PKC by DAG as well as Ca^{2+} (see **Introduction, Section 1.4.2**). This results in a direct activation

of the Raf1-MEK-ERK1/2 signalling cascade (Marinissen *et al.*, 2001). Alternatively, $G\alpha_{q/11}$-induced $[Ca^{2+}]_i$ increases may promote activation of Ras guanine nucleotide-releasing factor (Ras-GRF) to activate ERK via a Ras-Raf1-MEK-ERK1/2 pathway, or via Sos-Ras-Raf1-MEK-ERK1/2 (Marinissen *et al.*, 2001). GPCRs can also activate ERK1/2 signalling through a G protein-independent pathway. Thus, as the ligand-receptor-β-arrestin complex forms at the cell-surface, bound β-arrestin-2 recruits proteins for assembling an active MAP kinase signalling complex (DeFea *et al.*, 2000a; Pierce *et al.*, 2002). Receptor bound β-arrestin (β-arrestin1) may induce ERK1/2 activation via interaction with c-Src leading to ERK activation as seen with β_2-adrenoceptors (Pierce *et al.*, 2002). Alternatively, activation of ERK1/2 may occur by direct interaction of β-arrestin with the Raf-MEK-ERK complex (Pierce *et al.*, 2002). G protein-dependent activation of ERK can target phospho-ERK to the nucleus and this is involved in a wide range of actions including transcription, proliferation, differentiation, apoptosis, cell survival, angiogenesis and cancer (Marinissen *et al.*, 2001). Although it has been well documented for several GPCRs that the ligand-receptor-β-arrestin-MAPK complex, when internalized to endosomes can continue ERK1/2 signalling, this signalling tends to be restricted to the cytosol and indeed nuclear signalling of ERK1/2 has been observed to be inhibited (DeFea *et al.*, 2000b; Pierce *et al.*, 2002). Regulation of ERK signalling between cytosol and nucleus seems to play an important and specific role in physiological systems. For example, ERK1/2 cytosolic signalling inhibited agonist-induced proliferation while nuclear translocation of ERK is involved in cell differentiation (Kolch, 2005). G protein-independent activation of ERK accounts for sustained ERK1/2 activation of class B GPCRs, such as the NK_1 receptor, where inhibition of ECE-1 prolongs ERK1/2 activation (Cottrell *et al.*, 2009). In the present study, inhibition of ECE-1 by SM-19712 prolonged ERK1/2 activation approximately two fold and extended ERK1/2 activation for at least a further hour. Thus, ECE-1 may influence not only the resensitization profile of NMU2, but also may directly impact on ERK signalling and its consequences.

The majority of evidence supporting a role for ECE-1 has come from studies in HEK293 cells that possess endogenous ECE-1 activity (Padilla *et al.*, 2007 229; Roosterman *et al.*, 2007 229; Roosterman *et al.*, 2008 552). ECE-1 has four different isoenzymes, a-d, which share an identical *C*-terminus that contains the catalytic activity

(Muller *et al.*, 2003). All ECE-1 isoenzymes are found in HEK293 cells and are expressed both at the cell-surface and in early and large recycling endosomes. However, ECE-1a and c are mainly expressed at the cell membrane, while ECE-1 b and d isoenzymes are primarily localized at the endosomal membrane (Padilla *et al.*, 2007; Roosterman *et al.*, 2007). Despite the fact that ECE-1c is mainly localized at the plasma membrane, a previous study showed that the greatest resensitization of substance P-mediated Ca^{2+} responses and substance P degradation at endosomal pH was observed in cells transfected with ECE-1c (Roosterman *et al.*, 2007). Given that both mRNA and protein levels of ECE-1 are reportedly up-regulated by incubation of cells in high glucose in a time- and concentration-dependent manner (Keynan *et al.*, 2004; Khamaisi *et al.*, 2009), the current study explored the impact of high glucose on the resensitization of NmU-mediated signalling. The increase in ECE-1 expression in response to high glucose may be due to up-regulation of PKCδ (Keynan *et al.*, 2004; Khamaisi *et al.*, 2009). In addition to increased expression, incubation of cells expressing ECE-1 in high glucose (25 mM) promotes ECE-1 translocation from the cell-surface to the cytoplasm and these actions are mediated via PKC-dependent phosphorylation (Jafri *et al.*, 2006; Keynan *et al.*, 2004; Khamaisi *et al.*, 2009). The enhancement in the resensitization of NmU-25-mediated Ca^{2+} responses following incubation of HEK-NMU2 cells with high glucose (25 mM) for 24-72 h was SM-19712-sensitive, consistent with a high glucose-dependent increase in ECE-1 expression. Additionally, the ability of PKC inhibition to block the effects of high glucose is consistent with a role of PKC in regulating ECE-1 expression. It is quite difficult to interpret these findings, at least in the current study, due to the fact that high glucose and/or PKC inhibitor treatment is likely to have diverse effects at the cellular level. However, it has been shown that incubation of the cells for 72 h with high glucose results in a 20 fold increase in the expression of ECE-1 protein compared to 2 fold increase after 24 h incubation, which may explain the enhancement of resensitization of hNmU-25-mediated Ca^{2+} signalling (Keynan *et al.*, 2004; Khamaisi *et al.*, 2009).

These current data, together with the high specificity of SM-19712 (Umekawa *et al.*, 2000) and broad substrate specificity of ECE-1 (Johnson *et al.*, 1999), suggest the involvement of ECE-1 in the resensitization of NMU2. Further studies are needed to confirm a role for ECE-1 in NMU2 resensitization, including co-localization of hNmU-

25/ECE-1 and the susceptibility of hNmU-25 to cleavage by ECE-1 at either physiological or endosomal pH.

6.3.5 Resensitization of NMU2 following activation by different NmU versions or NmS

The peptides hNmU-25 and hNmS-33 are equipotent, full agonists at NMU2. However, the recoveries from exposure to each agonist follow distinct time-courses. Thus, recovery of Ca^{2+} responses in HEK-NMU2 desensitized with hNmS-33 was substantially slower than cells desensitized with hNmU-25. Full resensitization was observed for hNmU-25-treated cells in contrast to only 68% recovery in hNmS-33-treated cells after 6 h recovery. The delayed resensitization of Ca^{2+} responses to hNmS-33 is consistent with the *in vivo* activity of the peptide, as intracerebroventricular (ICV) injection of NmS results in a more prolonged anorexigenic effect than rNmU-23 in rats (Ida *et al.*, 2005). In contrast to what has been demonstrated here for hNmU-25-NMU2 recovery, SM-19712 had essentially no effect on the time-course of recovery following hNmS-33 challenge of HEK-NMU2. These experiments were completed in parallel and the reason behind the lack of the inhibitory effect of SM-19712 on hNmS-33-stimulated Ca^{2+} responses is as yet unclear. However, data here suggest that ECE-1 differentially modulates hNmU-25-NMU2 and hNmS-33-NMU2 complexes. Whether this is due to the substrate specificity of ECE-1 or other factors is unknown. In contrast, both hNmU-25-NMU2 and hNmS-33-NMU2 complexes are trafficked in a dynamin-dependent manner.

In the light of these findings, the study was extended to different NMU agonists. Previous functional contractile responses of different NmU versions highlighted the importance of the extension of the *N*-terminus of the ligand on the potency, maximum responses and duration of responses. For example, intravenous administration of NmU-25 resulted in more potent mesenteric vasoconstriction than NmU-8 (Gardiner *et al.*, 1990). Further, pNmU-25 induces a longer hypertensive effect than pNmU-8 in the rat and the contractile effect was three times as potent as pNmU-8 on rat uterus (Minamino *et al.*, 1985a). Based on these reports and the fact that pNmU-8 is the shortest bioactive version of NmU, pNmU-8 was chosen for further studies. This peptide is essentially equipotent to

hNmU-25 and a full agonist at NMU2. Resensitization following exposure to pNmU-8 occurred significantly more rapidly than was seen for hNmU-25, especially at 1 h and 3 h recovery time-points, and again this time-course was unaffected by SM-19712. Interestingly, incubation of HEK-NMU2 in high glucose medium for 48 h increased the rate of recovery of the Ca^{2+} responses in pNmU-8-desensitized cells, but again this was not SM-19712-sensitive. This enhancement of pNmU-8 resensitization independently of ECE-1 activity supports the idea that the high glucose environment may cause other intracellular changes in addition to ECE-1 up-regulation which may participate in resensitization of NMU2.

6.3.6 Are there any differences in the resensitization profiles of NMU1 and NMU2?

NMU1 and NMU2 share 51% homology mainly in the transmembrane domains (Howard *et al.*, 2000). However, variations can be observed at the third intracellular (i3) loop, where NMU2 is shorter than NMU1 by nine amino acids. Additionally, the NMU2 *C*-terminus consists of 88 amino acids, compared to the 70 amino acid *C*-terminus of NMU1. Unlike NMU1, the *C*-terminus of NMU2 contains a specific sequence, (-YQSF) that is considered as a tyrosine motif (Tyr-X-X-Ø, where X is any amino acid, and Ø is a bulky hydrophobic residue) that reportedly binds directly to the clathrin-coated pit (CCP) adaptor protein AP-2. This allows subsequent CCP-mediated GPCR internalization and trafficking (Marchese *et al.*, 2008). Because of these differences in receptor structure some of the consequences of pseudo-irreversible ligand binding were also explored in HEK-NMU1. The early time-course of recovery of responsiveness (e.g. at 60 min) following hNmU-25 exposure appeared somewhat more rapid for NMU1 versus NMU2. For instance, 10-20% of hNmU-25-mediated Ca^{2+} response resensitized in HEK-NMU2 after 1 h recovery compared to ~50% resensitization of the Ca^{2+} response observed in HEK-NMU1. However, both receptor subtypes required 6 h for full recovery. Pre-addition of SM-19712 had a marked inhibitory effect on NMU1 recovery suggesting that ECE-1 processing at the NmU-NMU1 complex is also important. Although the effect of ECE-1 inhibition on processing the hNmS-33-NMU1 complex was less marked, the

inhibitor did have a significant effect. These data suggest that there may be NMU1 versus NMU2 regulatory differences.

Unfortunately, a failure to find a model in which responses to native NMUs could be measured makes it more difficult to generalize these findings. Further studies are needed to characterize the pharmacological effects of different NmU or NmS peptides on NMUs to support these findings as well as to dissect out any differences in NMU1 and NMU2 regulation.

Chapter 7
Discussion

7.1 Summary

The current work has shown that both NmU and NmS are equipotent in causing Ca^{2+} mobilization via a $G\alpha_{q/11}$-dependent, PTX-insensitive pathway, and inhibition of adenylyl cyclase activity through a $G\alpha_{i/o}$-dependent, PTX-sensitive pathway in HEK293 cells recombinantly expressing either human NMU1 or NMU2. Pseudo-irreversible binding of NmU to NMU1 and NMU2 was demonstrated by the failure to remove bound Cy3B-pNmU-8 and by the lack of Ca^{2+} signalling on reapplication of hNmU-25 following attempts to remove an initial challenge by extended washing with physiological buffer. Application of a range of acidic pH solutions also failed to remove ligand until the solution pH had been reduced to pH 2.0. Brief exposure (~20 s) to pH 2.0 was sufficient to remove ligand without a detrimental effect on ligand-stimulated Ca^{2+} responses or cell viability.

Exposure to maximal concentration of hNmU-25 (30 nM) for 5 min was sufficient to cause maximum desensitization of hNmU-25-mediated Ca^{2+} responses to repetitive applications of hNmU-25. The desensitized hNmU-25-mediated Ca^{2+} responses in HEK-NMU1 and HEK-NMU2 required approximately 6 h to fully resensitize compared to the $\leq$2 h necessary to observe full recovery on removal of the ligand by brief acid washing. NMU1 showed a faster rate of resensitization during the first hour compared to NMU2. The resensitization times of both NMU1 and NMU2 were influenced by the length of the *N*-terminus of the neuropeptide ligand. For instance, desensitized Ca^{2+} responses following hNmS-33 challenge for both receptors did not fully recover by 6 h, while a similar extent of desensitization caused by pNmU-8 required only 3 h to achieve an almost full recovery.

Resensitization of hNmU-25-, hNmS-33- and pNmU-8-mediated Ca^{2+} responses in both HEK-NMU1 and -NMU2 was markedly slowed by an inhibitor of the dynamin-dependent internalization pathway. In HEK-NMU2, resensitization of hNmU-25-

mediated Ca^{2+} responses was dramatically inhibited by interfering with the recycling pathway, but was not affected by blockade of *de novo* protein synthesis.

Inhibition of ECE-1 activity in both NMU1- and NMU2-expressing cell-lines significantly inhibited resensitization of Ca^{2+} responses after desensitizing challenge with hNmU-25, but not pNmU-8. On the other hand, recovery of hNmS-33-mediated Ca^{2+} responses was significantly inhibited in HEK-NMU1 following inhibition of ECE-1, but not in HEK-NMU2. Activation of ERK1/2 signalling in HEK-NMU2 by hNmU-25 was significantly prolonged by ECE-1 inhibition. Additionally, prolonged exposure of HEK-NMU2 to a high-glucose medium significantly enhanced the recovery rate of Ca^{2+} responses to hNmU-25 and this enhancement was attenuated by either ECE-1 or protein kinase C inhibition. Interestingly, chronic exposure to high-glucose medium also hastened the recovery of desensitized Ca^{2+} responses by pNmU-8, but in this case inhibition of ECE-1 was without effect.

7.2 Discussion and future work

The present study has demonstrated coupling of NMU1 and NMU2 to both $G\alpha_{q/11}$ and $G\alpha_{i/o}$. In addition to the ability of hNmS-33 to evoke $[Ca^{2+}]_i$ mobilization in both NMU1- and NMU2-expressing cells, which is in agreement with previous reports (Aiyar *et al.*, 2004; Brighton *et al.*, 2004a; Mori *et al.*, 2005; Raddatz *et al.*, 2000). The current study showed for the first time that hNmS-33 can also induce coupling of NMU1 and NMU2 to $G\alpha_{i/o}$-linked signalling pathways.

Although coupling of NMU1 and NMU2 to $G\alpha_{i/o}$ is consistent with previous reports from this laboratory (Brighton *et al.*, 2004a; Brighton *et al.*, 2008), there is a debate as to whether activation of NMU1 and/or NMU2 can inhibit adenylyl cyclase activity (Aiyar *et al.*, 2004; Hosoya *et al.*, 2000; Hsu *et al.*, 2007; Szekeres *et al.*, 2000). In studies with recombinant receptors, coupling may be cell-type-dependent and/or influenced by expression levels, as a high expression level can promote promiscuous G protein coupling, especially to $G\alpha_i$ (Hermans, 2003). However, in the present study rNmU-23 mediated a PTX-sensitive inhibition of adenylyl cyclase activity in a concentration-dependent manner in rat cardiac myocytes, suggesting that NMU coupling to $G\alpha_{i/o}$ can

occur in physiological systems and is consistent with the fact that NMU(s) were shown to couple to $G\alpha_{q/11}$ as well as $G\alpha_{i/o}$ in cultured colonic myocytes (Brighton *et al.*, 2008). This is also consistent with other GPCRs, either recombinantly or natively expressed, including M_1 and M_3 muscarinic, A_3 adenosine and endothelin ET_A receptors (Hermans, 2003). However, it is unclear if coupling of NMUs to one or more Gα subunit in physiological systems is tissue-specific or receptor subtype-specific, as NMU coupling to $G\alpha_{q/11}$ was not detected in cardiac myocytes. A lack of $G\alpha_{q/11}$ coupling may be due to the fact that this pathway is not commonly active in these cells (Woodcock *et al.*, 2005). Thus, the availability of different physiological systems, naturally expressing specific NMU subtypes, should hopefully provide answers to these questions.

Pseudo-irreversible binding of NmU to NMUs, as demonstrated in the current study, is consistent with previous work in either recombinant or native cells naturally expressing NMUs (Brighton *et al.*, 2004a; Brighton *et al.*, 2008). However, the rapid and full reversibility, and lack of any sign of desensitization, of NmU-mediated contractile responses observed previously in strips of rat colonic smooth muscle, adds further complexity for fully understanding ligand-receptor interactions at NMUs and raised several questions (Brighton *et al.*, 2008). For example, does the intact tissue, but not isolated cells, contain factors (e.g. proteolytic activities, protein phosphatases, etc.) that facilitate dissociation of the ligand from the receptor and allow rapid resensitization of the receptor? Further, we may question whether irreversibility is ever observed in intact physiological tissue preparations and whether culturing rat colonic myocytes (or other cells from intact tissues) leads to the loss of these relevant factors? It is also possible that irreversible binding is species- and/or tissue-specific. Other studies of NmU-mediated contraction do, however, at least suggest high-affinity and prolonged ligand-receptor interactions. For example, the contractile responses to pNmU-8, pNmU-25, rNmU-23 or hNmU-25 in canine urinary bladder showed partial desensitization following addition of NmU even after a prolonged, 45 min wash (Westfall *et al.*, 2002). Further, intravenous administration of NmU to anaesthetized dogs resulted in sustained rises in urinary bladder pressure (Westfall *et al.*, 2002). Additionally, another study showed that the repetitive contractile response to gpNmU-8 in guinea-pig uterus was lost upon cumulative addition of gpNmU-9 (0.01-1 μM), while rat and mouse uterine responded appropriately to

cumulative additions of rNmU-23 or mNmU-23, respectively (Prendergast *et al.*, 2006). In addition, the present study has provided further evidence that pseudo-irreversible binding in both HEK-NMU1 and -NMU2 requires about 6 h for full recovery after exposure to hNmU-25. Interestingly, the length of the ligand *N*-terminus seems to be related to the duration of resensitization. For instance, full recovery of desensitized NMU1 or NMU2 following challenge with hNmS-33 required more than 6 h, while recovery following exposure to the shortest natural agonist, pNmU-8, required ≤3 h.

Pseudo-irreversible binding has also been shown for other GPCRs as described earlier (see **Chapter 3, Sections 3.3.2 and 3.3.3**), including urotensin II to the UT receptor and endothelin-1 to the ET_A receptor (Hilal-Dandan *et al.*, 1997; Qi *et al.*, 2005). Taking the endothelin-1-ET_A receptor association as an example, the prolonged [^{3}H]$InsP_x$ generation or inhibition of adenylyl cyclase activity following exposure of ET_A receptor to endothelin-1 for 5 min in isolated cardiac myocytes, could not be terminated by addition of antagonist, even at a high concentration. Further, ligand binding was partially resistant to either acid wash (pH 2.5, 10 min) or reducing agents, such as dithiothreitol (Hilal-Dandan *et al.*, 1997). It has been shown that agonistic activity at the ET_B receptor requires only the *C*-terminal fragment of endothelin-1, but high-affinity, irreversible binding requires the full length peptide (Lattig *et al.*, 2009). Although this was observed in isolated cells, pseudo-irreversible binding of endothelin-1 has also been demonstrated both in whole tissue *in vitro*, where the sustained contraction of rat mesenteric artery was shown to be resistant to extended wash, and *in vivo*, where vasopressor effects persisted even following lung and kidney clearance of circulating endothelin-1 (Mey *et al.*, 2009; Yanagisawa *et al.*, 1988). In contrast to the failure of the ET_A receptor antagonist, BQ123, to terminate endothelin-1-ET_A receptor binding and therefore signalling, it has recently been shown that the peptide, CGRP, appears to be responsible for the dissociation of endothelin-1 from the ET_A receptor and is thus able to terminate signalling and the persistent contractile actions of endothelin-1 (Meens *et al.*, 2010; Meens *et al.*, 2009). These studies suggest that CGRP works as an allosteric modulator, rather than as an antagonist, and might be considered a more tractable therapeutic target to facilitate the termination of ligand-receptor pseudo-irreversible binding and sustained receptor signalling. Although the recently discovered selective NMU2 antagonist will certainly

facilitate our future understanding of NmU-NMU2 pseudo-irreversible binding (Liu *et al.*, 2009), the endothelin-1-ET_A receptor studies highlight the importance of also seeking allosteric modulators to alter pseudo-irreversible ligand-receptor interactions.

The possibility of pseudo-irreversible binding of NmU to its receptors in physiological systems might contribute to the failure to detect responses to NmU in all screened primary cells and cell-lines in this study. For instance, it has been recently shown that freshly isolated rat calvarial osteoblast-like (ROB) cells exhibit high expression of NmU and low expression of NMU2 (Rucinski *et al.*, 2008). In contrast, following the culture of ROB cells for several days, the expression of NMU2 markedly increases, while NmU levels fall to below detectable levels (Rucinski *et al.*, 2008). Similar observations have been reported in peritoneal macrophages that express both NMU1 and NmU (Moriyama *et al.*, 2006a). That study demonstrated that knocking-down NmU resulted in a considerable up-regulation of NMU1 expression (Moriyama *et al.*, 2006a). Thus, the presence of an autocrine/paracrine action of NmU may prevent binding and responses to exogenous NmU. Further, another recent study, using immunocytochemistry, demonstrated that NMU2 is highly localized in the cytoplasm and nuclear area in human pancreatic cancer cells (Ketterer *et al.*, 2009). The latter finding may suggest that NMU2 has a natural, partially cytoplasmic localization, or that NMU2 might internalize following binding of endogenous NmU that is also reported to be present in these cells. Such studies may highlight the essential role of endogenous NmU in regulating the expression of NMUs and might suggest a new strategy for screening cells or tissues that reportedly naturally express NMUs.

Although, dynamin may also be involved in both CCP and caveolae-mediated internalization (Sandvig *et al.*, 2008), previous work has demonstrated that NMU internalization can be inhibited by pre-treatment with concanavalin A, which interferes with CCP-mediated endocytosis (Brighton, 2005). Together with the fact that dynasore inhibits both NMU1 and NMU2 resensitization of Ca^{2+} responses to pNmU-8, hNmU-25 and hNmS-33, this would suggest that internalization of NMUs is dynamin- and CCP-dependent. The availability of a dynamin marker and a CCP marker (EPS15) along with eGFP-tagged NMU1/2 might be used further to confirm these pathways. However, it is

important to ensure that the internalization of NMU1/2-eGFP is not affected by the *C*-terminal tagging since the present study has suggested that this modification abolishes coupling to $G\alpha_{i/o}$ (see **Chapter 4, Section 4.2.2**).

The current study also demonstrated the essential role of endosomal acidification and receptor recycling mechanisms on resensitization of Ca^{2+} responses to hNmU-25 in HEK-NMU2. However, due to the fact that NMU1 resensitization showed a faster recovery than NMU2 in the first hour and both receptors exhibit different characteristics in the intracellular domains and *C*-terminal tails, it will be important to assess more thoroughly recycling/degradation pathways for NMU1. Furthermore, it will also be important to repeat aspects of the present work using other ligands, as recovery rates showed a high dependency on the *N*-terminal length of NmU as described earlier.

Although the mechanism by which an inhibitor of endosomal acidification attenuates NMU2 resensitization is unclear, several studies have demonstrated the role of endosomal pH in ligand-receptor dissociation, receptor dephosphorylation and proteolytic degradation of the ligand (Krueger *et al.*, 1997; Mellman *et al.*, 1986; Padilla *et al.*, 2007; Roosterman *et al.*, 2007; Roosterman *et al.*, 2008). The present study also addressed the importance of ECE-1 activity on resensitization of hNmU-25-mediated Ca^{2+} responses in HEK-NMU1 and -NMU2. In addition to the distribution of ECE-1 isoenzymes at the plasma and endosomal membranes (Roosterman *et al.*, 2007), ECE-1a and c seem to be constitutively internalized to early endosomes via a dynamin-dependent mechanism, after which they recycle back to the cell-surface (Muller *et al.*, 2003). Further, phosphorylation of ECE-1a by PKC promotes its translocation to organellar compartments (Jafri *et al.*, 2006). Thus, activation of an NMU-$G\alpha_{q/11}$ pathway might stimulate PKC, which may phosphorylate and translocate ECE-1a. NMUs may internalize with other ECE-1 isoenzymes, via a dynamin-dependent pathway, to endosomes and this may contribute to NMU resensitization. Together with the lack of effect of SM-19712 on resensitization of Ca^{2+} responses to a low-affinity, small molecule ligand (carbachol at the M_3 muscarinic receptor; **Chapter 6**) or other peptide ligands, such as angiotensin II (Padilla *et al.*, 2007), and the high-selectivity of SM-19712 towards ECE-1 among other peptidases (Umekawa *et al.*, 2000) clearly highlights a role for ECE-1 in NmU-NMU1/2 processing.

The different effects of ECE-1 inhibition on resensitization of Ca^{2+} responses to hNmS-33 between NMU1- and NMU2-expressing cells and the absence of an effect of ECE-1 inhibition on the recovery rate of Ca^{2+} responses to pNmU-8 in HEK-NMU2 require further exploration of ECE-1involvement in NMU signalling. For example, it will be important to assess the susceptibility of different NMU ligands to ECE-1 proteolytic activity at both physiological and endosomal pH. Understanding the substrate specificity of ECE-1 may provide important clues about which ligand-receptor combinations are likely to be processed in an ECE-1-dependent manner and could allow development of ligands resistant to, or with enhanced sensitivity to ECE-1. It will also be essential to assess subcellular co-localization of ECE-1 with the ligand-receptor complex. Knocking-down ECE-1 in HEK-NMU1 and -NMU2 is an alternative approach to investigate its role in NMU resensitization and ligand processing, and would potentially highlight the isoenzyme(s) involved. Validation of the use of eGFP-tagged NMUs will substantially facilitate identification of the intracellular localization of NMUs on challenge with different NMU ligands. Indeed, the availability of several intracellular markers, such as markers of early endosomes (Rab5 GTPase and EEA1), recycling endosomes (Rab4 and 11) and lysosomes (Rab7 and LAMP) would be useful tools to localize and monitor NMU trafficking.

Although NMUs exhibit pseudo-irreversible ligand binding and have a slow rate of resensitization, it is unclear if NMUs belong to the Oakley et al. (2000) defined class A (low affinity β-arrestin binding and favouring β-arrestin-2) or class B (high affinity with no preference between β-arrestins) GPCRs. Furthermore, pseudo-irreversible ligand-receptor binding may not be an exclusive property of class B GPCRs, since the ET_A receptor, which binds irreversibly to endothelin-1, is classified as a class A GPCR (Moore *et al.*, 2007). Additionally, ECE-1 activity also is not only found to be important for ligands at class B GPCRs since this peptidase also regulates resensitization of the NK_3 receptor, which is a class A GPCR (Padilla *et al.*, 2007). Studying the recruitment of different β-arrestin isoforms, the kinetics of their interaction with the receptor, and examinations of β-arrestin-dependent signalling readouts (e.g. ERK1/2) should provide a clearer picture of the classification of NMUs and any potential ligand-dependence.

The present study has also highlighted the more sustained NMU2-mediated ERK1/2 activation when ECE-1 activity is inhibited. Future investigations of the association kinetics of NMUs with β-arrestins and the role of ECE-1 in the termination of ERK1/2 signalling may have therapeutic relevance. For instance, substance P activates the NK_1 receptor, which then binds β-arrestins and promotes signalling by a MAPK complex (Cottrell *et al.*, 2009). This stimulates phosphorylation and expression of nuclear death receptors (nur77) leading to cell death. However, ECE-1-mediated degradation of substance P disrupts the ligand-receptor-β-arrestin-ERK1/2 complex, which terminates ERK1/2 signalling and promotes cell survival (Cottrell *et al.*, 2009).

Disruption of endosomal acidification results in a greater inhibition of the recovery of hNmU-25-mediated Ca^{2+} responses in NMU2 than that observed by ECE-1 inhibition, highlighting additional mechanisms involved in NMU2 resensitization. Further investigation is needed to examine potential of other mechanisms, such as a role for receptor dephosphorylation by phosphatases. For example, resensitization of Ca^{2+} responses to substance P in HEK293 cells expressing the NK_1 receptor is dependent on both receptor dephosphorylation and cellular proteolytic activity (Murphy *et al.*, 2011).

Finally, culture of HEK-NMU2 in high-glucose medium was able to increase the rate of recovery of hNmU-2-mediated Ca^{2+} responses, whereas inhibition of ECE-1 antagonized the enhancement of hNmU-25-mediated Ca^{2+} responses. Preliminary experiments in our laboratory using Western blotting have demonstrated an increase of ECE-1 expression in HEK293 cells in response to culture in high glucose, which is consistent with the current findings and previous reports (Keynan *et al.*, 2004; Khamaisi *et al.*, 2009). However, the increase in the recovery rate of Ca^{2+} responses to pNmU-8 in HEK-NMU2 incubated in high glucose was resistant to ECE-1 inhibition thereby providing additional evidence for the involvement of other factor(s) regulating NMU signalling and trafficking.

The current study has shown the essentially irreversible binding of NmU to NMU and the subsequent internalization of the ligand-receptor complex through a dynamin-dependent pathway. This complex is likely processed via the endosomal recycling pathway but the rate at which this occurs is dependent upon a variety of factors including endosomal acidification and, at least for some ligands, the proteolytic activity of ECE-1.

Removal of the ligand from the receptor following endosomal acidification and/or proteolytic cleavage and the subsequent processing of ligand, potentially by ECE-1, may facilitate the recycling of the receptor and allow mechanisms such as receptor dephosphorylation to generate resensitized receptors in the plasma membrane. Further, the rate of such trafficking may influence the duration of G protein-dependent and G protein-independent signalling. This work shows the potential importance of the nature of the ligand in such processing and highlights the need to understand such ligand/receptor interactions under patho-physiological conditions and in drug design and development.

REFERENCES

Abbondanzo SJ, Manfra DJ, Chen SC, Pinzon-Ortiz M, Sun Y, Phillips JE, *et al.* (2009). Nmur1-/- mice are not protected from cutaneous inflammation. *Biochem Biophys Res Commun* **378**(4)**:** 777-782.

Aiyar N, Disa J, Foley JJ, Buckley PT, Wixted WE, Pullen M, *et al.* (2004). Radioligand binding and functional characterization of recombinant human NmU1 and NmU2 receptors stably expressed in clonal human embryonic kidney-293 cells. *Pharmacology* **72**(1)**:** 33-41.

Alevizos I, Mahadevappa M, Zhang X, Ohyama H, Kohno Y, Posner M, *et al.* (2001). Oral cancer in vivo gene expression profiling assisted by laser capture microdissection and microarray analysis. *Oncogene* **20**(43)**:** 6196-6204.

Alexander SP, Mathie A, Peters JA (2008). Guide to Receptors and Channels (GRAC), 3rd edition. *Br J Pharmacol* **153 Suppl 2:** S1-209.

Allison JH, Blisner ME, Holland WH, Hipps PP, Sherman WR (1976). Increased brain myo-inositol 1-phosphate in lithium-treated rats. *Biochem Biophys Res Commun* **71**(2)**:** 664-670.

Atsuchi K, Asakawa A, Ushikai M, Ataka K, Tanaka R, Kato I, *et al.* (2010). Centrally administered neuromedin S inhibits feeding behavior and gastroduodenal motility in mice. *Horm Metab Res* **42**(7)**:** 535-538.

Austin C, Lo G, Nandha KA, Meleagros L, Bloom SR (1995). Cloning and characterization of the cDNA encoding the human neuromedin U (NmU) precursor: NmU expression in the human gastrointestinal tract. *J Mol Endocrinol* **14**(2)**:** 157-169.

Bechtold DA, Ivanov TR, Luckman SM (2009). Appetite-modifying actions of pro-neuromedin U-derived peptides. *Am. J. Physiol.-Endocrinol. Metab.* **297**(2)**:** E545-E551.

Benito-Orfila MA, Domin J, Nandha KA, Bloom SR (1991). The motor effect of neuromedin U on rat stomach in vitro. *Eur J Pharmacol* **193**(3)**:** 329-333.

Bennett VJ, Perrine SA, Simmons MA (2002). A novel mechanism of neurokinin-1 receptor resensitization. *J Pharmacol Exp Ther* **303**(3)**:** 1155-1162.

Berkova Z, Morris AP, Estes MK (2003). Cytoplasmic calcium measurement in rotavirus enterotoxin-enhanced green fluorescent protein (NSP4-EGFP) expressing cells loaded with Fura-2. *Cell Calcium* **34**(1)**:** 55-68.

Bohm SK, Khitin LM, Grady EF, Aponte G, Payan DG, Bunnett NW (1996). Mechanisms of desensitization and resensitization of proteinase-activated receptor-2. *J Biol Chem* **271**(36)**:** 22003-22016.

Bohme I, Beck-Sickinger AG (2009). Illuminating the life of GPCRs. *Cell Commun Signal* **7:** 16.

Bolsover S, Ibrahim O, O'Luanaigh N, Williams H, Cockcroft S (2001). Use of fluorescent Ca2+ dyes with green fluorescent protein and its variants: problems and solutions. *Biochem J* **356**(Pt 2)**:** 345-352.

Bonfiglio JJ, Inda C, Refojo D, Holsboer F, Arzt E, Silberstein S (2011). The corticotropin-releasing hormone network and the hypothalamic-pituitary-adrenal axis: molecular and cellular mechanisms involved. *Neuroendocrinology* **94**(1)**:** 12-20.

Boselli C, Govoni S, Vicini D, Lanni C, Racchi M, D'Agostino G (2002). Presence and passage dependent loss of biochemical M3 muscarinic receptor function in human detrusor cultured smooth muscle cells. *J Urol* **168**(6)**:** 2672-2676.

Brauner-Osborne H, Wellendorph P, Jensen AA (2007). Structure, pharmacology and therapeutic prospects of family C G-protein coupled receptors. *Curr Drug Targets* **8**(1)**:** 169-184.

Brighton P (2005). *The activation and regulation of mammalian neuromedin U receptor isoforms*. edn. University of Leicester: Leicester.

Brighton PJ, Szekeres PG, Willars GB (2004b). Neuromedin U and its receptors: structure, function, and physiological roles. *Pharmacol Rev* **56**(2)**:** 231-248.

Brighton PJ, Szekeres PG, Wise A, Willars GB (2004a). Signaling and ligand binding by recombinant neuromedin U receptors: evidence for dual coupling to Galphaq/11 and Galphai and an irreversible ligand-receptor interaction. *Mol Pharmacol* **66**(6)**:** 1544-1556.

Brighton PJ, Wise A, Dass NB, Willars GB (2008). Paradoxical behavior of neuromedin U in isolated smooth muscle cells and intact tissue. *J Pharmacol Exp Ther* **325**(1)**:** 154-164.

BROWN BL (1971). A Simple and Sensitive Saturation Assay Method for the Measurement of Adenosine
3': 5'-Cyclic Monophosphate. *Biochem. J.* **121:** 561-562.

Bunnett NW, Cottrell GS (2010). Trafficking and Signaling of G Protein-Coupled Receptors in the Nervous System: Implications for Disease and Therapy. *Cns & Neurological Disorders-Drug Targets* **9**(5)**:** 539-556.

Cabrera-Vera TM, Vanhauwe J, Thomas TO, Medkova M, Preininger A, Mazzoni MR, *et al.* (2003). Insights into G protein structure, function, and regulation. *Endocr Rev* **24**(6)**:** 765-781.

Cahalan MD (2009). STIMulating store-operated Ca(2+) entry. *Nat Cell Biol* **11**(6)**:** 669-677.

Campfield LA, Smith FJ, Guisez Y, Devos R, Burn P (1995). Recombinant mouse OB protein: evidence for a peripheral signal linking adiposity and central neural networks. *Science* **269**(5223)**:** 546-549.

Cao CQ, Yu XH, Dray A, Filosa A, Perkins MN (2003). A pro-nociceptive role of neuromedin U in adult mice. *Pain* **104**(3)**:** 609-616.

Cattaruzza F, Cottrell GS, Vaksman N, Bunnett NW (2009). Endothelin-converting enzyme 1 promotes re-sensitization of neurokinin 1 receptor-dependent neurogenic inflammation. *Br J Pharmacol* **156**(5)**:** 730-739.

Challiss RAJ, Mistry R, Gray DW, Nahorski SR (1994). MODULATION OF MUSCARINIC CHOLINOCEPTOR-STIMULATED INOSITOL 1,4,5-TRISPHOSPHATE ACCUMULATION BY N-METHYL-D-ASPARTATE IN NEONATAL RAT CEREBRAL-CORTEX. *Neuropharmacology* **33**(1)**:** 15-25.

Chen T, Zhou M, Walker B, Harriot P, Mori K, Miyazato M, *et al.* (2006). Structural and functional analogs of the novel mammalian neuropeptide, neuromedin S (NmS), in the dermal venoms of Eurasian bombinid toads. *Biochem Biophys Res Commun* **345**(1)**:** 377-384.

Cherezov V, Rosenbaum DM, Hanson MA, Rasmussen SG, Thian FS, Kobilka TS, *et al.* (2007). High-resolution crystal structure of an engineered human beta2-adrenergic G protein-coupled receptor. *Science* **318**(5854)**:** 1258-1265.

Chu C, Jin Q, Kunitake T, Kato K, Nabekura T, Nakazato M, *et al.* (2002). Cardiovascular actions of central neuromedin U in conscious rats. *Regul Pept* **105**(1)**:** 29-34.

Clapham DE, Neer EJ (1997). G protein beta gamma subunits. *Annu Rev Pharmacol Toxicol* **37:** 167-203.

Conlon JM, Domin J, Thim L, DiMarzo V, Morris HR, Bloom SR (1988). Primary structure of neuromedin U from the rat. *J Neurochem* **51**(3)**:** 988-991.

Coopman K, Huang Y, Johnston N, Bradley SJ, Wilkinson GF, Willars GB (2010). Comparative effects of the endogenous agonist glucagon-like peptide-1 (GLP-1)-(7-36) amide and the small-molecule ago-allosteric agent "compound 2" at the GLP-1 receptor. *J Pharmacol Exp Ther* **334**(3)**:** 795-808.

Cordeaux Y, Briddon SJ, Megson AE, McDonnell J, Dickenson JM, Hill SJ (2000). Influence of receptor number on functional responses elicited by agonists acting at the human adenosine A(1) receptor: evidence for signaling pathway-dependent changes in agonist potency and relative intrinsic activity. *Mol Pharmacol* **58**(5)**:** 1075-1084.

Cordeaux Y, Hill SJ (2002). Mechanisms of cross-talk between G-protein-coupled receptors. *Neurosignals* **11**(1)**:** 45-57.

Cottrell GS, Padilla B, Pikios S, Roosterman D, Steinhoff M, Grady EF, *et al.* (2007). Post-endocytic sorting of calcitonin receptor-like receptor and receptor activity-modifying protein 1. *J Biol Chem* **282**(16)**:** 12260-12271.

Cottrell GS, Padilla BE, Amadesi S, Poole DP, Murphy JE, Hardt M, *et al.* (2009). Endosomal endothelin-converting enzyme-1: a regulator of beta-arrestin-dependent ERK signaling. *J Biol Chem* **284**(33)**:** 22411-22425.

Dass NB, Bassil AK, North-Laidler VJ, Morrow R, Aziz E, Tuladhar BR, *et al.* (2007). Neuromedin U can exert colon-specific, enteric nerve-mediated prokinetic activity, via a pathway involving NMU1 receptor activation. *Br J Pharmacol* **150**(4)**:** 502-508.

DeFea KA, Vaughn ZD, O'Bryan EM, Nishijima D, Dery O, Bunnett NW (2000a). The proliferative and antiapoptotic effects of substance P are facilitated by formation of a beta -arrestin-dependent scaffolding complex. *Proc Natl Acad Sci U S A* **97**(20)**:** 11086-11091.

DeFea KA, Zalevsky J, Thoma MS, Dery O, Mullins RD, Bunnett NW (2000b). beta-arrestin-dependent endocytosis of proteinase-activated receptor 2 is required for intracellular targeting of activated ERK1/2. *J Cell Biol* **148**(6)**:** 1267-1281.

Domin J, Benito-Orfila MA, Nandha KA, Aitken A, Bloom SR (1992). The purification and sequence analysis of an avian neuromedin U. *Regul Pept* **41**(1)**:** 1-8.

Domin J, Ghatei MA, Chohan P, Bloom SR (1986). Characterization of neuromedin U like immunoreactivity in rat, porcine, guinea-pig and human tissue extracts using a specific radioimmunoassay. *Biochem Biophys Res Commun* **140**(3)**:** 1127-1134.

Domin J, Ghatei MA, Chohan P, Bloom SR (1987). Neuromedin U--a study of its distribution in the rat. *Peptides* **8**(5)**:** 779-784.

Domin J, Yiangou YG, Spokes RA, Aitken A, Parmar KB, Chrysanthou BJ, *et al.* (1989). The distribution, purification, and pharmacological action of an amphibian neuromedin U. *J Biol Chem* **264**(35)**:** 20881-20885.

Eckman EA, Reed DK, Eckman CB (2001). Degradation of the Alzheimer's amyloid beta peptide by endothelin-converting enzyme. *J Biol Chem* **276**(27)**:** 24540-24548.

Egecioglu E, Ploj K, Xu X, Bjursell M, Salome N, Andersson N, *et al.* (2009). Central NMU signaling in body weight and energy balance regulation: evidence from NMUR2 deletion and chronic central NMU treatment in mice. *Am J Physiol Endocrinol Metab* **297**(3)**:** E708-716.

Euer NI, Kaul S, Deissler H, Mobus VJ, Zeillinger R, Weidle UH (2005). Identification of L1CAM, Jagged2 and Neuromedin U as ovarian cancer-associated antigens. *Oncol Rep* **13**(3)**:** 375-387.

Fahnoe DC, Knapp J, Johnson GD, Ahn K (2000). Inhibitor potencies and substrate preference for endothelin-converting enzyme-1 are dramatically affected by pH. *J Cardiovasc Pharmacol* **36**(5 Suppl 1)**:** S22-25.

Fang L, Zhang M, Li C, Dong S, Hu Y (2006). Chemical genetic analysis reveals the effects of NMU2R on the expression of peptide hormones. *Neurosci Lett* **404**(1-2)**:** 148-153.

Fujii R, Hosoya M, Fukusumi S, Kawamata Y, Habata Y, Hinuma S, *et al.* (2000). Identification of neuromedin U as the cognate ligand of the orphan G protein-coupled receptor FM-3. *J Biol Chem* **275**(28)**:** 21068-21074.

Funes S, Hedrick JA, Yang S, Shan L, Bayne M, Monsma FJ, Jr., *et al.* (2002). Cloning and characterization of murine neuromedin U receptors. *Peptides* **23**(9)**:** 1607-1615.

Gambone JE, Dusaban SS, Loperena R, Nakata Y, Shetzline SE (2011). The c-Myb target gene neuromedin U functions as a novel cofactor during the early stages of erythropoiesis. *Blood*.

Garcia Lopez MA, Aguado Martinez A, Lamaze C, Martinez AC, Fischer T (2009). Inhibition of dynamin prevents CCL2-mediated endocytosis of CCR2 and activation of ERK1/2. *Cell Signal* **21**(12)**:** 1748-1757.

Gardiner SM, Compton AM, Bennett T, Domin J, Bloom SR (1990). Regional hemodynamic effects of neuromedin U in conscious rats. *Am J Physiol* **258**(1 Pt 2)**:** R32-38.

Gartlon J, Szekeres P, Pullen M, Sarau HM, Aiyar N, Shabon U, *et al.* (2004). Localisation of NMU1R and NMU2R in human and rat central nervous system and effects of neuromedin-U following central administration in rats. *Psychopharmacology (Berl)* **177**(1-2)**:** 1-14.

Graham ES, Littlewood P, Turnbull Y, Mercer JG, Morgan PJ, Barrett P (2005). Neuromedin-U is regulated by the circadian clock in the SCN of the mouse. *Eur J Neurosci* **21**(3)**:** 814-819.

Graham ES, Turnbull Y, Fotheringham P, Nilaweera K, Mercer JG, Morgan PJ, *et al.* (2003). Neuromedin U and Neuromedin U receptor-2 expression in the mouse and rat hypothalamus: effects of nutritional status. *J Neurochem* **87**(5)**:** 1165-1173.

Graham FL, van der Eb AJ (1973). A new technique for the assay of infectivity of human adenovirus 5 DNA. *Virology* **52**(2)**:** 456-467.

Gray JA, Sheffler DJ, Bhatnagar A, Woods JA, Hufeisen SJ, Benovic JL, *et al.* (2001). Cell-type specific effects of endocytosis inhibitors on 5-hydroxytryptamine(2A) receptor desensitization and resensitization reveal an arrestin-, GRK2-, and GRK5-independent mode of regulation in human embryonic kidney 293 cells. *Mol Pharmacol* **60**(5)**:** 1020-1030.

Guan XM, Yu H, Jiang Q, Van Der Ploeg LH, Liu Q (2001). Distribution of neuromedin U receptor subtype 2 mRNA in the rat brain. *Brain Res Gene Expr Patterns* **1**(1)**:** 1-4.

Gudermann T, Schoneberg T, Schultz G (1997). Functional and structural complexity of signal transduction via G-protein-coupled receptors. *Annu Rev Neurosci* **20:** 399-427.

Haigler HT, Maxfield FR, Willingham MC, Pastan I (1980). Dansylcadaverine inhibits internalization of 125I-epidermal growth factor in BALB 3T3 cells. *J Biol Chem* **255**(4)**:** 1239-1241.

Hall CJ (2011). *The effect of GPCR crosstalk on intracellular Ca2+ responses and downstream signalling*. edn. University of Leicester: Leicester.

Hanada R, Nakazato M, Murakami N, Sakihara S, Yoshimatsu H, Toshinai K, *et al.* (2001). A role for neuromedin U in stress response. *Biochem Biophys Res Commun* **289**(1)**:** 225-228.

Hanada R, Teranishi H, Pearson JT, Kurokawa M, Hosoda H, Fukushima N, *et al.* (2004). Neuromedin U has a novel anorexigenic effect independent of the leptin signaling pathway. *Nat Med* **10**(10)**:** 1067-1073.

Hanada T, Date Y, Shimbara T, Sakihara S, Murakami N, Hayashi Y, *et al.* (2003). Central actions of neuromedin U via corticotropin-releasing hormone. *Biochem Biophys Res Commun* **311**(4)**:** 954-958.

Hanyaloglu AC, Zastrow M (2008). Regulation of GPCRs by endocytic membrane trafficking and its potential implications. *Annu. Rev. Pharmacol. Toxicol.* **48:** 537-568.

Harding MA, Theodorescu D (2007). RhoGDI2: a new metastasis suppressor gene: discovery and clinical translation. *Urol Oncol* **25**(5)**:** 401-406.

Harten SK, Esteban MA, Shukla D, Ashcroft M, Maxwell PH (2011). Inactivation of the von Hippel-Lindau tumour suppressor gene induces Neuromedin U expression in renal cancer cells. *Mol Cancer* **10**(1)**:** 89.

Hashimoto T, Masui H, Uchida Y, Sakura N, Okimura K (1991). Agonistic and antagonistic activities of neuromedin U-8 analogs substituted with glycine or D-amino acid on contractile activity of chicken crop smooth muscle preparations. *Chem Pharm Bull (Tokyo)* **39**(9)**:** 2319-2322.

Heasman SJ, Ridley AJ (2008). Mammalian Rho GTPases: new insights into their functions from in vivo studies. *Nat Rev Mol Cell Biol* **9**(9)**:** 690-701.

Hedrick JA, Morse K, Shan L, Qiao X, Pang L, Wang S, *et al.* (2000). Identification of a human gastrointestinal tract and immune system receptor for the peptide neuromedin U. *Mol Pharmacol* **58**(4)**:** 870-875.

Hermans E (2003). Biochemical and pharmacological control of the multiplicity of coupling at G-protein-coupled receptors. *Pharmacol Ther* **99**(1)**:** 25-44.

Hilal-Dandan R, Merck DT, Lujan JP, Brunton LL (1994). Coupling of the type A endothelin receptor to multiple responses in adult rat cardiac myocytes. *Mol Pharmacol* **45**(6)**:** 1183-1190.

Hilal-Dandan R, Urasawa K, Brunton LL (1992). Endothelin inhibits adenylate cyclase and stimulates phosphoinositide hydrolysis in adult cardiac myocytes. *J Biol Chem* **267**(15)**:** 10620-10624.

Hilal-Dandan R, Villegas S, Gonzalez A, Brunton LL (1997). The quasi-irreversible nature of endothelin binding and G protein-linked signaling in cardiac myocytes. *J Pharmacol Exp Ther* **281**(1)**:** 267-273.

Hoang MV, Turner AJ (1997). Novel activity of endothelin-converting enzyme: hydrolysis of bradykinin. *Biochem J* **327 (Pt 1):** 23-26.

Hokfelt T, Bartfai T, Bloom F (2003). Neuropeptides: opportunities for drug discovery. *Lancet neurology* **2**(8)**:** 463-472.

Hosoya M, Moriya T, Kawamata Y, Ohkubo S, Fujii R, Matsui H, *et al.* (2000). Identification and functional characterization of a novel subtype of neuromedin U receptor. *J Biol Chem* **275**(38)**:** 29528-29532.

Howard AD, Wang R, Pong SS, Mellin TN, Strack A, Guan XM, *et al.* (2000). Identification of receptors for neuromedin U and its role in feeding. *Nature* **406**(6791)**:** 70-74.

Hsu SH, Luo CW (2007). Molecular dissection of G protein preference using Gsalpha chimeras reveals novel ligand signaling of GPCRs. *Am J Physiol Endocrinol Metab* **293**(4)**:** E1021-1029.

Huang Y (2011b). *Exploring the structure, function and regulation of the human glucagon-like peptide-1 receptor*. edn. University of Leicester: Leicester.

Huang Y, Willars GB (2011a). Generation of epitope-tagged GPCRs. *Methods Mol Biol* **746:** 53-84.

Huotari J, Helenius A (2011). Endosome maturation. *EMBO J* **30**(17)**:** 3481-3500.

Ida T, Mori K, Miyazato M, Egi Y, Abe S, Nakahara K, *et al.* (2005). Neuromedin s is a novel anorexigenic hormone. *Endocrinology* **146**(10)**:** 4217-4223.

Ivanov TR, Lawrence CB, Stanley PJ, Luckman SM (2002). Evaluation of neuromedin U actions in energy homeostasis and pituitary function. *Endocrinology* **143**(10)**:** 3813-3821.

Ivanov TR, Le Rouzic P, Stanley PJ, Ling WY, Parello R, Luckman SM (2004). Neuromedin U neurones in the rat nucleus of the tractus solitarius are catecholaminergic and respond to peripheral cholecystokinin. *J Neuroendocrinol* **16**(7)**:** 612-619.

Ivic L, Zhang C, Zhang X, Yoon SO, Firestein S (2002). Intracellular trafficking of a tagged and functional mammalian olfactory receptor. *J Neurobiol* **50**(1)**:** 56-68.

Jacobson KA, Boeynaems JM (2010). P2Y nucleotide receptors: promise of therapeutic applications. *Drug Discov Today* **15**(13-14)**:** 570-578.

Jafri F, Ergul A (2006). Phosphorylation of endothelin converting enzyme-1 isoforms: relevance to subcellular localization. *Exp Biol Med (Maywood)* **231**(6)**:** 713-717.

Jaszberenyi M, Bagosi Z, Thurzo B, Foldesi I, Telegdy G (2007). Endocrine and behavioral effects of neuromedin S. *Horm Behav* **52**(5)**:** 631-639.

Jethwa PH, Small CJ, Smith KL, Seth A, Darch SJ, Abbott CR, *et al.* (2005). Neuromedin U has a physiological role in the regulation of food intake and partially mediates the effects of leptin. *Am J Physiol Endocrinol Metab* **289**(2)**:** E301-305.

Jethwa PH, Smith KL, Small CJ, Abbott CR, Darch SJ, Murphy KG, *et al.* (2006). Neuromedin U partially mediates leptin-induced hypothalamo-pituitary adrenal (HPA) stimulation and has a physiological role in the regulation of the HPA axis in the rat. *Endocrinology* **147**(6)**:** 2886-2892.

Johnson EN, Appelbaum ER, Carpenter DC, Cox RF, Disa J, Foley JJ, *et al.* (2004). Neuromedin U elicits cytokine release in murine Th2-type T cell clone D10.G4.1. *J Immunol* **173**(12)**:** 7230-7238.

Johnson GD, Stevenson T, Ahn K (1999). Hydrolysis of peptide hormones by endothelin-converting enzyme-1. A comparison with neprilysin. *J Biol Chem* **274**(7)**:** 4053-4058.

Jones NA, Morton MF, Prendergast CE, Powell GL, Shankley NP, Hollingsworth SJ (2006). Neuromedin U stimulates contraction of human long saphenous vein and gastrointestinal smooth muscle in vitro. *Regul Pept* **136**(1-3)**:** 109-116.

Kaczmarek P, Malendowicz LK, Fabis M, Ziolkowska A, Pruszynska-Oszmalek E, Sassek M, *et al.* (2009). Does somatostatin confer insulinostatic effects of neuromedin u in the rat pancreas? *Pancreas* **38**(2)**:** 208-212.

Kaczmarek P, Malendowicz LK, Pruszynska-Oszmalek E, Wojciechowicz T, Szczepankiewicz D, Szkudelski T, *et al.* (2006). Neuromedin U receptor 1 expression in the rat endocrine pancreas and evidence suggesting neuromedin U suppressive effect on insulin secretion from isolated rat pancreatic islets. *Int J Mol Med* **18**(5)**:** 951-955.

Kage R, O'Harte F, Thim L, Conlon JM (1991). Rabbit neuromedin U-25: lack of conservation of a posttranslational processing site. *Regul Pept* **33**(2)**:** 191-198.

Kalatskaya I, Schussler S, Seidl C, Jochum M, Faussner A (2006). C-terminal fusion of eGFP to the bradykinin B2 receptor strongly affects down-regulation but not receptor internalization or signaling. *Biol Chem* **387**(5)**:** 603-610.

Kangawa K, Minamino N, Fukuda A, Matsuo H (1983a). Neuromedin K: a novel mammalian tachykinin identified in porcine spinal cord. *Biochem Biophys Res Commun* **114**(2)**:** 533-540.

Kawai T, Shibata A, Kurosawa K, Sato Y, Kato S, Ohki K, *et al.* (2006). Structure-activity relationships of neuromedin U. V. study on the stability of porcine neuromedin U-8 at the C-terminal asparagine amide under mild alkaline and acidic conditions. *Chem Pharm Bull (Tokyo)* **54**(5)**:** 659-664.

Ketterer K, Kong B, Frank D, Giese NA, Bauer A, Hoheisel J, *et al.* (2009). Neuromedin U is overexpressed in pancreatic cancer and increases invasiveness via the hepatocyte growth factor c-Met pathway. *Cancer Lett* **277**(1)**:** 72-81.

Keynan S, Khamaisi M, Dahan R, Barnes K, Jackson CD, Turner AJ, *et al.* (2004). Increased expression of endothelin-converting enzyme-1c isoform in response to high glucose levels in endothelial cells. *J Vasc Res* **41**(2)**:** 131-140.

Khamaisi M, Dahan R, Hamed S, Abassi Z, Heyman SN, Raz I (2009). Role of protein kinase C in the expression of endothelin converting enzyme-1. *Endocrinology* **150**(3)**:** 1440-1449.

Kim SJ, Kim MY, Lee EJ, Ahn YS, Baik JH (2004). Distinct regulation of internalization and mitogen-activated protein kinase activation by two isoforms of the dopamine D2 receptor. *Mol Endocrinol* **18**(3)**:** 640-652.

Koenig JA, Edwardson JM (1997). Endocytosis and recycling of G protein-coupled receptors. *Trends Pharmacol Sci* **18**(8)**:** 276-287.

Kojima M, Haruno R, Nakazato M, Date Y, Murakami N, Hanada R, *et al.* (2000). Purification and identification of neuromedin U as an endogenous ligand for an orphan receptor GPR66 (FM3). *Biochem Biophys Res Commun* **276**(2)**:** 435-438.

Kolch W (2005). Coordinating ERK/MAPK signalling through scaffolds and inhibitors. *Nat Rev Mol Cell Biol* **6**(11)**:** 827-837.

Kowalski TJ, Spar BD, Markowitz L, Maguire M, Golovko A, Yang S, *et al.* (2005). Transgenic overexpression of neuromedin U promotes leanness and hypophagia in mice. *J Endocrinol* **185**(1)**:** 151-164.

Kozasa T, Jiang X, Hart MJ, Sternweis PM, Singer WD, Gilman AG, *et al.* (1998). p115 RhoGEF, a GTPase activating protein for Galpha12 and Galpha13. *Science* **280**(5372)**:** 2109-2111.

Krueger KM, Daaka Y, Pitcher JA, Lefkowitz RJ (1997). The role of sequestration in G protein-coupled receptor resensitization. Regulation of beta2-adrenergic receptor dephosphorylation by vesicular acidification. *J Biol Chem* **272**(1)**:** 5-8.

Lalo U, Allsopp RC, Mahaut-Smith MP, Evans RJ (2010). P2X1 receptor mobility and trafficking; regulation by receptor insertion and activation. *J Neurochem* **113**(5)**:** 1177-1187.

Lattig J, Oksche A, Beyermann M, Rosenthal W, Krause G (2009). Structural determinants for selective recognition of peptide ligands for endothelin receptor subtypes ETA and ETB. *J Pept Sci* **15**(7)**:** 479-491.

Law PY, Erickson LJ, El-Kouhen R, Dicker L, Solberg J, Wang W, *et al.* (2000). Receptor density and recycling affect the rate of agonist-induced desensitization of mu-opioid receptor. *Mol Pharmacol* **58**(2)**:** 388-398.

Lee WH, Liu SB, Shen JH, Jin Y, Lai R, Zhang Y (2005). Identification and molecular cloning of a novel neuromedin U analog from the skin secretions of toad Bombina maxima. *Regul Pept* **129**(1-3)**:** 43-47.

Liu JJ, Payza K, Huang J, Liu R, Chen T, Coupal M, *et al.* (2009). Discovery and pharmacological characterization of a small-molecule antagonist at neuromedin U receptor NMUR2. *J Pharmacol Exp Ther* **330**(1)**:** 268-275.

Lo G, Legon S, Austin C, Wallis S, Wang Z, Bloom SR (1992). Characterization of complementary DNA encoding the rat neuromedin U precursor. *Mol Endocrinol* **6**(10)**:** 1538-1544.

Macia E, Ehrlich M, Massol R, Boucrot E, Brunner C, Kirchhausen T (2006). Dynasore, a cell-permeable inhibitor of dynamin. *Dev Cell* **10**(6)**:** 839-850.

Maggi CA, Patacchini R, Giuliani S, Turini D, Barbanti G, Rovero P, *et al.* (1990). Motor response of the human isolated small intestine and urinary bladder to porcine neuromedin U-8. *Br J Pharmacol* **99**(1)**:** 186-188.

Magnan R, Masri B, Escrieut C, Foucaud M, Cordelier P, Fourmy D (2010). Regulation of membrane cholecystokinin-2 receptor by agonists enables classification of partial agonists as biased agonists. *J Biol Chem* **286**(8)**:** 6707-6719.

Maier W, Adilov B, Regenass M, Alcedo J (2010). A neuromedin U receptor acts with the sensory system to modulate food type-dependent effects on C. elegans lifespan. *PLoS Biol* **8**(5)**:** e1000376.

Malendowicz LK, Andreis PG, Markowska A, Nowak M, Warchol JB, Neri G, *et al.* (1994). Effects of neuromedin U-8 on the secretory activity of the rat adrenal cortex: evidence for an indirect action requiring the presence of the zona medullaris. *Res Exp Med (Berl)* **194**(2)**:** 69-79.

Malendowicz LK, Nussdorfer GG, Nowak KW, Mazzocchi G (1993). Effects of neuromedin U-8 on the rat pituitary-adrenocortical axis. *In Vivo* **7**(5)**:** 419-422.

Mangold C, Ksiazek I, Yun SW, Berger E, Binkert C (2008). Distribution of neuromedin U binding sites in the rat CNS revealed by in vitro receptor autoradiography. *Neuropeptides* **42**(4)**:** 377-386.

Marchese A, Paing MM, Temple BR, Trejo J (2008). G protein-coupled receptor sorting to endosomes and lysosomes. *Annu Rev Pharmacol Toxicol* **48:** 601-629.

Marinissen MJ, Gutkind JS (2001). G-protein-coupled receptors and signaling networks: emerging paradigms. *Trends Pharmacol Sci* **22**(7)**:** 368-376.

Maruyama K, Kaiya H, Miyazato M, Konno N, Wakasugi T, Uchiyama M, *et al.* (2011). Isolation and characterisation of two cDNAs encoding the neuromedin U receptor from goldfish brain. *J Neuroendocrinol* **23**(3)**:** 282-291.

Maruyama K, Konno N, Ishiguro K, Wakasugi T, Uchiyama M, Shioda S, *et al.* (2008). Isolation and characterisation of four cDNAs encoding neuromedin U (NMU) from the brain and gut of goldfish, and the inhibitory effect of a deduced NMU on food intake and locomotor activity. *J Neuroendocrinol* **20**(1)**:** 71-78.

McLean AJ, Milligan G (2000). Ligand regulation of green fluorescent protein-tagged forms of the human beta(1)- and beta(2)-adrenoceptors; comparisons with the unmodified receptors. *Br J Pharmacol* **130**(8)**:** 1825-1832.

Meens MJ, Compeer MG, Hackeng TM, van Zandvoort MA, Janssen BJ, De Mey JG (2010). Stimuli of sensory-motor nerves terminate arterial contractile effects of endothelin-1 by CGRP and dissociation of ET-1/ET(A)-receptor complexes. *PLoS One* **5**(6)**:** e10917.

Meens MJ, Fazzi GE, van Zandvoort MA, De Mey JG (2009). Calcitonin gene-related peptide selectively relaxes contractile responses to endothelin-1 in rat mesenteric resistance arteries. *J Pharmacol Exp Ther* **331**(1)**:** 87-95.

Mellman I, Fuchs R, Helenius A (1986). Acidification of the endocytic and exocytic pathways. *Annu Rev Biochem* **55:** 663-700.

Mey JGRD, Compeer MG, Meens MJ (2009). Endothelin-1, an Endogenous Irreversible Agonist in Search of an Allosteric Inhibitor. *Mol Cell Pharmacol* **5**(1)**:** 246-257.

Millar RP, Newton CL (2010). The year in G protein-coupled receptor research. *Mol Endocrinol* **24**(1)**:** 261-274.

Minamino N, Kangawa K, Fukuda A, Matsuo H (1984b). Neuromedin L: a novel mammalian tachykinin identified in porcine spinal cord. *Neuropeptides* **4**(2)**:** 157-166.

Minamino N, Kangawa K, Honzawa M, Matsuo H (1988). Isolation and structural determination of rat neuromedin U. *Biochem Biophys Res Commun* **156**(1)**:** 355-360.

Minamino N, Kangawa K, Matsuo H (1983b). Neuromedin B: a novel bombesin-like peptide identified in porcine spinal cord. *Biochem Biophys Res Commun* **114**(2)**:** 541-548.

Minamino N, Kangawa K, Matsuo H (1984a). Neuromedin C: a bombesin-like peptide identified in porcine spinal cord. *Biochem Biophys Res Commun* **119**(1)**:** 14-20.

Minamino N, Kangawa K, Matsuo H (1984c). Neuromedin N: a novel neurotensin-like peptide identified in porcine spinal cord. *Biochem Biophys Res Commun* **122**(2)**:** 542-549.

Minamino N, Kangawa K, Matsuo H (1985a). Neuromedin U-8 and U-25: novel uterus stimulating and hypertensive peptides identified in porcine spinal cord. *Biochem Biophys Res Commun* **130**(3)**:** 1078-1085.

Mitchell JD, Maguire JJ, Kuc RE, Davenport AP (2009). Expression and vasoconstrictor function of anorexigenic peptides neuromedin U-25 and S in the human cardiovascular system. *Cardiovasc Res* **81**(2)**:** 353-361.

Miyazato M, Mori K, Ida T, Kojima M, Murakami N, Kangawa K (2008). Identification and functional analysis of a novel ligand for G protein-coupled receptor, Neuromedin S. *Regul Pept* **145**(1-3)**:** 37-41.

Mollenhauer HH, Morre DJ, Rowe LD (1990). Alteration of intracellular traffic by monensin; mechanism, specificity and relationship to toxicity. *Biochim Biophys Acta* **1031**(2)**:** 225-246.

Mondal MS, Date Y, Murakami N, Toshinai K, Shimbara T, Kangawa K, *et al.* (2003). Neuromedin U acts in the central nervous system to inhibit gastric acid secretion via CRH system. *Am J Physiol Gastrointest Liver Physiol* **284**(6)**:** G963-969.

Moore CA, Milano SK, Benovic JL (2007). Regulation of receptor trafficking by GRKs and arrestins. *Annu Rev Physiol* **69:** 451-482.

Mori K, Miyazato M, Ida T, Murakami N, Serino R, Ueta Y, *et al.* (2005). Identification of neuromedin S and its possible role in the mammalian circadian oscillator system. *Embo J* **24**(2)**:** 325-335.

Moriyama M, Fukuyama S, Inoue H, Matsumoto T, Sato T, Tanaka K, *et al.* (2006b). The neuropeptide neuromedin U activates eosinophils and is involved in allergen-induced eosinophilia. *Am J Physiol Lung Cell Mol Physiol* **290**(5)**:** L971-977.

Moriyama M, Matsukawa A, Kudoh S, Takahashi T, Sato T, Kano T, *et al.* (2006a). The neuropeptide neuromedin U promotes IL-6 production from macrophages and endotoxin shock. *Biochem Biophys Res Commun* **341**(4)**:** 1149-1154.

Moriyama M, Sato T, Inoue H, Fukuyama S, Teranishi H, Kangawa K, *et al.* (2005). The neuropeptide neuromedin U promotes inflammation by direct activation of mast cells. *J Exp Med* **202**(2)**:** 217-224.

Morley JE, Levine AS (1982). Corticotrophin releasing factor, grooming and ingestive behavior. *Life Sci* **31**(14)**:** 1459-1464.

Muller L, Barret A, Etienne E, Meidan R, Valdenaire O, Corvol P, *et al.* (2003). Heterodimerization of endothelin-converting enzyme-1 isoforms regulates the subcellular distribution of this metalloprotease. *J Biol Chem* **278**(1)**:** 545-555.

Mundell SJ, Barton JF, Mayo-Martin MB, Hardy AR, Poole AW (2008). Rapid resensitization of purinergic receptor function in human platelets. *J Thromb Haemost* **6**(8)**:** 1393-1404.

Murphy JE, Roosterman D, Cottrell GS, Padilla BE, Feld M, Brand E, *et al.* (2011). Protein Phosphatase 2a Mediates Resensitization of the Neurokinin 1 Receptor. In: *Am J Physiol Cell Physiol*, 2011/07/29 edn.

Murphy R, Turner CA, Furness JB, Parker L, Giraud A (1990). Isolation and microsequence analysis of a novel form of neuromedin U from guinea pig small intestine. *Peptides* **11**(3)**:** 613-617.

Nakahara K, Hanada R, Murakami N, Teranishi H, Ohgusu H, Fukushima N, *et al.* (2004a). The gut-brain peptide neuromedin U is involved in the mammalian circadian oscillator system. *Biochem Biophys Res Commun* **318**(1)**:** 156-161.

Nakahara K, Katayama T, Maruyama K, Ida T, Mori K, Miyazato M, *et al.* (2010). Comparison of feeding suppression by the anorexigenic hormones neuromedin U and neuromedin S in rats. *J Endocrinol* **207**(2)**:** 185-193.

Nakahara K, Kojima M, Hanada R, Egi Y, Ida T, Miyazato M, *et al.* (2004b). Neuromedin U is involved in nociceptive reflexes and adaptation to environmental stimuli in mice. *Biochem Biophys Res Commun* **323**(2)**:** 615-620.

Nakazato M, Hanada R, Murakami N, Date Y, Mondal MS, Kojima M, *et al.* (2000). Central effects of neuromedin U in the regulation of energy homeostasis. *Biochem Biophys Res Commun* **277**(1)**:** 191-194.

Nandha KA, Benito-Orfila MA, Jamal H, Akinsanya KO, Bloom SR, Smith DM (1999). Effect of steroids and the estrous cycle on uterine neuromedin U receptor expression. *Peptides* **20**(10)**:** 1203-1209.

Nandha KA, Benito-Orfila MA, Smith DM, Bloom SR (1993). Characterization of the rat uterine neuromedin U receptor. *Endocrinology* **133**(2)**:** 482-486.

Niimi M, Murao K, Taminato T (2001). Central administration of neuromedin U activates neurons in ventrobasal hypothalamus and brainstem. *Endocrine* **16**(3)**:** 201-206.

Novak CM, Zhang M, Levine JA (2006). Neuromedin U in the paraventricular and arcuate hypothalamic nuclei increases non-exercise activity thermogenesis. *J Neuroendocrinol* **18**(8)**:** 594-601.

O'Harte F, Bockman CS, Abel PW, Conlon JM (1991a). Isolation, structural characterization and pharmacological activity of dog neuromedin U. *Peptides* **12**(1)**:** 11-15.

O'Harte F, Bockman CS, Zeng W, Abel PW, Harvey S, Conlon JM (1991b). Primary structure and pharmacological activity of a nonapeptide related to neuromedin U isolated from chicken intestine. *Peptides* **12**(4)**:** 809-812.

Oakley RH, Laporte SA, Holt JA, Barak LS, Caron MG (1999). Association of beta-arrestin with G protein-coupled receptors during clathrin-mediated endocytosis dictates the profile of receptor resensitization. *J Biol Chem* **274**(45)**:** 32248-32257.

Oakley RH, Laporte SA, Holt JA, Caron MG, Barak LS (2000). Differential affinities of visual arrestin, beta arrestin1, and beta arrestin2 for G protein-coupled receptors delineate two major classes of receptors. *J Biol Chem* **275**(22)**:** 17201-17210.

Offermanns S, Wieland T, Homann D, Sandmann J, Bombien E, Spicher K, *et al.* (1994). Transfected muscarinic acetylcholine receptors selectively couple to Gi-type G proteins and Gq/11. *Mol Pharmacol* **45**(5)**:** 890-898.

Ozaki Y, Onaka T, Nakazato M, Saito J, Kanemoto K, Matsumoto T, *et al.* (2002). Centrally administered neuromedin U activates neurosecretion and induction of c-fos messenger ribonucleic acid in the paraventricular and supraoptic nuclei of rat. *Endocrinology* **143**(11)**:** 4320-4329.

Padilla BE, Cottrell GS, Roosterman D, Pikios S, Muller L, Steinhoff M, *et al.* (2007). Endothelin-converting enzyme-1 regulates endosomal sorting of calcitonin receptor-like receptor and beta-arrestins. *Journal of Cell Biology* **179**(5)**:** 981-997.

Pahl C, Novak I (1993). Effect of vasoactive intestinal peptide, carbachol and other agonists on the membrane voltage of pancreatic duct cells. *Pflugers Arch* **424**(3-4)**:** 315-320.

Palczewski K, Kumasaka T, Hori T, Behnke CA, Motoshima H, Fox BA, *et al.* (2000). Crystal structure of rhodopsin: A G protein-coupled receptor. *Science* **289**(5480)**:** 739-745.

Palmer TM, Gettys TW, Stiles GL (1995). Differential interaction with and regulation of multiple G-proteins by the rat A3 adenosine receptor. *J Biol Chem* **270**(28)**:** 16895-16902.

Peier A, Kosinski J, Cox-York K, Qian Y, Desai K, Feng Y, *et al.* (2009). The antiobesity effects of centrally administered neuromedin U and neuromedin S are mediated predominantly by the neuromedin U receptor 2 (NMUR2). *Endocrinology* **150**(7)**:** 3101-3109.

Peier AM, Desai K, Hubert J, Du X, Yang L, Qian Y, *et al.* (2011). Effects of Peripherally Administered Neuromedin U on Energy and Glucose Homeostasis. *Endocrinology*.

Perret BG, Wagner R, Lecat S, Brillet K, Rabut G, Bucher B, *et al.* (2003). Expression of EGFP-amino-tagged human mu opioid receptor in Drosophila Schneider 2 cells: a potential expression system for large-scale production of G-protein coupled receptors. *Protein Expr Purif* **31**(1)**:** 123-132.

Pierce KL, Premont RT, Lefkowitz RJ (2002). Seven-transmembrane receptors. *Nat Rev Mol Cell Biol* **3**(9)**:** 639-650.

Pitcher JA, Freedman NJ, Lefkowitz RJ (1998). G protein-coupled receptor kinases. *Annu Rev Biochem* **67:** 653-692.

Prendergast CE, Morton MF, Figueroa KW, Wu X, Shankley NP (2006). Species-dependent smooth muscle contraction to Neuromedin U and determination of the receptor subtypes mediating contraction using NMU1 receptor knockout mice. *Br J Pharmacol* **147**(8)**:** 886-896.

Qi JS, Minor LK, Smith C, Hu B, Yang J, Andrade-Gordon P, *et al.* (2005). Characterization of functional urotensin II receptors in human skeletal muscle myoblasts: comparison with angiotensin II receptors. *Peptides* **26**(4)**:** 683-690.

Quayle JM, Dart C, Standen NB (1996). The properties and distribution of inward rectifier potassium currents in pig coronary arterial smooth muscle. *J Physiol* **494 (Pt 3):** 715-726.

Raddatz R, Wilson AE, Artymyshyn R, Bonini JA, Borowsky B, Boteju LW, *et al.* (2000). Identification and characterization of two neuromedin U receptors differentially expressed in peripheral tissues and the central nervous system. *J Biol Chem* **275**(42)**:** 32452-32459.

Rahman AA, Shahid IZ, Pilowsky PM (2011). Intrathecal neuromedin U induces biphasic effects on sympathetic vasomotor tone, increases respiratory drive and attenuates sympathetic reflexes in rat. *Br J Pharmacol*.

Rashid AJ, O'Dowd BF, George SR (2004). Minireview: Diversity and complexity of signaling through peptidergic G protein-coupled receptors. *Endocrinology* **145**(6)**:** 2645-2652.

Rasmussen SG, Choi HJ, Rosenbaum DM, Kobilka TS, Thian FS, Edwards PC, *et al.* (2007). Crystal structure of the human beta2 adrenergic G-protein-coupled receptor. *Nature* **450**(7168)**:** 383-387.

Rink R, Arkema-Meter A, Baudoin I, Post E, Kuipers A, Nelemans SA, *et al.* (2010). To protect peptide pharmaceuticals against peptidases. *J Pharmacol Toxicol Methods* **61**(2)**:** 210-218.

Roosterman D, Cottrell GS, Padilla BE, Muller L, Eckman CB, Bunnett NW, *et al.* (2007). Endothelin-converting enzyme 1 degrades neuropeptides in endosomes to control receptor recycling. *Proceedings of the National Academy of Sciences of the United States of America* **104**(28)**:** 11838-11843.

Roosterman D, Kempkes C, Cottrell GS, Padilla BE, Bunnett NW, Turck CW, *et al.* (2008). Endothelin-converting enzyme-1 degrades internalized somatostatin-14. *Endocrinology* **149**(5)**:** 2200-2207.

Rovati GE, Capra V, Neubig RR (2007). The highly conserved DRY motif of class A G protein-coupled receptors: beyond the ground state. *Mol Pharmacol* **71**(4)**:** 959-964.

Rucinski M, Ziolkowska A, Neri G, Trejter M, Zemleduch T, Tyczewska M, *et al.* (2007). Expression of neuromedins S and U and their receptors in the hypothalamus and endocrine glands of the rat. *Int J Mol Med* **20**(2)**:** 255-259.

Rucinski M, Ziolkowska A, Tyczewska M, Szyszka M, Malendowicz LK (2008). Neuromedin U directly stimulates growth of cultured rat calvarial osteoblast-like cells acting via the NMU receptor 2 isoform. *Int J Mol Med* **22**(3)**:** 363-368.

Sakura N, Ohta S, Uchida Y, Kurosawa K, Okimura K, Hashimoto T (1991). Structure-activity relationships of rat neuromedin U for smooth muscle contraction. *Chem Pharm Bull (Tokyo)* **39**(8)**:** 2016-2020.

Salio C, Lossi L, Ferrini F, Merighi A (2006). Neuropeptides as synaptic transmitters. *Cell Tissue Res* **326**(2)**:** 583-598.

Salmon AL, Johnsen AH, Bienert M, McMurray G, Nandha KA, Bloom SR, *et al.* (2000). Isolation, structural characterization, and bioactivity of a novel neuromedin U analog from the defensive skin secretion of the Australasian tree frog, Litoria caerulea. *J Biol Chem* **275**(7)**:** 4549-4554.

Sambrook Ra (2001). *Molecular Cloning: A Laboratory Manual*. 3 edn, vol. 3. Cold Spring Harbor Laboratory Press.

Sandvig K, Torgersen ML, Raa HA, van Deurs B (2008). Clathrin-independent endocytosis: from nonexisting to an extreme degree of complexity. *Histochem Cell Biol* **129**(3)**:** 267-276.

Sasaki T, Shimizu T, Wakiguchi H, Yokotani K (2008). Centrally administered neuromedin U elevates plasma adrenaline by brain prostanoid TP receptor-mediated mechanisms in rats. *Eur J Pharmacol* **592**(1-3)**:** 81-86.

Sato S, Hanada R, Kimura A, Abe T, Matsumoto T, Iwasaki M, *et al.* (2007). Central control of bone remodeling by neuromedin U. *Nat Med* **13**(10)**:** 1234-1240.

Savarese TM, Wang CD, Fraser CM (1992). Site-directed mutagenesis of the rat m1 muscarinic acetylcholine receptor. Role of conserved cysteines in receptor function. *J Biol Chem* **267**(16)**:** 11439-11448.

Schmidlin F, Dery O, DeFea KO, Slice L, Patierno S, Sternini C, *et al.* (2001). Dynamin and Rab5a-dependent trafficking and signaling of the neurokinin 1 receptor. *Journal of Biological Chemistry* **276**(27)**:** 25427-25437.

Shan L, Qiao X, Crona JH, Behan J, Wang S, Laz T, *et al.* (2000). Identification of a novel neuromedin U receptor subtype expressed in the central nervous system. *J Biol Chem* **275**(50)**:** 39482-39486.

Sharman JL, Mpamhanga CP, Spedding M, Germain P, Staels B, Dacquet C, *et al.* (2011). IUPHAR-DB: new receptors and tools for easy searching and visualization of pharmacological data. *Nucleic Acids Res* **39**(Database issue)**:** D534-538.

Shetzline SE, Rallapalli R, Dowd KJ, Zou S, Nakata Y, Swider CR, *et al.* (2004). Neuromedin U: a Myb-regulated autocrine growth factor for human myeloid leukemias. *Blood* **104**(6)**:** 1833-1840.

Shousha S, Nakahara K, Miyazato M, Kangawa K, Murakami N (2005). Endogenous neuromedin U has anorectic effects in the Japanese quail. *Gen Comp Endocrinol* **140**(3)**:** 156-163.

Shousha S, Nakahara K, Sato M, Mori K, Miyazato M, Kangawa K, *et al.* (2006). Effect of neuromedin S on feeding regulation in the Japanese quail. *Neurosci Lett* **391**(3)**:** 87-90.

Singer CA, Vang S, Gerthoffer WT (2002). Coupling of M(2) muscarinic receptors to Src activation in cultured canine colonic smooth muscle cells. *Am J Physiol Gastrointest Liver Physiol* **282**(1)**:** G61-68.

Skalli O, Pelte MF, Peclet MC, Gabbiani G, Gugliotta P, Bussolati G, *et al.* (1989). Alpha-smooth muscle actin, a differentiation marker of smooth muscle cells, is present in microfilamentous bundles of pericytes. *J Histochem Cytochem* **37**(3)**:** 315-321.

Strader CD, Fong TM, Tota MR, Underwood D, Dixon RA (1994). Structure and function of G protein-coupled receptors. *Annu Rev Biochem* **63:** 101-132.

Sumi S, Inoue K, Kogire M, Doi R, Takaori K, Suzuki T, *et al.* (1987). Effect of synthetic neuromedin U-8 and U-25, novel peptides identified in porcine spinal cord, on splanchnic circulation in dogs. *Life Sci* **41**(13)**:** 1585-1590.

Syme CA, Zhang L, Bisello A (2006). Caveolin-1 regulates cellular trafficking and function of the glucagon-like Peptide 1 receptor. *Mol Endocrinol* **20**(12)**:** 3400-3411.

Szekeres PG, Muir AI, Spinage LD, Miller JE, Butler SI, Smith A, *et al.* (2000). Neuromedin U is a potent agonist at the orphan G protein-coupled receptor FM3. *J Biol Chem* **275**(27)**:** 20247-20250.

Takahashi K, Furukawa C, Takano A, Ishikawa N, Kato T, Hayama S, *et al.* (2006). The neuromedin U-growth hormone secretagogue receptor 1b/neurotensin receptor 1 oncogenic signaling pathway as a therapeutic target for lung cancer. *Cancer Res* **66**(19)**:** 9408-9419.

Tan CP, McKee KK, Liu Q, Palyha OC, Feighner SD, Hreniuk DL, *et al.* (1998). Cloning and Characterization of a Human and Murine T-Cell Orphan G-Protein-Coupled Receptor Similar to the Growth Hormone Secretagogue and Neurotensin Receptors* 1. *Genomics* **52**(2)**:** 223-229.

Tanida M, Satomi J, Shen J, Nagai K (2009). Autonomic and cardiovascular effects of central neuromedin U in rats. *Physiol Behav* **96**(2)**:** 282-288.

Tarasova NI, Stauber RH, Choi JK, Hudson EA, Czerwinski G, Miller JL, *et al.* (1997). Visualization of G protein-coupled receptor trafficking with the aid of the green fluorescent protein. Endocytosis and recycling of cholecystokinin receptor type A. *J Biol Chem* **272**(23)**:** 14817-14824.

Thompson EL, Murphy KG, Todd JF, Martin NM, Small CJ, Ghatei MA, *et al.* (2004). Chronic administration of NMU into the paraventricular nucleus stimulates the HPA axis but does not influence food intake or body weight. *Biochem Biophys Res Commun* **323**(1)**:** 65-71.

Tong J, Du GG, Chen SR, MacLennan DH (1999). HEK-293 cells possess a carbachol- and thapsigargin-sensitive intracellular Ca2+ store that is responsive to stop-flow medium changes and insensitive to caffeine and ryanodine. *Biochem J* **343 Pt 1:** 39-44.

Torres R, Croll SD, Vercollone J, Reinhardt J, Griffiths J, Zabski S, *et al.* (2007). Mice genetically deficient in neuromedin U receptor 2, but not neuromedin U receptor 1, have impaired nociceptive responses. *Pain* **130**(3)**:** 267-278.

Trejter M, Neri G, Rucinski M, Majchrzak M, Nussdorfer GG, Malendowicz LK (2008). Neuromedin-U stimulates enucleation-induced adrenocortical regeneration in the rat. *Int J Mol Med* **21**(6)**:** 683-687.

Tsubota Y, Kakimoto N, Owada-Makabe K, Yukawa K, Liang XM, Mune M, *et al.* (2003). Hypotensive effects of neuromedin U microinjected into the cardiovascular-related region of the rat nucleus tractus solitarius. *Neuroreport* **14**(18)**:** 2387-2390.

Tusnady GE, Simon I (2001). The HMMTOP transmembrane topology prediction server. *Bioinformatics* **17**(9)**:** 849-850.

Ubl JJ, Sergeeva M, Reiser G (2000). Desensitisation of protease-activated receptor-1 (PAR-1) in rat astrocytes: evidence for a novel mechanism for terminating Ca2+ signalling evoked by the tethered ligand. *J Physiol* **525 Pt 2:** 319-330.

Umekawa K, Hasegawa H, Tsutsumi Y, Sato K, Matsumura Y, Ohashi N (2000). Pharmacological characterization of a novel sulfonylureid-pyrazole derivative, SM-19712, a potent nonpeptidic inhibitor of endothelin converting enzyme. *Jpn J Pharmacol* **84**(1)**:** 7-15.

Verdich C, Madsen JL, Toubro S, Buemann B, Holst JJ, Astrup A (2000). Effect of obesity and major weight reduction on gastric emptying. *Int J Obes Relat Metab Disord* **24**(7)**:** 899-905.

Vigo E, Roa J, Pineda R, Castellano JM, Navarro VM, Aguilar E, *et al.* (2007a). Novel role of the anorexigenic peptide neuromedin U in the control of LH secretion and its regulation by gonadal hormones and photoperiod. *Am J Physiol Endocrinol Metab* **293**(5)**:** E1265-1273.

Wang F, Zhang Y, Jiang X, Zhang L, Gong S, Liu C, *et al.* (2011). Neuromedin U inhibits T-type Ca2+ channel currents and decreases membrane excitability in small dorsal root ganglia neurons in mice. *Cell Calcium* **49**(1)**:** 12-22.

Warne T, Serrano-Vega MJ, Baker JG, Moukhametzianov R, Edwards PC, Henderson R, *et al.* (2008). Structure of a beta1-adrenergic G-protein-coupled receptor. *Nature* **454**(7203)**:** 486-491.

Westfall TD, McCafferty GP, Pullen M, Gruver S, Sulpizio AC, Aiyar VN, *et al.* (2002). Characterization of neuromedin U effects in canine smooth muscle. *J Pharmacol Exp Ther* **301**(3)**:** 987-992.

Widdop S, Daykin K, Hall IP (1993). Expression of muscarinic M2 receptors in cultured human airway smooth muscle cells. *Am J Respir Cell Mol Biol* **9**(5)**:** 541-546.

Willars GB, Nahorski SR (1995). Quantitative comparisons of muscarinic and bradykinin receptor-mediated Ins (1,4,5)P3 accumulation and Ca2+ signalling in human neuroblastoma cells. *Br J Pharmacol* **114**(6)**:** 1133-1142.

Wojcikiewicz RJ, Tobin AB, Nahorski SR (1994). Muscarinic receptor-mediated inositol 1,4,5-trisphosphate formation in SH-SY5Y neuroblastoma cells is regulated acutely by cytosolic Ca2+ and by rapid desensitization. *J Neurochem* **63**(1)**:** 177-185.

Woodcock EA, Matkovich SJ (2005). Ins(1,4,5)P3 receptors and inositol phosphates in the heart-evolutionary artefacts or active signal transducers? *Pharmacol Ther* **107**(2)**:** 240-251.

Wren AM, Small CJ, Abbott CR, Jethwa PH, Kennedy AR, Murphy KG, *et al.* (2002). Hypothalamic actions of neuromedin U. *Endocrinology* **143**(11)**:** 4227-4234.

Wu Y, McRoberts K, Berr SS, Frierson HF, Jr., Conaway M, Theodorescu D (2007). Neuromedin U is regulated by the metastasis suppressor RhoGDI2 and is a novel promoter of tumor formation, lung metastasis and cancer cachexia. *Oncogene* **26**(5)**:** 765-773.

Yamashita K, Upadhyay S, Osada M, Hoque MO, Xiao Y, Mori M, *et al.* (2002). Pharmacologic unmasking of epigenetically silenced tumor suppressor genes in esophageal squamous cell carcinoma. *Cancer Cell* **2**(6)**:** 485-495.

Yanagisawa M, Kurihara H, Kimura S, Tomobe Y, Kobayashi M, Mitsui Y, *et al.* (1988). A novel potent vasoconstrictor peptide produced by vascular endothelial cells. *Nature* **332**(6163)**:** 411-415.

Yang G, Su J, Yao Y, Lei Z, Zhang G, Liu Y, *et al.* (2010). Distribution of neuromedin S and its receptor NMU2R in pigs. *Res Vet Sci*.

Yao ST (2009). Alpha-adrenergic receptors in the nucleus tractus solitarii: fitting a new piece to a complex puzzle. *Exp Physiol* **94**(7)**:** 771-772.

Yu R, Hinkle PM (1997). Effect of cell type on the subcellular localization of the thyrotropin-releasing hormone receptor. *Mol Pharmacol* **51**(5)**:** 785-793.

Yu XH, Cao CQ, Mennicken F, Puma C, Dray A, O'Donnell D, *et al.* (2003). Pro-nociceptive effects of neuromedin U in rat. *Neuroscience* **120**(2)**:** 467-474.

Zeng H, Gragerov A, Hohmann JG, Pavlova MN, Schimpf BA, Xu H, *et al.* (2006). Neuromedin U receptor 2-deficient mice display differential responses in sensory perception, stress, and feeding. *Mol Cell Biol* **26**(24)**:** 9352-9363.

Zhang Y, Jiang D, Zhang J, Wang F, Jiang X, Tao J (2010). Activation of neuromedin U type 1 receptor inhibits L-type Ca2+ channel currents via phosphatidylinositol 3-kinase-dependent protein kinase C epsilon pathway in mouse hippocampal neurons. *Cell Signal* **22**(11)**:** 1660-1668.

Zhu X, Gilbert S, Birnbaumer M, Birnbaumer L (1994). Dual signaling potential is common among Gs-coupled receptors and dependent on receptor density. *Mol Pharmacol* **46**(3)**:** 460-469.

Zhu X, Jiang M, Birnbaumer L (1998). Receptor-activated Ca2+ influx via human Trp3 stably expressed in human embryonic kidney (HEK)293 cells. Evidence for a non-capacitative Ca2+ entry. *J Biol Chem* **273**(1)**:** 133-142.

Ziolkowska A, Macchi C, Trejter M, Rucinski M, Nowak M, Nussdorfer GG, *et al.* (2008). Effects of neuromedin-U on immature rat adrenocortical cells: in vitro and in vivo studies. *Int J Mol Med* **21**(3)**:** 303-307.